Design, Synthesis and Photo-physical Studies of Donor-Acceptor Systems for Achieving Long-Lived Charge-Separated State

by
Daisymol K. B.
10CC15J39005

A thesis submitted to the
Academy of Scientific & Innovative Research
for the award of the degree of
DOCTOR OF PHILOSOPHY
in
SCIENCE

Under the supervision of
Dr. K. R. Gopidas

CSIR-National Institute for Interdisciplinary Science and Technology (CSIR-NIIST)
Thiruvananthapuram

Academy of Scientific and Innovative Research
AcSIR Headquarters, CSIR-HRDC campus
Sector 19, Kamla Nehru Nagar,
Ghaziabad, U.P. – 201 002, India
2023

सीएसआईआर- राष्ट्रीय अंतर्विषयी विज्ञान तथा प्रौद्योगिकी संस्थान

CSIR-NATIONAL INSTITUTE FOR
INTERDISCIPLINARY SCIENCE & TECHNOLOGY

इंडस्ट्रियल इस्टेट पी.ओ., तिरुवनंतपुरम - 695 019, केरल, भारत

Industrial Estate P.O., Thiruvananthapuram - 695 019, Kerala, INDIA.

डॉ. के.आर. गोपिदास, एफ.ए.एससी.

Dr. K. R. Gopidas F.A.Sc.

सीएसआईआर एमेरिटस वैज्ञानिक

CSIR Emeritus Scientist

रसायन विज्ञान तथा प्रौद्योगिकी प्रभाग

Chemical Sciences and Technology Division

January 6, 2023

<u>CERTIFICATE</u>

This is to certify that the work incorporated in this Ph.D. thesis entitled **"Design, Synthesis and Photo-physical Studies of Donor-Acceptor Systems for Achieving Long-Lived Charge-Separated State"** submitted by Mrs. *Daisymol K. B.* to Academy of Scientific and Innovative Research (AcSIR) in fulfillment of the requirements for the award of the Degree of *Doctor Of Philosophy in Science*, embodies original research work under my supervision/guidance. We, further certify that this work has not been submitted to any other University or Institution in part or full for the award of any degree or diploma. Research material(s) obtained from other source(s) and used in this research work has/have been duly acknowledged in the thesis. Image(s), illustration(s), figure(s), table(s) etc., used in the thesis from other source(s), have also been duly cited and acknowledged.

Daisymol K. B.

Dr. K. R. Gopidas

(Thesis Supervisor)

टेलीफोन /Telephone: 91-471-2515390(O), 9446520537(M)

फ़ैक्स /Fax : +91-471-2491712, ई-मेल /E-mail: gopidaskr@gmail.com

STATEMENTS OF ACADEMIC INTEGRITY

I Daisymol K.B., a Ph.D. student of the Academy of Scientific and Innovative Research (AcSIR) with Registration No. 10CC15J39005 hereby undertake that, the thesis entitled **"Design, Synthesis and Photo-physical Studies of Donor-Acceptor Systems for Achieving Long-Lived Charge-Separated State"** has been prepared by me and that the document reports original work carried out by me and is free of any plagiarism in compliance with the UGC Regulations on *"Promotion of Academic Integrity and Prevention of Plagiarism in Higher Educational Institutions (2018)"* and the CSIR Guidelines for *"Ethics in Research and in Governance (2020)"*.
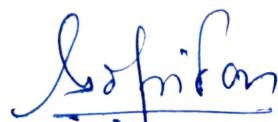
Signature of the Student
Date   : 06-01-2023
Place   : Thiruvananthapuram

It is hereby certified that the work done by the student, under my/our supervision, is plagiarism-free in accordance with the UGC Regulations on *"Promotion of Academic Integrity and Prevention of Plagiarism in Higher Educational Institutions (2018)"* and the CSIR Guidelines for *"Ethics in Research and in Governance (2020)"*.

Signature of the Supervisor
Name : Dr. K. R. Gopidas
Date   : 06-01-2023
Place : Thiruvananthapuram

DECLARATION

I, Daisymol K. B. bearing AcSIR Registration No. 10CC15J39005 declare:

(a) that the plagiarism detection software is currently not available at my work-place institute.

(b) that my thesis entitled, ""**Design, Synthesis and Photo-physical Studies of Donor-Acceptor Systems for Achieving Long-Lived Charge-Separated State**" is plagiarism free in accordance with the UGC Regulations on *"Promotion of Academic Integrity and Prevention of Plagiarism in Higher Educational Institutions (2018)"* and the CSIR Guidelines for *"Ethics in Research and in Governance (2020)"*.

(c) that I would be solely held responsible if any plagiarised content in my thesis is detected, which is violative of the UGC regulations 2018.

(Signature of the Student)
Date: 06-01-2023
Place: Thiruvananthapuram

Daisymol K. B.

CONTENTS

CHAPTER 1: **Photoinduced Charge Separation and Charge Recombination in Donor-Acceptor Dyads: an Overview**

CHAPTER 2: **Photoinduced Electron Transfer Studies of 9,10-Bis(phenylethynyl)-2,6-di-*tert*-butylanthracene-Phenothiazine and 9,10-Bis(phenylethynyl)-2,6-di(1-adamantyl)anthracene-Phenothiazine Dyads**

CHAPTER 3: **Photoinduced Electron Transfer Studies of Adamantane-Bridged Dyads with *N,N*-dimethylaniline Donor and Hydrocarbon Acceptors**

CHAPTER 4: **Photoinduced Electron Transfer Studies of Adamantane-Bridged Dyads with Hydrocrbon Donors and Nitrobenzene Acceptor**

LIST OF FIGURES

LIST OF SCHEMES

LIST OF TABLES

LIST OF ABBREVIATIONS

1	^{1}HNMR	Proton NMR
2	3, BuBPEA	2,6-di-*tert*-butyl-BPEA
3	4, ADBPEA	2,6-diadamantyl-BPEA
4	AD	Adamantane
5	AN	Antracene
6	AN-AD-DMA	Anthracene-dimethylaniline
7	B	Bridge
8	BCI	Bacteriochlorophyll molecules
9	BET	Back Electron Transfer
10	BP	Benzophenone
11	BPEA	bis(phenylethynyl)anthracene
12	BPEP	Bis(phenylethynyl)pyrene
13	BPh	Bacteriopheophytins
14	CCD	Charge-Coupled Device
15	CH	Chlorin

16	CR	Charge Recombination
17	CS	Charge Separated
18	CV	Cyclic Voltammetry
19	D-A	Donor-Acceptor
20	DCV	Dicyanovinyl
21	DMN	1,4-dimethoxynaphthalene
22	DNB	Dinitrobenzene
23	DNP	2-methylaminonaphthalene
24	DPA	Diphenyl anthracene
25	EnT	Energy Transfer
26	ESR	Electron Spin Resonance
27	ET	Electron Transfer
28	FC	Franck-Condon
29	FT-IR	Fourier-transform infrared spectroscopy
30	HOMO	Highest Occupied Molecular Orbital
31	ICT	Intramolecular Charge Transfer
32	ISC	Inter System Crossing
33	LED	Light Emitting Diode
34	MLCT	Metal to Ligand Charge Transfer
35	NB	Nitrobenzene
36	NBCD	mono-6-*p*-nitrobenzoyl- -cyclodextrin
37	Nd-YAG	Neodymium Yttrium Aluminum Garnet
38	NP	Naphthalene
39	P	Porphyrin

40	PE	Perylene
41	PET	Photoinduced Electron Transfer
42	PT	Phenothiazine
43	PY	Pyrene
44	PY-AD-DMA	Pyrene-dimethylaniline
45	Q	Quinones
46	Q_A	Menaquinone
47	Q_B	Ubiquinone
48	RC	Reaction Center
49	RuBP	*tris*-bipyridylruthenium(II)dichloride
50	S	Spacer
51	SOC	Spin-Orbit Coupling
52	T	Temperature
53	TICT	Twisted Intramolecular Charge Transfer
54	T-T	Triplet-Triplet
55	UV	Ultra Violet
56	UV/Vis-NIR	Ultraviolet-Visible-Near Infrared spectrophotometry
57	VIS	Visible

PREFACE

Photogenerated radical-ion pairs in linked donor-acceptor (D-A) dyads are extremely short-lived because of the very fast charge recombination (CR) reaction either to the D-A ground state or to a low-lying local triplet ($^3D^*$ or $^3A^*$). Applications of photoinduced electron transfer (PET) in practically relevant areas such as artificial photosynthesis, solar water splitting and photocatalytic reactions require radical ion pairs (also known as charge separated (CS) state) with near-microsecond lifetimes and hence enhancing the CS state lifetimes is a major goal in photochemistry. Most of the studies in this area envisaged the natural photosynthetic reaction center as a model and designed covalently linked triads, tetrads and higher order systems. However, covalent synthesis of large molecular arrays is highly inefficient and expensive and hence assembling such arrays through non-covalent interactions were also attempted. The covalent and non-covalent approaches have very little success in extending the radical ion pair lifetimes beyond the nanosecond domain. The amount of energy that can be stored in the radical ion pair is also very important. In large molecular arrays, long-lived RP is possible because of sequential electron transfer steps that increases the distance between the charge centers. Energy is lost in each of these steps and as a result the RP state will store only about fifty percent of the excitation energy. In this context, design of compact dyads that can generate long-lived radical ions and also store energy in excess of 2.0 eV, looks extremely attractive and important. All the compact dyads designed till date exhibited sub-nanosecond lifetimes. In this thesis, we have attempted the design and study of donor-acceptor dyads that exhibit charge separated state lifetimes in the near microsecond regime.

The thesis is divided into four chapters. The first chapter gives a detailed overview of photoinduced electron transfer and the importance of long-lived photoinduced charge separation. Strategies employed by previous workers for generating long-lived charge separated states, such as design and study of triads, tetrads, etc. are discussed. The advantages of dyads over the polyads are discussed. A survey of donor-acceptor dyads studied previously is also included in the chapter.

Formation of long-lived CS states in two D-A dyads with bis(phenylethynyl)anthracene as light absorber and electron acceptor and phenothiazine as donor were investigated in Chapter 2. The bis(phenylethynyl)anthracene core was substituted with *tert*-butyl or 1-adamantyl groups at the 2- and 6-positions in order to increase the solubility of these molecules in polar solvents. The absorption spectra indicated that the donor and acceptor moieties do not have any ground-state interaction. Fluorescence of the bis(phenylethynyl)anthracene core was efficiently quenched by the donor moieties and this was attributed to electron transfer from the phenothiazine to bis(phenylethynyl)anthracene singlet excited state. Nanosecond flash photolysis experiments gave long-lived transient absorptions assignable to phenothiazine radical cation and bis(phenylethynyl)anthracene radical anion. Although the triplet energy of bis(phenylethynyl)anthracene lies below the energy of the CS state, the bis(phenylethynyl)anthracene triplet is not formed due to the absence of spin-orbit coupling or hyperfine interaction in this molecule. Electron transfer in these systems is analyzed in the light of Marcus theory and the slow back electron transfer was attributed to inverted region effects. Substitution of *tert*-butyl or 1-adamantyl group did not increase the solubility of the molecules in polar solvents and hence temperature dependent studies of electron transfer could not be carried out.

Synthesis, characterization and photoinduced electron transfer studies of adamantane-bridged anthracene-dimethylaniline (AN-AD-DMA) and pyrene-dimethylaniline (PY-AD-DMA) systems are reported in Chapter 3. The adamantane bridge separates the donor dimethylaniline and acceptor anthracene (or pyrene) by three carbon atoms (or four C-C single bonds) and the edge-to-edge D-A distance is about 4.6 Å. A comparison can be made to AN-$(CH_2)_3$-DMA and PY-$(CH_2)_3$-DMA, which were studied in great detail in the past. In

AN-$(CH_2)_3$-DMA, PET occurs in 2.7 ps and lifetime of the CS state was only 700 ps. For PY-$(CH_2)_3$-DMA, the CS state is formed within 11 ps of photoexcitation and lifetime was 1.1 ns. In the adamantane bridged systems, the CS state formation was 1-2 orders of magnitude slower. Most surprisingly, lifetimes of the CS states were enhanced thousand-fold to nearly 1.0 microsecond. In the –$(CH_2)_3$- chain linked systems, the ^{1}CS state did not undergo intersystem crossing to ^{3}CS state because the electron spin – nuclear spin hyperfine interaction energy ΔE_{hfi} is much lower than the spin exchange interaction 2J. In the adamantane bridged systems we see formation of local triplet state with quantum yield of 0.2, in addition to the long-lived CS state, which suggest that the AD bridge is also capable of reducing the spin exchange interaction energy. Long-lived CS state formation and intersystem crossing in the singlet radical pair were not observed previously in compact dyads. These new properties observed in the case of AN-AD-DMA and PY-AD-DMA are attributed to the adamantane bridge.

In Chapter 4 of the thesis, the newly observed ability of adamantane to enhance the CS state lifetime is confirmed using few other adamantane-bridged compact donor-acceptor systems. Nitrobenzene (NB) moiety is used as the acceptor and aromatic hydrocarbons such as AN, PY, diphenylanthracene (DPA) and perylene (PER) were used as donors. In Chapter 4, we report the synthesis, characterization and photophysical studies of four adamantane bridged dyads, AN-AD-NB, PY-AD-NB, DPA-AD-NB and PER-AD-NB. Single crystal X-ray structures of two of the compact dyads are also presented in this chapter. We observed that the fluorescence of the aromatic hydrocarbons is efficiently quenched by the appended NB moiety, which is attributed to PET occurring in these dyads. Nanosecond laser flash photolysis gave transients assignable to triplets of the hydrocarbons in addition to

nitrobenzene radical anion and hydrocarbon radical cations. The radical ions exhibited lifetimes close to a microsecond. Thus, our studies reported in Chapters 3 and 4 confirm that the adamantane bridge can be used to enhance charge separated states in compact dyads.

Note: The abbreviations of various compounds given here correspond to those given under the respective Chapters.

Photoinduced Charge Separation and Charge Recombination in Donor-Acceptor Dyads: An Overview

1.1. INTRODUCTION

Donor-Acceptor (D-A) systems capable of transferring an electron from D to A upon light irradiation is at the core of all the important photo-processes such as artificial photosynthesis, photovoltaics and photocatalysis.[1-7] Upon irradiation, D or A gets excited, and the excited state either donates or accepts an electron to/from the partner and generates the donor radical cation, $D^{\bullet+}$ and acceptor radical anion $A^{\bullet-}$. The charge separated (CS) state lifetime actually determines the efficiencies of the light-induced processes. The process is referred to as photoinduced electron transfer (PET). PET processes are generally very inefficient because $A^{\bullet-}$ quickly transfers the electron back to $D^{\bullet+}$ and the ground-state reactants are regenerated. This process is termed charge recombination (CR) or back electron transfer (BET). Generally, CR reactions are as fast or faster than the charge separation reactions and hence the quantum yield (Φ_{CS}) and lifetime (τ_{CS}) of the CS states are very low.

The importance of Φ_{CS} and τ_{CS} in PET reactions can be illustrated by considering the light-induced water splitting reaction. In principle, water can be split into hydrogen and oxygen through a PET reaction as shown in equations (1.1) to (1.3).[8-11]

$$D + A \xrightarrow{h\nu} D^{\bullet+} + A^{\bullet-} \qquad (1.1)$$

$$2A^{\bullet-} + 2H_2O \xrightarrow{\text{Catalyst 1}} 2A + H_2 + 2OH^- \qquad (1.2)$$

$$4D^{\bullet+} + 2H_2O \xrightarrow{\text{Catalyst 2}} 4D + O_2 + 4H^+ \qquad (1.3)$$
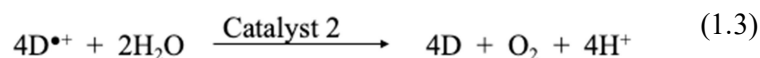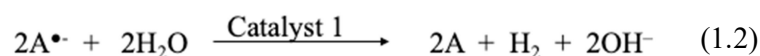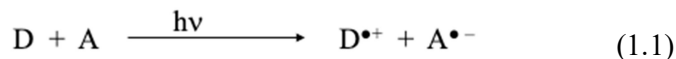
The PET reaction in equation (1.1) is a single-electron transfer reaction. The water reduction reaction is a two-electron reaction and the water oxidation reaction requires four electrons. The electron residing on $A^{\bullet-}$ is transferred quickly to a suitable catalyst, which after accumulating sufficient number of electrons carry out the water reduction. Similarly, the hole acquired by D is transferred to a catalyst, which performs the oxidation reaction after accumulating sufficient number of holes. These reactions require that $D^{\bullet+}$ and $A^{\bullet-}$ are formed in sufficient amount and their lifetimes should be sufficient so that they can participate in bimolecular reactions. In order to participate in bimolecular reactions, lifetimes in the microsecond range is required. Water splitting using sunlight is an extremely important research area because the hydrogen thus generated can be used for energy creation.

PET reactions can be performed in the bimolecular mode (free D and A molecules) or in a unimolecular manner (linked D-A system). In the bimolecular mode, the reaction is diffusion controlled. If D is the molecule that is excited, then D^* and A diffuses towards each other and form an encounter complex. Electron transfer then occurs within the encounter complex to form the ion pairs. D^* and A are in close contact when electron transfer occurs and $D^{\bullet+}$ and $A^{\bullet-}$ are formed, which leads to extremely fast CR to the ground state. A small fraction of the ion pairs escapes to form free ions. Continuous irradiation will lead to formation of the required radical ion, if scavengers are used. For example, for hydrogen generation reaction, secondary electron donors (D_1) are used as scavengers, which reacts with $D^{\bullet+}$ as shown in equation (1.4).

$$D^{\bullet+} + D_1 \longrightarrow D + D_1{}^{\bullet+} \qquad (1.4)$$
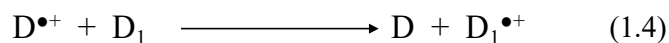
D_1 is a better electron donor than D and it gives an electron to $D^{\bullet+}$ and regenerates D, thus reducing the rate of CR. The $D_1{}^{\bullet+}$ formed undergo very fast, irreversible decomposition and is not available for CR. This leads to accumulation of $A^{\bullet-}$ for the water reduction.

The bimolecular PET reactions are not desirable because of the wastage of large amounts of chemicals. If we are exciting D, then concentration of D employed is around 10^{-4} M, because of the limitations of the Beer-Lambert law. Up on irradiation, D^* is formed in concentrations less than 10^{-5} M. If D^* is in the singlet excited state, its lifetime will be in the 1-5 ns range. To capture all the D^* in to an encounter complex within the short time, large amounts of A are required. Normally $0.1 - 0.01$ M of A is required. The amount of $D^{\bullet+}$ formed is $\leq [D^*] \sim 10^{-5}$ M. In order to capture all the $D^{\bullet+}$ formed, large amounts of the sacrificial donor is also required. Although few strategies to enhance the lifetime of CS state in bimolecular reactions are reported in the literature, we will not discuss those here. Our discussion will be confined to linked D-A systems. Enhancing Φ_{CS} and τ_{CS} in linked D-A systems have been important goals of PET research for the last few decades. [8-11]

The reaction center (RC) in photosynthetic bacteria exhibits very high quantum yield of photoinduced charge separation ($\Phi_{CS} \approx 1$) and CS state lifetime ($\tau_{CS} \approx 1$ s). The photosynthetic bacteria achieve this remarkable feat by arranging several chromophores at specific distances and orientations within a protein matrix. The way in which the chromophores, electron donors and electron acceptors are arranged in the RC of *Rhodopseudomonas viridis* is given below in Figure 1.1.[12,13] The photosynthetic reaction centre in Figure 1.1 consists of four bacteriochlorophyll molecules (BCl), two bacteriopheophytins (BPh), a molecule of menaquinone (Q_A), a molecule of ubiquinone (Q_B) and a non-heme iron.[12,13] Two of the BCl molecules are aligned very closely. These exhibit very strong electronic coupling and known as "special pair", which is designated here as $(BCl)_2$. Except for the iron atom that is shown in the lower middle part, all other constituent molecules exist in pairs because of which the reaction center is said to have C_2 symmetry. The right-hand side is designated as L-side and the left-hand side as M-side. It has been

stated that the left-hand side has no role in the photochemical process taking place in the reaction center.
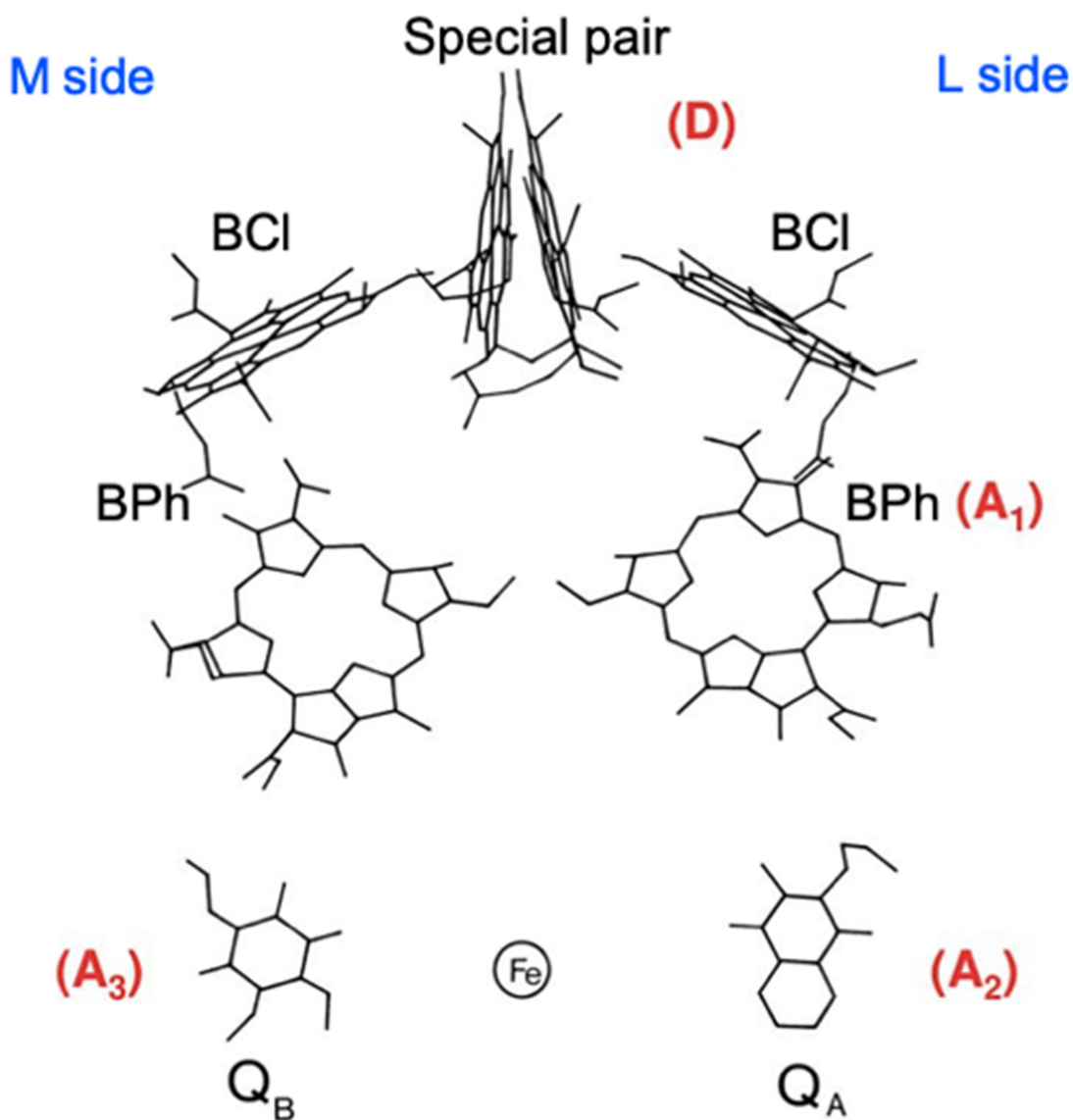
Figure 1.1. Arrangement of chromophores, electron donors and electron acceptors in the RC of *Rhodopseudomonas viridis*.

Present day knowledge of the working of RC is acquired through the combined efforts of a large number of scientists employing several state-of-the art optical and electron spin techniques, X-ray crystallography, electronic structure calculations and molecular modelling

simulations.[14-19] Light falling on the RC leads to excitation of $(BCl)_2$, which serve as the light absorber and primary electron donor (D). Within 3 ps an electron is transferred from $^1(BCl)_2^*$ to the adjacent BPh, which is the primary acceptor A_1, to form the radical ion products $(BCl)_2^{•+}$ and $BPh^{•-}$. The BCl monomer on the L-side is known to assist this electron transfer. CR reaction between $(BCl)_2^{•+}$ and $BPh^{•-}$ is prevented by ultrafast transfer of the electron from $BPh^{•-}$ to the secondary acceptor menaquinone (A_2) within 200 ps. Within 100 μs, the electron is transported to the ubiquinone (A_3). These electron transfers leave a positively charged $(BCl)_2$, which then accepts an electron from a Fe-porphyrin placed on the outer side of the membrane. The sequence of electron transfers result in charge separation across the membrane, which is long-lived. Quantum yield of the long-lived CS state is close to unity.

The reactions taking place in the reaction center can be better understood by using the reaction scheme in Figure 1.2. Excitation leads to formation of $^*(BCl)_2$ which transfers an electron to BPh with rate constant $k_{et} = 4.3 \times 10^{11}$ s^{-1}. $BPh^{•-}$ transfers that electron to Q_A with $k_{et} = 5.0 \times 10^9$ s^{-1}, which in turn is transferred to Q_B with $k_{et} = 1.0 \times 10^4$ s^{-1}. Each electron transfer in the sequence increases the distance between the radical ion centers and consequently reduces the CR rate. It can be seen from Figure 1.2 that the CR rate in the first step is 10^8 s^{-1}, which reduces to 1.0 s^{-1} in the last step. In each of the electron transfer steps k_{et} $\gg k_{CR}$, which reduces the CR reactions significantly. For example, in $(BCl)_2^{•+}\cdots BPh^{•-}$ $\cdots Q_A\cdots Q_B$ the ratio of k_{et}/k_{CR} is ~50 and this value increases to 1000 in $(BCl)_2^{•+}\cdots BPh\cdots Q_A\cdots Q_B^{•-}$. Thus, the bacterial reaction center effectively eliminates the CR reactions and generates the CS state in nearly quantitative yield.
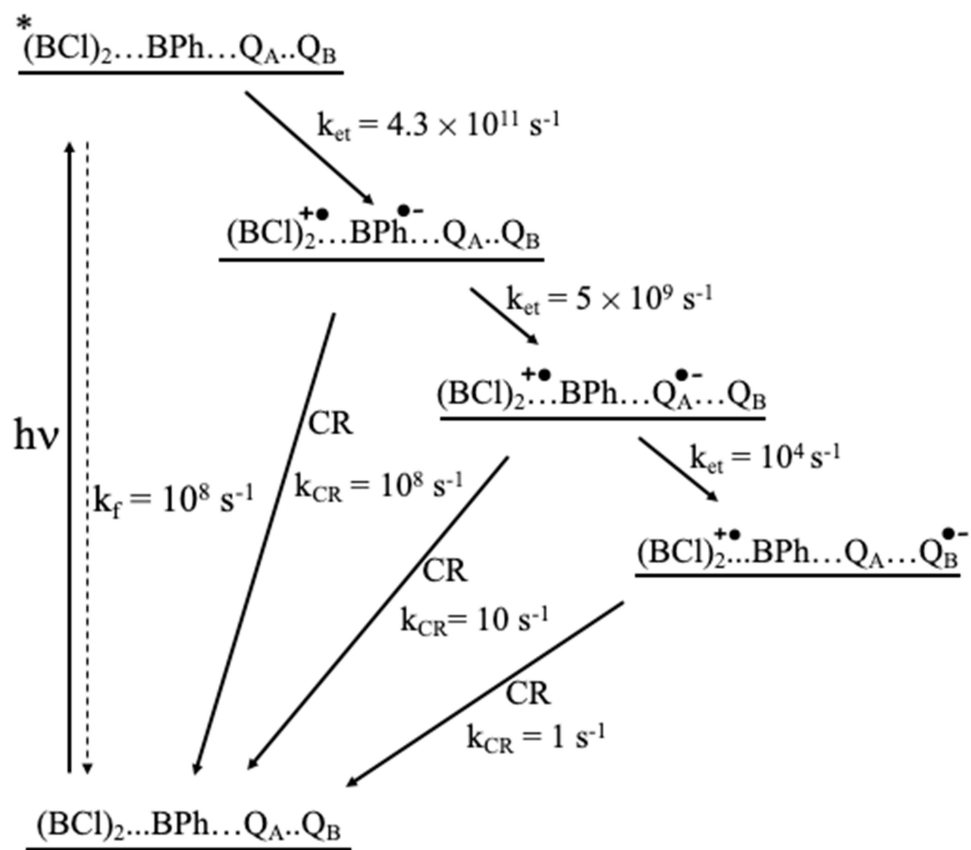
Figure 1.2. Sequential electron transfer scheme in the photoreaction center

The RC in bacteria became the inspiration for researchers to design molecular systems for solar energy harvesting through PET reactions. In the reaction center the molecular components are kept at fixed distances with proper orientations with the help of the protein scaffold.[12,13] The laboratory chemist does not have access to such a scaffold and hence uses covalent or non-covalent bonding interactions to assemble D-A systems for long CS state lifetimes. Large numbers of linked dyads, triads and tetrads, where the D and A components are covalently linked for sequential electron transfer, were synthesized and studied in the laboratory.[20] It is to be mentioned that synthesis and purification of these molecules are cumbersome and considerable effort and time are to be expended to achieve the synthesis of these polyads. Although the synthetic systems are capable of sequential

electron transfer as in the bacterial RC, none of these systems exhibited the high Φ_{CS} and τ_{CS} as in the bacterial RC. D-A systems capable of sequential electron transfer were assembled non-covalently also, but Φ_{CS} and τ_{CS} reported in these systems were also low.[21,22]

Imahori, Fukuzumi and co-workers have synthesized and studied the ferrocene-zincporphyrin-freebaseporphyrin-fullerene (Fc-ZnP-H$_2$P-C$_{60}$) tetrad shown in Figure 1.3.[23] The Fc-ZnP-H$_2$P-C$_{60}$ tetrad exhibited the cascade type electron transfer seen in the photosynthetic bacteria. Excitation of the ZnP component leads ultimately to the generation of the final CS state Fc$^{\bullet+}$-ZnP-H$_2$P-C$_{60}$$^{\bullet-}$ in solution and frozen media. In frozen benzonitrile the final CS state survived for 0.38 s, which is at least ten times larger than τ_{CS} of other tetrads.

1

Figure 1.3. Structure of the Fc-ZnP-H$_2$P-C$_{60}$ molecular tetrad studied by Imahori et al.

The cascade of energy and electron transfer processes taking place following the excitation of Fc-ZnP-H$_2$P-C$_{60}$ is shown schematically in Figure 1.4. Excitation of the molecule leads to formation of Fc-ZnP*-H$_2$P-C$_{60}$ and/or Fc-ZnP-H$_2$P*-C$_{60}$. Since H$_2$P* is lower in energy compared to ZnP*, the excitation localized on ZnP can be transferred to H$_2$P. The Fc-ZnP-H$_2$P*-C$_{60}$, generated by direct excitation or energy transfer from Fc-ZnP*-H$_2$P-C$_{60}$, transfers an electron from H$_2$P* to C$_{60}$ to give Fc-ZnP-H$_2$P$^{\bullet+}$-C$_{60}$$^{\bullet-}$. Successive electron
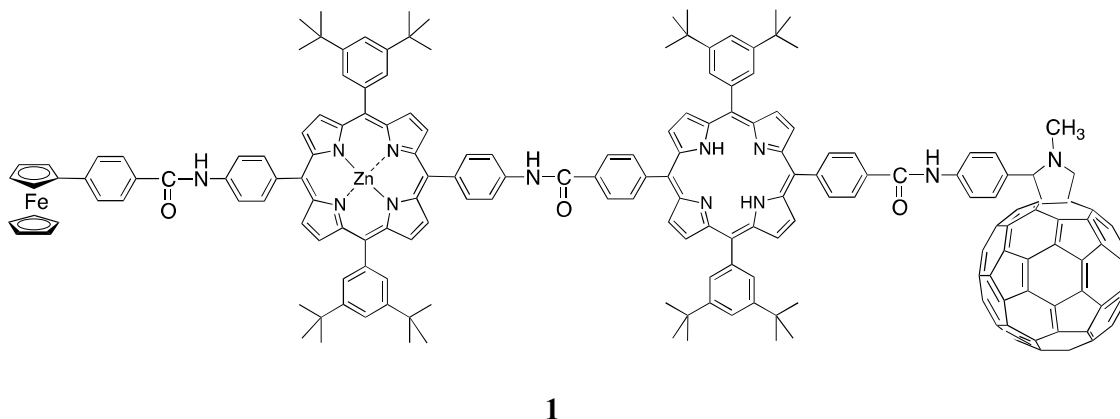
transfers from ZnP to $H_2P^{\bullet+}$ and then from Fc to $ZnP^{\bullet+}$ occurs leading ultimately to the final

CS state $Fc^{\bullet+}$-ZnP-H_2P-$C_{60}^{\bullet-}$.
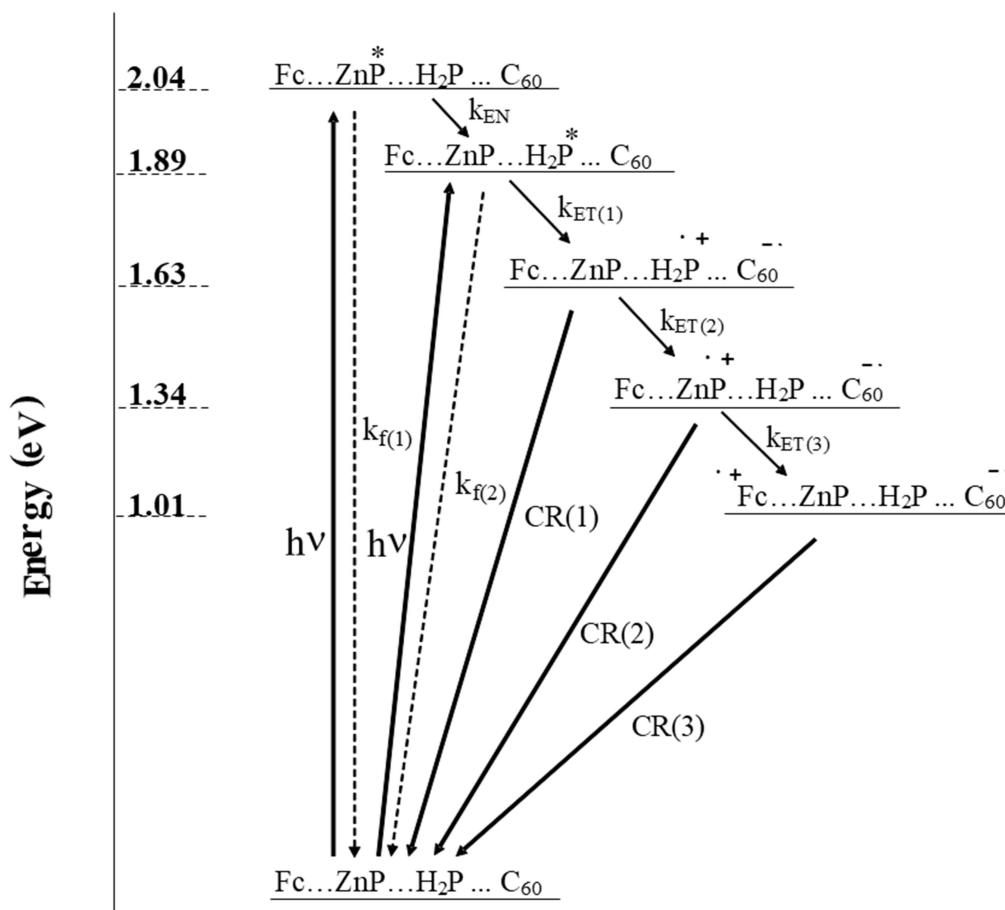
Figure 1.4. Cascade of energy and electron transfer processes taking place in Fc-ZnP-H_2P-C_{60}.

In contrast to the bacterial reaction center, CR reactions (CR(1), CR(2) and CR(3)) are competitive with forward ET reactions in this tetrad and hence the quantum yield for the formation of the final CS state is only about 0.2. The lifetime of the final CS state in benzonitrile solution at room temperature was 0.01 s ($k_{CR(3)} \sim 10^2$ s^{-1}). The CS state lifetime is enhanced to 0.38 s in frozen benzonitrile.

An important aspect that is not often discussed in the study of polyads is the loss of energy encountered at each step in the cascade. The left-hand side of Figure 1.4 shows the

energy of each of the intermediates in the cascade. The initial Fc-ZnP*-H$_2$P-C$_{60}$ excited state is produced by absorption of photons having 2.04 eV energy. At each step in the cascade some energy is lost and the final CS state Fc$^{\bullet+}$-ZnP-H$_2$P-C$_{60}$$^{\bullet-}$ has only 1.01 eV energy. Thus, nearly 50% of the absorbed energy is lost in the cascade energy and electron transfer processes.

Loss of energy at each step of the electron transfer cascade is unavoidable in polyads. Recently, attention is being refocused into the design of dyads that can generate long-lived CS states. Since only one electron transfer step is involved in dyads, the energy loss will be minimal. But the lifetimes of the CS states in dyads are generally less than 1.0 ns, with a few exceptions. In few cases, lifetimes of the CS states are prolonged due to factors that affect the kinetic aspects of electron transfer. Kinetic aspects of electron transfer are best described by Marcus theory and essential aspects of the theory are presented in the following section. Knowledge of Marcus theory is essential to understand the factors responsible for long lifetimes of CS states reported for few dyads.

1.2. MARCUS THEORY OF ELECTRON TRANSFER

In classical theory D and A are assumed to be within close contact and hence are coupled weakly. These reactions are referred to as outer sphere electron transfer. Prior to the electron transfer, the donor, acceptor and surrounding solvent molecules will have to undergo a thermally induced reorganization to create a favorable geometry for electron transfer and this constitute the activation barrier for the electron transfer. Professor Rudolf Marcus derived equation 1.5, which connects the free energy of activation ($\Delta G^{\ddagger}$) for outer sphere electron transfer with the free energy (ΔG_{et}) of the redox reaction and reorganization energy λ.[24-27]

$$\Delta G^{\ddagger} = (\lambda + \Delta G_{et})^2 / 4\lambda \qquad (1.5)$$

The Marcus equation for activation-controlled electron transfer reaction has the same form as the Eyring equation

$$k_{et} = A \exp - (\lambda + \Delta G_{et})^2 / 4\, \lambda RT) \qquad (1.6)$$

The reorganization energy $\lambda = \lambda_o + \lambda_i$, where λ_o refers to outer shell reorganization energy and λ_i refers to inner shell reorganization energy.

The outer shell or solvent reorganization refers to the energy required for reorienting the solvent molecules surrounding D and A. If D and A are neutral molecules, the products $D^{\bullet+}$ and $A^{\bullet-}$ will be charged entities and hence the orientational and electronic polarization of the solvent molecules will be different for the reactants and products. Initially D and A are in thermal equilibrium within a solvent cage. In the transition state D and A are polarized electronically and to stabilize the polarized state the solvent molecules undergo orientational polarization. When the electron is transferred and $D^{\bullet+}$ and $A^{\bullet-}$ are generated, the electronic polarization responds instantly to stabilize the charges generated. As the product state is formed, the orientational and electronic polarizations of the solvent adjusts to minimize the energy of the product state. The outer shell reorganization energy is given by the equation 1.7.

$$\lambda_o = \Delta e^2 \left(\frac{1}{2r_D} + \frac{1}{2r_A} - \frac{1}{d_{cc}} \right) \left(\frac{1}{\varepsilon_{op}} - \frac{1}{\varepsilon_s} \right) \qquad (1.7)$$

Equation 1.7 assumes that D and A are spherical and are in a solvent cage. In the equation, r_D and r_A are the radii of D and A, respectively, d_{cc} is the center-to-center distance between these molecules, and ε_{op} and ε_s are the optical and static dielectric constants of the solvent. Since ε_s is large for polar solvents, the equation suggests that λ_o will be larger for polar solvents. This equation also suggests that λ_o will be smaller when the reactant sizes are large. λ_o also depends on the separation distance d_{cc} and its value will be higher when d_{cc} is large.

The inner shell reorganization energy λ_i is associated with the bond length changes that occur when D goes to $D^{\bullet+}$ and A goes to $A^{\bullet-}$. λ_i is given by equation 1.8.

$$\lambda_i = \sum_i \left[\frac{f(R)_i f(P)_i}{f(R)_i + f(P)_i} \right] [\Delta q_i]^2 \qquad (1.8)$$

In equation 1.8 Δq_i is the difference in equilibrium bond distance between the reactant and product state corresponding to an ith vibration, $f(R)_i$ and $f(P)_i$ are the force constants for this vibration for the reactant and product states. The quantity in the bracket is referred to as the 'reduced force constant'. The equation includes the summation of all vibrational modes. For rigid aromatic molecules such as pyrene and spherical molecules such as C_{60}, bond length changes associated with redox reactions are very small. Hence λ_i will be very small for these molecules.

Equation 1.5 is a quadratic relationship between the driving force (ΔG_{et} or Gibbs free energy) and activation energy for electron transfer reactions. The ΔG_{et} for PET reactions is usually obtained using the Weller equation,[28]

$$\Delta G_{et} = E_{ox} - E_{red} - E_{00} - e^2/\varepsilon_s \, d_{cc} \qquad (1.9)$$

where E_{ox} is the oxidation potential of D, E_{red} is the reduction potential of A and E_{00} is the excitation energy of the light absorber (D or A). For a thermodynamically allowed PET reaction, ΔG_{et} will be negative. The physical meaning of the Marcus equation will become very clear if we evaluate the rate constants of electron transfer reactions from a donor with a series of homologous acceptors using equation 1.6. The reorganization energy λ is a positive number. If we assume that for the homologous electron transfer reactions, λ is constant (say ~1.0 eV) and ΔG_{et} varies from, say, +1.0 to -3.0 eV, the plot of k_{et} against ΔG_{et} will be bell shaped as shown in Figure 1.5.

Figure 1.5. Plot of k_{et} vs. ΔG_{et} (eq. 1.2) showing different regions of the Marcus parabola

Figure 1.5 shows that rate of electron transfer increases initially with increase in driving force (ie., as ΔG_{et} becomes more negative), reaches a maximum and then decreases with further increase in driving force. This happens because λ is +ve and ΔG_{et} is -ve and at some point in the curve $-\Delta G_{et} = \lambda$. At this point the activation energy $\Delta G^{\ddagger}$ will be zero as per equation 1.5. The electron transfer reaction will be activation-less at this point and the rate will be maximum. The region where the rate increases with increase in driving force is termed 'normal' region and the domain where rate decreases with increase in driving force is termed 'inverted' region (Figure 1.5). Existence of the inverted region was an important prediction of Marcus theory. Marcus theory was proposed in the late 1950s, but the existence of the inverted region was experimentally verified only in the 1980s.

The classical Marcus theory is intended for weakly adiabatic electron transfer. In the quantum mechanical treatment, electron transfer is assumed to take place within a super molecule consisting of D, A and the solvent molecules. Within the super molecule all atoms

of the reactants and medium are constantly undergoing low and high frequency vibrations. Nuclear bond deformations correspond to high frequency vibrations and the vibrational and rotational modes of the solvent constitute low frequency vibrations. The transition between the reactant and product surfaces is then visualized as an isoenergetic crossing involving the coupling of the wavefunctions of the reactant and product vibrational modes. The coupling strength depends on the electronic coupling matrix and the vibrational overlap integral. Under these circumstances the electron transfer is described as a non-adiabatic radiation-less transition, whose rate is given by the Fermi Golden Rule expression,

$$k_{et} = \frac{2\pi}{\hbar} |H_{el}|^2 \, FC \qquad (1.10)$$

where H_{el} is the quantum mechanical counter part of the classical electron transfer matrix that couples the reactant and product electronic wave functions and FC is the Franck-Condon factor, which represents the weighted density of final states at the initial energy. The term is proportional to the matrix element describing the overlap of nuclear wave functions between the initial and final thermally averaged vibronic states. In the high temperature limit, the Marcus equation assumes its semi-classical form given in equation 1.11.[26,27]

$$k_{et} = \frac{2\pi}{\hbar} |H_{el}|^2 \, \frac{\exp[-(\Delta G_{et} + \lambda)^2 / 4\lambda k_B T]}{\sqrt{4\pi\lambda k_B T}} \qquad (1.11)$$

In equation 1.11, k_B is the Boltzmann constant and T is the temperature. The equation has a form similar to the classical Marcus equation except that the inverted region is somewhat shallow. The electron transfer reaction is considered non-adiabatic when $H_{el} < 200$ cm^{-1}.

It may be mentioned that the Marcus-type behavior, as shown in Figure 1.5, will be observed in fixed distance electron transfer reactions only. Detailed investigation of the dependence of electron transfer rate on free energy was first attempted by Rehm and Weller.[28] In their experiment quenching of the fluorescence of several aromatic hydrocarbons

by large number of donors and acceptors were studied. In this study the ΔG values ranged from 0.26 to -2.7 eV, but the plot of quenching constant against ΔG did not show the inverted region. They found that the quenching rate rapidly rises in the normal region, reached a limiting value and stayed there with further increase in driving force as shown in Figure 1.6. This behavior, where the rate for electron transfer increases with decrease in free energy, reaches a maximum and remains pegged to the maximum with further increase in driving force, came to be known as 'Rehm-Weller behavior'. The Rehm-Weller behavior seems to be the rule for luminescence quenching through electron transfer in solution.

Figure 1.6. Rehm-Weller plot for bimolecular PET reaction

Early Studies of D-A Dyads

A dyad for PET reaction can be designated as D ⌇⌇⌇ A where the donor D is attached to the acceptor A using a flexible or rigid spacer. Excitation of D or A then leads to electron transfer from D to A to give $D^{\bullet+}$⌇⌇⌇$A^{\bullet-}$. CR then occurs to regenerate the dyad in its ground state. In designing dyads for PET reactions, the following aspects are very important. (i) Quantum yield of the charge separation process Φ_{CS}, (ii) lifetime of the CS state τ_{CS} (= $1/k_{CR}$) and (iii) free energy for charge recombination, ΔG_{CR}. In most of the cases

studied, D or A, which is excited, is fluorescent and hence rate of PET can be determined using time resolved fluorescence experiments. If τ_0 is the fluorescence lifetime of D and τ_1 the fluorescence lifetime of the dyad, then rate constant for PET is given by equation 1.12.[20]

$$k_{et} = 1/\tau_1 - 1/\tau_0 \qquad (1.12)$$

Φ_{CS} is then given by equation 1.9.

$$\Phi_{CS} = k_{et} \times \tau_1 \qquad (1.13)$$

In order to characterize the charge separated state $D^{\bullet+} \sim\sim\sim A^{\bullet-}$, laser flash photolysis in the nanosecond or femtosecond time domain is required. Radical ions $D^{\bullet+}$ and $A^{\bullet-}$ can be identified using their absorption bands in the transient spectrum. The decay of the radical ions can be followed in these studies to obtain the τ_{CS}. ΔG_{CR} is generally estimated from the redox potentials of D and A using equation 1.14.[20]

$$\Delta G_{CR} = E_{red} - E_{ox} \qquad (1.14)$$

If the CS state is stable (i.e., large τ_{CS}), the energy stored in the CS state can be used to do work. Thus, PET reaction is a means for converting light energy into chemical potential. If sunlight can be used to carryout PET reactions to give long-lived CS states, then PET would be one of the important methods for solar energy harvesting. For practical systems τ_{CS} should be in the microsecond time domain so that the CS state can participate in diffusion-controlled reactions. In the search for long-lived photoinduced CS state, large numbers of polyads have been designed and studied during the last three decades. Since this thesis deals with dyads, we will mention studies related to dyads only in this chapter.

Warman et al. have designed the dyad **2**, which consist of the donor 1,4-dimethoxynaphthalene (DMN) linked to the dicynanovinyl (DCV) acceptor through a rigid spacer.[29-31] The edge-to-edge distance between the donor and acceptor in this dyad is 4.6 Å.

2   **3**

Figure 1.7. Structures of DMN-DCV dyads studied by Warman et al.

PET takes place in **2** with k_{et} = 5.0 × 10^{11} s^{-1}. Because of the very small edge-to-edge distance, CR reaction was very facile which reduced the lifetime of the CS state to < 0.5 ns. These authors have extended the work on DMN-DCV dyads by systematically increasing the edge-to-edge distance using rigid spacers of different length. In molecule **3** studied, the edge-to-edge distance between DMN and DCV is 14.2 Å. Rates of both PET and CR are reduced because of the large distance separating D and A. For **3**, k_{et} was 1.2 × 10^8 s^{-1} and τ_{CS} was 1050 ns.

Porphyrin (P) or zinc porphyrin (ZP) was used as donor for most of the dyads synthesized in the early period. Synthetic porphyrins were used because of their similarity to the chromophores in natural photosynthetic systems. Their stability, redox properties and absorption properties were highly suited for the design of systems for artificial photosynthesis. Quinones (Q) and C_{60} are used frequently as acceptors. The P-Q dyads **3A,B** (Figure 1.8) were studied by Asahi et al. using time resolved fluorescence and femtosecond flash photolysis.[32]

3A,B

Figure 1.8. Structures of P-Q dyads studied by Asahi et al.

When Q = benzoquinone, values of the important parameters were τ_{P-BQ} = 6.2 ps, k_{et} = 16 × 10^{10} s^{-1}, Φ_{CS} = 0.992 and τ_{CS} = 140 ps. When Q = naphthaquinone, the corresponding parameters were: τ_{P-NQ} = 14.0 ps, k_{et} = 7.0 × 10^{10} s^{-1}, Φ_{CS} = 0.98 and τ_{CS} = 400 ps. The experiments suggested that both CS and CR reactions are slow in the NQ substituted system.

In the free base chlorin – zinc porphyrin (CH-ZnP, **4**) studied by Wasielewsky et al.[33] the CH moiety acts as the excited state electron acceptor. In non-polar toluene, charge separation does not occur in this molecule, but in polar solvents PET reaction is possible.

4

Figure 1.9. Structure of the CH-ZnP dyad studied by Wasielewsky et al.

Excitation of a butyronitrile solution of **4** at 610 nm, where the CH absorbs most of the light, leads to formation of the CS state CH$^{\bullet-}$-ZnP$^{\bullet+}$ with k_{et} = 2.5 × 10^{11} s^{-1}. The CR reaction is also very fast and hence the CS state lifetime was only 43 ps.

Fe(III) porphyrins are very good electron acceptors and have been used as the acceptor moiety in several dyads and polyads. McLendon and coworkers studied the P-Fe(III)P dyad **5**, where the free base porphyrin is linked to Fe(III) porphyrin via a *meso* phenyl group.[34,35] Excitation of P-Fe(III)P in methanol leads to electron transfer from the excited free base porphyrin to Fe(III)P with k_{et} = 10^{11} s^{-1}. The CS state P$^{\bullet+}$-Fe(II)P is very short-lived because of the very fast CR reaction.

5

Figure 1.10. Structure of P-Fe(III)P dyad studied by McLendon and coworkers.

C_{60} is a very good electron acceptor and several of P-C_{60} and ZnP-C_{60} dyads were evaluated for PET. The porphyrins or metallated porphyrins have very good absorption in the visible region. C_{60} absorbs throughout the visible region till 710 nm, but the extinction coefficients are much lower than those of P or ZnP. In most cases of P-C_{60} and ZnP-C_{60}, both chromophores absorb light, but because of the higher extinction coefficients the P or ZnP are preferentially excited. Since the absorption onset for C_{60} is 710 nm, excitation energy can be transferred from $^1P^*$ or $^1(ZnP)^*$ to C_{60} through singlet-singlet energy transfer (EnT).

Gust, Moore and co-workers have synthesized the P-C_{60} dyad **6** (Figure 1.10) for PET studies.[36] For this molecule PET does not take place when excited in a non-polar solvent such as toluene. Upon excitation in benzonitrile $^1P^*$-C_{60} is formed, which decays by a combination of PET and EnT. PET occurs with $k_{et} = 1.8 \times 10^{11}$ s^{-1} to generate $P^{\bullet+}$-$C_{60}^{\bullet-}$ and EnT occurs with $k_{EnT} = 7.1 \times 10^{10}$ s^{-1} to give P-$^1C_{60}^*$. The P-$^1C_{60}^*$ formed by EnT also undergo PET to give the CS state. The CS state in this case is readily identified using femtosecond transient absorption spectroscopy through the absorptions of $P^{\bullet+}$ in the 600-700 nm region and $C_{60}^{\bullet-}$ around 1000 nm. The overall quantum yield for formation of the CS state through both the pathways is 0.99. The $P^{\bullet+}$-$C_{60}^{\bullet-}$ state decays by CR to the ground state with $k_{CR} = 3.4 \times 10^9$ s^{-1} ($\tau_{CS} = 294$ ps).

6

Figure 1.11. Structure of the P-C_{60} dyad studied by Gust, Moore and coworkers.

Imahori et al. have synthesized and studied the ZnP-C_{60} dyad **7** (Figure 1.11).[37] In **7,** the ZnP donor is linked to the C_{60} acceptor through a flexible amide bond. Excitation in benzonitrile generated the singlet excited state of ZnP, which donates an electron to C_{60} with $k_{et} = 9 \times 10^9$ s^{-1} to form the CS state ZnP$^{\bullet+}$-$C_{60}$$^{\bullet-}$. The CS state undergo CR reaction to regenerate the ground state of the molecule with $k_{CR} = 2 \times 10^9$ s^{-1} ($\tau_{CS} = 500$ ps). The relatively low k_{et} and k_{CR} values of **7** are attributed to the large D-A distance in this case.
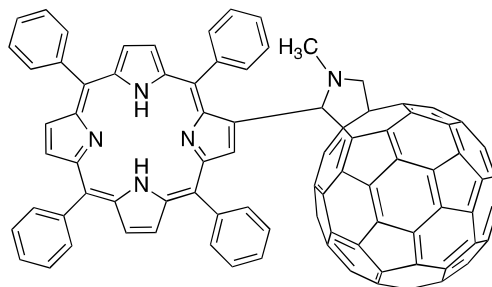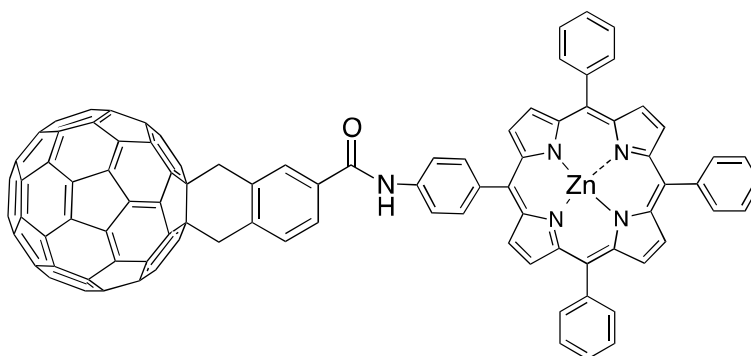
7

Figure 1.12. Structure of the P-C_{60} dyad studied by Imahori et al.

1.3.   Charge Separated State with Triplet Multiplicity

PET reactions proceed with spin conservation. This means that if the CS state is formed from a singlet excited state, the CS state produced will have singlet multiplicity. Dyads **1-7** discussed in the previous section are all generated from singlet excited states and these states have very low lifetimes because of the very fast, spin allowed Charge recombination (CR) to the ground state. In contrast, if the CS states are generated in the triplet state, they are expected to exhibit long lifetimes because of the forbidden nature of the CR to the ground state. In principle, ^{3}CS state can be generated in two ways; (1) The ^{1}CS state generated by PET reaction from a singlet excited state can undergo ISC to give the ^{3}CS state and, (2) the ^{1}D* (or ^{1}A*) produced by light absorption can undergo ISC to ^{3}D* (or ^{3}A*) which then undergo PET to give the ^{3}CS. If the center-to-center distance d_{cc} is large in a dyad, the exchange interaction between the singlet and triplet CS states will be low and the energy difference between ^{1}CS and ^{3}CS will also be very low.[1] In compact dyads (i.e., very low d_{cc} value), the exchange energy is expected to be large and hence the energy difference between ^{1}CS and ^{3}CS could be larger.

1.3.1.   Generation of ^{3}CS from ^{1}CS

For a large number of dyads, the energies of local triplet states ^{3}D*-A or D-^{3}A* lie below the ^{1}CS/^{3}CS energy levels and in these cases the CS state undergo charge recombination to give the local triplet states. For example, in anthracene-dimethylaniline (AN-(CH$_2$)$_n$-DMA) and pyrene-dimethylaniline (PY-(CH$_2$)$_n$-DMA) dyads (Figure 1.12), excitation of the AN or PY leads to PET from DMA to give the CS state. Very fast CR reaction then occurs leading to formation of ^{3}AN or ^{3}PY, when $n > 6$. When $n < 6$, the CS states are very short-lived and will not be observed in nanosecond flash photolysis experiments.[38,39]

AN-DMA   **PY-DMA**

Figure 1.13. Structures of AN-DMA and PY-DMA dyads, n = 1-3.

In a few dyads, energies of the CS states depend on solvent polarity. Energies of the singlet and triplet CS states will be higher than local triplet states in non-polar solvents, but in very polar solvents such as acetonitrile (ACN), the CS state energies fall below the local triplet levels as shown in Figure 1.13.[40]

Figure 1.14. Tuning of ^{1,3}CS state energy by changing solvent polarity

For this system energies of the locally excited singlet states D-^{1}A* and ^{1}D*-A are above the ^{1}CS state and hence PET is possible from these singlet excited states. The local triplet states D-^{3}A* and ^{3}D*-A are placed below the CS state in non-polar solvents. This is a general

feature exhibited by large number of dyads. The local singlet and triplet energy levels are generally affected very little by changes in solvent polarity. The CS state, however, is highly polar and gets stabilized in polar solvents. It has been observed that in few cases of dyads, the CS state energies fall below the local triplet levels in polar solvents as shown in Figure 1.13. In these cases, the ^{1}CS state generated can undergo CR reaction to the ground state or undergo singlet- triplet exchange to generate the ^{3}CS state. The ^{3}CS state thus generated will be long-lived because of the forbidden nature of triplet CR reaction. The quantum yield of ^{3}CS state formation, however, will be low as this process occurs in competition with singlet CR reaction.

Fukuzumi and coworkers have designed the chlorin-C_{60} dyads **8**[41] and **9**[42] and the zinc-imidazoporphyrin-C_{60} dyad **10**[43] (Figure 1.14) which exhibited long-lived CS states. In the case of **8**, nanosecond flash photolysis gave absorptions corresponding to the zinc chlorin radical cation and fullerene radical anion. Absorptions corresponding to these radical ions decayed via first order kinetics with a lifetime of ~ 110 μs. Formation of the CS state is confirmed in this case by using ESR spectroscopy.

| **8** | **9** | **10** |
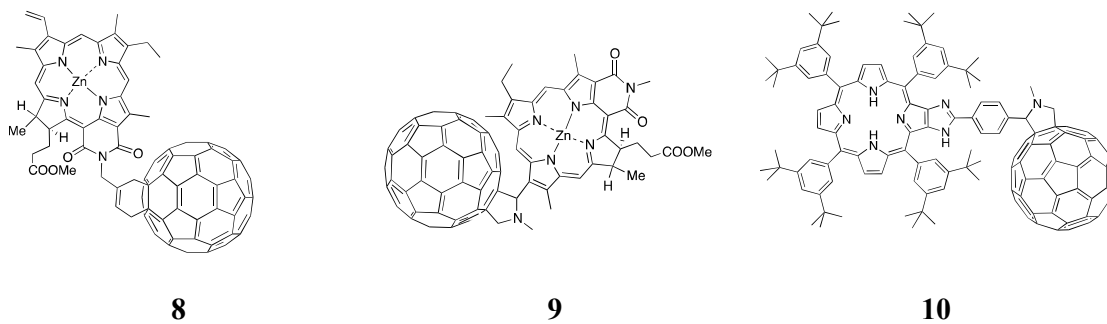
Figure 1.15. Structures of dyads exhibiting long-lived 3CS states

Dyad **9** is also a chlorin-C_{60} dyad, but in this case the linker is very short and rigid. Absorption spectrum of the **9** showed that there is no significant electronic interaction between the D and A units in the ground state. Fluorescence lifetime of **9** was significantly

smaller than that of free zinc chlorin molecule. From the fluorescence data the rate constant of electron transfer k_{et} was obtained as 1.0×10^{11} s^{-1}. Transient absorption studies in benzonitrile confirmed formation of zinc chlorin radical cation (λ_{max} 790 nm) and $C_{60}^{\bullet-}$ (λ_{max} = 1000 nm). Decays of both transients were first order with 230 μs lifetime. The quantum yield of the long-lived transient, however, was only 12%. The zinc-imidazoporphyrin-C_{60} **10** also exhibited very similar results. Excitation of **10** at 298 K gave the CS state with 260 μs lifetime. At 278 K, the CS state lifetime increased to 310 μs. In all the above three cases, the energy stored in the CS state is low (< 1.5 eV).

Fukuzumi and coworkers claimed that the CS states in **8**, **9** and **10** are long-lived due to the inverted region effects.[41-43] In all these cases C_{60} is the acceptor and d_{cc} values are small. Fullerenes have remarkably small reorganization energies of electron transfer due to delocalization of the π-electrons over three dimensions along with the rigid, confined structure of the π cloud. Small d_{cc} helps in reducing λ_o values (equation 1.3). Smaller λ values lead to acceleration of k_{et} and deceleration of k_{CR}. For **8**, **9** and **10**, λ values are ~ 0.5 eV. For such systems the onset of the inverted behavior occurs at ΔG ~ -0.5 eV. For these molecules ΔG_{CS} ~ -1.3 eV, which falls in the deep inverted region. Fukuzumi and coworkers argue that τ_{CS} values are very large for **8**, **9** and **10** because ΔG_{CS} falls in the deep inverted region.

Harriman, Verhoeven and coworkers have questioned the claims of Fukuzumi and coworkers regarding the long CS state lifetimes of **8**, **9** and **10**.[40] These authors have reinvestigated the photophysical processes in these molecules and came up with alternate explanations. These molecules are examples of cases where the CS state energy is lower than local triplet energies (as in shown in the right-hand side of Figure 1.13). In these cases, PET occur from the singlet excited state of chlorin or porphyrin leading to formation of CS states

whose energies are lower than those of local triplet states. Part of ^{1}CS generated undergoes CR reaction to the ground state and a small fraction undergo ISC to ^{3}CS, which is long-lived. It may be noted that the quantum yield of CS state in the case of **9** is only 12%, which gives support to the conclusion of Harriman and Verhoeven and coworkers. Because of this reason we have included **8**, **9** and **10** in this section dealing with ^{3}CS states, although Fukuzumi's group attributed the observed long CS state lifetimes in these cases to inverted region behavior.

1.3.2. Generation of ^{3}CS Directly from Triplet Excited States

Molecules that exhibit very high triplet quantum yields can act as excited state donor or excited state acceptor to generate ^{3}CS states directly. For example, benzophenone (BP) upon excitation to the singlet excited state, undergo ultrafast ISC ($k_{ISC} \sim 10^{11}$ s^{-1}) to the triplet state and generates ^{3}BP* with $\Phi_T = 1.0$.[44] ^{3}BP* is a very good electron acceptor. If an electron donor capable of donating an electron to ^{3}BP* is attached to BP through a suitable spacer S, then PET can occur and the ^{3}CS state will be generated directly with high quantum yield as shown in Figure 1.15.
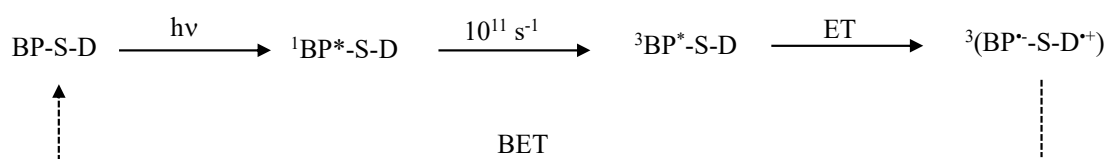
Figure 1.16. Generation of ^{3}CS using ^{3}BP* as acceptor

Other molecules that exhibit $\Phi_T \sim 1.0$ are phenalenedione, naphthalimide etc. C_{60} also exhibits very high triplet quantum yield ($\Phi_T > 0.9$), but in this case PET will also occur from $^1C_{60}^*$, which will reduce the yield of ^{3}CS state. If $^3C_{60}^*$ is generated through T-T energy transfer, then the ^{3}CS can be generated in high yields. Another important molecule that can generate ^{3}CS state is *tris*-bipyridylruthenium(II) dichloride (RuBP), which upon excitation

produces the ^{3}MLCT state with unit quantum efficiency. The ^{3}MLCT state of this molecules can act as electron acceptor to produce Ru(I) or electron donor to generate the Ru(III) state. In molecules undergoing PET from the triplet state, the ^{3}CS state will be lower in energy compared to the local triplets and hence CR reaction will not lead to formation of local triplet states. Although CR reaction from ^{3}CS to the ground dyad state is spin forbidden, the reaction generally is very facile due to the spin-orbit coupling or heavy atom effect operating in the ^{3}(D$^{\bullet+}$-A$^{\bullet-}$) ion pair system. Few examples of PET reactions that directly generate the ^{3}CS states are presented in Figure 1.16.
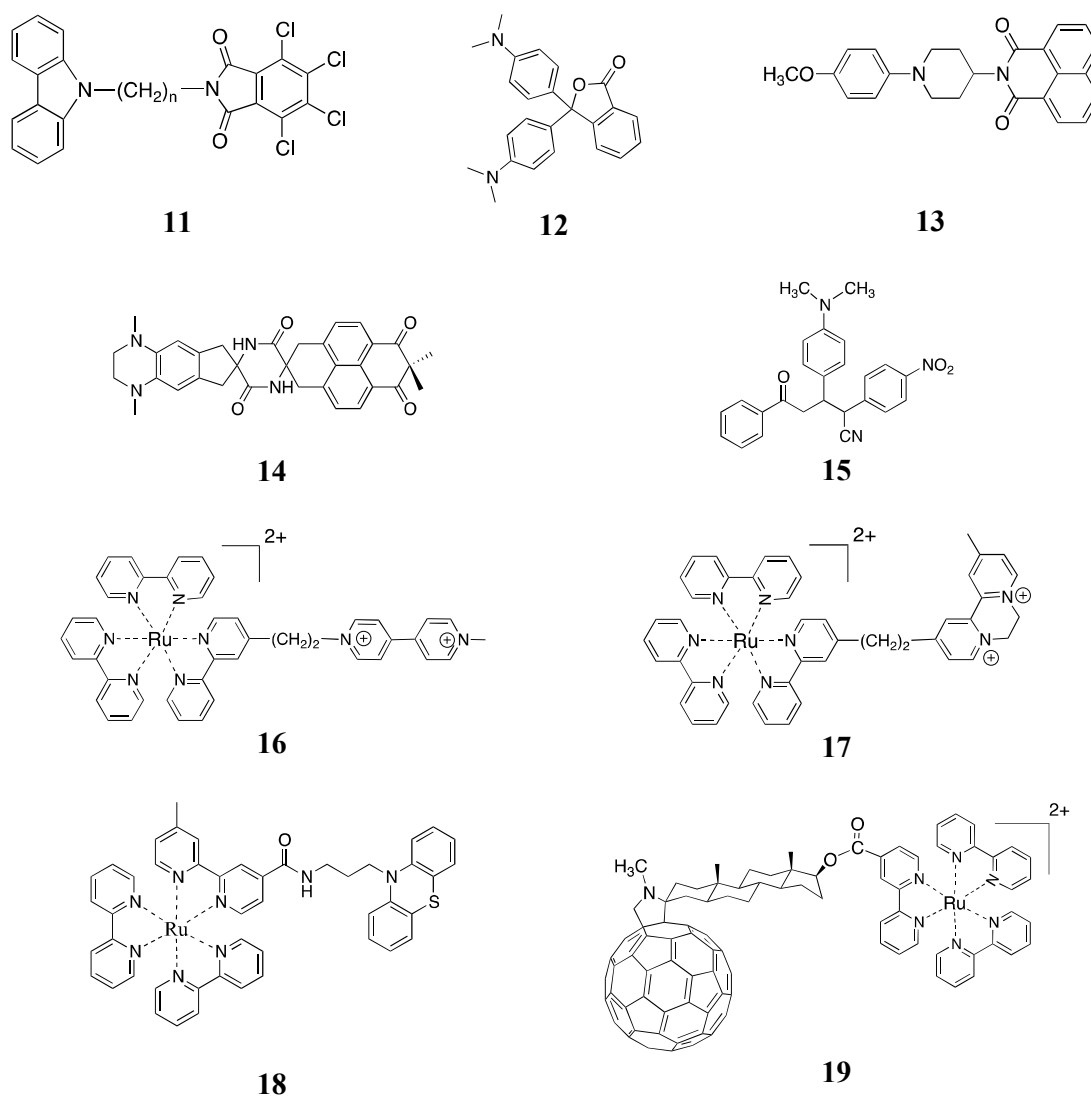
Figure 1.17. Examples for dyads that generate ^{3}CS states directly

Excitation of **11** leads to formation of ^{3}CS state in ~ 55% yield.[45] The quantum yield is less most probably because of PET taking place from the singlet excited state also. Lifetime of the ^{3}CS state is 2.4 μs in cyclohexane. In the case of **12**, the ^{3}CS state is generated with ~ 30% efficiency and exhibited lifetime of 20 ns in acetonitrile.[46] ^{3}CS states of **13**[47] and **14**[48] are generated with near 100% efficiency in polar solvents. ^{3}CS state lifetimes for **14** is 3.35 μs in THF and 1.0 μs in acetonitrile. In the case of **15**, the ^{3}CS state is formed when excited in deoxygenated acetonitrile and exhibited lifetime of 330 ns.[40]

In molecules **16**[49] and **17**,[50] the ^{3}MLCT state of RuBP act as electron donors and the paraquat/diaquat moiety acts as the electron acceptor. Lifetimes of the CS states were very low for these molecules and it is explained by invoking the heavy atom effect of the Ru atoms in these dyads. Because of the heavy atom effect, the ^{1}MLCT state of RuBP undergoes ultrafast ISC to ^{3}MLCT with k_{ISC} ~ 10^{12} s^{-1}. The heavy atom effect operates in the ^{3}CS state as well, and this facilitates the CR reaction to the ground singlet state. In the case of **18**, nanosecond flash photolysis experiments have identified formation of absorptions corresponding to Ru(I) and phenothiazine radical cation generated as a result of electron transfer from phenothiazine to ^{3}[RuBP]*. Lifetime of the CS state was 30 ns in this case, which was attributed to conformational effects.[51] In the case of **19**, excitation of the RuBP chromophore in acetonitrile leads to formation of the ^{3}CS state which exhibited 100 ns lifetime.[52] The long lifetime of the CS state is attributed to the rigid spacer which keeps the D and A components at distances greater than 10 Å. In this molecule the ^{3}CS state energy is higher than that of $^3C_{60}{}^*$, and hence CR occurs to generate $^3C_{60}{}^*$.

1.4. Long-Lived CS State due to Inverted Region Effect

It has been suggested that dyads exhibiting long-lived CS states can be designed with the aid of the Marcus parabola (Figure 1.5). A suitable D-A system selected to demonstrate

this concept will have k_{PET} value lying at the top of the Marcus parabola and k_{CR} value lying deep in the inverted region. For this hypothetical system ΔG_{PET} would be ~ -1.0 eV, ΔG_{BET} ~ -2.0 eV, and the reorganization energy λ ~ 1.0 eV (Figure 1.5). Figure 1.5 shows that for this system k_{PET} ~ 10^{11} s^{-1} and k_{CR} ~ 10^5 s^{-1} and hence τ_{CS} ~ 10 μs. k_{PET}/k_{CR} value will be > 10^4 in this case and it would be possible to observe a long-lived CS state. However, straight forward demonstration of this "inverted effect" has been very rare in the literature. It is generally observed that when $-\Delta G_{BET}$ is very large, other channels of deactivation, such as jumps to low-lying triplet states, will become possible. It is suggested that nuclear tunneling is very important at large free energies and hence Marcus equation may not adequately describe electron transfer in this regime. There are, however, few papers which claimed long-lived CS state formation due to the inverted region effects. These studies are reported in this section. Some of these reports are severely criticized and these are also included in this discussion.

Fukuzumi et al. have claimed that 9-mesityl-10-methylacridinium perchlorate (Acr[+]-Mes, **20**, Figure 1.17) exhibited long-lived photoinduced charge separation.[53] In this molecule the electron donor, mesityl moiety, is directly linked to the acceptor, acridinium ion at the 9-position. The Acr[+] acceptor is selected because its λ value for electron self-exchange between Acr[+] and the one electron reduced radical Acr[•] is the smallest (0.3 eV) among redox active organic compounds.[54] The Mes group is directly connected to Acr[+] at the 9-position to minimize d_{cc}.

20
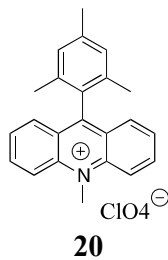
Figure 1.18. Structure of Acr[+]-Mes

Thus, the solvent reorganization is minimized and the total reorganization energy expected for the PET reaction is only about 0.7 eV. Photoexcitation of Acr^+-Mes gave a transient, which was identified as $Acr^{\bullet}$-$Mes^{\bullet+}$ formed as a result of electron transfer from Mes to $^1Acr^{+*}$, in 98% yield. The transient exhibited lifetime of 2 h at 203 K and virtually infinite lifetime at 77 K. ΔG_{CR} for the BET reaction from $Acr^{\bullet}$ to $Mes^{\bullet+}$, calculated from redox potentials, is -2.37 eV. Since $\lambda = 0.7$ eV, the Marcus parabola will have maximum at $\Delta G = -0.7$ eV, and hence $\Delta G_{CR} = -2.37$ eV would fall in the deep inverted region. Fukuzumi et al. made the claim that the transient observed in the case of Acr^+-Mes is very long lived because the free energy for back electron transfer falls in the deep inverted region.[53] The authors also reported EPR spectrum of the radicals at low temperature to support the assignment of the transient. They also claimed that the CS state, $Acr^{\bullet}$-$Mes^{\bullet+}$, undergo secondary electron transfer reactions with donors such as anthracene and acceptors such as naphthalene diimide and methyl viologen. It is also claimed that the CS state $Acr^{\bullet}$-$Mes^{\bullet+}$ can perform a variety of photoredox reactions such as cycloaddition, oxygenation, atom-transfer cyclization, C-H functionalization and bond-cleavage reactions because of the very high oxidizing and reducing abilities of the radical ion pairs.[55-61]

Fukuzumi et al. also reported long-lived CS state formation due to inverted region effect in dyad **21** (Figure 1.18).[62] In **21**, the anthraquinone moiety is the excited state electron acceptor and the formanilide group is the electron donor.
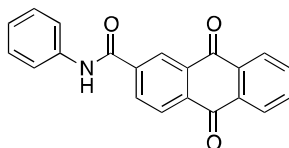
21

Figure 1.19. Structure of anthraquinone-formanilide dyad

The calculated ΔG_{PET} and ΔG_{BET} values for **21** are -0.21 and -2.24 eV, respectively. Flash photolysis gave a transient assigned to the CS state with 900 µs lifetime. In the case of **21** excitation populates the triplet state of anthraquinone within 1.7 ps and hence PET leads to ^{3}CS state. Hence this molecule could have been included under section 1.4.2 dealing with direct generation of ^{3}CS states. But the lifetime reported is too large and the authors claimed that the long lifetime is due to inverted region effects.

Harriman, Verhoeven and co-workers have challenged the claims of long-lived charge separation in **20** and **21**.[63-68] Fukuzumi et al. claimed that **20** is even better than the natural photosynthetic system in terms of both the energy content and lifetime of the CS state. They estimated the energy of the CS state at 2.37 eV. According to Harriman and others the actual energy is 2.57 eV, which is very close to the singlet excited state of Acr$^+$. Based on the onset of phosphorescence spectrum they placed the triplet energy of Acr$^+$ at 1.94 eV. According to Harriman, Verhoeven and co-workers, the energy levels for **20** is as shown in Figure 1.19.

^{1}Acr^{+*}-Mes ——————— 2.67 eV

5 ps

^{1,3}(Acr$^•$-Mes$^{•+}$) - - - - - - - 2.57 eV

6 ns

^{3}Acr^{+*}-Mes - - - - - - - 1.94 eV

Acr$^+$-Mes ———————
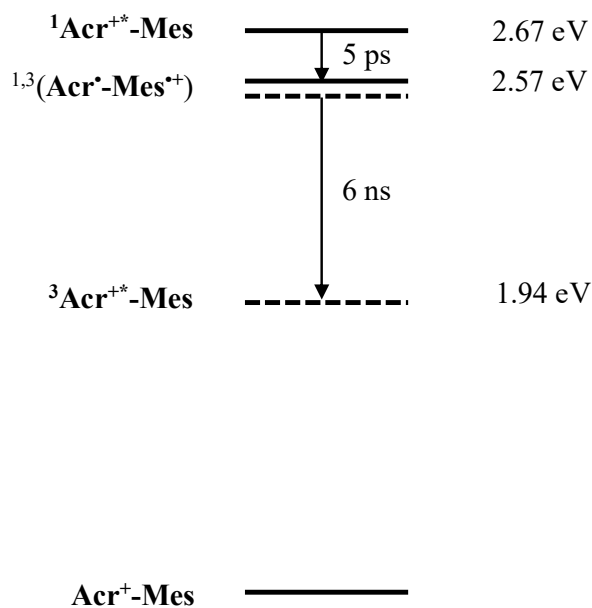
Figure 1.20. Energy level diagram proposed for **20** by Harriman and others

According to Harriman, Verhoeven and co-workers, ^{3}Acr^{+*} is below ^{1,3}CS state and hence the CS state would undergo CR to ^{3}Acr^{+*} and the transient observed by Fukuzumi et al. is actually ^{3}Acr^{+*}-Mes. According to this group the secondary reactions reported by Fukuzumi et al. are reactions of either ^{3}Acr^{*+} or due to radicals obtained by decomposition of Acr$^{\bullet}$-Mes$^{\bullet+}$. According to Harriman, Verhoeven and others, the lifetime of Acr$^{\bullet}$-Mes$^{\bullet+}$ is only 6 ns. Fukuzumi group has published several papers supporting their claim.[55-61] In a paper published in 2017, the group insisted that the transient obtained is Acr$^{\bullet}$-Mes$^{\bullet+}$, but stated that the CS state has triplet multiplicity.[61]

Dyad **21** had been studied earlier and long-lived CS state was not reported in these studies.[69,70] Harriman, Verhoeven and co-workers therefore synthesised **21** and reinvestigated its photochemistry.[66] They did not observe long-lived CS states in solvents such as acetonitrile or benzonitrile. In DMSO, which was the solvent used by Fukuzumi group, they observed formation of long-lived transient which was identified as anthraquinone radical anion, formed by the reaction of triplet anthraquinone with DMSO, which served as a sacrificial electron donor. Thus observation of long-lived CS state in the case of **21** is also dismissed by Harriman, Verhoeven and co-workers.

Our research group has reported formation of long-lived CS states upon photoexcitation of dyads **22** and **23** (Figure 1.20).[71-73] In these molecules bis(phenyletynyl)anthracene (BPEA) or bis(phenylethynyl)pyrene (BPEP) is the excited state electron acceptor and the phenothiazine (PT) molecule on either side served as electron donor. For both systems there are no interactions between the donor and acceptor components in the ground state. Fluorescence of the BPEA/BPEP chromophores were efficiently quenched by the attached phenothiazine groups, which is attributed to electron transfer taking place from phenothiazine to the excited singlet state of BPEA/BPEP.

Picosecond transient absorption studies suggested formation of the CS state directly from the singlet excited states of BPEA/BPEP. Nanosecond flash photolysis gave transient absorptions due to phenothiazine radical cation and BPEA/BPEP radical anions. Lifetime of the charge separated states are ~ 30 μs in both cases. We have attributed the long lifetime of the CS state to inverted region effects based on the energy level diagrams for these compounds.

22

23
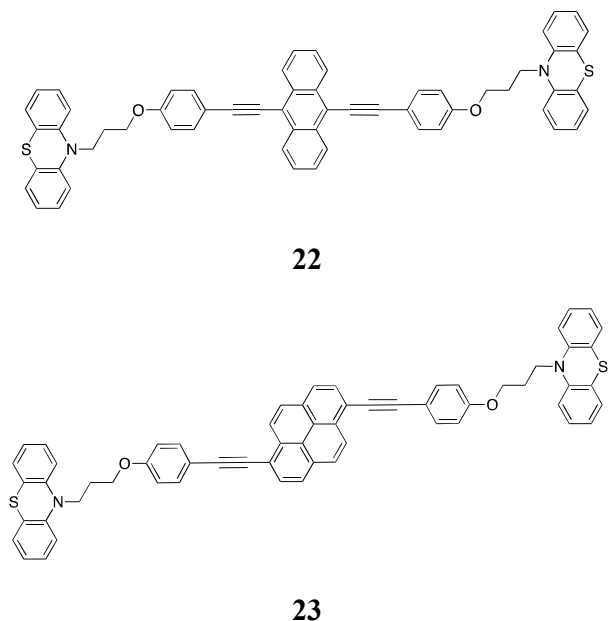
Figure 1.21. BPEA-PT and BPEP-PT dyads studied in our group

1.5.   Enhancing CS State Lifetime using Spacer Groups

In the design of dyads, normally a spacer group (S), sometimes designated as 'bridge' (B), is incorporated between D and A. The spacer can control the distance between the donor and acceptor and their relative orientation. This aspect has encouraged the use of rigid hydrocarbon spacers in the design of polyads. According to the Marcus equation (equation 1.11), there are three important variables that determine the rate of electron transfer reactions, namely, ΔG_{et}, λ and H_{el}. The importance of ΔG_{et} and λ are discussed earlier in this chapter. The electronic coupling matrix element H_{el} is affected by

the donor-acceptor distance. If D and A are separated by distance d, then H_{el} is given by equation 1.15.

$$(H_{el})^2 = (Hel^0)^2 \exp(-\beta(d-d_0)) \qquad (1.15)$$

where H_{el}^0 is the coupling matrix element at distance d_0 (contact distance between D and A) and β is known as the damping factor.[26] The value of β depends on the electronic structure and conducting nature of the spacer. The exponential dependence of electron transfer rate on distance is well established in the literature.[74] In the case of long-range electron transfer where D and A are separated by distances that exceeds the sum of their van der Waals radii, H_{el} is generally small (< 150 cm^{-1}). In order to understand the role of H_{el} and the effect of different parameters on H_{el}, several spacer groups have been introduced. Structures of some of the spacer groups employed are shown in Figure 1.21.
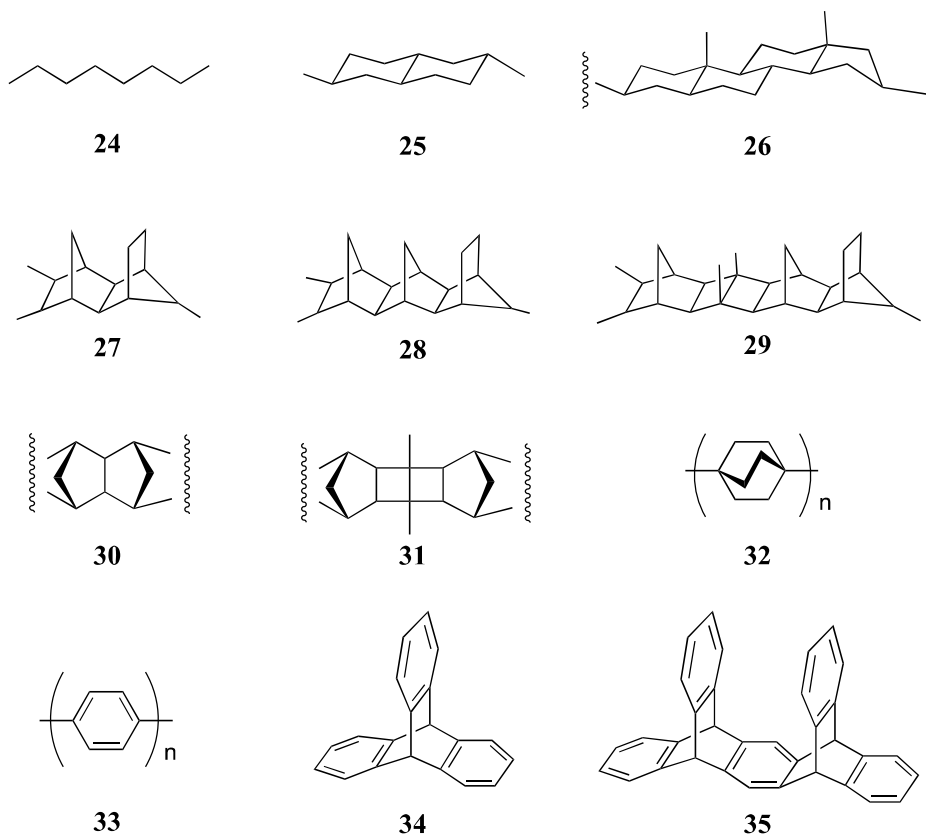
Figure 1.22. Structures of few spacer groups employed in D-S-A systems

Methylene chains (**24**) are the simplest type of spacers one can think of and several groups have employed this spacer in D-S-A systems.[49-51,75-77] If the methylene chains assume a linear, all-*trans* configuration, the edge-to-edge D-A distance is given by $(n \times 1.27)$ Å, where 'n' is the number of methylene groups in the chain.[49] Most of the time the methylene chains do not assume the linear conformation and the actual distance will be much smaller. It was observed that the electron transfer rates decrease by a factor of 10 for every methylene group.[20] Rigid *trans*-decaline (**25**) and steroidal (**26**) spacers have been employed by Closs et al. to study intramolecular electron transfer from 4-biphenyl radical anion to 2-naphthyl acceptors.[78-80] Paddon-Row and co-workers have employed rigid norbornylogous bridges **27-31** to study the distance dependence of electron transfer in DMN – DCV systems (see Figure 1.6 also).[29-31,81,82] Dervan and co-workers have changed the edge-to-edge distance in porphyrin-quinone systems from 6 – 14 Å by employing bicyclo[2,2,2]octane (**32**) spacer groups.[83-85] Phenyl (**33**)[86] and 'ipticene' bridges (**34**, **35**)[87] were also employed to study the distance dependence of PET reactions.

The distance dependence of H_{el} provides yet another pathway to design long-lived CS states. This can be illustrated using compounds **2** and **3** (Figure 1.6).[29-31] The D-A edge to edge distance in **2** is 4.6 Å. The rigid norbornylogous spacer in **3** increased the distance to 14.2 Å. Increasing the distance decreased k_{CR} considerably and hence τ_{CS} increased from ~ 2 ps in **2** to 1050 ns in **3**. In the work of Dervan and co-workers the edge-to-edge D-A distance in P-Q systems were increased from 6 to 14 Å using spacer **32**.[83-85] They were able to increase the CS state lifetime from 130 ps to 50 ns in this way. Although the distance dependence of H_{el} can be tuned to get long-lived CS states, the experimental work involved in incorporating the long spacers in between D and A components is very cumbersome, and hence is not a very attractive one.

Wasielewski et al. have used 'pentiptycene' spacers to vary the orientation

between the D and A components in P-Q systems as shown in Figure 1.22.[87] In the *syn*-isomer **36** the center-to-center distance between the porphyrin donor and quinone acceptor is 11 Å, and the same is 16 Å in the *anti*-isomer **37**. However, the electron transfer rate constants k_{et} and k_{CR} are slower by a factor of two for the *syn*-isomer.

36   **37**
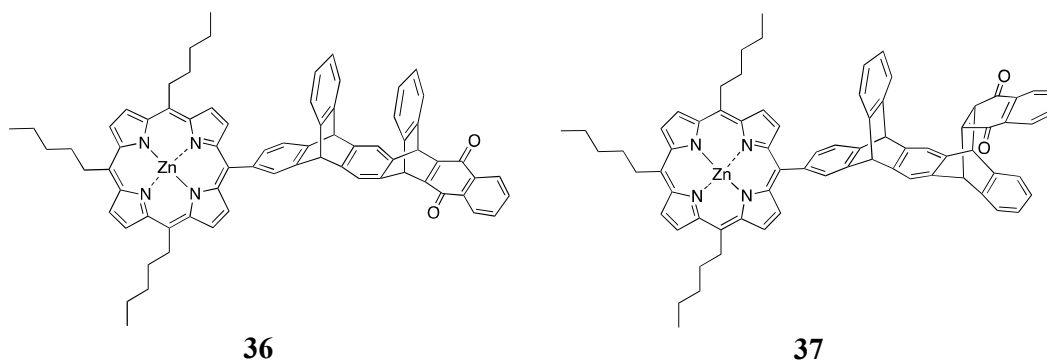
Figure 1.23. Structures of *syn*- and *anti*-P-Q systems studied by Wasielewski et al.

Similar results were reported by others also. For example, Oliver et al. studied DMN-DCV systems with rigid hydrocarbon spacers with an all-*trans* arrangement of single bonds or a single s-*cis* kink in the chain.[88] They observed that the all-*trans* isomer exhibited faster electron transfer rates. Closs, Miller and co-workers found that in the intramolecular electron transfer from biphenyl radical anion to naphthalene linked by rigid 1,4-cyclohexadiyl spacers, the electron transfer rates were lower for the cis isomers although the distance is shorter. [89-90] Higher k_{et} and k_{CR} values for the *trans* isomers was attributed to better H_{el} values for these molecules. Calculations by Ohta et al. showed that when cyclohexyl ring is used as the spacer, the equatorial-equatorial conformation where the C-C bonds exist in an all *trans* arrangement exhibit higher H_{el} values compared to other conformations.[91] Thus the spacer group can affect rate of electron transfer through the distance and orientation effects.

1.7 Origin of the thesis

Existence of the inverted region was one of the most important predictions of Marcus theory. The 'inverted region effect' was very controversial from the time of its proposal in 1956 until experimental proof for the same was presented in 1986.[78,79] The inverted region effect is now confirmed in a large number of charge recombination and charge shift reactions. However, in all these reports, the normal region of the parabola only had k_{et} values and the inverted region only had k_{CR} values. Our group was among the first to establish the normal and inverted regions of the parabola using only k_{et} values. Considerable amount of work was carried out in our research group previously in this area [92-94].

Our group has shown that compounds **22** and **23** exhibit long-lived photoinduced CS states due to the inverted region effect.[71-73] The fluorescence quantum yields of both compounds are close to 100%. This feature is derived from the BPEA/BPEP core in these molecules which also exhibit $\Phi_F \sim 1.0$. The ISC efficiency is close to zero and triplet states of these molecules cannot be populated by direct excitation. These molecules have triplet levels which are at lower energies compared to the CS states. However the CS states do not undergo CR to local triplets and we believe that this is due to very low ISC efficiency of the CS state. Compounds **22** and **23**, however, have very less solubility in most of the common solvents. These molecules are insoluble in polar solvents such as acetonitrile. This has hindered detailed studies of the inverted region effects in polar solvents using these compounds. We thought that substituting the BPEA core using solubilising groups such as *tert*-butyl will enhance the solubility in polar solvents. In Chapter 2 of the thesis we describe the synthesis, photophysical and electron transfer studies of 2,6-di-*tert*-butyl and 2,6-di-adamantyl- substituted BPEA derivatives.

Adamantane (AD, **38**, Figure 1.23) is among the most rigid hydrocarbons that is photochemically and electrochemically silent and ideally suited as spacer unit in PET

studies. AD has four identical bridge-head positions. If we attach a donor unit to one of the bridge-head positions, the other three bride-head positions have identical spatial disposition with respect to the one substituted. If we attach an acceptor group to one of these positions we will get a D-S-A system where the D and A are separated by a rigid, three carbon spacer with an edge-to-edge distance of < 5.0 Å. This distance is not sufficient to bring about any distance effect on k_{CR}, but could provide interesting orientational effects. In Chapters 3 and 4 of this thesis, PET reactions of D-S-A systems, where S is adamantyl group, are reported.

38   **39**
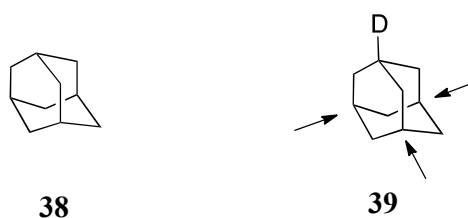
Figure 1.24. Structure of adamantane (**38**) and bridge-substituted adamantane (**39**)

To the best of our knowledge the AD spacer has not been employed in any PET reactions. The AD spacer was however used in energy transfer studies by Tan et al.[95] These authors have employed AD groups as spacers in a phenanthrene-biphenyl-naphthalene (PBN) trichromophoric molecule **40** (Figure 1.24).

40
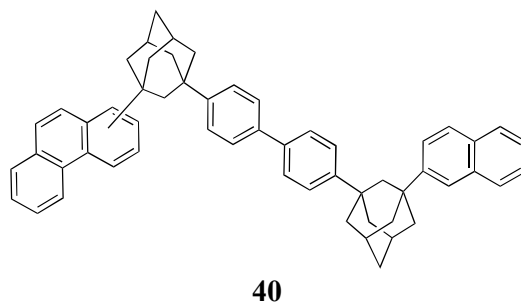
Figure 1.25. Structure of trichormophoric molecule PBN.

Molecule **40** was selected for the study because of its favourable spectral characteristics and energy levels. The singlet state energies (E_S) for the biphenyl, naphthalene and

phenanthrene chromophores are 97, 92 and 85 kcal M^{-1}, respectively. The corresponding triplet energies (E_T) are 64.2, 62.1 and 61.6 kcal M^{-1}, respectively. Both singlet-singlet and triplet-triplet energy transfers were studied using this molecule. This study confirmed that the AD spacer is a good conduit for energy transfer. We anticipated that AD will be a good conduit for PET also and may exert conformational effect on rates of PET and CR reactions.

1.8. References

1. Hou, Y.; Zhang, X.; Chen, K.; Liu, D.; Wang, Z.; Liu, Q.; Zhao, J.; Barbon, A. Charge Separation, Charge Recombination, Long-Lived Charge Transfer State Formation and Intersystem Crossing in Organic Electron Donor/Acceptor Dyads, *J. Mater. Chem. C*. **2019**, *7*, 12048-12074.

2. Fukuzumi, S.; Lee, Y.-M.; Nam W. Mimicry and Functions of Photosynthetic Reaction Centers. *Biochem. Soc. Trans*. **2018**, *46*, 1279-1288.

3. Llansola-Portoles, M. J.; Gust, D.; Moore, T. A.; Moore, A. L. Artificial Photosynthetic Antennas and Reaction Centers. *C. R. Chimie* **2017**, *20*, 296-313.

4. Yuan, Y.-J.; Yu, Z.-T.; Chen, D.-Q.; Zou, Z.-G. Metal-Complex Chromophores for Solar Hydrogen Generation. *Chem. Soc. Rev*. **2017**, *46*, 603-631.

5. Rudolf, M.; Kirner, S. V.; Guldi, D. M. A Multicomponent Molecular Approach to Artificial Photosynthesis – The Role of Fullerenes and Endohedral Metallofullerenes. *Chem. Soc. Rev*. **2016**, *45*, 612-630.

6. Mulfort, K. L.; Utschig, L. M. Modular Homogeneous Chromophore−Catalyst Assemblies. *Acc. Chem. Res*. **2016**, *49*, 835-843.

7. Strauss, V.; Roth, A.; Sekita, M.; Guldi, D. M. Efficient Energy-Conversion Materials for the Future: Understanding and Tailoring Charge-Transfer Processes in Carbon Nanostructures. *Chem* **2016**, *1*, 531-556.

8. Kavarnos, G. J.; Turro, N. J. Photosensitization by Reversible Electron Transfer: Theories, Experimental Evidence, and Examples. *Chem. Rev.* **1986**, *86*, 401-449.

9. Kavarnos, G. J. *Fundamentals of Photoinduced Electron Transfer*, VCH Publishers, New York, 1993.

10. Fox, M. A.; Channon, M. (Eds.), *Photoinduced Electron Transfer*, *Parts A-D*, Elsevier, Amsterdam, 1988.

11. Mattay, J. (Ed.), *Photoinduced Electron Transfer*, *Parts I – IV*, Springer Verlag, Heidelberg, 1990.

12. Deisenhofer, J.; Epp, O.; Miki, K.; Huber, R.; Michel, H. Structure of the Protein Subunits in the Photosynthetic Reaction Centre of Rhodopseudomonas Viridis at 3Å Resolution. *Nature* **1985**, *318*, 618-628.

13. Feher, G.; Allen, J. P.; Okamura, M. Y.; Rees, D. C. Structure and Function of Bacterial Photosynthetic Reaction Centres. *Nature* **1989**, *339*, 111-116.

14. Friesner, R.; Wertheimer, R. Model for Primary Charge Separation in Reaction Centers of Photosynthetic Bacteria. *Proc. Natl. Acad. Sc. USA*. **1982**, *79*, 2138-2142.

15. Friesner, R. A.; Won, Y. Photochemical Charge Separation in Photosynthetic Reaction Centers. *Photochem. Photobiol.* **1989**, *50*, 831-839.

16. Holzapfel, W.; Finkele, U.; Kaiser, W.; Oesterhelt, D.; Scheer, H.; Stiltz, H. U.; Zinth, W. Initial Electron-Transfer in the Reaction Center from Rhodobacter Sphaeroids. *Proc. Natl. Acad. Sci. USA*. **1990**, *87*, 5168-5172.

17. Tanaka, S.; Marcus, R. A. Electron Transfer Model for the Electric Field Effect on Quantum Yield of Charge Separation in Bacterial Photosynthetic Reaction Centers. *J. Phys. Chem. B* **1997**, *101*, 5031-5045.

18. Bixon, M.; Jortner, J. Electric Field Effects on the Primary Charge Separation in Bacterial Photosynthesis. *J. Phys Chem.* **1988**, *92*, 7148-7156.

19. Plato, M.; Möbius, K.; Michel-Beyerle, M. E.; Bixon, M.; Jortner, J. Intermolecular Electronic Interactions in the Primary Charge Separation in Bacterial Photosynthesis. *J. Am. Chem. Soc.* **1988**, *110*, 7279-7285.

20. Balzani, V. (Ed.), *Electron Transfer in Chemistry*, Wiley-VCH, Weinheim, 2001, Vol. III, Part 3, pp 177-403.

21. El-Khouly, M. E.; El-Mohsnawy, E.; Fukuzumi, S. Solar Energy Conversion: From Natural to Artificial Photosynthesis. *J. Photochem. Photobiol. C* **2017**, *31*, 36-83.

22. K. C, C. B.; D'Souza, F. Design and Photochemical Study of Supramolecular Donor–Acceptor Systems Assembled via Metal–Ligand Axial Coordination. *Coord. Chem. Rev*. **2016**, *322*, 104 -141.

23. Imahori, H.; Guldi, D. M.; Tamaki, K.; Yoshida, Y.; Luo, C.; Sakata, Y.; Fukuzumi, S. Charge Separation in a Novel Artificial Photosynthetic Reaction Center Lives 380 ms. *J. Am. Chem. Soc.* **2001**, *123*, 6617-6628.

24. Marcus, R. A. Exchange Reactions and Electron Transfer Reactions Including Isotopic Exchange. Theory of Oxidation-Reduction Reactions Involving Electron Transfer. Part 4 - A Statistical-Mechanical Basis for Treating Contributions from Solvent, Ligands, and Inert Salt. *Disc. Faraday Soc.* **1960***, 29,* 21-31.

25. Marcus, R. A. On the Theory of Oxidation – Reduction Reactions Involving Electron Transfer. V. Comparison and Properties of Electrochemical and Chemical Rate Constants. *J. Phys. Chem.* **1963***, 67,* 853-857.

26. Marcus, R. A.; Sutin, N. Electron Transfers in Chemistry and Biology. *Biochim. Biophys. Acta* **1985**, *811*, 265-322.

27. Marcus, R. A. Electron Transfer Reactions in Chemistry: Theory and Experiment (Nobel Lecture). *Angew. Chem., Int. Ed.* **1993**, *32*, 1111-1121.

28. Rehm, D.; Weller, A. Kinetics of Fluorescence Quenching by Electron and H-Atom

Transfer. *Isr. J. Chem.* **1970**, *8*, 259-271.

29. Paddon-Row, M. N.; Oliver, A. M.; Warman, J. M.; Smit, K. J.; de Haas, M. P.; Oevering, H.; Verhoeven, J. W. Factors Affecting Charge Separation and Recombination in Photoexcited Rigid Donor-Insulator-Acceptor Compounds. *J. Phys. Chem.* **1988**, *92,* 6958-6962.

30. Warman, J. M.; de Haas, M. P.; Paddon-Row, M. N.; Cotsaris, E.; Hush, N. S.; Oevering, H.; Verhoeven, J. W. Light-induced giant dipoles in simple model compounds for photosynthesis. *Nature* **1986**, *320*, 615-616.

31. Warman, J. M.; de Haas, M. P.; Verhoeven, J. W.; Paddon-Row, M. N. Photoinduced Electron Transfer within Donor-Spacer-Acceptor Molecular Assemblies Studied by Time-Resolved Microwave Conductivity. *Adv. Chem. Phys.* **1999**, *106,* 571-601.

32. Asahi, T.; Ohkohchi, M.; Matsusaka, R.; Mataga, N.; Zhang, R. P.; Osuka, A.; Maruyama, K. Intramolecular Photoinduced Charge Separation and Charge Recombination of the Product Ion Pair States of a Series of Fixed-Distance Dyads of Porphyrins and Quinones: Energy Gap and Temperature Dependences of the Rate Constants. *J. Am. Chem. Soc.* **1993**, *115*, 5665-5674.

33. Wasielewski, M. R.; Johnson, D. J.; Niemczyk, M. P.; Gaines, G. L. III; O'Neil, M. P.; Svec, W. A. Chlorophyll-Porphyrin Heterodimers with Orthogonal □ Systems. Solvent Polarity Dependent Photophysics. *J. Am. Chem. Soc.* **1990**, *112*, 6482-6488.

34. Heiler, D.; McLendon, G.; Rogalskyj, P. Synthesis and Electron-Transfer Rates of Coplanar Bisporphyrins: Models for (Heme) Protein-Protein Electron-Transfer Reactions. *J. Am. Chem. Soc.* **1987**, *109,* 604-606.

35. Helms, A.; Heiler, D.; McLendon, G. Electron Transfer in Bis-Porphyrin Donor-Acceptor Compounds with Polyphenylene Spacers Show a Weak Distance Dependence. *J. Am. Chem. Soc.* **1992**, *114*, 6227-6238.

36. Kuciauskas, D.; Lin, S**.;** Seely, G. R.; Moore, A. L.; Moore, T. A.; Gust, D.; Drovetskaya, T.; Reed, C. A.; Boyd, P. D. W. Energy and Photoinduced Electron Transfer in Porphyrin−Fullerene Dyads. *J. Phys. Chem.* **1996**, *100*, 15926-15932.

37. Imahori, H.; Hagiwara, K.; Aoki, M.; Akiyama, T.; Taniguchi, S.; Okada, T.; Shirakawa, M.; Sakata, Y. Linkage and Solvent Dependence of Photoinduced Electron Transfer in Zincporphyrin-C_{60} Dyads. *J. Am. Chem. Soc.* **1996**, *118*, 11771-11782.

38. Orbach, N; Ottolenghi, M. in *The Exciplex*, Gordon, M.; Ware, W. R. (Eds.), Academic Press Inc. New York, 1975, pp 75-111.

39. Weller, A.; Staerk, H.; Treichel, R. Magnetic Field Effects on Geminate Radical-Pair Recombination. *Faraday Discuss. Chem. Soc.* **1984**, *78*, 271-278.

40. Verhoeven, J. W.; van Ramesdonk, H. J.; Groeneveld, M. M.; Benniston, A. C.; Harriman, A. Long-Lived Charge-Transfer States in Compact Donor-Acceptor Dyads. *ChemPhysChem* **2005**, *6*, 2251-2260.

41. Ohkubo, K.; Imahori, H.; Shao, J.; Ou, Z.; Kadish, K. M.; Chen, Y.; Zheng, G.; Pandey, R. K.; Fujitsuka, M.; Ito O.; Fukuzumi, S. Small Reorganization Energy of Intramolecular Electron Transfer in Fullerene-Based Dyads with Short Linkage. *J. Phys. Chem. A* **2002**, *106*, 10991-10998.

42. Ohkubo, K.; Kotani, H.; Shao, J.; Ou, Z.; Kadish, K. M.; Li, G.; Pandey, R. K.; Fujitsuka, M.; Ito, O.; Imahori, H.; Fukuzumi, S. Production of an Ultra-Long-Lived Charge-Separated State in a Zinc Chlorin–C_{60} Dyad by One-Step Photoinduced Electron Transfer *Angew. Chem. Int. Ed.* **2004**, *43*, 853-856.

43. Kashiwagi, Y.; Ohkubo, K.; McDonald, J. A.; Blake, I. M.; Crossley, M. J.; Araki, Y.; Ito, O.; Imahori, H.; Fukuzumi, S. Long-Lived Charge-Separated State Produced by Photoinduced Electron Transfer in a Zinc Imidazoporphyrin-C_{60} Dyad. *Org. Lett.* **2003**, *5*, 2719-2721.

44. Turro, N. J.; Ramamurthy, V.; Scaiano, J. C. *Modern Molecular Photochemistry*, University Science Books, California, 2010, p. 300.

45. Smit, K. J.; Warman, J. M. The Formation of Singlet and Triplet Charge Transfer States on Photoexcitation of Carbazole-$(CH_2)_n$-Tetrachlorophthalimide Compounds Studied by Time-Resolved Microwave Conductivity. *J. Lumin.* **1988**, *19*, 149-154.

46. Karpiuk, J. Photoinduced Electron Transfer in Malachite Green Lactone. *Phys. Chem. Chem. Phys.* **2003**, *5*, 1078-1090.

47. van Dijk, S. I.; Groen, C. P.; Hartl, F.; Brouwer, A. M.; Verhoeven, J. W. Long-Lived Triplet State Charge Separation in Novel Piperidine-Bridged Donor-Acceptor Systems. *J. Am. Chem. Soc.* **1996**, *118*, 8425-8432.

48. Anglos, D.; Bindra, V.; Kuki, A. Photoinduced Electron Transfer and Long-Lived Charge Separation in Rigid Peptide Architectures. *J. Chem. Soc. Chem. Commun.* **1994**, 213-215.

49. Yonemoto, E. H.; Riley, R. L.; Kim, Y. II; Atherton, S. J.; Schmehl, R. H.; Mallouk, T. E. Photoinduced Electron Transfer in Covalently Linked Ruthenium Tris(bipyridyl)-Viologen Molecules: Observation of Back Electron Transfer in the Marcus Inverted Region. *J. Am. Chem. Soc.* **1992**, *114*, 8081-8087.

50. Ryu, C. K.; Wang, R.; Schmehl, R. H.; Ferrere, S.; Ludwikow, M.; Merkert, J. W.; Headford, C. E. L.; Elliott, C. M. Photoinduced Electron Transfer in Linked Ruthenium(II) Diimine-Diaquat Complexes: Linkage Dependence. *J. Am. Chem. Soc*. **1992**, *114*, 430-438.

51. Ajayakumar, G.; Gopidas, K. R. Long-Lived Photoinduced Charge Separation in New Ru(bipyridine)$_3{}^{2+}$-Phenothiazine Dyads. *Photochem. Photobiol. Sci.* **2008**, *7*, 826-833.

52. Maggini, M.; Guldi, D. M.; Mondini, S.; Scorrano, G.; Paolucci, F.; Ceroni, P.; Roffia, S. Photoinduced Electron Transfer in a Tris(2,2'-bipyridine)-C_{60}-ruthenium(II)

Dyad: Evidence of Charge Recombination to a Fullerene Excited State. *Chem. Eur. J.* **1998**, 4, 1992-2000.

53. Fukuzumi, S.; Kotani, H.; Ohkubo, K.; Ogo, S.; Tkachenko, N. V.; Lemmetyinen, H. Electron-transfer States of 9-Mesityl-10-methylacridinium Ion with Much Longer Lifetime and Higher Energy Than That of the Natural Photosynthetic Reaction Center. *J. Am. Chem. Soc.* **2004**, *126*, 1600-1601.

54. Fukuzumi, S.; Ohkubo, K.; Suenobu, T.; Kato, K.; Fujitsuka, M.; Ito, O. Photoalkylation of 10-Alkylacridinium Ion via Charge-Shift Type of Photoinduced Electron Transfer Controlled by Solvent Polarity. *J. Am. Chem. Soc*. **2001**, *123*, 8459-8467.

55. Ohkubo, K.; Kotani, H.; Fukuzumi, S. Misleading Effects of Impurities Derived from the Extremely Long-Lived Electron-Transfer State of 9-Mesityl-10-methylacridinium Ion. *Chem. Commun.* **2005**, 4520-4522.

56. Kotani, H.; K. Ohkubo, K.; S. Fukuzumi, S. Photocatalytic Oxygenation of Anthracenes and Olefins with Dioxygen via Selective Radical Coupling Using 9-Mesityl-10-methylacridinium Ion as an Effective Electron-Transfer Photocatalyst. *J. Am. Chem. Soc.* **2004**, *126*, 15999-16006.

57. Hasobe, T.; Hattori, S.; Kamat, P.V.; Wada, Y.; Fukuzumi, S. Organization of Supramolecular Assembly of 9-Mesityl-10-carboxymethylacridinium Ion and Fullerene Clusters on TiO_2 Nanoparticles for Light Energy Conversion. *J. Mater. Chem.* **2005**, *15*, 372-380.

58. Ohkubo, K.; Nanjo, T.; Fukuzumi, S. Efficient Photocatalytic Oxygenation of Aromatic Alkene to 1,2-Dioxetane with Oxygen via Electron Transfer. *Org. Lett.* **2005**, *7*, 4265-4268.

59. Fukuzumi, S.; Ohkubo, K.; Suenobu, T. Long-Lived Charge Separation and

Applications in Artificial Photolysis. *Acc. Chem. Res.* **2014**, *47*, 1455-1464.

60. Fukuzumi, S.; Ohkubo, K. Selective Photocatalytic Reactions with Organic Photocatalysts. *Chem. Sci.* **2013**, *4*, 561-574.

61. Tsudaka, T.; Kotani, H.; Ohkubo, K.; Nakagawa, T.; Tkachenko, N. V.; Lammetyinen, H.; Fukuzumi, S. Photoinduced Electron Transfer in 10-Methylacridinium Ions. *Chem. Eur. J.* **2017**, *23*, 1306-1317.

62. Okamoto, K.; Hasobe, T.; Tkachenko, N. V.; Lemmetyinen, H.; Kamat, P. V.; Fukuzumi, S. Drastic Difference in Lifetimes of the Charge-Separated State of the Formanilide-Anthraquinone Dyad versus the Ferrocene-Formanilide-Anthraquinone Triad and Their Photoelectrochemical Properties of the Composite Films with Fullerene Clusters. *J. Phys. Chem. A* **2005**, *109*, 4662-4670.

63. Benniston, A. C.; Harriman, A.; Li, P.; Rostron, J. P.; Verhoeven, J. W. Illumination of the 9-Mesityl-10-methylacridinium Ion Does Not Give a Long-Lived Photoredox State. *Chem. Commun.* **2005**, 2701-2703.

64. Benniston, A. C., Harriman, A.; Li, P.; Rostron, J. P.; Ramesdonk, H. J.; Groeneveld, M. M.; Zhang, H.; Verhoeven, J. W. Charge Shift and Triplet State Formation in the 9-Mesityl-10-methylacridinium Cation. *J. Am. Chem. Soc.* **2005**, *127*, 16054-16064.

65. Verhoeven, J. W.; van Ramesdonk, H. J.; Zhang, H.; Groeneveld, M. M.; Benniston, A. C.; Harriman, A. Long-Lived Charge-Transfer States in 9-Aryl-Acridinium Ions; A Critical Reinvestigation. *Int. J. Photoenergy* **2005**, *7*, 103-108.

66. van Ramesdonk, H. J.; Bakker, B. H.; Groeneveld, M. M.; Verhoeven, J. W.; Allen, B. D.; Rostron, J. P.; Harriman, A. Ultrafast Intersystem Crossing in 9,10-Anthraquinones and Intramolecular Charge Separation in an Anthraquinone-Based Dyad. *J. Phys. Chem. A* **2006**, *110*, 13145-13150.

67. Benniston, A. C.; Harriman, A.; Verhoeven, J. W. Comment: Electron-Transfer

Reactions in the 9-Mesityl-10-methylacridinium ion: Impurities, Triplet States and Infinitely Long-Lived Charge-Shift States? *Phys. Chem. Chem. Phys.* **2008**, *10*, 5156-5158.

68. Verhoeven, J. W. On the Role of Spin Correlation in the Formation, Decay, and Detection of Long-Lived, Intramolecular Charge-Transfer States. *J. Photochem. Photobiol. C* **2006**, *7*, 40-60.

69. Hamanoue, K.; Nakayama, T.; Nanshow, H.; Hanada, T.; Naruta, Y.; Kodo, T.; Maruyama, K. Photoinduced Intramolecular Charge Separation in an Anthraquinone-Linked All-*cis* 5, 10, 15, 20-*meso*-Tetrakis (2-aminophenyl)porphyrin Derivative Studied by Picosecond and Nanosecond Laser Spectroscopy. *J. Chem. Soc. Faraday Trans.* **1993**, *89*, 3243-3250.

70. Allen, N.S.; Pullen, G.; Shah, M.; Edge, M.; Holdsworth, D.; Weddell, I.; Swart, R.; Catalina, F. Photochemistry and Photoinitiator Properties of 2-Substituted Anthraquinones 1. Absorption and Luminescence Characteristics. *J. Photochem. Photobiol. A: Chem.* **1995**, *91*, 73-79.

71. Suneesh, C. V.; Gopidas, K. R. Long-Lived Photoinduced Charge Separation in Flexible 9,10-Bis(phenylethynyl)anthracene-Phenothiazine Dyads. *J. Phys. Chem. C* **2009**, *113*, 1606-1614.

72. Suneesh, C. V.; Gopidas, K. R. Long-Lived Photoinduced Charge Separation Due to Inverted Region Effect in 1,6-Bis(phenylethynyl)pyrene-Phenothiazine Dyad. *J. Phys. Chem. C*, **2010**, *114*, 18725-18734.

73. Suneesh, C. V.; Vinayak, M. V.; Gopidas, K. R. Photoinduced Charge Separation in two Bis(phenylethynyl)anthracene Based Triads: Inverted Region Effect vs. Distance Effect on Back Electron Transfer. *J. Phys. Chem. C*, **2010**, *114*, 18735-18744.

74. Wasielewski, M. R. In *Photoinduced Electron Transfer*, *Part A*; Fox, M. A., Channon,

M., (Eds.), Elsevier: Amsterdam, 1988; pp 161- 206.

75. Crawford, M. K.; Wang, Y.; Eisenthal, K. B. Effects of Conformation and Solvent Polarity on Intramolecular Charge Transfer: A Picosecond Laser Study. *Chem. Phys. Lett.* **1981**, *79*, 529-533.

76. Mataga, N. Photochemical Charge Transfer Phenomena – Picosecond Laser Photolysis Studies. *Pure Appl. Chem.* **1984**, *56*, 1255-1268.

77. Mataga, N. Photoinduced Electron Transfer and Multiple States Mechanisms. *Pure Appl. Chem.* **1993,** 65, 1605-1610.

78. Closs, G. L.; Calcaterra, L. T.; Green, N. J.; Penfield, K. W.; Miller, J. R. Distance, Stereoelectronic Effects, and the Marcus Inverted Region in Intramolecular Electron Transfer in Organic Radical Anions. *J. Phys. Chem.* **1986**, *90*, 3673-3683.

79. Closs, G. L.; Miller, J. R. Intramolecular Long-Distance Electron Transfer in Organic Molecules. *Science* **1988**, *240,* 440-447.

80. Johnson, M. D.; Miller, J. R.; Green, N. S.; Closs, G. L. Distance Dependence of Intramolecular Hole and Electron Transfer in Organic Radical Ions. *J. Phys. Chem.* **1989,** *93,* 1173-1176.

81. Paddon-Row, M. N.; Cotsaris, E.; Patney, H. K. The Synthesis of Rigid Norbornylogs for the Purpose of Studying Orbital Interactions Through Bonds. *Tetrahedron* **1986**, *42*, 1779-1788.

82. Oevering, H.; Paddon-Row, M. N.; Heppener, M.; Oliver, A. M.; Cotsaris, E.; Verhoeven, J. W.; Hush, N. S. Long-Range Photoinduced Through-Bond Electron Transfer and Radiative Recombination via Rigid Nonconjugated Bridges: Distance and Solvent Dependence. *J. Am. Chem. Soc.* **1987**, *109*, 3258-3269.

83. Joran, A. D.; Leland, B. A.; Geller, G. G.; Hopfield, J. J.; Dervan, P. B. Models for Photochemical Electron Transfer at Fixed Distances. Porphyrin-Bicyclo[2.2.2]octane-

Quinone and Porphyrin-Bisbicyclo[2.2.2]octane-Quinone. *J. Am. Chem.* Soc. **1984**,*106*, 6090-6092.

84. Leland, B. A.; Joran, A. D.; Felker, P. M.; Hopfield, J. J.; Zewail, A. H.; Dervan, P. B. Porphyrins Linked to Quinones at Two Different Fixed Distances. *J. Phys. Chem.* **1985**, *89*, 5571-5573.

85. Joran, A. D.; Leland, B. A.; Felker, P. M.; Zewail, A. H.; Hopfield, J. J.; Dervan, P. B. Effect of Exothermicity on Electron Transfer Rates in Photosynthetic Molecular Models. *Nature* **1987**, *327*, 508-511.

86. Heitele, H.; Michael-Beyerle, M. E. Electron Transfer Through Aromatic Spacer in Bridged Electron-Donor-Acceptor Molecules. *J. Am. Chem. Soc.* **1985**, *107*, 8286-8288.

87. Wasielewski, M. R.; Niemczyk, M. P.; Johnson, D. G.; Svec, W. A.; Minsek, D. W. Ultrafast Photoinduced Electron Transfer in Donor-Spacer-Acceptor Molecules: Modification of Spacer Energetics as a Probe for Superexchange. *Tetrahedron* **1989**, *45*, 4785-4806.

88. Oliver, A. M.; Craig, D. C.; Paddon-Row, M. N.; Kroon, J.; Verhoeven, J. W. Strong Effects of the Bridge Configuration on Photoinduced Charge Separation in Rigidly Linked Donor-Acceptor Systems. *Chem. Phys. Lett.* **1988**, *150*, 366-373.

89. Calcaterra, L. T.; Closs, G. L.; Miller, J. R. Fast Intramolecular Electron Transfer in Radical Ions Over Long Distances Across Rigid Saturated Hydrocarbon Spacers. *J. Am. Chem. Soc.* **1983**, *105*, 670-672.

90. Miller, J. R.; Calcaterra, L. T.; Closs, G. L. Intramolecular Long-Distance Electron Transfer in Radical Anions. The Effects of Free Energy and Solvent on the Reaction Rates. *J. Am. Chem. Soc.* **1984**, *106*, 3047-3049.

91. Ohta, K.; Gloss, G. L.; Morokuma, K.; Green, N. J. Stereoelectronic Effects in

Intramolecular Long-Distance Electron Transfer in Radical Anions as Predicted by Ab-initio MO Calculations. *J. Am. Chem. Soc*. **1986**, *108*, 1319-1320.

92. Prasad, E.; Gopidas, K. R. Photoinduced Electron Transfer in Hydrogen Bonded Donor-Acceptor Systems. Study of the Dependence of Rate on Free Energy and Simultaneous Observation of the Marcus and Rehm-Weller Behaviors. *J. Am. Chem. Soc.* **2000**, *122*, 3191-3196.

93. Smitha, M. A.; Prasad, E.; Gopidas, K. R. Photoinduced Electron Transfer in Hydrogen Bonded Donor-Acceptor Systems. Free Energy and Distance Dependence Studies and an Analysis of the Role of Diffusion. *J. Am. Chem. Soc.* **2001**, *123*, 1159-1165.

94. Balan, B.; Gopidas. K. R. Photoinduced Electron Transfer in α-Cyclodextrin Based Supramolecular Dyads: A Free Energy Dependence Study. *Chem. Eur. J.* **2006**, *12*, 6701-6710.

95. Tan, Z.; Kote, R.; Samaniego, W. N.; Weininger, S. J.; McGimpsey, W. G. Intramolecular Singlet-Singlet and Triplet-Triplet Energy Transfer in Adamantyl-Linked Trichromophores. *J. Phys. Chem.* **1999**, *103*, 7612-7620.

Photoinduced Electron Transfer Studies of 9,10-Bis(phenylethynyl)-2,6-di-*tert*-butylanthracene-Phenothiazine and 9,10-Bis(phenylethynyl)-2,6-di(1-adamantyl)anthracene-Phenothiazine Dyads

2.1. Abstract

Photoinduced electron transfer in two donor-acceptor dyads with bis(phenylethynyl) anthracene as light absorber and acceptor and phenothiazine as donor were investigated. The bis(phenylethynyl)anthracene core was substituted with tert-butyl or 1-adamantyl groups at the 2- and 6-positions. The absorption spectra indicated that the donor and acceptor moieties do not have any ground-state interaction. Fluorescence of the bis(phenylethynyl)anthracene core was efficiently quenched in polar solvents by the donor moieties and this was attributed to electron transfer from the phenothiazine to bis(phenylethynyl)anthracene singlet excited state. Nanosecond flash photolysis experiments gave long-lived transient absorptions assignable to phenothiazine radical cation and bis(phenylethynyl)anthracene radical anion. Electron transfer in these systems is analyzed in the light of Marcus theory and the slow back electron transfer was attributed to inverted region effects.

2.2. Introduction

Generation of long-lived photoinduced charge separation in bis(phenylethynyl)-anthracene -phenothiazine (**1**, BPEA-PT) and bis(phenylethynylpyrene)-phenothiazine (**2,** BPEP-PT) dyads were reported previously from our laboratory.[1,2] Structures of these molecules are shown in Figure 2.1.
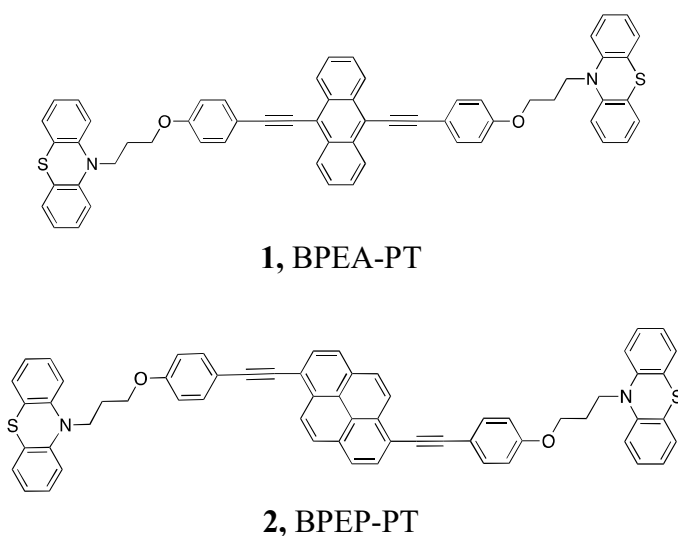
1, BPEA-PT

2, BPEP-PT

Figure 2.1. Structures of BPEA-PT and BPEP-PT

Upon photoirradiation, the BPEA core in **1** gets excited and accepts an electron from the donor PT. The fluorescence of BPEA is quenched due to the PET process. Rate constant for the forward electron transfer, k_{et}, obtained is 1.2×10^9 s^{-1}, using fluorescence decay analysis. The evolution of the transient absorption following excitation in the picosecond time window was probed using femtosecond flash photolysis. The transient obtained exhibited maximum at 570 nm and decayed monotonously, with a rate which was nearly identical to the fluorescence decay rate. Hence this was assigned to the $S_1 \rightarrow S_n$ absorption of the BPEA core. Transient absorption due the donor radical cation (PT$^{\bullet+}$) started developing around 600 ps, but absorption due to the

acceptor radical anion (BPEA$^{\bullet-}$) could not be observed, most probably due to its low extinction coefficient. Transient absorption spectra obtained in the nanosecond time scales showed long-lived absorptions due to PT$^{\bullet+}$ at 515 nm and BPEA$^{\bullet-}$ at 640 nm. The transients were long lived and the charge separated state lifetime (τ_{CS}) determined was 36 μs. The long lifetime of the CS state was attributed to the inverted region effects. As mentioned in the introduction section, formation of long-lived charge separation is a contentious issue, particularly when a local triplet level exists below the energy level of the CS state.[3-8] Energy levels of the various transients possible in the case of BPEA-PT are shown in Figure 2.2.
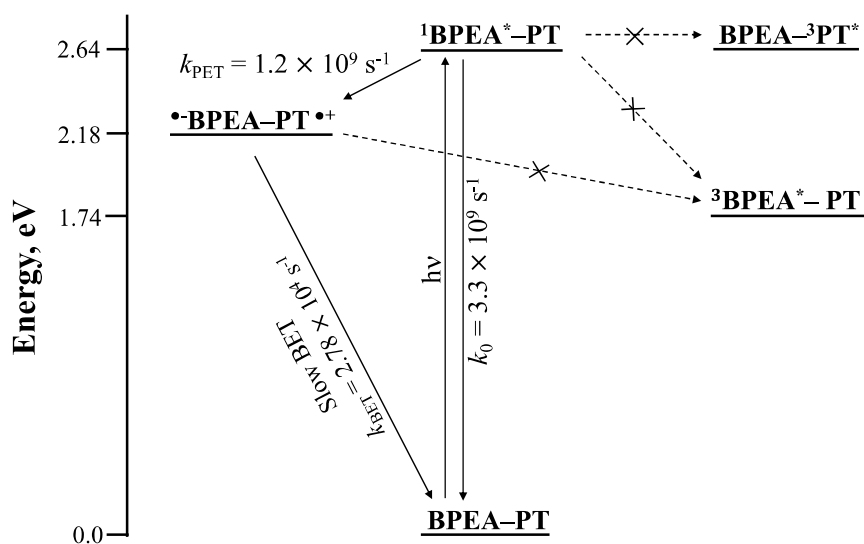
Figure 2.2. Energy levels of the transient species possible in the excitation of **BPEA-PT**

Excitation of BPEA-PT led to formation of the singlet excited state, where the excitation energy is localized on BPEA. This state lies at 2.64 eV above the ground state. The transient spectra clearly show that ET occurs from the PT moiety to ^{1}BPEA* leading to formation of the CS state,$^{\bullet-}$BPEA-PT$^{\bullet+}$ with singlet multiplicity, which lies at 2.18 eV above the ground state. Energy

levels of possible local triplets are shown on the right-hand side of the figure.

The ^{3}PT* is nearly isoenergetic with ^{1}BPEA*, but energy transfer from ^{1}BPEA* to ^{3}PT* is spin-forbidden and will not occur. The local triplet, ^{3}BPEA* lies at 1.74 eV and it can form in two possible ways: (1) intersystem crossing in ^{1}BPEA*-PT and (2) intersystem crossing in ^{1}($^{\bullet-}$BPEA-PT$^{\bullet+}$) to ^{3}($^{\bullet-}$BPEA-PT$^{\bullet+}$) followed by charge recombination. We did not see formation of ^{3}BPEA* in flash photolysis and concluded that both the above pathways are not operating in BPEA-PT. However, formation of ^{3}BPEA* was observed when the flash photolysis was conducted in heavy-atom containing solvents. The heavy atom induces spin-orbit coupling (SOC), which facilitates intersystem crossing either in ^{1}BPEA* or in ^{1}($^{\bullet-}$BPEA-PT$^{\bullet+}$), ultimately leading to formation of ^{3}BPEA*. In linked D-A systems, local triplets can be formed by the hyperfine-induced radical pair intersystem crossing mechanism. This mechanism is not operating in the ^{1}($^{\bullet-}$BPEA-PT$^{\bullet+}$) radical pair. In fact, the excitation of the BPEA core does not lead to ^{3}BPEA* due to very poor SOC in the molecule. We proposed that the lack of SOC in the core BPEA is persisting in the ion pair, ^{1}($^{\bullet-}$BPEA-PT$^{\bullet+}$), also. ^{1}($^{\bullet-}$BPEA-PT$^{\bullet+}$) lies at 2.18 eV and BET to the ground state is highly exergonic (ΔG_{BET} = -2.18 eV). The total reorganization energy for the BET process was estimated at 1.25 eV and this value is much less than -ΔG_{BET}, and hence BET falls in the deep inverted region. However, it may be noted that the inverted region is not the only reason for the long CS state lifetime. Lack of intersystem crossing in the ion-pair state has considerable influence in prolonging the CS state lifetime. We made very similar observations in the case of BPEP-PT dyad also.

BPEA-PT and BPEP-PT are two dyads that exhibit long-lived CS states. To what extent the inverted region effect contributes to the long CS state lifetime is to be established. Since the temperature term 'T' appear in the pre-exponential and exponential factors of the Marcus

equation, study of the effect of temperature on the BET rate can, in principle, provide some information. Time-resolved EPR experiments can be performed to distinguish between singlet and triplet radical pair states.[8-11] These studies are hampered by the extremely low solubility of the dyads in polar solvents such as acetonitrile. The studies reported above for the dyads were performed in the low polarity solvent, dichloromethane. In addition, the compounds exhibited very low extinction coefficients at the commonly accessible laser wavelengths of 355 and 532 nm. Because of this, very high concentrations were required for the laser studies. We thought that the situation may be improved by substituting the anthracene core in BPEA with alkyl groups. The BPEA core is constructed from 9,10-dibromoanthracene through Sonogashira coupling with terminal alkynes. Construction of the core may be affected if the 1- and 5- positions of anthracene are substituted with alkyl groups and hence we thought of introducing the alkyl groups at the 2- and 6- positions. A literature survey showed that the 2- and 6- positions of anthracene can be easily substituted with *tert*-butyl groups.[12-14] In Friedel-Crafts type alkylation of aromatics, the *tert*-butyl and 1-adamntayl groups behave similarly, and we reasoned that the 2- and 6- positions of anthracene can also be substituted easily with 1-adamantyl groups.[15,16] Based on these reasons we have synthesized and studied the 2,6-di-*tert*-butyl-BPEA (**3,** BuBPEA**)** and 2,6-diadamantyl-BPEA (**4,** ADBPEA) derivatives of BPEA. The donor PT groups were covalently linked to these BPEA cores to get the dyads BuBPEA-PT (**5**) and ADBPEA-PT (**6**). Structures of the core molecules and dyads prepared for the study are shown in Figure 2.3.

2.3. Results and Discussion

2.3.1. Synthesis and Characterization of Target Molecules

BuBPEA was synthesized starting from anthracene as shown in Scheme 2.1. Anthracene was refluxed in trifluoroacetic acid in the presence of excess *tert*-butanol to get the 2,6-di-*tert*-

butylanthracene (**8**). **8** was converted to the 9,10-dibromo derivative **9** by reaction with bromine in dichloromethane at 0 ^{0}C. The target molecule **4** was prepared by reaction of **9** with **10** under Sonogashira conditions. Synthesis of **10** was reported from our laboratory earlier.[1] Scheme for the synthesis of core molecule **3** is also shown in Scheme 2.1.

3, BuBPEA   **4**, ADBPEA

5, BuBPEA-PT

6, ADBPEA-PT
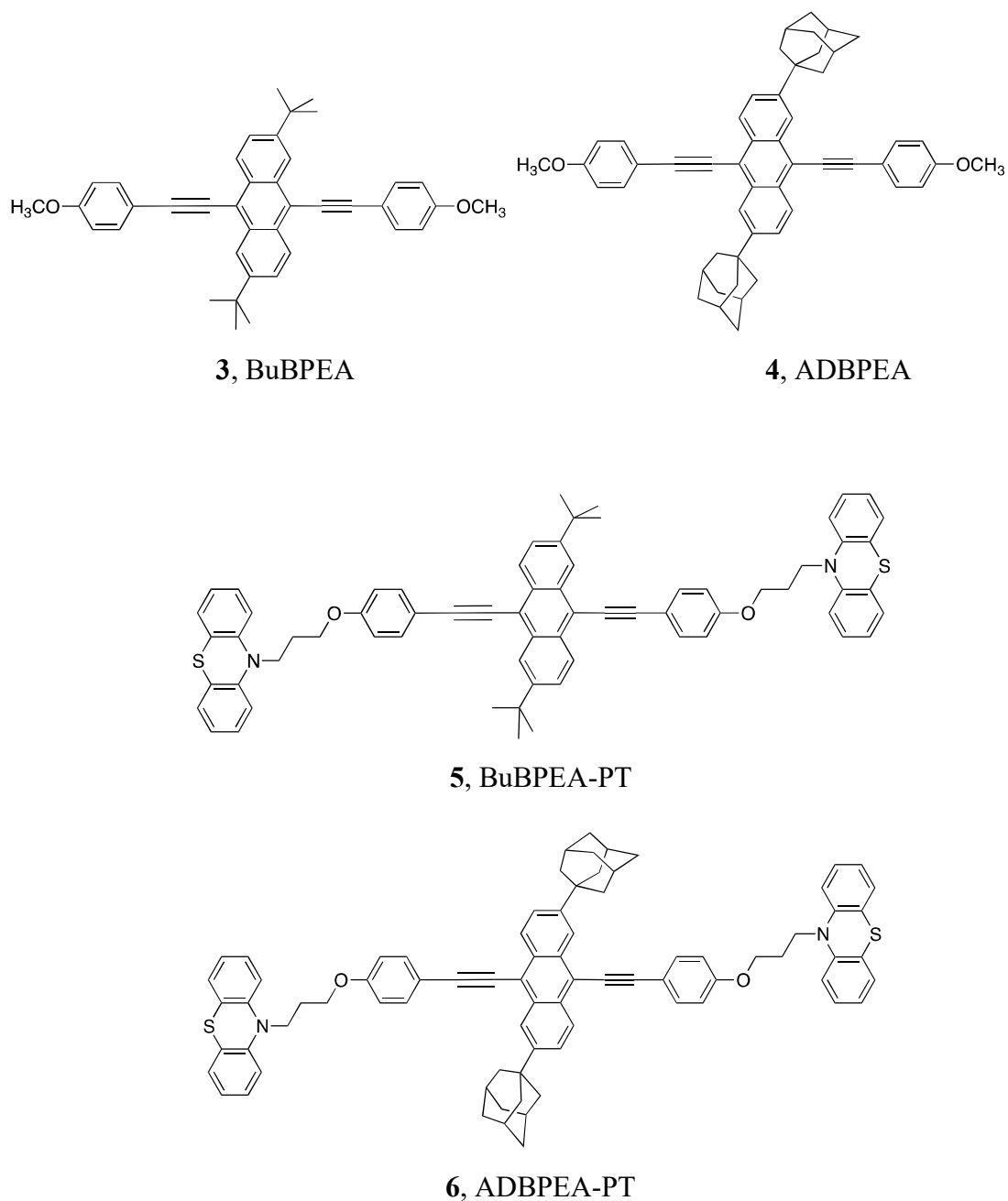
Figure 2.3. Structures of the molecules studied in this chapter
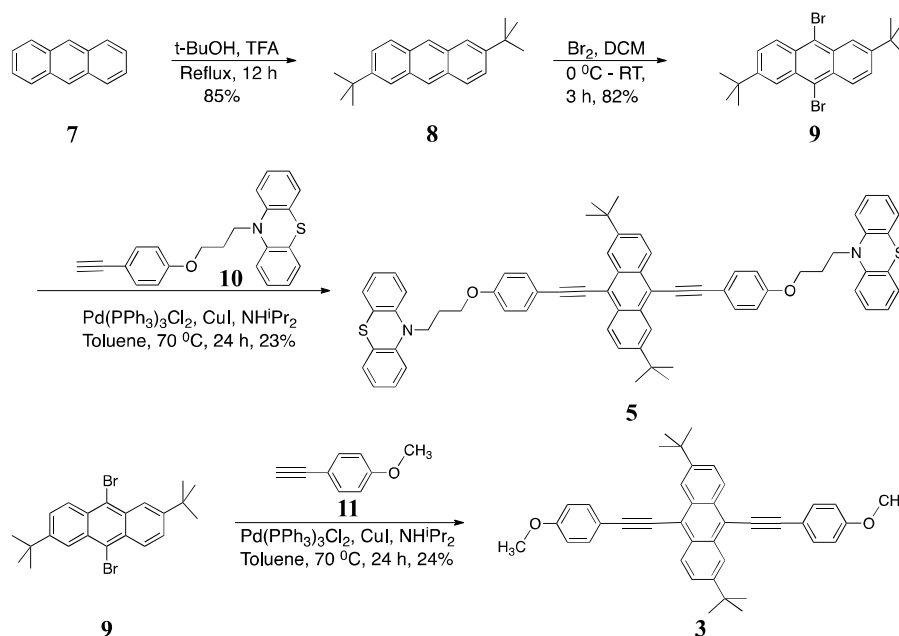
Scheme 2.1. Schemes for synthesis of target molecule **4** and core molecule **3**.

The adamantyl-substituted derivative **6** and the corresponding core molecule **4** were synthesized

in a similar manner. This is shown in Scheme 2.2.
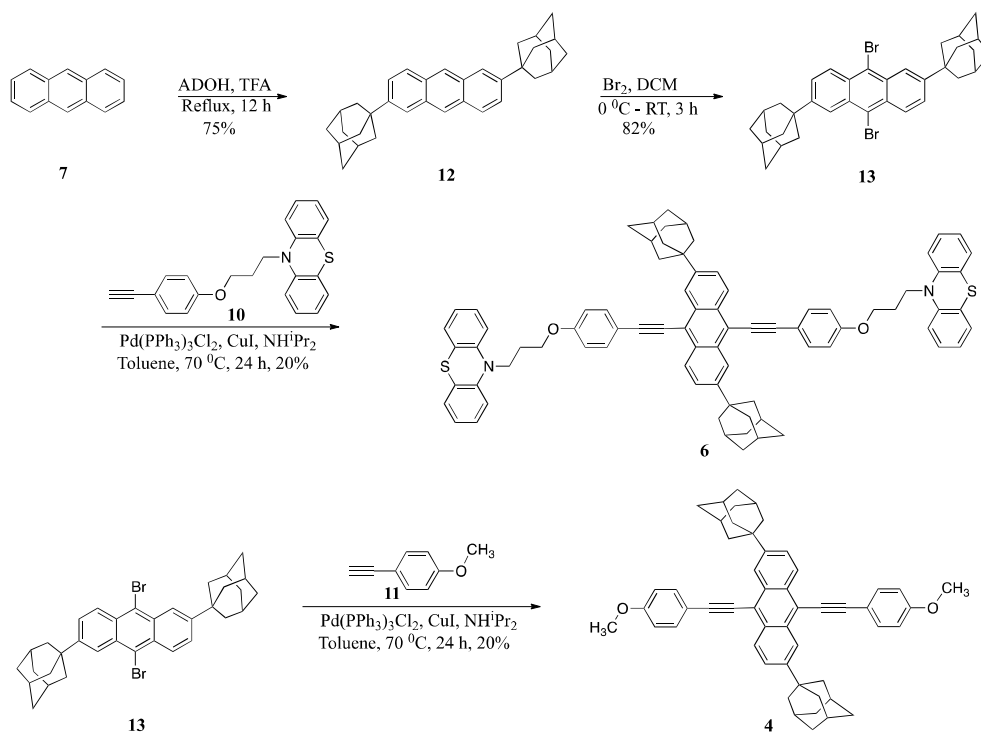
Scheme 2.2. Scheme for synthesis of target molecule **6** and core molecule **4**.

55

All the compounds synthesized were characterized using state-of-the art spectroscopic techniques. The details are given in the experimental section.

2.3.2. Photophysical Studies

BuBPEA-PT was soluble only in less polar solvents and insoluble in acetonitrile. ADBPEA-PT exhibited slight solubility in acetonitrile, but the solubility was not sufficient to conduct electrochemical or flash photolysis experiments in this solvent. Figure 2.4 shows the long-wavelength absorption band of BuBPEA-PT in few solvents. The spectrum exhibits two peaks and peak maxima in dichloromethane were 445 and 475 nm. In less polar solvents both peak maxima exhibited slight blue shifts. The absorption spectrum is almost identical to that of BPEA and the *tert*-butyl group substitution seems to have no effect on the spectrum. The long-wavelength absorption of BuBPEA and BuBPEA-PT were identical indicating that there is no ground state interaction between the donor and acceptor chromophores.
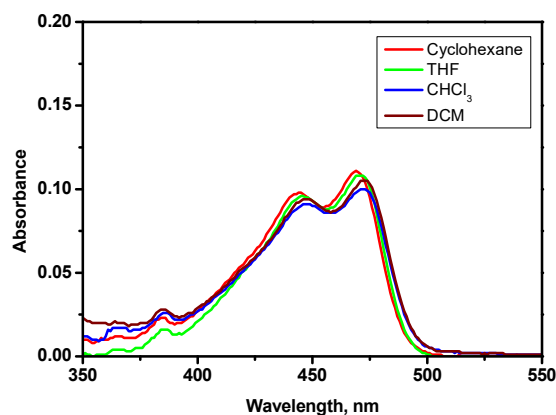
Figure 2.4. Absorption spectra of BuBPEA in few solvents.

The photophysical characteristics of BPEA molecule was investigated previously using polarized absorption and emission spectroscopy.[17-19] Based on these studies, the lowest energy transition in BPEA is assigned to a transition polarized along the long axis of the molecule. The studies also suggested the existence of an overlapping blue-shifted band with perpendicular polarization.

The normalized fluorescence spectra of BuBPEA-PT in few solvents are shown in Figure 2.5A. The spectrum exhibited maximum at 475 nm in cyclohexane and this is red-shifted to 490 nm in dichloromethane. The Stokes shift observed were very small in all solvents and the value was 778 cm^{-1} in dichloromethane. The spectra exhibited moderate quenching due to PET in medium polar solvents such as dichloromethane. Figure 2.5B compares the fluorescence spectra of the core molecule BuBPEA with that of BuBPEA-PT in dichloromethane.

A   B
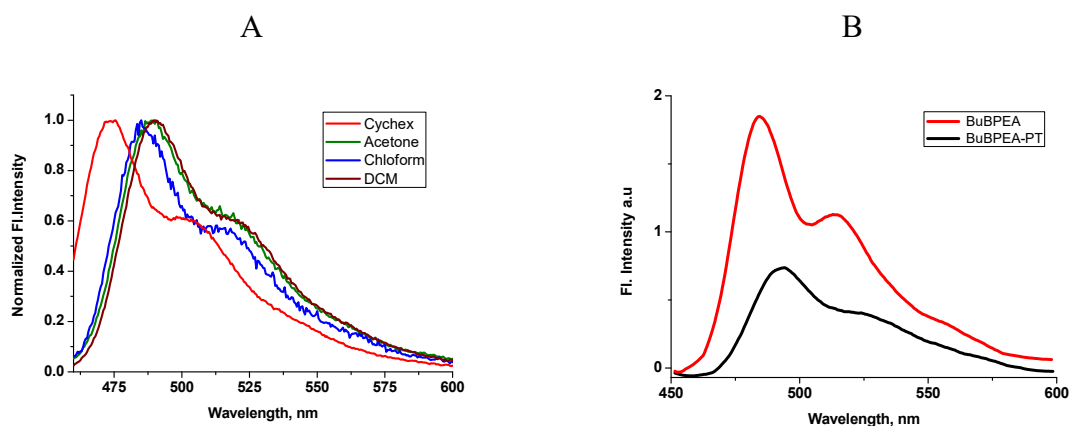
Figure 2.5. (A) Normalized fluorescence spectra of BuBPEA-PT in few solvents. (B) Fluorescence spectra of BuBPEA (red) and BuBPEA-PT (black) in dichloromethane

It can be seen from Figure 2.5B that the fluorescence emission is quenched very much in this solvent as a result of electron transfer from PT to ^{1}BuBPEP* core. In less polar solvents such as cyclohexane and chloroform, the spectra of BuBPEA and BuBPEA-PT were nearly identical, suggesting the absence of PET in these solvents.

Figure 2.6 shows the absorption spectra of ADBPEP compared with that of the dyad ADBPEA-PT in dichloromethane in the 300-500 nm range. In the region of the long wavelength absorption, the spectra are identical, suggesting that substitution of the PT group did not influence the electronic states of ADBPEA core.
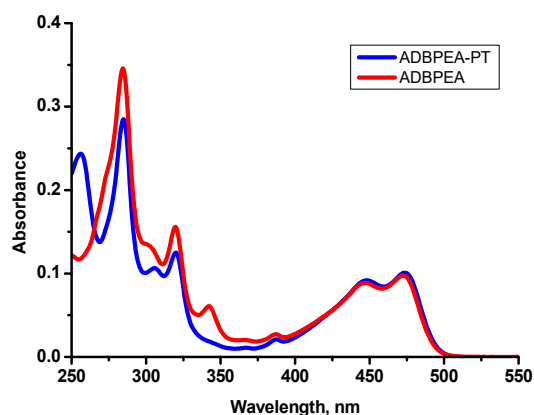
Figure 2.6. Absorption spectra of ADBPEA and ADBPEA-PT in dichloromethane.

ADBPEA-PT exhibits slight solubility in acetonitrile, which is sufficient to record its emission spectrum and fluorescence decay in this solvent. No attempt was made to perform other studies in this solvent. Figure 2.7 shows the absorption and fluorescence spectra of ADBPEP-PT in dichloromethane compiled in one plot.
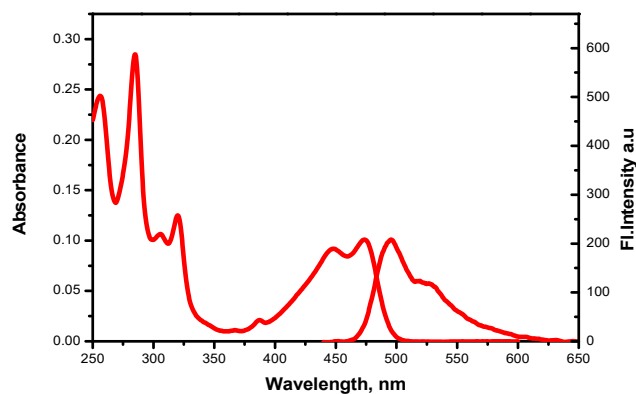
Figure 2.7. Absorption and fluorescence spectra of ADBPEA-PT in dichloromethane

The observed Stokes shift is 936 cm^{-1}, which is slightly larger than that observed for the *tert*-butyl derivative. In polar solvents the emission of ADBPEA-PT is quenched with respect to the ADBPEA as shown in Figure 2.8A,B. The quenching is much more in acetonitrile compared to that in dichloromethane. In Figure 2.8C, normalized fluorescence spectra of ADBPEA-PT in

different solvents are shown. Except for the small red-shift (~ 5 nm), the spectral profile remains

the same in all solvents.
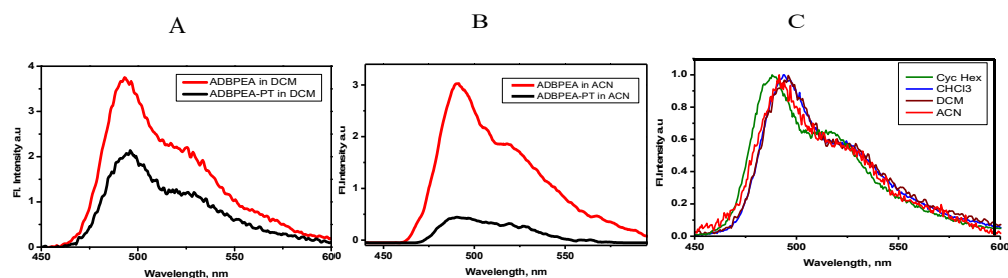
Figure 2.8. Fluorescence spectra of ADBPEA and ADBPEA-PT compared in (A) dichloromethane and (B) acetonitrile. (C) shows the normalized fluorescence spectra of ADBPEA-PT in different solvents.

2.3.3. Electrochemical studies

Redox potentials of BuBPEA-PT and ADBPEA-PT were measured (vs. Ferrocenium/ferrocene) in dichloromethane using square-wave voltammetry. Redox potentials of the core BPEA moiety was unaffected by substitution. This molecule exhibited an oxidation potential at 0.96 V and reduction potential at -1.46 V. The square-wave voltammogram obtained for ADBPEA-PT is given in Figure 2.9.
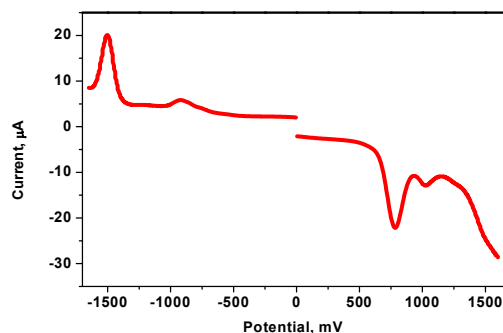
Figure 2.9. Square-wave voltammogram obtained for ADBPEA-PT in dichloromethane

The voltammogram exhibited reduction peak corresponding to the BPEA core at -1.5 V and a

new oxidation peak, corresponding to the PT moiety appeared at 0.78 V. Thus, in these dyads the

BPEA core is the acceptor and PT is the electron donor. The free energy for the PET reaction can

be calculated using the Weller equation (Chapter 1, equation 1.9). The excitation energy $E_{0,0}$ was calculated from the point of intersection of the absorption and fluorescence spectral profiles in Figure 2.7. The wavelength at this point was 485 nm and the corresponding energy is 2.56 eV. The center-to-center distance term in equation 1.9 was 16.8 Å, as obtained from ChemBioDraw software. Dielectric constant ε_s for dichloromethane is 8.93. Substituting these values in equation 1.9, we get $\Delta G = -0.376$ eV for ADBPEA-PT. Same value is obtained for BuBPEA-PT. Thus, PET is exergonic in both the dyads and we expect the following processes to take place upon excitation of ADBPEA-PT.

$$\text{ADBPEA-PT} \xrightarrow{\text{h}\nu > 350 \text{ nm}} {}^{1}\text{ADBPEA}^{*}\text{-PT} \qquad (2.1)$$

$$^{1}\text{ADBPEA}^{*}\text{-PT} \xrightarrow{\text{ET}} {}^{\bullet-}\text{ADBPEA-PT}^{\bullet+} \qquad (2.2)$$

$$^{\bullet-}\text{ADBPEA-PT}^{\bullet+} \xrightarrow{\text{BET}} \text{ADBPEA-PT} \qquad (2.3)$$
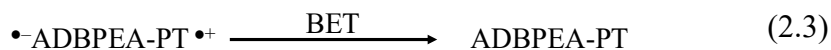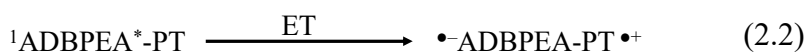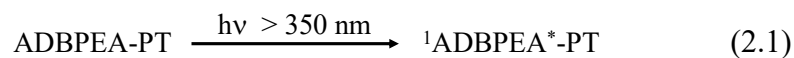
Rate constants for the PET and BET reactions were obtained from fluorescence lifetime and flash photolysis studies.

2.3.4. Fluorescence Lifetime Studies

The model compound BuBPEA exhibited monoexponential decay in dichloromethane with lifetime 3.65 ns. Decays of BuBPEA-PT were monoexponential in cyclohexane and chloroform with lifetime 2.8 ns (τ_0). Figure 2.10 shows the decay profiles of BuBPEA in dichloromethane and BuBPEA-PT in different solvents. In dichloromethane the decay was biexponential with lifetimes 1.12 (76%) and 2.24 (24%) ns. The short component (τ_1) is due to PET process in the dyad and long component may be assigned to conformers which did not undergo PET. Substituting values of τ_1 and τ_0 in equation 1.12, the rate constant for PET is obtained as 5.35×10^8 s^{-1}. Substituting this value in equation 1.13, we get the $\Phi_{\text{PET}} = 0.6$.
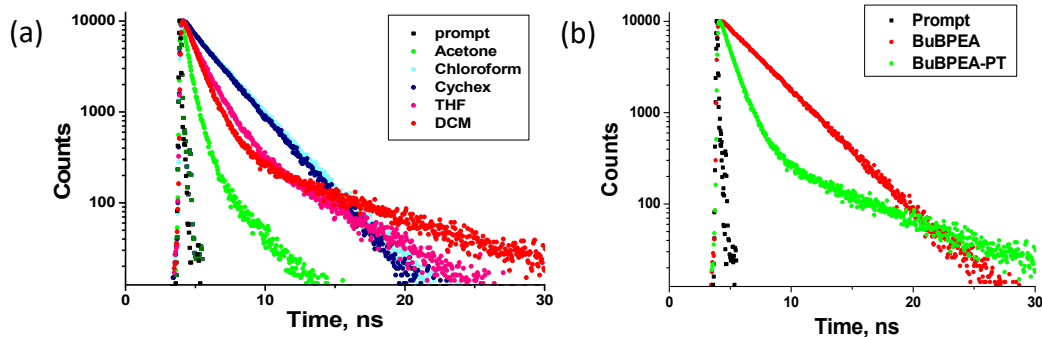
Figure 2.10. Fluorescence decay profiles of a) BuBPEA-PT in different solvents. b) BuBPEA and BuBPEA-PT in dichloromethane

Since ADBPEA and ADBPEA-PT exhibited slight solubility in acetonitrile, fluorescence decay profiles were recorded in this solvent. Fluorescence decay profiles of these molecules are shown in Figure 2.11.
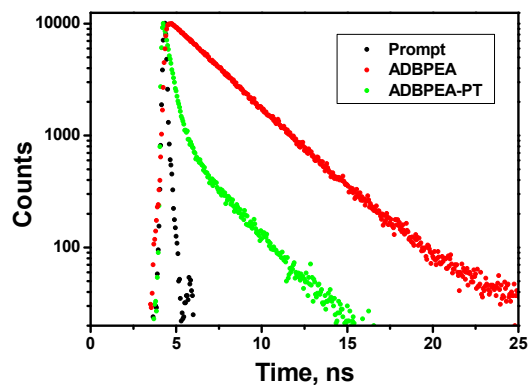
Figure 2.11. Fluorescence decay profiles of ADBPEA and ADBPEA-PT in acetonitrile.

The model compound exhibited monoexponential decay with lifetime (τ_0) = 3.29 ns. ADBPEA-PT dyad exhibited biexponential decay with τ_1 = 0.42 ns and τ_2 = 2.94 ns. The short component

arises due to PET in the dyad and equation 1.12 was used to obtain k_{PET}. The value obtained was 2.1×10^9 s^{-1}. Using this value of k_{PET}, we obtained $\Phi_{PET} = 0.88$.

2.3.5. Laser Flash Photolysis Studies

In order to visualize the formation of the radical ion pairs that arise due to the transfer of electron from PT to the singlet excited state of BPEP in the dyads as per equation 2.2, nanosecond flash photolysis experiments were carried out in de-aerated dichloromethane solution using the 355 nm light from a Nd-YAG laser. The transient absorption spectrum obtained in the case of BuBPEA-PT at 1.0 µs following the laser flash, is shown in Figure 2.12. The spectrum exhibited an intense peak at 510 nm and a broad peak centered around 640 nm. The inserts show decay profiles of the transients at 510 and 640 nm.
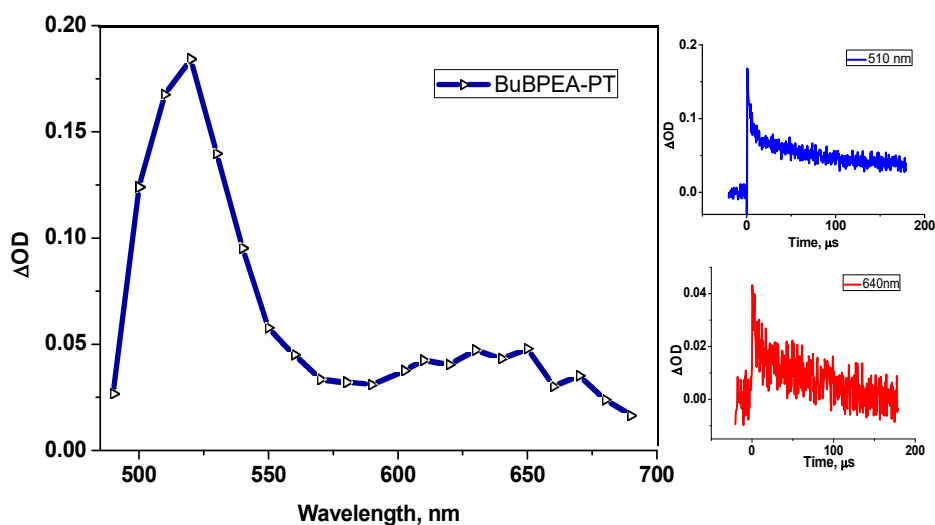
Figure 2.12. Transient absorption spectrum obtained in the flash photolysis of BuBPEA-PT in dichloromethane. Inserts show transient decays at 510 and 640 nm.

Figure 2.13 shows the transient absorption spectrum obtained in the case of ADBPEA-PT. In this case also, absorptions were observed at 510 and 640 nm. It is widely accepted that the

phenothiazine radical cation exhibits strong absorption at 510-520 nm.[2,23] Hence, we assign the peak at 515 nm to phenothiazine radical cation formed as a result of PET to the BPEA core.
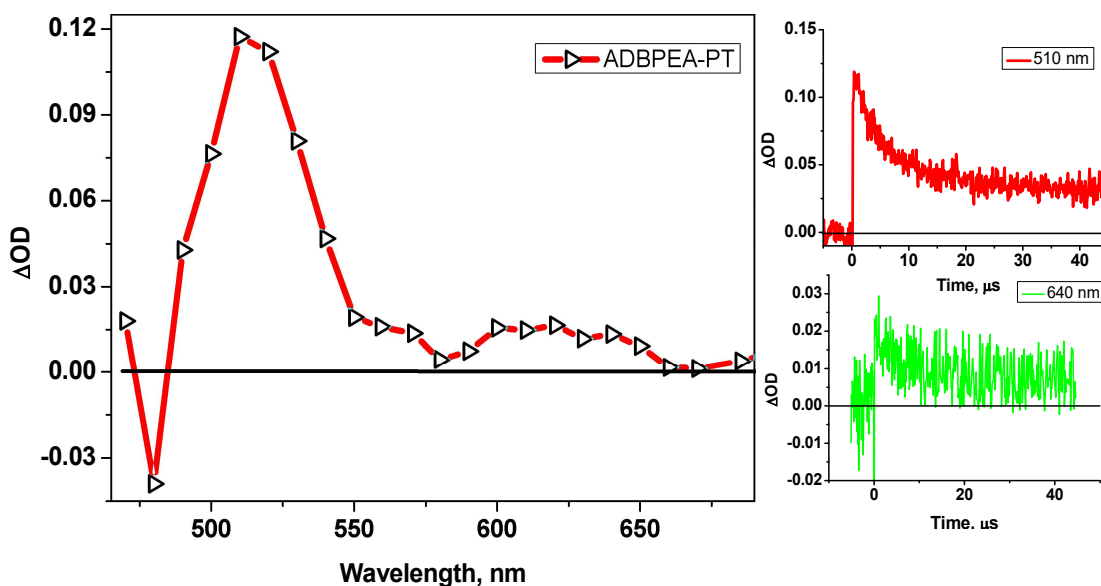
Figure 2.13. Transient absorption spectrum obtained at 1.0 ms after the flash for ADBPEA- in dichloromethane. Inserts show the decay profiles of transients at 510 and 640 nm.

Albinsson and co-workers have studied the BPEA core as an electron accepting unit in various systems and have reported that radical anion of BPEA absorbs around 640 nm.[24] Hence, we assign the broad absorption in this region to BPEA$^{\bullet-}$. In the case of BuBPEA-PT, the radical ion pair state exhibited lifetime τ_{CS} = 24 μs (k_{BET} = $1/\tau_{CS}$ = 4.25 × 10^4 s^{-1}). In the case of ADBPEA-PT, the observed radical ion pair lifetime was 6.45 μs (k_{BET} = 1.5 × 10^5 s^{-1}). The lifetimes obtained are in the microsecond domain and these are similar to those of BPEA-PT and BPEP-PT systems reported by us earlier.[1,2]

The photophysical and electron transfer properties of BuBPEA-PT and ADBPEA-PT we report in this chapter are nearly identical to those of BPEA-PT and BPEP-PT reported by us previously[1,2] and can be described by the energy level diagram in Figure 2.2. The singlet excited

states of these molecules are around 2.56 eV above the ground state and this is slightly lower than that for BPEA-PT. Energy of the CS state is at 2.38 eV, which is 0.2 eV higher than that of BPEA-PT. Substitution of *tert*-butyl or 1-adamantyl groups at the 2- and 6- positions of anthracene did not lead to significant changes in the absorption and emission profiles of the model molecules. Thus, we do not expect the *tert*-butyl or 1-adamantyl group substitution to cause any significant change in the energy level of the local triplet state. The fact that both BuBPEA-PT and ADBPEA-PT did not generate the local triplet suggest that spin-orbit coupling or hyperfine-induced intersystem crossing pathways are not operating in these molecules. Thus, the long-lived CS state in these molecules can be attributed to the inverted region effect, which is made possible by lack of intersystem crossing in the parent hydrocarbon.

2.4. Conclusions

In this chapter we have studied the photophysical and electron transfer properties of BuBPEA-PT and ADBPEA-PT. These compounds were prepared hopping that substitution of tert-butyl and/or adamantyl groups will enhance the solubility of the BPEA core so that PET processes in these molecules can be investigated in polar solvents, such as acetonitrile. However, the solubilities did not increase and studies could not be done as planned. Hence we have not investigated these systems any further.

2.5. Experimental Section

2.5.1. Methods

Melting points were determined on a Mel-Temp II melting point apparatus and are uncorrected. ^{1}HNMR data were recorded on a 500 MHz Bruker Avance DPX spectrometer. FT-IR spectra were recorded on a Shimadzu IR Prestige 21 spectrometer. High resolution mass spectra were obtained by using a JOEL JMS600 mass spectrometer. Absorption spectra were

obtained using a Shimadzu 3101PC UV/Vis-NIR scanning spectrophotometer. Steady state fluorescence experiments were performed with a Perkin Elmer LS 55 Fluorescence Spectrometer using optically dilute solutions. Electrochemical experiments were performed using a BAS 50W voltammetric analyser employing *tetra-n-*butylammonium hexafluorophosphate as supporting electrolyte. Fluorescence lifetime experiments were performed by using an IBH picoseconds single photon counting system employing 440 nm Nano-LED excitation source and a Hamamatsu C4878-02 micro channel plate (MCP) detector. Nanosecond laser flash photolysis experiments were performed by using an Applied Photophysics Model LKS-20 laser kinetic spectrometer by using the third harmonic (355 nm) from a GCR-12 series Quanta Ray Nd: YAG laser. Solutions for laser flash photolysis studies were de-aerated by purging with argon for 20 min before experiments.

2.5.2. Synthesis of Compounds

2.5.2.1. Synthesis of BuBPEA and BuBPEA-PT

2.5.2.1.1. Synthesis of 2,6-Di-tert-butylanthracene (8): A mixture of anthracene (8.9 g, 50 mmol), trifluoroacetic acid (50 mL) and *tert*-butanol (20 mL) were refluxed for 12 h. The mixture was cooled and filtered and the solid was washed with water several times. It was then dried in the air and crystallized from petroleum ether/ethyl acetate to get **8** as colourless flaky crystals. Yield: 12.3 g (85%), mp. 250 – 252 ^{0}C. HRMS: Calculated for $C_{22}H_{26}$: 290.20; Observed: 290.29. ^{1}H NMR (CDCl$_3$, 500 MHz) δ: 1.4 (s,18 H), 7.5 (d, 2H), 7.8 (s, 2H), 7.9 (d, 2H), 8.3 (s, 2H) ppm. ^{13}C NMR (CDCl$_3$, 125 MHz) δ: 31.1, 35.3, 123.6, 124.7, 125.5, 127.8, 130.4, 132.6, 147.4 ppm. IR (KBr) ν_{max}: 3064, 2953, 1927, 1627, 1473, 1360, 1247, 1199, 1085, 965, 807, 612 cm^{-1}.

2.5.2.1.2. Synthesis of 9,10-dibromo-2,6-ditert-butylanthracene (**9**): **8** (5.0 g, 17.24 mmol) was dissolved in dichloromethane (90 mL) in a 250 mL three-necked flask equipped with a reflux condenser, dropping funnel and gas absorption device. Bromine (3.0 mL, 9.3 g, 58 mmol) was taken in the dropping funnel. The flask was cooled to 0 ^{0}C and bromine was slowly added with stirring over a period of 1 h. Stirring was continued at this temperature for 2 h more. A saturated solution of sodium bicarbonate (50 mL) was taken in the dropping funnel and added to the flask slowly until the red colour disappeared. The mixture was then taken in a separating funnel and layers separated. The organic layer was separated, washed with brine and dried over anhydrous sodium sulfate. The solvent was removed to get the crude product. This was suspended in methanol, sonicated for 5 min. and filtered to get the pure product. Yield: 6.3 g (82%), MP. 209 – 210 ^{0}C. HRMS: Calculated for $C_{22}H_{24}Br_2$: 448.02; Observed: 448.01. ^{1}H NMR (CDCl$_3$, 500 MHz) δ: 1.4 (s, 18 H), 7.7 (d, 2H), 8.4 (s, 2H), 8.5 (d, 2H) ppm. 13C NMR (CDCl$_3$, 125 MHz) δ: 31.2, 35.3, 123.2, 129.9, 130.2, 149.7 ppm. IR (KBr) v_{max}: 2953, 1931, 1673, 1585, 1466, 1363, 1100,961, 873, 814, 737 cm^{-1}.

2.5.2.1.3. Synthesis of BuBPEP-PT (**5**): A mixture of **9** (362 mg, 0.58 mmol), dichlorobis(triphenylphosphene)palladium(II) (50 mg, 0.0728 mmol) and copper(I) iodide (30 mg, 0.03 mmol) were dissolved in dry toluene (30 mL) in an argon flushed RB. Dry diisopropyl amine (10 mL) and compound **10** (454 mg, 1.27 mmol) were added and the mixture heated at 70 ^{0}C for 24 h under argon. The solvent was then removed and the residue chromatographed over silica gel. Elution with hexane/chloroform (7:3) gave the product as orange solid. Yield: 130 mg (23%), mp. 209 – 210 ^{0}C. ^{1}H NMR (CDCl$_3$, 500 MHz) δ: 1.5 (s, 18H), 2.3 (m, 4H), 4.1 (t, 4H), 4.2 (t, 4H), 6.9 (m, 12H), 7.2 (t, 8H), 7.6 (m, 2H), 7.7 (m, 4H), 8.6 (m, 4H) ppm. ^{13}C NMR (CHCl$_3$, 125 MHz) δ: 26.72, 30.96, 35.21, 43.78, 65.42, 77.01, 85.79, 102.16, 114.87, 115.78,

117.58, 121.55, 122.66, 125.58, 125.94, 127.30, 130.60, 131.69, 132.98, 145.15, 148.78, 159.08

ppm. IR (KBr) ν_{max}: 3217, 2951, 1734, 1686, 1542, 1505, 1463, 1294, 1180 cm^{-1}.

2.5.2.1.4. Synthesis of Model Compound 3: A mixture of **9** (500 mg, 1.12 mmol), dichlorobis(triphenylphosphene)palladium(II) (65 mg, 0.1 mmol), and copper(I) iodide (20 mg, 0.1 mmol) were dissolved in dry THF (40 mL) in a argon degassed RB. Dry diisopropyl amine (10 mL) and phenylacetylene (420 mg, 3.18 mmol) were added and reaction mixture stirred at 70 ^{0}C under argon atmosphere for 24 h. The solvent was removed and residue chromatographed over silica gel. Elution with hexane gave the product, which was crystallized from dichloromethane and the crystals washed with cold ether. Yield: 130 mg (24%). mp. 219-220 ^{0}C. ^{1}H NMR (CDCl$_{3}$, 500 MHz) δ: 1.58 (s, 18H), 3.89 (s, 6H), 7.34 (m, 2H), 7.45 (m, 2H), 7.48 (m, 4H), 7.57 (m, 2H), 8.63 (d, 2H), 8.64 (m, 2H) ppm.

2.5.2.2. Synthesis of ADBPEA and ADBPEA-PT

2.5.2.2.1. Synthesis of 2,6-Diadamantylanthracene (12): This molecule was prepared in the same way as for **8**, except that the *tert*-butanol was replaced by 1-adamantanol (17g, 110 mmol). After filtration of the solid, excess adamantanol was removed by stirring with cold hexane and filtering. The product was crystallized from petroleum ether/ethyl acetate mixture.

Yield: 11.2 g (75%). HRMS: Calculated for C$_{34}$H$_{38}$: 446.3; Observed: 446.2. ^{1}H NMR (CDCl$_{3}$, 500 MHz) δ: 1.8 (s, 6H), 2.1 (s, 12H), 2.8 (m, 12H), 7.5 (d, 2H), 7.8 (d, 2H), 8.3 (s, 2H) ppm. ^{13}C NMR (CDCl$_{3}$, 125 MHz) δ: 31.1, 35.3, 123.6, 124.7, 125.5, 127.8, 130.4, 132.6, 147.4 ppm.

2.5.2.2.2. Synthesis of 9,10-dibromo-2,6-Diadamantylanthracene (13): The reaction was done as in the case of **9**. Yield: 45%. Mass (HRMS): Calculated for C$_{34}$H$_{36}$Br$_{2}$: 602.12; found: 602.78; ^{1}H NMR (CDCl$_{3}$, 500MHz) δ: 8.41 (s, 2H), 8.1 (d, 2H), 7.5 (d, 2H), 2.8(m, 12H), 2.1(s, 12H), 1.8 (s, 6H) ppm.

2.5.2.2.3 Synthesis of ADBPEA-PT(6) : To an argon degassed RB flask, 2, 6-diadamantyl-9,10-dibromoanthracene(**13**, 0.2780 g, 0.46 mmol), dichlorobis(triphenylphosphene) palladium(II) (50mg, .0728 mmol) and copper(I)iodide (30 mg,0.03 mmol) were dissolved in dry THF (30mL). Dry diisopropylamine(7 mL) and compound **10** (0.4114g, 1.15 mmol) were added. The mixture was refluxed for 24 h at 70 ^{0}C under argon. The solvent was removed and residue was purified by column chromatography over silica using chloroform/hexane (3:7) to obtain **6** as orange solid. (mp > 300 ^{0}C.). ^{1}H NMR (CDCl$_3$, 500MHz) δ: 1.86 (s, 12H), 2.2 (s, 12H), 2.3 (s, 6H), 2.32 (s, 4H), 4.1 (m, 8H), 6.9 (m, 13H), 7.18 (q, 9H), 7.64 (m, 3H), 7.72 (t, 2H), 8.56 (m, 3H) ppm. ^{13}CNMR (CDCl$_3$, 125MHz) δ: 160.2, 148, 143.9, 135.2, 132.6, 131.9, 129.1, 128.8, 127.2, 125.1, 123.6, 120.6, 119.1, 114.6, 114.2, 112, 94.6, 72.6, 46.5, 42.7, 36.1, 35.6, 28.6, 26.1 ppm.

2.6. References

1. Suneesh, C. V.; Gopidas, K. R. Long-Lived Photoinduced Charge Separation in Flexible 9,10-Bis(phenylethynyl)anthracene-Phenothiazine Dyads. *J. Phys. Chem. C* **2009**, *113*, 1606-1614.

2. Suneesh, C. V.; Gopidas, K. R. Long-Lived Photoinduced Charge Separation Due to the Inverted Region Effect in 1,6-Bis(phenylethynyl)pyrene-Phenothiazine Dyad. *J. Phys. Chem. C* **2010**, *114*, 18725-18734.

3. Benniston, A. C.; Harriman, A.; Li, P.; Rostron, J. P.; Verhoeven, J. W. Illumination of the 9-Mesityl-10-methylacridinium Ion Does Not Give a Long-Lived Photoredox State. *Chem. Commun*. **2005**, 2701-2703.

4. Benniston, A. C., Harriman, A.; Li, P.; Rostron, J. P.; Ramesdonk, H. J.; Groeneveld, M. M.; Zhang, H.; Verhoeven, J. W. Charge Shift and Triplet State Formation in the 9-Mesityl-10-methylacridinium Cation. *J. Am. Chem. Soc.* **2005**, *127*, 16054-16064.

5. Verhoeven, J. W.; van Ramesdonk, H. J.; Zhang, H.; Groeneveld, M. M.; Benniston, A. C.; Harriman, A. Long-Lived Charge-Transfer States in 9-Aryl-Acridinium Ions; A Critical Reinvestigation. *Int. J. Photoenergy* **2005**, *7*, 103-108.

6. van Ramesdonk, H. J.; Bakker, B. H.; Groeneveld, M. M.; Verhoeven, J. W.; Allen, B. D.; Rostron, J. P.; Harriman, A. Ultrafast Intersystem Crossing in 9,10-Anthraquinones and Intramolecular Charge Separation in an Anthraquinone-Based Dyad. *J. Phys. Chem. A* **2006**, *110*, 13145-13150.

7. Benniston, A. C.; Harriman, A.; Verhoeven, J. W. Comment: Electron-Transfer Reactions in the 9-Mesityl-10-methylacridinium ion: Impurities, Triplet States and Infinitely Long-Lived Charge-Shift States? *Phys. Chem. Chem. Phys.* **2008**, *10*, 5156-5158.

8. Verhoeven, J. W. On the Role of Spin Correlation in the Formation, Decay, and Detection of Long-Lived, Intramolecular Charge-Transfer States *J. Photochem. Photobiol. C* **2006**, *7*, 40-60.

9. Kawai, A.; Shibuya, K. Electron Spin Dynamics in a Pair Interaction Between Radical and Electronically-Excited Molecule as Studied by a Time-Resolved ESR Method. *J. Photochem. Photobiol. C* **2006**, *7*, 89-103.

10. Dance, Z. E. X.; Mickley, S. M.; Wilson, T. M.; Ricks, A. B.; Scott, A. M.; Ratner, M. A.; Wasielewski, M. R. Intersystem Crossing Mediated by Photoinduced Intramolecular Charge Transfer: Julolidine-Anthracene Molecules with Perpendicular π Systems. *J. Phys. Chem. A* **2008**, *112*, 4194-4201.

11. Hou, Y.; Zhang, X.; Chen, K.; Liu, D.; Wang, Z.; Liu, Q.; Zhao, J.; Barbon, A. Charge Separation, Charge Recombination, Long-Lived Charge Transfer State Formation and

Intersystem Crossing in Organic Electron Donor/Acceptor Dyads. *J. Mater. Chem. C* **2019**, *7*, 12048-12074.

12. Zgorzelak, M.; Grajewski, J.; Gawronski, J.; Kwit, M. Solvent-Assisted Synthesis of a Shape-Persistent Chiral Polyaza Gigantocycle Characterized by a Very Large Internal Cavity and Extraordinarily High Amplitude of the ECD Exciton Couplet. *Chem. Commun.* **2019,** *55*, 2301-2304.

13. Geiger, T.; Haupt, A.; Maichle-Mössmer, C.; Schrenk, C.; Schnepf, A.; Bettinger, H. F. Synthesis and Photodimerization of 2- and 2,3-Disubstituted Anthracenes: Influence of Steric Interactions and London Dispersion on Diastereoselectivity. *J. Org. Chem.* **2019**, *84*, 10120-10135.

14. Niladari Raju, M. V.; Mohanty, M. E.; Bangal, P. R.; Vaidya, J. R. Synthesis and Ultrafast Dynamics of a Donor-Acceptor-Donor Molecule Having Optoelectronic Properties. *J. Phys. Chem. C* **2015**, *119*, 8563-8575.

15. Wrona-Pitrowicz, A.; Makal, A. Zakrzewski, J. Triflic Acid Promoted Adamantylation and *tert*-Butylation of Pyrene: Fluorescent Properties of Pyrene-Decorated Adamantanes and a Channeled Crystal Structure of 1,3,5-Tris(pyren-2-yl)adamantane. *J. Org. Chem.* **2020**, *85*, 11134-1139.

16. Miura, Y.; Yamano, E.; Tanaka, A. Generation, Isolation and Characterization of *N*-(Arylthio)-7-*tert*-butyl- and *N*-(Arylthio)-2,7-di-*tert*-butyl-1-pyreneylaminyl Radicals. *J. Org. Chem.* **1994**, *59*, 3294-3300.

17. Levitus, M.; Garcia-Garibay, M. A. Polarized Electronic Spectroscopy and Photophysical Properties of 9,10-Bis(phenylethynyl)anthracene. *J. Phys. Chem. A* **2000**, *104*, 8632-8637.

18. Zhu, A.; White, J. O.; Drickamer, H. G. The Effect of Pressure and of Controlled Stretch on the Luminescent Properties of 9,10-Bis(phenylethynyl) Anthracene. *J. Phys. Chem. A* **2002**, *106*, 9209-9212.

19. Beeby, A.; Findlay, K. S.; Goeta, A. E.; Porrès, L.; Rutter, S. R.; Thompson, A. L. Engineering a Twist in 9,10-Diethynylanthracenes by Steric Interactions. *Photochem. Photobiol. Sci.* **2007**, *6*, 982-986.

20. Moroi, Y.; Braun, A. M.; Graetzel, M. Light-Initiated Electron Transfer in Functional Surfactant Assemblies. 1. Micelles with Transition Metal Counter Ions. *J. Am. Chem. Soc.* **1979**. *101*, 567-572.

21. Chen, P.; Duesing, R.; Graff, D. K.; Meyer, T. J. Intramolecular Electron Transfer in the Inverted Region. *J. Phys. Chem.* **1991**, *95*, 5850-5858.

22. Klumpp, T.; Linsenmann, M.; Larson, S. L.; Limoges, B. R.; Bürssner, D.; Krissinel, E. B.; Elliott, C. M.; Steiner, U. E. Spin Chemical Control of Photoinduced Electron-Transfer Processes in Ruthenium(II)-Trispyridine-Based Supramolecular Triads. *J. Am. Chem. Soc.* **1999**, *121*, 1076-1087.

23. Ajayakumar, G.; Gopidas, K. R. Long-Lived Photoinduced Charge Separation in New Ru(bipyridine)$_3{}^{2+}$-Phenothiazine dyads. *Photochem. Photobiol. Sci.* **2008**, *7*, 826-833.

24. Winters, M. U.; Pattersson, K.; Mårtensson, J.; Albinsson, B. Competition Between Superexchange-Mediated and Sequential Electron Transfer in a Bridged Donor-Acceptor System. *Chem. Eur. J.* **2005**, *11*, 562-573.

<div align="right">**Chapter 3**</div>

Photoinduced Electron Transfer Studies of Adamantane-Bridged Dyads with *N,N*-dimethylaniline Donor and Hydrocarbon Acceptors

3.1. Abstract

Photoinduced electron transfer studies in adamantane bridged anthracene-dimethylaniline (AN-AD-DMA) and pyrene-dimethylaniline (PY-AD-DMA) are reported in this chapter. In the adamantane bridged dyads, the donor and acceptor are separated by four C-C single bonds only, and hence these can be classified as compact dyads. Excitation of anthracene or pyrene in these dyads leads to electron transfer from dimethylaniline to the singlet excited state of these hydrocarbons, which leads to quenching of the hydrocarbon fluorescence. The photoinduced electron transfer rates in the adamantane-bridged systems is 1-2 orders of magnitude slower compared to methylene chain linked anthracene-dimethylaniline and pyrene-dimethylaniline systems studied earlier by others. The charge separated states were long-lived (~ 1 µs) in these dyads which could be observed in nanosecond flash photolysis. Compared to the methylene chain linked systems, the charge separated state lifetimes were nearly thousand-fold larger in the adamantane bridged systems. A fraction of the singlet charge-separated state undergoes intersystem crossing to the triplet manifold, which underwent recombination to generate the hydrocarbon triplets. Long-lived charge separated state formation and intersystem crossing in the singlet radical pair were not observed previously in compact dyads. These new properties are attributed to the adamantane bridge.

3.2. Introduction

Aromatic amines are among the most widely used donor molecules in organic chemistry.[1] The donor strength of a molecule can be related to its HOMO energy or ionization potential. The gas phase ionization potentials of most aryl amines are in the 6.0 – 8.0 eV range.[1] Most aryl amines have their first oxidation potential around + 1.0 V (vs SCE) and hence can be oxidized easily by a variety of reagents. They can be oxidized electrochemically and photochemically. One electron oxidation leads to formation of the radical cation of the aryl amine, the stability of which varies widely depending on the structure of the aryl amine. Radical cations of few aryl amines are very stable, and in these cases the electrochemical oxidations are completely reversible.[2] Most aryl amine radical cations are coloured and the absorption spectra of a large number of aryl amine radical cations are compiled.[3] Due to the facile electron donating nature, several aryl amines act as hole-transport materials in various applications such as xerography,[4,5] light-emitting diodes,[6-9] and photorefractive systems.[10-12] They also find applications as second and third order non-linear materials[13-15] and in solar cells.[16-19]

Aryl amines are the most frequently used electron donors in bimolecular PET reactions.[20-47] The most frequently used aryl amines are dialkylanilines (**1**), triaryl amines (**2**), phenothiazines (**3**), carbazoles (**4**) and benzidines (**5**) (Figure 3.1; R = alkyl or aryl). In most of the PET studies mentioned, the aryl amines act as ground state electron donors. The molecules acting as excited state acceptors in these studies are also listed in Figure 3.1. Aromatic hydrocarbons such as anthracene (AN, **6**) and pyrene (PY, **7**) in their singlet excited states can accept an electron from these amines, although electron transfer to the triplet excited states of these molecules from aryl amines are exergonic (vide infra). Aryl ketones (**8**) and quinones (**9**, **10**) are good electron acceptors and generate their triplet excited states with high quantum yield

up on excitation. The aryl amines can quench the triplet excited states of these ketones and quinones through electron transfer or hydrogen abstraction. Electron transfer from amines to the excited states of coumarins (**11**) is discussed in several papers. The singlet excited states of C_{60} (**12**) and C_{70} are also quenched by amines by electron transfer mechanism. Another molecule of interest is *tris*-bipyridylruthenium(II) (Rubp, **13**), the MLCT excited state of which readily accepts an electron from aryl amines.
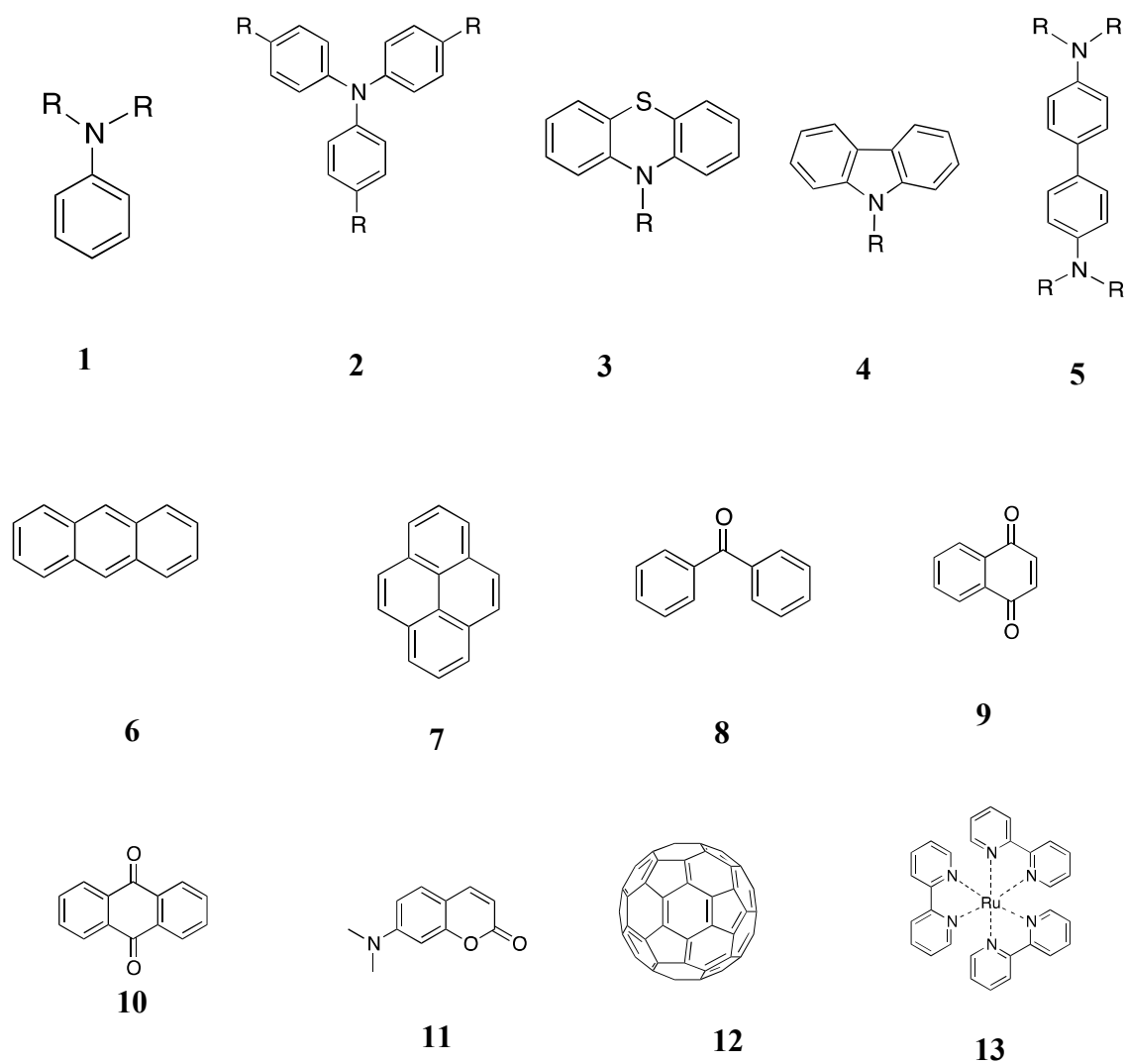
Figure 3.1. Structures of aryl amines (**1 – 5**) and common excited state electron acceptors (**6 – 13**) employed in PET studied of aryl amine – acceptor systems

PET from the aryl amines to the excited states of **6 – 13** were studied by steady-state and time-resoled fluorescence and nanosecond-femtosecond laser flash photolysis techniques. In the flash photolysis experiments radical cations of the amines and radical anions of the acceptors were detected. The radical ions then undergo very facile charge recombination reactions to regenerate the starting materials in their ground states. CS and CR reactions of aryl amine – acceptor systems on silica gel surfaces,[36,44] ionic liquids[45] and zeolite cavities[46] were also studied. In this chapter we report PET reactions between DMA and photoexcited AN and PY, bridged through a rigid adamantane spacer. The DMA-AN and DMA-PY donor-acceptor systems have been studied in great detail and these will be discussed later in this chapter.

Although aryl amines act as donor components in large numbers of bimolecular PET reactions, very few examples of covalently linked dyads containing aryl amine donors are reported in the literature (Figure 3.2). Among these dyads **14-17** were synthesized for applications in solar cells and charge transport systems, and detailed studies of PET processes and charge separation in these systems were not attempted.[48-51] Synthesis of **18** is reported along with its absorption and fluorescence spectra. The fluorescence quantum yield of this molecule is very low compared to Rubp due to electron transfer from the appended amine donor groups.[52] The phenothiazine – Rubp donor-acceptor system **19** was studied by our group.[53] PET processes in this molecule was studied by steady-state and time resolved fluorescence and nanosecond laser flash photolysis. CS in **19** occurs with $\Phi_{CS} = 0.82$ and $k_{CS} = 2.47 \times 10^8$ s^{-1}. The CS state observed in nanosecond flash photolysis exhibited lifetime of 26 ns, which corresponds to $k_{CR} = 3.8 \times 10^7$ s^{-1}.

14

15

16

17

18

19
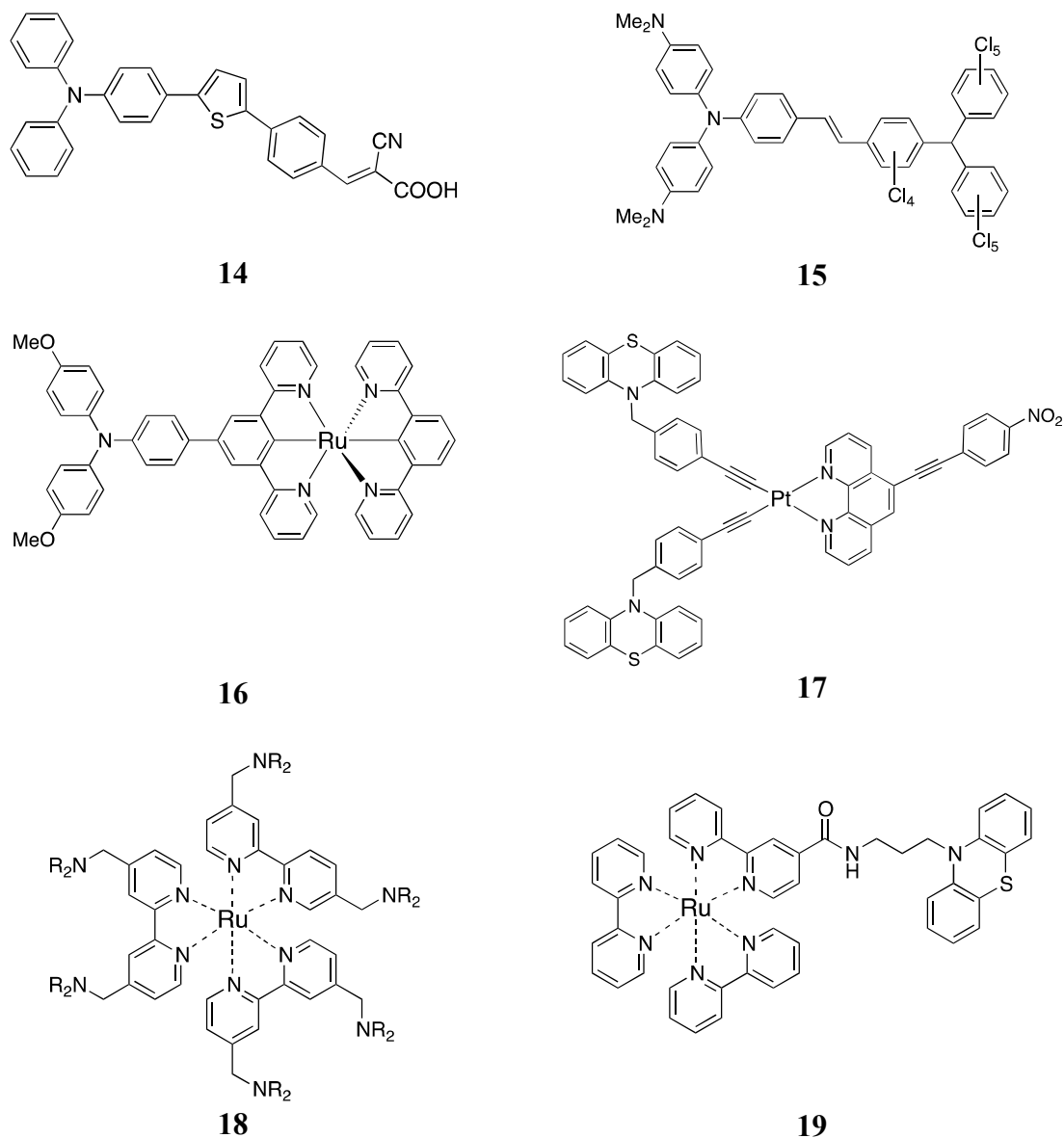
Figure 3.2. Structures of few aryl amine – acceptor systems reported in the literature.

A few non-covalently linked aryl amine – acceptor systems are also reported in the literature. Our group has reported PET reactions in AN-DMA and PY-DMA systems assembled through the hydrogen bonding interactions involving carboxylic acids as shown in Figure 3.3.[54,55] Rates of PET determined were 4.3×10^8 s^{-1} and 9.0×10^8 s^{-1}, respectively, for **20** and **21**.
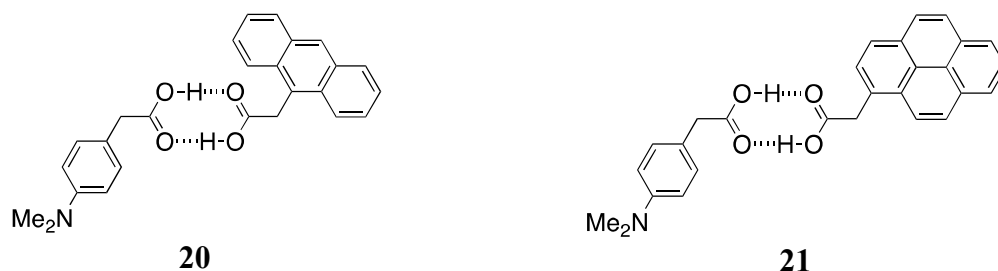
Figure 3.3. Hydrogen bonded AN-DMA and PY-DMA systems studied in our group.

Sessler et al. reported assembling of AN-DMA system held together by guanosine-cytidine Watson-Crick base-pairing interaction as shown in **22** (Figure 3.4).[56,57]
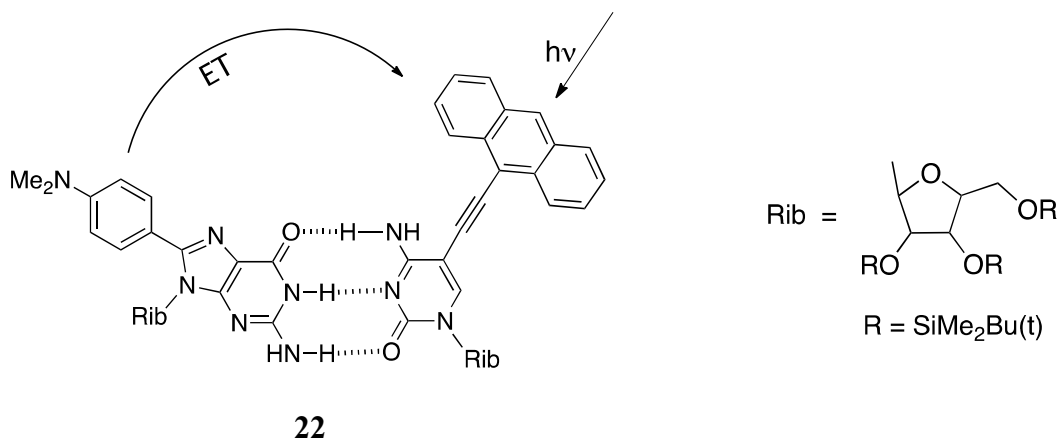
Figure 3.4. AN-DMA system studied by Sessler et al.

PET processes in **22** was studied by time-resolved fluorescence and picosecond flash photolysis. In toluene solution, the rate constants for PET and subsequent CR reactions obtained were $k_{CS} = 3.5 \times 10^{10}$ s^{-1} and $k_{CR} = 1.42 \times 10^{9}$ s^{-1}, respectively.

As mentioned previously, PET reactions of AN-DMA and PY-DMA systems were studied in great detail.[58-69] The studies include bimolecular PET reactions and PET reactions in linked systems. The various processes taking place in bimolecular PET reactions of AN-DMA

can be summarised as in Scheme 3.1. Similar processes will be occurring in the case of PY-DMA system also.

Separated species | Encounter complex | Exciplex

$$AN + DMA \xrightarrow{h\nu} {}^1AN^* + DMA \longrightarrow ({}^1AN^* + DMA) \longrightarrow ({}^1AN^* \cdots DMA)$$

path 'a'

$${}^3AN^* + DMA \xleftarrow{\text{path 'd'}} {}^3(AN^{\bullet-} \ DMA^{\bullet+}) \xleftarrow{\text{path 'd'}} {}^1(AN^{\bullet-} \ DMA^{\bullet+}) \qquad ({}^3AN^* \cdots DMA)$$

path 'c' | path 'b'

$$AN + DMA \xleftarrow[\text{CR}]{\text{CR}} AN^{\bullet-} + DMA^{\bullet+} \xrightarrow[\text{CR}]{\text{path 'c'}} {}^3AN^* + DMA$$
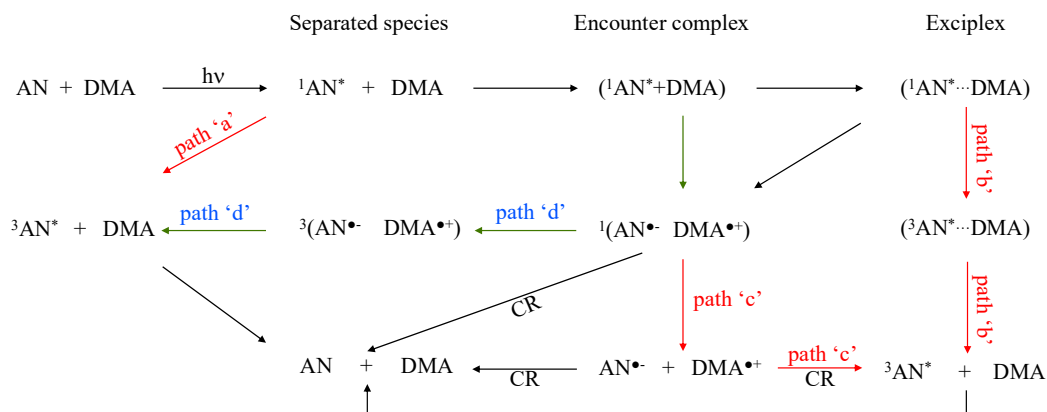
Scheme 3.1. General reaction scheme for fluorescence quenching of AN by DME

AN is excited to its singlet excited state which accepts an electron from DMA to give the CS state, which can be detected in flash photolysis experiments. But CR takes place to the ground state reactants or to the triplet excited state of AN. According to Scheme 3.1, the molecular triplet, ${}^3AN^*$ can be formed in four different pathways (paths a-d). Path 'a' is formation of ${}^3AN^*$ from ${}^1AN^*$ through intersystem crossing. In path 'b', the exciplex formed in the singlet state undergo intersystem crossing to triplet exciplex, which then dissociate to ${}^3AN^*$ and ground state DMA. In path 'c' the ${}^3AN^*$ is formed by recombination of radical ions that has escaped from the cage (this is termed homogeneous recombination). In path 'd', the ${}^3AN^*$ is formed by geminate recombination in the triplet radical pair, which is formed from the singlet radical pair state. In this case the triplet state formation requires spin realignment in the radical pair state. This spin multiplicity change occurs through the hyperfine-coupling-induced coherent spin motion of the unpaired electron spins.[70-73] The hyperfine interaction can couple the singlet and triplet states only if the interaction energy ΔE_{hfi} is greater than spin exchange interaction ($2J$). At the

encounter distance of ~ 7 Å, $2J > \Delta E_{hfi}$ and hence the spin multiplicity change will not occur. But $2J$ decreases exponentially with distance and if the radical pairs separate to distances close to 15 Å within its lifetime, ΔE_{hfi} will become larger than $2J$, and spin realignment can occur in the geminate radical pair. $^3AN^*$ formation through paths 'a' and 'b' involve spin-orbit-coupling-induced intersystem crossing and this is not affected by external magnetic fields. When AN is irradiated in the presence of DMA in nonpolar solvents ($\varepsilon_s < 10$), electron transfer does not occur and $^3AN^*$ is formed through paths 'a' or 'b' and its yield is not affected by external magnetic field. But when the experiment is performed in polar solvents ($\varepsilon_s > 20$), PET occurs and triplet is generated through paths 'c' or 'd'. The triplet formation shows a fast component (~ 10 ns) arising from the geminate recombination and slow component (~ 600 ns) arising from the homogeneous recombination. External magnetic field does not affect the homogeneous component, but slows down the geminate component by a factor of 1.5. Thus, study of magnetic field effect can isolate the two components of radical recombination and provide information about the structure and dynamics of radical pairs and influence of exchange and hyperfine interactions on the electron spin motion.

Covalently linked AN-DMA and PY-DMA systems were also studied in detail. The covalent linker in most cases are –$(CH_2)_n$-, where n varied from 0-16. Scheme 3.2 shows the process taking place in alkyl chain-linked AN-DMA systems when the AN moiety is excited.

$$AN\text{-}(CH_2)_n\text{-}DMA \xrightarrow{h\nu} {}^1AN^*\text{-}(CH_2)_n\text{-}DMA \xrightarrow{k_{CS}} {}^1(^\bullet AN^*\text{-}(CH_2)_n\text{-}DMA^{\bullet +})$$

$$k_{CR}$$

$$^3AN^*\text{-}(CH_2)_n\text{-}DMA \longleftarrow {}^3(^{\bullet -}AN^*\text{-}(CH_2)_n\text{-}DMA^{\bullet +})$$
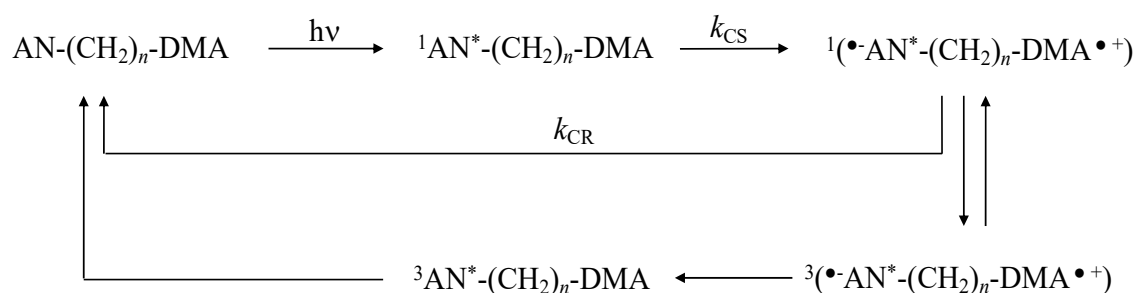
Scheme 3.2. Photo-process taking place in AN-$(CH_2)_n$-DMA

All the diffusion processes possible for unlinked systems (Scheme 3.1) will be absent in linked systems. Excitation of the AN moiety in the dyad leads to $^1AN^*$, which accepts an electron from DMA to give the CS state. Since electron transfer takes place in the singlet manifold, the CS state is formed with overall singlet spin. Since the radical ion centers are close in space, the spins will be correlated. In systems where $n < 6$, the CS state formed is short-lived, but can be detected in picosecond-femtosecond flash photolysis. Since the lifetimes are so short, spin realignment and triplet formation will not occur in these systems. When $n > 6$, the CS states have slightly longer lifetimes and R_e is large such that $2J \sim \Delta E_{hfi}$ and spin realignment to triplet state can occur in the radical pair. For systems with n is 6 - 8, R_e values are less than 15 Å and in these cases, although ^3CS state is formed through spin alignment, the quantum yields are low. For systems with $n > 9$, spin realignment in the radical pair is very facile as $2J < \Delta E_{hfi}$. $^3AN^*$ is formed with high quantum yields in these cases.

In this chapter we have explored the PET processes in the AD spaced dyads AN-AD-DMA and PY-AD-DMA. Structures of these molecules are given in Figure 3.5. In these systems the donor and acceptor are separated by 3 carbon atoms or 4 *trans* C-C single bonds. The edge-to-edge donor-acceptor distances in the AD bridged systems will be similar to the corresponding C3-alkyl chain bridged systems. Structures of the C3 chain bridged systems are also given in Figure 3.5. One major difference between the alkyl chain bridged systems with the AD spaced systems is to be mentioned here. In AN-AD-DMA, attachment of DMA is through the 2-position of AN, whereas in AN-$(CH_2)_3$-DMA the attachment is through the 9-position of AN. Similarly, in PY-AD-DMA the attachment of DMA is through the 2- position of PY, whereas in PY-$(CH_2)_3$-DMA the attachment is through the 1- position of PY. These differences, however, are not expected to make any differences in the PET processes. The rigidity of the AD bridge and

the orientation of the AN or PY with respect to the orientation of DME in the 1,3-AD substituted systems are expected to make some contribution to the PET reactions of the AD-bridged systems.
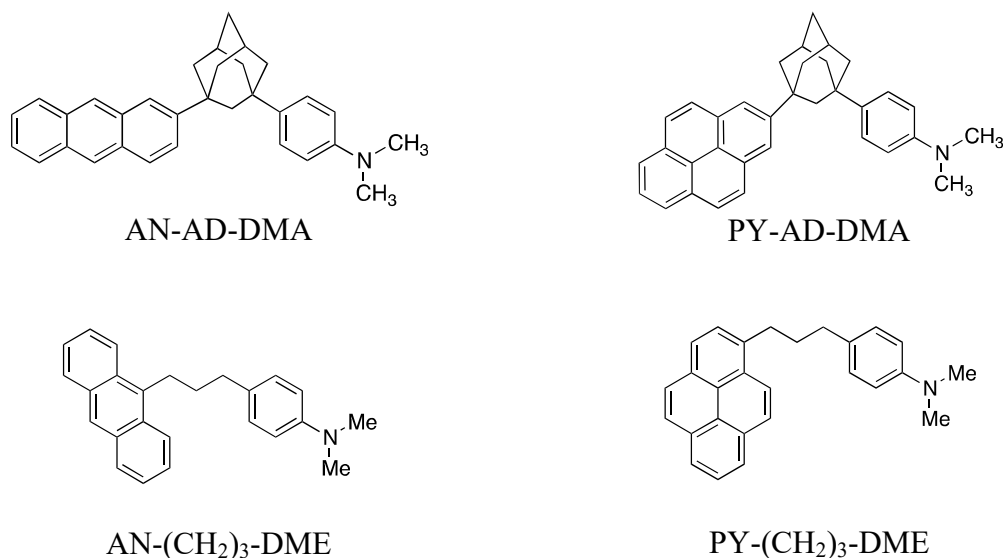
Figure 3.5. Structures of the molecules studied in this chapter.

AN-(CH$_2$)$_3$-DMA and PY-(CH$_2$)$_3$-DMA exhibit very similar photophysics, which depends on the polarity of the solvent employed. Photo processes taking place in AN-(CH$_2$)$_3$-DMA are shown in Figure 3.6.[60-64] Upon excitation ^{1}AN*-(CH$_2$)$_3$-DMA is generated, which in nonpolar solvents undergo intramolecular exciplex formation. In hexane solution emission from the exciplex can be observed around 470-480 nm, which is red shifted by ~ 50 nm in 2-propanol. The intramolecular exciplex is formed only if the AN and DMA moieties can achieve certain geometries. If the alkyl chain length is less ($n < 3$), this geometry is not achieved and intramolecular exciplex is not formed in nonpolar solvents. In polar solvents such as acetonitrile, electron transfer occurs from DMA to ^{1}AN* to generate the CS state, $^{\bullet+}$AN-(CH$_2$)$_3$-DMA$^{\bullet-}$. The CS state is very short lived. Mataga et al. reported that for AN-(CH$_2$)$_3$-DMA, the CS state is

formed within 2.7 ps and exhibited lifetime of 700 ps in acetonitrile.[67] The corresponding values

reported for PY-$(CH_2)_3$-DMA were 11 ps and 1.1 ns. Okada et al. reported that for PY-$(CH_2)_3$-

DMA in acetonitrile, the CS state is formed within 100 ps and exhibited lifetime of 800 ps.[60]
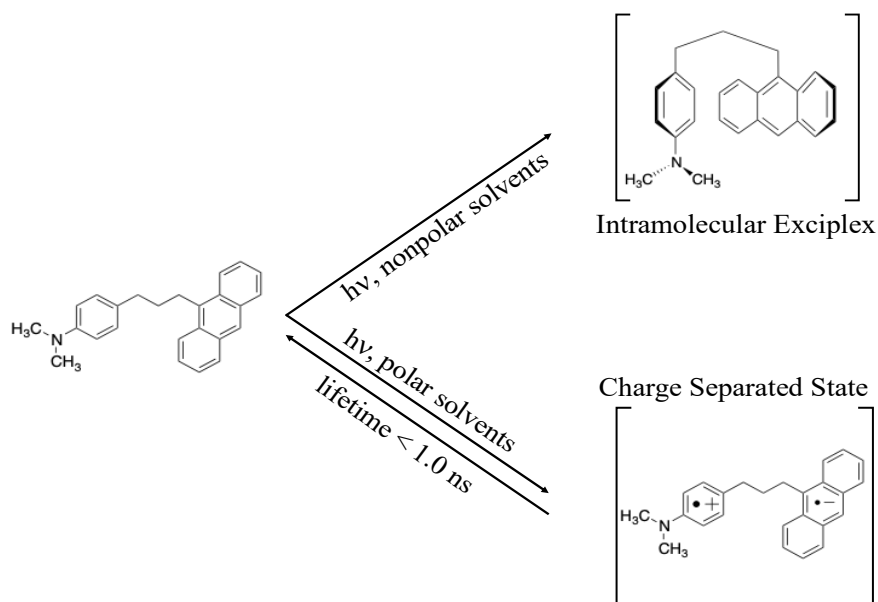
Figure 3.6. Excited state processes in AN-C3-DMA.

3.3. Results and Discussion

3.3.1. Synthesis and Characterization of AN-AD-DMA and PY-AD-DMA

AN-AD-DMA and PY-AD-DMA were prepared by the triflic acid mediated Friedel-

Crafts reaction of 3-(4-nitrophenyl)-1-adamantanol (**27**) with AN or PY followed by reductive

methylation. The adamantane derivative **27** was prepared as shown in Scheme 3.3. Friedel-Crafts

alkylation of benzene with 1-bromoadamantane (**23**) in the presence of anhydrous $FeCl_3$ catalyst

gave 1-phenyladamantane (**24**) in good yield. This was nitrated using fuming nitric acid in

glacial acetic acid. Nitration occurs only at the para position of the phenyl ring due to the steric

bulk of the adamantyl group. Compound **24** was brominated to give 1-bromo-3-(4-

nitrophenyl)adamantane (**25**). Since the phenyl ring in **24** is deactivated by the presence of the

nitro group, the phenyl group will not be brominated. The bromo derivative is converted to the

hydroxy derivative by heating in DMF containing water.
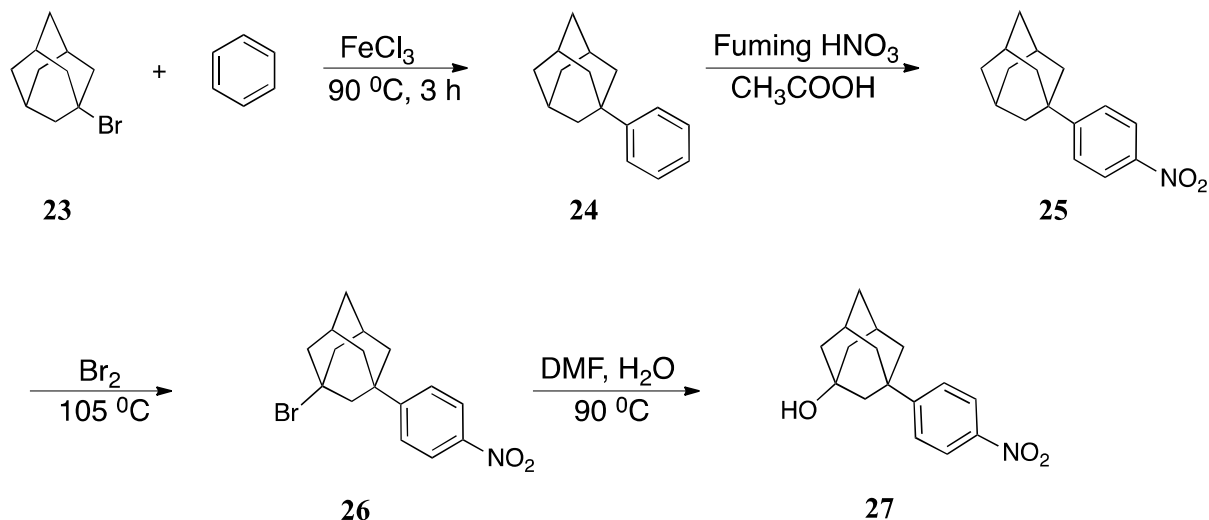
Scheme 3.3. Scheme for synthesis of 3-(4-nitrophenyl)-1-adamantanol

The target molecule AN-AD-DMA was prepared by the triflic acid catalysed Friedel-

Crafts reaction of **27** with anthracene followed by reductive methylation of the nitro group using

hydrogen and formaldehyde as shown in Scheme 3.4.
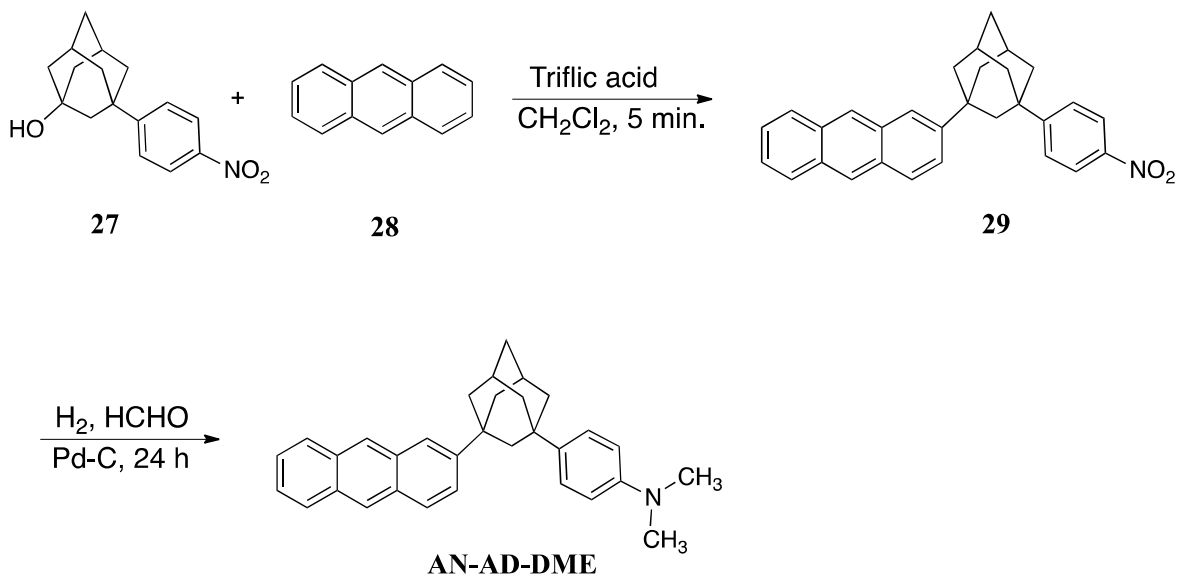
Scheme 3.4. Scheme for synthesis of AN-AD-DMA

PY-AD-DMA was prepared by a similar scheme (Scheme 3.5)
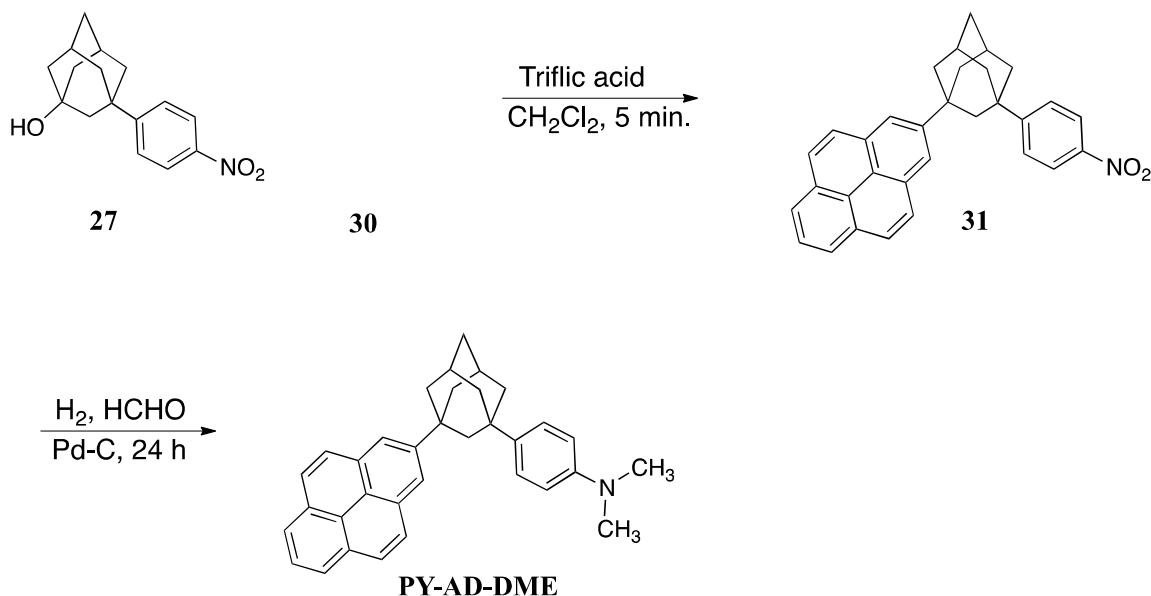
Scheme 3.5. Scheme for synthesis of PY-AD-DMA

In electrophilic substitution reactions such as Friedel-Crafts alkylation, AN and PY are normally substituted at the 1-position. Substitution of bulky alkyl groups such as *tert*-butyl or 1-adamantyl occurs at the 2-position of AN and PY. In case of di-substitution with these bulky groups, reaction occurs at the 2- and 6- positions of AN and 2- and 7- positions of pyrene. All the products and intermediates are characterised by spectroscopic techniques (see experimental).

3.3.2. Photophysical Studies

Figure 3.7A compares the absorption spectrum of AN and AN-AD-DMA in acetonitrile. Although the maxima of the 0-0 band remained the same for the two compounds, the intensities of the peaks are slightly dampened in AN-AD-DMA. The absorption features below 325 nm is attributed to the DMA chromophore. A small shoulder is seen near 400 nm. This shoulder on the absorption edge may be due to electronic interaction between the donor DMA and acceptor AN moieties. In order to see if this is due to charge-transfer interactions, we have obtained the

absorption spectra in solvents of different polarities and this is presented in Figure 3.7B. In less polar solvents, such as benzene and dichloromethane the spectra exhibited slight red shifts compared to the spectra obtained in polar solvents acetonitrile and methanol. In all solvents the shoulder pattern remains same and did not show solvatochromic shift. This suggests that this band is not due to any charge transfer interaction.

A

B
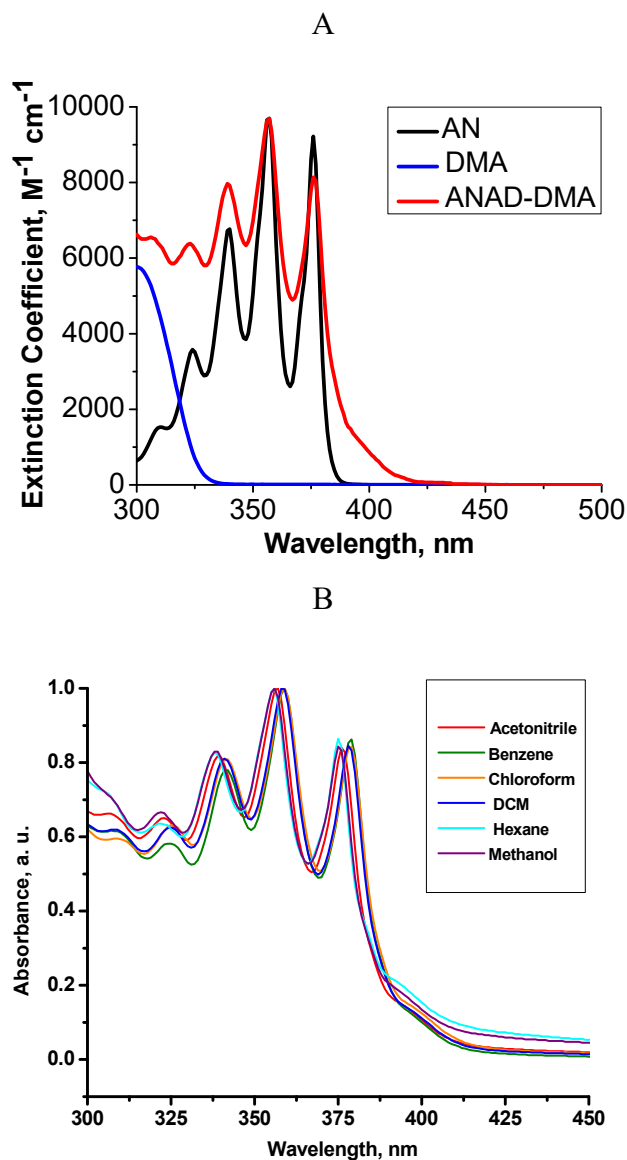
Figure 3.7. (A) Comparison of absorption spectra of AN and AN-AD-DMA in acetonitrile and (B) Absorption spectra of AN-AD-DMA is different solvents.

Figure 3.8A compares the absorption spectra of PY and PY-AD-DMA in acetonitrile. As can be seen in the figure, the maxima of all the three absorption peaks are red-shifted slightly for the DMA substituted system. All the three peaks are dampened in intensity and small absorption is seen in the 350-400 nm region. As in the case of the AN system, this broad absorption may be due to electronic interaction between the PY and DMA moieties.
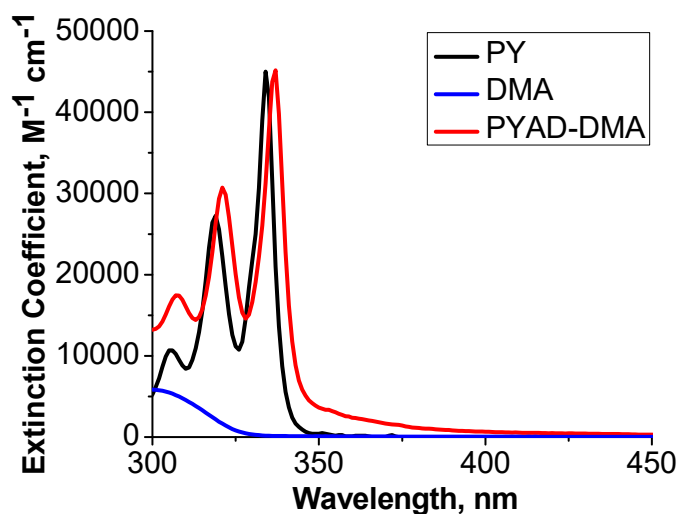
Figure 3.8. (A) Comparison of absorption spectra of PY and PY-AD-DMA in acetonitrile

Figure 3.9A compares the fluorescence of AN with that of AN-AD-DMA in acetonitrile. The figure shows that the presence of DMA leads to considerable quenching of the fluorescence of the AN chromophore. The PY-AD-DMA exhibited some aggregation in acetonitrile. Hence the emission spectrum of this compound was taken in dichloromethane. In Figure 3.9B, the emission spectra of PY is compared with that of PY-AD-DMA. It can be noted that the emission is quenched very much (but not as much as that in Figure 3.9A). It may also be noted that the emission spectra of PY-AD-DMA extends beyond 500 nm and this is most probably due to excimer or exciplex. However, how excimer or exciplex formation occurs in PY-AD-DMA is not clear at this stage.
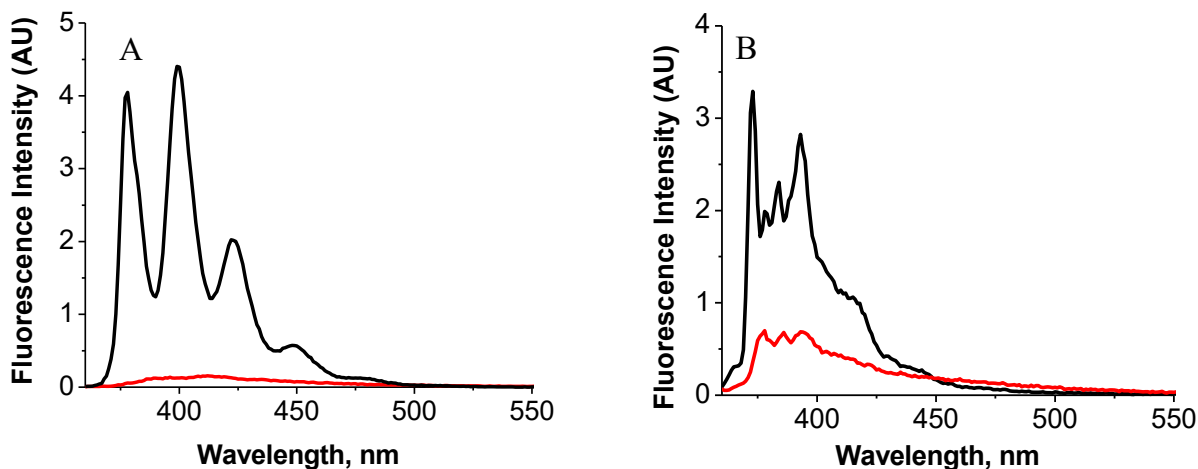
Figure 3.9. (A) Comparison of the emission spectra of AN (—) and AN-AD-DMA (—) in acetonitrile and (B) PY (—) and PY-AD-DMA (—) in dichlromethane. Excitation wavelength was 340 nm for the AN systems and 330 nm for the PY systems.

3.3.3. Electrochemical Aspects

Photoinduced electron transfer in AN-DMA and PY-DMA systems are very well studied and the redox potentials of these molecules are available even in several books.[74,75] Hence no attempts were made to determine the redox potentials in the AD-bridged dyads. We assumed that AD bridging did not affect the redox potentials of AN, PY and DMA or the excitation energies of AN and PY. We used the following values from the literature. DMA: E_{ox} = 0.81 V vs. SCE; AN: $E_{0,0}$ = 3.31 eV, E_{red} = -1.93 V vs. SCE; PY: $E_{0,0}$ = 3.33 eV, E_{red} = -2.09 vs. SCE. Values of the redox potentials and excitation energies were used in the Weller equation (equation 1.9, Chapter 1) to get the ΔG for electron transfer from DMA to singlet excited states of AN and PY. The center-to-center distance d_{cc} in equation 1.9 is assumed as 12 Å. ΔG_{PET} values obtained for the AN-AD-DMA and PY-AD-DMA systems were -0.602 eV and -0.462 eV, respectively. ΔG_{PET} values were negative and thermodynamically allowed for both the systems. Taking the AN based system as example, the following reactions will occur upon irradiation.

$$\text{AN-AD-DMA} \xrightarrow{\text{h}\nu\ =\ 355\ \text{nm}} {}^1\text{AN}^*\text{-AD-DMA} \qquad (3.1)$$

$$^1\text{AN}^*\text{-AD-DMA} \xrightarrow{\text{ET}} {}^{\bullet-}\text{AN-AD-DMA}^{\bullet+} \qquad (3.2\ )$$

$$^{\bullet-}\text{AN-AD-DMA}^{\bullet+} \xrightarrow{\text{CR}} \text{AN-AD-DMA} \qquad (3.3)$$
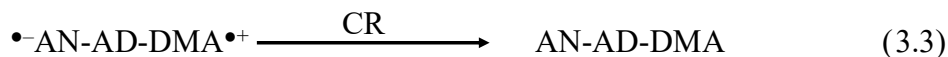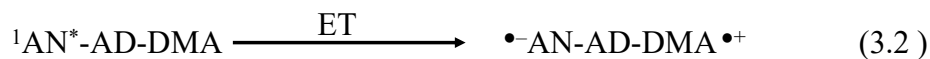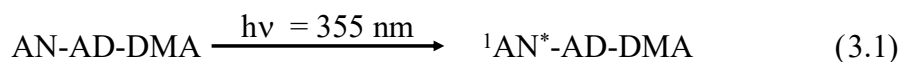
Rate constant for the PET reaction (k_{PET}) can be obtained from fluorescence lifetime studies. Free energy change for the charge recombination reaction (ΔG_{CR}) were calculated using equation 1.14 (Chapter 1) and the values obtained for AN-AD-DMA and PY-AD-DMA were -2.74 eV and -2.9 eV, respectively. These reactions are expected to be in the deep inverted region and the rate constant can be obtained from transient absorption studies.

3.3.4. Fluorescence Lifetime Studies

AN and PY exhibited exponential decays and the lifetimes (τ_0) obtained were 4.8 and 100 ns, respectively. Fluorescence decays of AN-AD-DMA and PY-AD-DMA were biexponential and are presented in Figure 3.10.
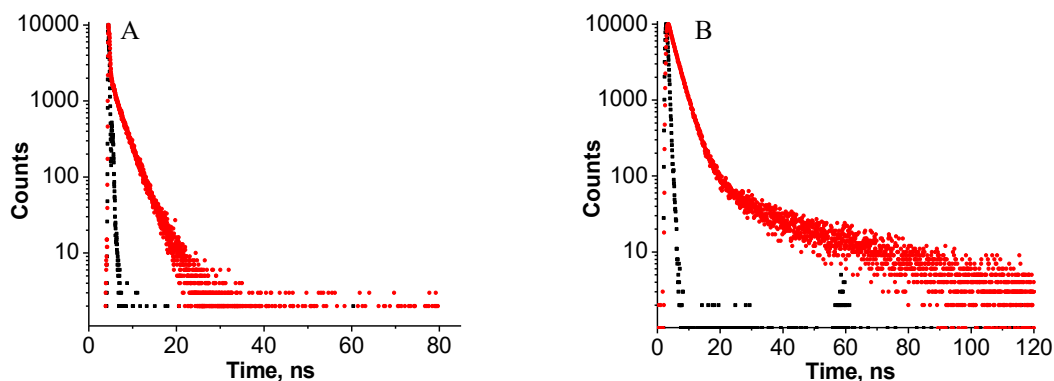
Figure 3.10. Fluorescence decay profiles of (A) AN-AD-DMA and (B) PY-AD-DMA. The lamp profiles are also shown (•••). Excitation was by a 331 nm Nano-LED. For AN-AD-DMA emission was collected at 400 nm and for PY-AD-DMA emission was collected at 380 nm.

The decays were fitted using biexponential function and the parameters obtained are given in Table 3.1.

Table 3.1. Parameters obtained in the fluorescence decay analysis

Dyad	τ_1 ns, (%)	τ_2 ns, (%)	χ^2
AN-AD-DMA	0.234, (94.5%)	3.0, (5.5%)	1.18
PY-AD-DMA	2.13, (93%)	15, (7%)	1.19

The fast component of the decays (τ_1) contributes to about 95% and this is attributed to PET process. The long lifetime component (τ_2), which contributes to about 5% of the decay is attributed to small amounts of aggregates or excimers present in the solution. The fast component is used for calculation of k_{PET}. The k_{PET} values were calculated using equation 1.12 (Chapter 1). Substituting the values of τ_1 and τ_0 in equation 1.12, we get $k_{PET} = 4.06 \times 10^9$ s^{-1} for AN-AD-DMA and 4.60×10^8 s^{-1} for PY-AD-DMA. Inspection of the ΔG_{PET} values for these electron transfers (-0.602 eV for AN-AD-DMA and -0.462 eV for PY-AD-DMA) suggests that these systems fall in the normal region of the Marcus parabola. The AN-AD-DMA has more driving force and the rate is higher for this system.

3.3.5. Laser Flash Photolysis Studies

It is clear from the above studies that excitation of AN in AN-AD-DMA (or PY in PY-AD-DMA) leads to electron transfer from ground state DMA to the singlet excited state of AN (or PY). In order to get detailed information about these processes, AN-AD-DMA and PY-AD-DMA were subjected to laser flash photolysis using the 355 nm light of a Nd-YAG laser. The transient absorption spectra obtained at 390 ns, 780 ns and 1.24 μs following the laser excitation are shown in Figure 3.11A. The spectra exhibited absorptions at 430, 470 and 710 nm. Figures 3.11B,C show the decay profiles of the transients at 430 and 470 nm.
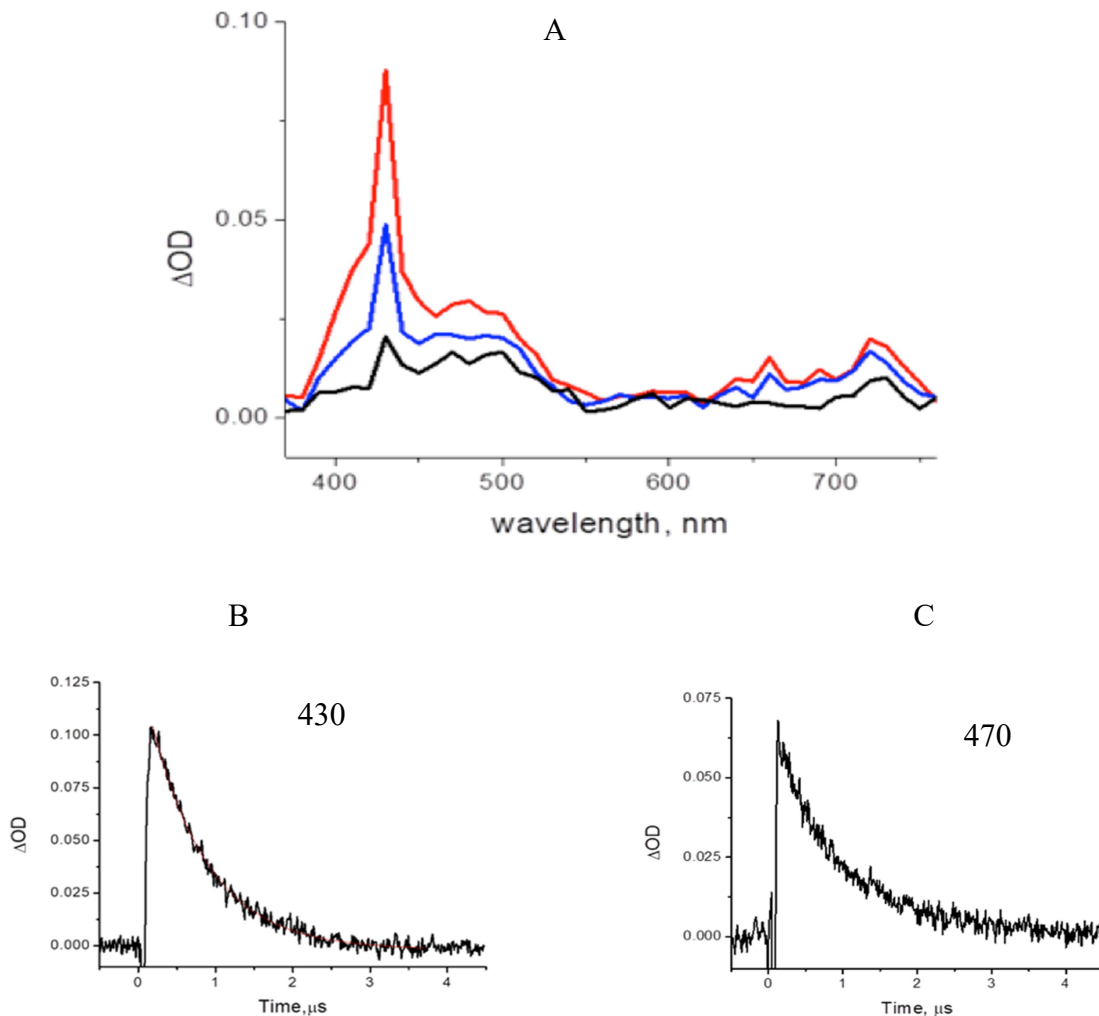
Figure 3.11. (A) Transient absorption spectra obtained at 390 ns (red), 780 ns (blue) and 1.24 μs (black) in the flash photolysis of AN-AD-DMA in acetonitrile. (B) and (C) show decay kinetics of transients at 430 and 470 nm.

The transient spectrum obtained at 390 ns is nearly identical to the transient absorption spectrum obtained in the flash photolysis of AN in the presence of high concentrations of DMA (0.3 M). This is shown in Figure 3.12. The 430 nm absorption was assigned to $^3AN^*$, the 470 nm absorption was assigned to $DMA^{\bullet+}$ and the absorptions above 580 nm were assigned to $AN^{\bullet-}$. It may be noted that at longer time windows, the absorptions due to $DMA^{\bullet+}$ and $AN^{\bullet-}$ are absent and only the absorption due to the triplet is observed. Based on this and other reports,[74,76,77] we

have assigned the transients in Figure 3.11A to $^3AN^*$ (430 nm), $DMA^{\bullet+}$ (470 nm) and $AN^{\bullet-}$ (710 nm). $DMA^{\bullet+}$ and $AN^{\bullet-}$ are formed by the electron transfer reaction in equation 3.2.
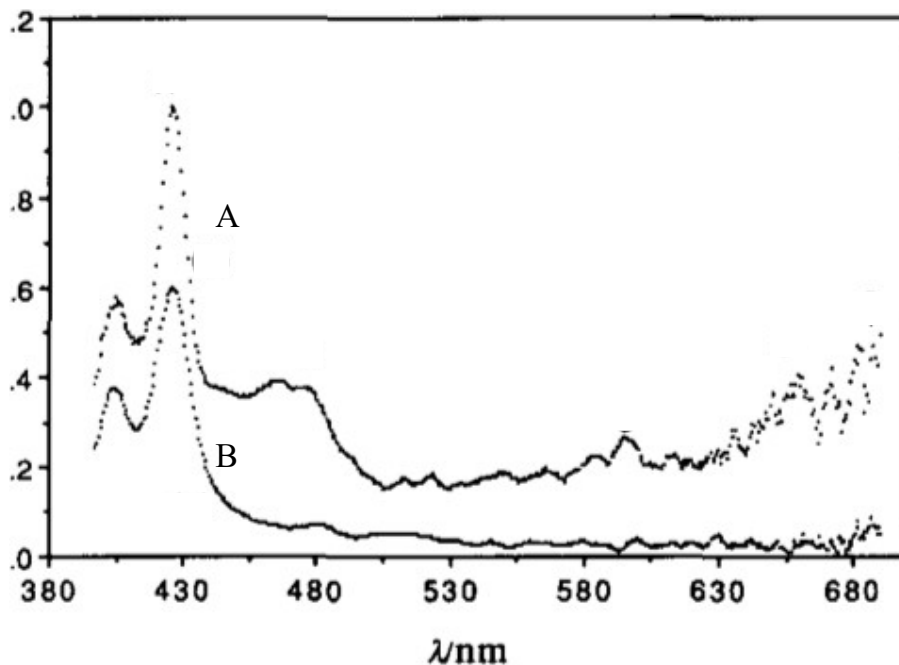
Figure 3.12. Transient absorption spectra obtained in the flash photolysis of AN in the presence of excess DMA. (A) Spectrum taken at 40 ns and (B) spectrum obtained at 160 ns. Taken from reference 43.

Fitting the decay in Figure 3.12B, the lifetime of $^3AN^*$ is obtained as 740 ns. The decay rates of $DMA^{\bullet+}$ at 470 nm (Figure 3.12C) and $AN^{\bullet-}$ at 710 nm were same and attributed to CR reaction to the ground state. Fitting the decay at 470 nm gave the CR rate $k_{CR} = 1.15 \times 10^6$ s^{-1}, which gave $\tau_{CS} = 1/k_{CR} = 872$ ns.

Figure 3.13A shows the transient absorption spectra obtained at 250 and 750 ns following excitation of PY chromophore in PY-AD-DMA. The absorption is very broad and covers the entire region from 400 to 575 nm. As in the case of AN-AD-DMA system, we expect formation of triplet along with radical ions in PY-AD-DMA. The absorptions maxima of $^3PY^*$ (415 and

470 nm)[74], DMA$^{\bullet+}$ (470 nm)[76,77] and PY$^{\bullet-}$ (495 nm)[78] are very close and the broad absorption observed is due to overlapping of these absorptions.

A

B   C   D
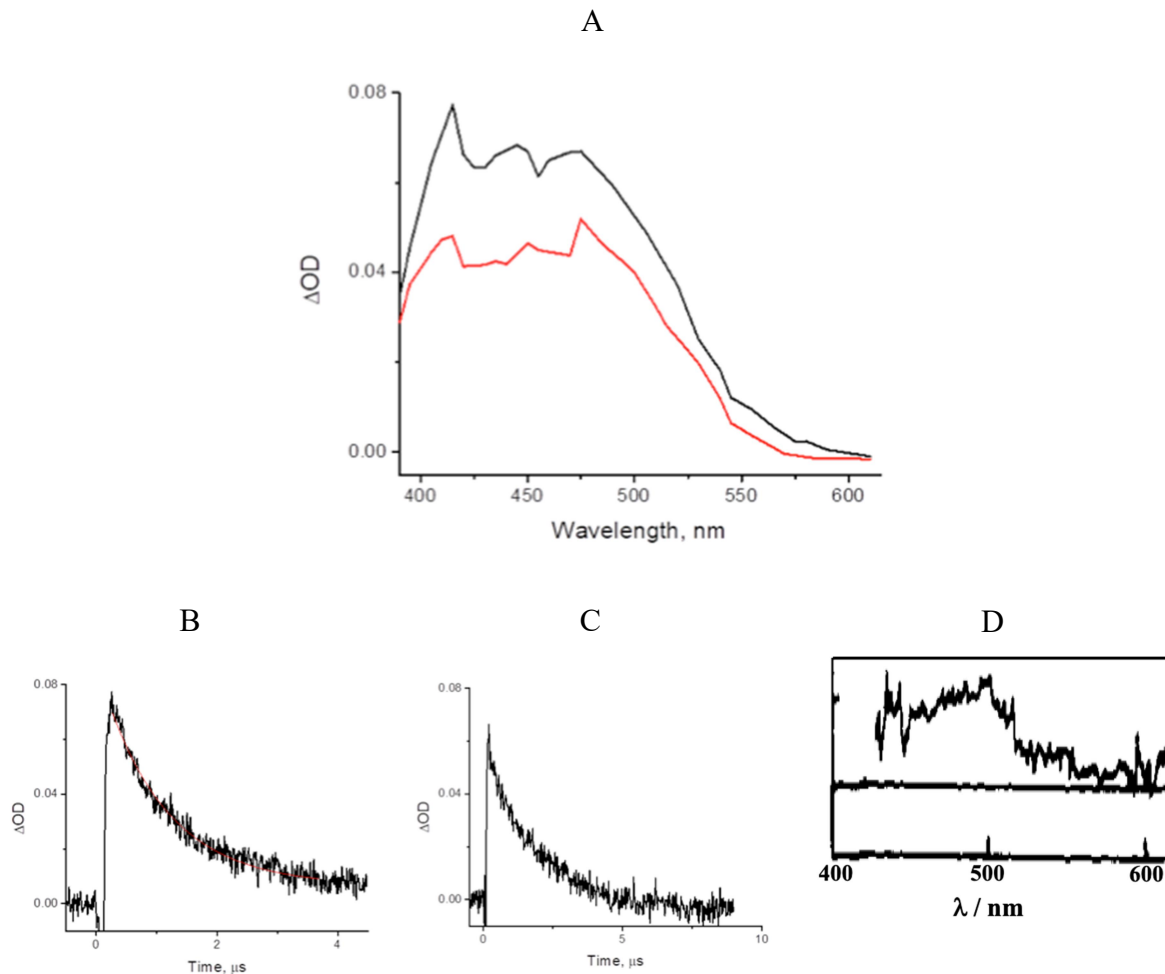
Figure 3.13. (A) Transient absorption spectra obtained at 250 (black) and 750 ns (red) following excitation of PY-AD-DMA; (B) and (C) shows transient decays at 415 and 470 nm, respectively, and (D) is the transient spectrum obtained for PY-(CH$_2$)$_3$-DMA at 2.5 ns (from ref. 79).

Figures 3.13B,C show the decay profiles of transients at 415 and 470 nm. Since the absorptions due to the transients are overlapping, we have not tried to fit the decays to get lifetimes. But it can be seen from the figures that the decays are in the microsecond time domain. In fact, overlapping absorptions due to DMA$^{\bullet+}$ and PY$^{\bullet-}$ are reported at short time scales in the flash

photolysis of PY-(CH$_2$)$_3$-DMA.[79] This is copied in Figure 3.13D. ^{3}PY* was not formed in this study and except for this Figures 3.13A and 3.13D are similar.

In order to understand the origin of triplet formation, the flash photolysis experiments were carried out at shorter timescales. We observed that ^{3}AN* and ^{3}PY* formation is associated with a slow growth process extending to ~ 100 ns, as shown in Figure 3.14.
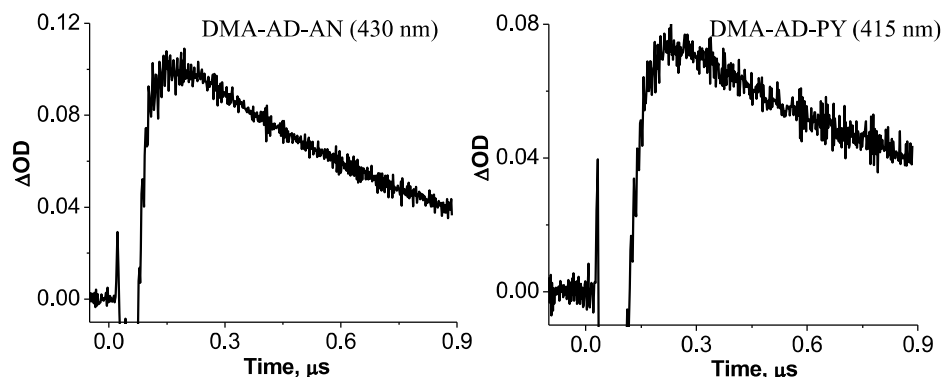
Figure 3.14. Slow growth of triplet absorptions in the flash photolysis of AN-AD-DMA and PY-AD-DMA.

In the case of AN-AD-DMA and PY-AD-DMA, the singlet excited state undergoes electron transfer within 5 ns ($k_{PET} > 2 \times 10^8$ s^{-1}), but triplet formation requires ~ 100 ns. This suggests that the triplet is not formed directly from the singlet excited state through intersystem crossing. Most probably the triplets are formed through intersystem crossing in the singlet RP followed by CR reaction to the triplet, as shown in equation 3.4 and 3.5, respectively.

$$^1(^{\bullet-}\text{AN-AD-DMA}^{\bullet+}) \xrightarrow{\text{ISC}} {}^3(^{\bullet-}\text{AN-AD-DMA}^{\bullet+}) \qquad (3.4)$$

$$^3(^{\bullet-}\text{AN-AD-DMA}^{\bullet+}) \xrightarrow{\text{CR}} {}^3\text{AN}^*\text{-AD-DMA} \qquad (3.5)$$
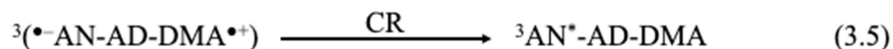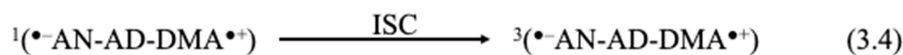
In the case of AN-AD-DMA, the triplet exhibited sharp absorption maximum at 430 nm (Figure 3.11A). This enabled us to determine the quantum yield of triplet formation (Φ_T) using

relative actinometry. An optically matched solution of AN in acetonitrile was used as reference

(R). The decay profiles obtained in the flash photolysis of AN-AD-DMA (referred as sample, S)

and optically matched AN (referred as R) are shown in Figure 3.15.

AN-AD-DMA   Reference solution
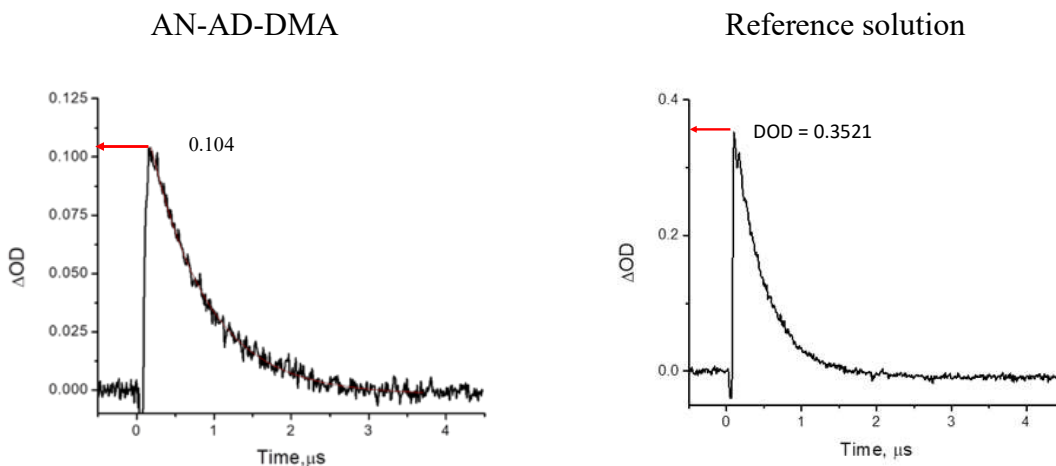
Figure 3.15. Decays profiles of the 430 nm transients in the flash photolysis of DMA-AD-AN
and optically matched solution of AN in acetonitrile.

Equation 3.6 was used to calculate Φ_T,

$$\Phi_{T(S)} = \Phi_R \left[\frac{\Delta OD_S \, \varepsilon_R}{\Delta OD_R \, \varepsilon_S} \right] \qquad (3.6)$$

where Φ_R is the quantum yield for the reference solution, ΔODs are the end-of-pulse optical

densities of the sample and reference solutions and ε_S are the extinction coefficients of the

absorptions. Since the triplets are due to AN, $\varepsilon_R = \varepsilon_S$. Using the known Φ_T value of AN (= 0.71),

we obtained $\Phi_T = 0.21$ for AN-AD-DMA in acetonitrile.

As mentioned in the introduction section of this chapter, in linked AN-$(CH_2)_n$-DMA and

PY-$(CH_2)_n$-DMA systems, formation of $^3AN^*$ or $^3PY^*$ were observed for $n \geq 6$, where R_e is > 8.8

Å. Similar results are also observed in rigid DMN[n]DCV dyads studied in great detail by

Paddon-Row et al.[80] In these cases, triplet formation was observed only for systems for which n

≥ 6 ($R_e \geq 6.8$ Å). For $n = 6$ system, Φ_T was 0.03, which increased to 0.4 for $n = 10$ ($R_e = 11.5$ Å).

For DMA-AD-AN, AN and DMA are separated by three carbon atoms and $R_e \sim 4.6$ Å, and hence formation of $^3AN^*$ with $\Phi_T \sim 0.2$ is unusual. Most probably, the AD spacer is also capable of reducing $2J$ values and the slow formation of $^3AN^*$ suggests that $2J \approx \Delta E_{hfi}$ for DMA-AD-AN. Based on these observations, the photo-processes taking place in AN-AD-DMA can be summarized as in Figure 3.16.
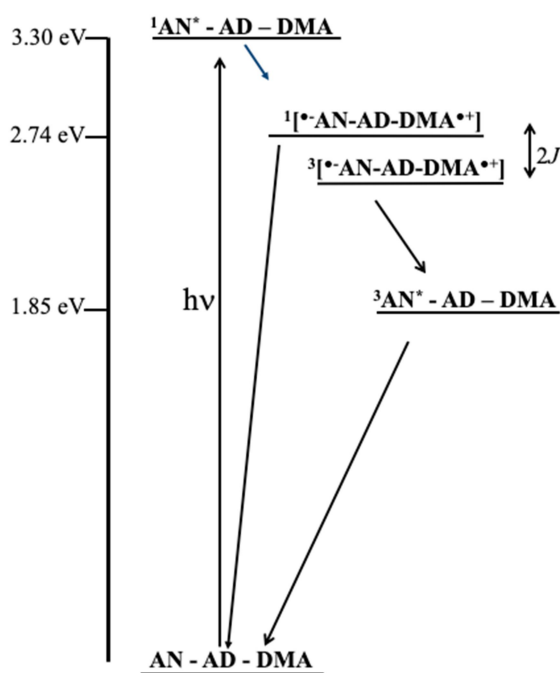
Figure 3.16. Possible photo-processes in AN-AD-DMA

Excitation of AN-AD-DMA with 355 nm laser generates the singlet excited state localised on the AN chromophore. The AN singlet excited state accepts an electron from DMA to generate the radical pair state $^{\bullet-}AN\text{-}AD\text{-}DMA^{\bullet+}$ with overall singlet multiplicity. A fraction of the ion pair state undergoes intersystem crossing to the triplet radical pair state, which undergo charge recombination to generate a triplet state localized on AN. The singlet radical pair state undergoes charge recombination to the ground state with lifetime of ~ 800 ns.

To the best of our knowledge, charge separated state lifetimes exceeding 1.0 ns has not been reported for any singlet excited state mediated electron transfer in compact dyads.[81,82] For the dyads reported in Chapter 2 of this thesis, microsecond lifetimes were possible because of the lack of intersystem crossing in the singlet radical pair state. The only unambiguous strategy for long-lived CS state generation in dyads today is the spin-control approach, in which the CS state is generated in the triplet manifold. The strategy works only if ^{3}CS is the lowest triplet in the dyad and only few examples are known.[83,84] Since the ^{3}CS state is very low in energy, the energy that can be stored in the radical pair is very low (< 1.5 eV) in these systems. For the alkyl chain bridged systems shown in Figure 3.5, $\tau_{CS} \leq 1.0$ ns.[67] In the case of rigid dyad DMN[4]DMV, where $R_e = 4.6$ Å, τ_{CS} was << 1.0 ns.[80] For DMN[6]DMV having $R_e = 6.8$ Å, τ_{CS} was 0.5 ns.[80] τ_{CS} values observed for AD bridged systems studied here are nearly thousand times larger. Even for most of the triad molecules also, τ_{CS} reported are less than 1.0 μs.[81,82] In this context, observation of $\tau_{CS} > 800$ ns for DMA-AD-AN and DMA-AD-PY is extremely important and constitute a significant advance in the study of PET reactions.

According to the Marcus equation (equation 1.11, Chapter 1), the rate constant for electron transfer (photoinduced electron transfer and charge recombination reactions), depend on H_{el}, which is the electronic matrix element which couples the reactant and product states, Gibbs free energy change (ΔG_{et}) and reorganization energy λ. For AN-AD-DMA, $k_{PET} = 4.06 \times 10^9$ s^{-1} and $k_{CR} = 1.15 \times 10^6$ s^{-1} (vide supra). Values obtained for PY-AD-DMA were similar. k_{PET} and k_{CR} values for the –(CH$_2$)$_3$- linked systems in Figure 3.5 were 1-3 orders larger.[67] Since the donor and acceptor chromophores are the same in the AD-bridged and alkyl chain-bridged systems (Figure 3.5), ΔG_{et} and λ values should be identical for both systems. Hence the observed differences in k_{PET} and k_{CR} values must be due to the differences in H_{el} values, attributable to the

AD bridge. For AN-AD-DMA, we have calculated the electronic coupling $H_{el(PET)}$ and $H_{el(CR)}$, respectively for the PET and CR reactions using experimentally observed k values and calculated ΔG and λ values. The reorganization energy $\lambda = \lambda_o + \lambda_i$. λ_o was calculated using equation 1.7 (Chapter 1). ε_{op} in equation 1.7 is the square of the refractive index (n) and ε_s is the dielectric constant. For acetonitrile solvent values reported for $n = 1.3441$ (and hence $\varepsilon_{op} = 1.8066$) and $\varepsilon_s = 37.5$. We also used values of $r_D = 3$ Å, $r_A = 4$ Å and $d_{cc} = 12$ Å (D = DMA and A = AN). Substituting these values, we obtained $\lambda_o = 1.58$ eV. For the reduction reaction of AN to AN$^{\bullet-}$, λ_i reported in the literature is 0.15 eV.[85] We used the same value for the oxidation of DMA to DMA$^{\bullet+}$. Thus, the total internal reorganization energy $\lambda_i = 0.3$ eV. Adding the values, we got $\lambda = 1.88$ eV. This value is assumed to be same for PET and CR reactions. In section 3.3.3 of this chapter we calculated $\Delta G_{PET} = -0.602$ eV and $\Delta G_{CR} = -2.74$ eV for AN-AD-DMA. For the calculation of Hel values, the Marcus equation was rearranged to equation 3.7.

$$H_{el}^2 = \frac{k_{et}}{(2\pi/\hbar)} \frac{\sqrt{4\pi\lambda k_B T}}{\exp[-(\Delta G^0 + \lambda)^2 / 4\lambda k_B T]} \qquad (3.7)$$

For calculating $H_{el(PET)}$ values, values of k_{PET} and ΔG_{PET} were used in equation 3.7. For calculation of $H_{el(CR)}$, values of k_{CR} and ΔG_{CR} were employed. Values of other parameters employed were: $\hbar = 6.5821 \times 10^{-16}$ eV; $k_B = 8.6173 \times 10^{-5}$ eV K^{-1}; T = 298 K; and 1 eV = 8065.73 cm^{-1}. The calculations gave $H_{el(PET)} = 322$ cm^{-1} and $H_{el(CR)} = 0.532$ cm^{-1}. The $H_{el(CR)}$ obtained is three orders of magnitude smaller compared to $H_{el(PET)}$. Thus, the long τ_{CS} obtained in the present study is attributed to the AD bridge, which exhibit extremely small electronic coupling for the CR reaction. The $H_{el(PET)}$ values reported here is comparable to the value of 392

cm^{-1} reported for the DMN[4]DMV system.[81] H$_{el(CR)}$ value was not calculated for this system because τ_{CR} was too short.

It has been recognized early that long CS state lifetimes can be achieved in principle, if H$_{el(PET)}$ is much larger than H$_{el(CR)}$. Early studies by Zeng and Zimmt,[86,87] Oliver et al.,[88] and Wasielewski et al.[89] employed tools such as molecular symmetry, molecular shape and geometrical isomerism, to increase CS state lifetimes, but the enhancements attained were small. Use of AD as bridge gave H$_{el(PET)}$:H$_{el(CR)}$ ratio > 600 for the AN/DMA and AN/PY systems reported in this chapter. If we can establish that use of the AD bridge is a general strategy to enhance this ratio in dyads, it would be an important development in the study of PET reactions.

3.4. Conclusions

In this chapter we employed adamantane as a bridge in the AN/DMA and PY/DMA donor acceptor systems. This is the first time that the AD bridge is used in PET studies. Very important and novel observations are presented in this chapter, which we attribute to the AD bridge. The PET rates in AN-AD-DMA and PY-AD-DMA were 1-2 orders of magnitude slower compared to the corresponding alkyl chain bridged systems shown in Figure 3.5. Remarkably, the charge separated state lifetimes were thousand-fold larger in the AD-bridged systems. We could use nanosecond flash photolysis to identify the radical ion pairs formed in the PET reactions. It appears that the AD spacer also influences the values of singlet-triplet coupling (2*J*) and the hyperfine coupling energy (ΔE_{hfi}) in the radical pair, such that intersystem crossing became possible in the radical pair at short D-A separations.

3.5. Experimental Section

3.5.1. Methods.

Experimental methods employed in this chapter are same as in Chapter 2.

3.5.2. Synthesis of compounds. Synthesis of AN-AD-DMA and PY-AD-DMA were accomplished using Schemes 3.3 – 3.5. Procedures for the synthesis and relevant data of compounds are given below.

3.5.2.1. Synthesis of 1-Phenyladamantane (24): A solution of 1-bromoadamantane (**23,** 4.4 g, 20.5 mmol) in benzene (30 mL) was added drop-wise over a period of 30 min. to a well-stirred mixture of freshly sublimed $FeCl_3$ (1.1 g, 6.75 mmol) and benzene (20 mL). After complete addition, the mixture was refluxed for 3 h and allowed to stand overnight. Poured into ice containing conc. HCl (5 mL). The benzene layer was separated, washed free of acid and dried over anhydrous $CaCl_2$. The benzene was removed and the residue obtained was crystallized from 90% ethanol-water mixture to give **24**. Yield: 3.0 g (69%), mp. 88-89 ^{0}C. ^{1}H NMR (CDCl$_3$, 500 MHz) δ: 1.773 (dd, 6H), 1.923 (s, 6H), 2.097 (s, 3H), 7.171 (m, 1H), 7.305-7.379 (m, 4H). ^{13}C NMR (CHCl$_3$, 125 MHz) δ: 29.0, 36.2, 36.9, 43.2, 124.9, 125.6, 128.2, 151.4. IR (KBr) ν_{max}: 2928, 2901, 2850, 1512, 1447, 1352, 989, 902, 845, 832, 809 cm^{-1}.

3.5.2.2. Synthesis of 1-(4-Nitrophenyl)adamantane (25): To an ice-cold mixture of **24** (2.0 g, 9.42 mmol) and glacial acetic acid (40 mL), fuming nitric acid (24 mL) was added over a period of 30 min. with vigorous stirring. Stirring was continued overnight and then poured into ice-cold water. The solid obtained was extracted with CH_2Cl_2, and the extract washed free of acid, dried and solvent removed to get **25**. Recrystallized from hexane. Yield: 2.0 g (83%), mp. 128-129 ^{0}C. ^{1}H NMR (CDCl$_3$, 500 MHz) δ: 1.792 (dd, 6H), 1.929 (s, 6H), 2.137 (s, 3H), 7.510 (d, 2H), 8.165 (d, 2H) ppm. ^{13}C NMR (CHCl$_3$, 125 MHz) δ: 28.69, 36.51, 36.99, 42.84, 123.40, 125.88, 145.89, 158.90 ppm.

3.5.2.3. Synthesis of 3-Bromo-1-(4-nitrophenyl)adamantane (26): A mixture of **25** (3.0 g, 11.7 mmol) and bromine (4 mL) was refluxed with stirring for 5 h, during which time the temperature was gradually raised from 30 to 105 ^{0}C. The mixture was cooled and the residue dissolved in CCl_4 (100 mL) and poured into water. The mixture was cooled in ice and excess bromine was removed using sodium thiosulfate solution. The CCl_4 layer was separated, dried over anhydrous $CaCl_2$ and solvent removed to get the product **26**. Yield: 2.75 g (70%),

^{1}H NMR ($CDCl_3$, 500 MHz) δ: 1.779 (dd, 2H), 1.945 (s, 4H), 2.387 (m, 6H), 2.521 (s, 2H), 7.498 (d, 2H), 8.188 (d, 2H) ppm. ^{13}C NMR ($CHCl_3$, 125 MHz) δ: 32.33, 34.45, 40.98, 41.67, 48.07, 53.67, 64.37, 123.64, 125.80, 146.30, 156.00 ppm.

3.5.2.4. Synthesis of 3-Hydroxy-1-(4-nitrophenyl)adamantane (27): Compound **26** (1.0 g, 2.97 mmol) was dissolved in DMF (10 mL) and heated to 90 ^{0}C. Water (5 mL) was added drop-wise at this temperature and heating continued for 24 h. The mixture was poured into HCl-ice mixture. The solid obtained was filtered, washed with excess water and dried to get the product **27**. Yield: 730 mg (90%), mp-129-130 ^{0}C NMR ($CDCl_3$, 500 MHz) δ: 1.674 (s, 2H), 1.780-1.889 (m, 10 H), 2.381 (s, 2H), 7.500 (d, 2H), 8.178 (d, 2H) ppm.

3.5.2.5. Synthesis of 1-(anthracen-2-yl)-3-(4-nitrophenyl)adamantane (29): To a mixture of anthracene (0.5 g, 2.81 mmol) and triflic acid (1.68 g, 11.2 mmol) in CH_2Cl_2 (30 mL), compound **27** (0.77 g, 2.82 mmol) was added in one lot with vigorous stirring. After 5 minutes of stirring, the reaction was quenched by adding ice-water. CH_2Cl_2 (50 mL) was added and layers separated. The CH_2Cl_2 layer was washed free of acid, dried with anhydrous Na_2SO_4 and solvent removed to get a residue, which was chromatographed over silica gel. Elution with hexane gave unreacted anthracene. Further elution with hexane-chloroform (8:2) mixture gave the product **29**. Yield:

490 mg (40%), mp-203-204 ^{0}C ^{1}H NMR (CDCl$_3$, 500 MHz) δ: 1.872 (s, 2H), 2.029-2.171 (m, 10H), 2.430 (s, 2H), 7.445 (m, 2H), 7.586 (m, 3H), 7.864 (s, 1H), 7.971-7.995 (m, 3H), 8.193 (d, 2H), 8.388 (d, 2H) ppm. ^{13}C NMR (CHCl$_3$, 125 MHz) δ: 29.34, 35.71, 37.49, 38.11, 41.70, 42.09, 48.19, 122.59, 123.52, 123.92, 125.11, 125.27, 125.68, 126.00, 126.17, 128.09, 128.11, 128.16, 130.50, 131.55, 131.82, 131.87, 146.08, 146.58, 158.11 ppm. HRMS calculated for C$_{30}$H$_{27}$NO$_2$: 433.2035, Observed: 433.20355.

3.5.2.6. Synthesis of AN-AD-DMA:

To mixture of Pd-C (0.03 g, 10 %) and **29** (0.43 g, 1 mmol) under vacuum conditions added 30 % Formaldehyde (0.30 g, 3 mmol) and 30 ml Ethanol and stirred well. The solution was then purged with Hydrogen gas for overnight. After the completion of reaction, confirmed using TLC silica gel plate, the mixture was passed through celite pad. The filtrate was concentrated to remove the solvent followed by washing with water to remove formaldehyde which was then chromatographed over silica gel. Elution with hexane-chloroform (8:2) mixture gave unreacted starting material. Further elution with hexane-chloroform (7:3) mixture gave the product **29**. Yield: (230 mg) 55 %, mp. 138-139 ^{0}C. ^{1}H NMR (CDCl$_3$, 500 MHz) δ: 1.619-1.989 (m, 2H), 2.074-2.150 (m, 4H), 2.365 (s, 2H), 2.936 (m, 6H), 6.786 (d, 2H), 7.255 (s, 2H), 7.320 (d,2H), 7.420-7.437 (t, 2H), 7.868 (s, 1H), 7.948-7.988(t, 3H). ^{13}C NMR (CHCl$_3$, 125 MHz) δ: 14.11, 22.69, 29.65, 36.06, 37.67, 42.52, 48.80, 122.31, 122.52, 124.94, 125.11, 125.59, 125.68, 126.1, 127.85, 128.1, 128.15, 130.52, 131.47, 131.96, 147.42 HRMS calculated for C$_{30}$H$_{27}$NO$_2$: 431.26, Observed: 432.27.

3.5.2.7. Synthesis of 1-(pyren-2-yl)-3-(4-nitrophenyl)adamantane (31):

To a mixture of Pyrene (0.5 g, 2.47 mmol) and triflic acid (1.49 g, 9.9 mmol) in CH$_2$Cl$_2$ (30 mL), compound **27** (0.68 g, 2.47 mmol) was added in one lot with vigorous stirring. After 5 minutes of

stirring, the reaction was quenched by adding ice-water. CH_2Cl_2 (50 mL) was added and layers separated. The CH_2Cl_2 layer was washed free of acid, dried with anhydrous Na_2SO_4 and solvent removed to get a residue, which was chromatographed over silica gel. Elution with hexane gave unreacted anthracene. Further elution with hexane-chloroform (8:2) mixture gave the product **29**. Yield: 450 mg (40%), 212-215 ^{0}C; ^{1}H NMR (CDCl$_3$, 500 MHz) δ: 1.870-1.950 (m, 2H), 1.989-1.2.052 (m, 4 H) 2.210-2.295 (m, 6H), 2.419 (s, 2H), 7.548(d, 2H), 7.911 (s, 1H), 7.925-7.993 (m, 4H), 8.087 - 8.146 (m, 6H). ^{13}C NMR (CHCl$_3$, 125 MHz) δ: 29.53, 35.72, 37.73, 38.32, 42.11, 42.65, 49.23, 121.69, 123.55, 124.87, 125.67, 126.05, 127.44, 128.09, 127.52, 130.99, 131.15, 147.32, 158.12. HRMS calculated for $C_{30}H_{27}NO_2$: 457.57, Observed: 457.57.

3.5.2.8. Synthesis of PY-AD-DMA:

To mixture of Pd-C (0.03 g, 10 %) and **29** (0.45 g, 1 mmol) under vacuum conditions added 30 % Formaldehyde (0.30 g, 3 mmol) and 30 ml Ethanol and stirred well at room temperature. The solution was then purged with Hydrogen gas for overnight. After the completion of reaction, confirmed using TLC silica gel plate, the mixture was passed through celite pad. The filtrate was concentrated to remove the solvent followed by washing with water to remove formaldehyde which was then chromatographed over silica gel. Elution with hexane-chloroform (8:2) mixture gave unreacted starting material. Further elution with hexane-chloroform (7:3) mixture gave the product **29**. Yield (135 mg) 30%. mp: 151-152 ^{0}C. ^{1}H NMR (CDCl$_3$, 500 MHz) δ: 1.811-1.865 (m, 2H), 1.930-1.956 (q, 2H), 1.985-2.157 (m, 2H), 2.344 (s, 2H), 2.860 (m, 6H), 6.700 (d, 2H), 7.278 (d, 2H), 7.872-7.902 (m, 4H), 7.973 (s, 1H), 8.064 (d, 2H), 8.156 (d, 2H). ^{13}C NMR (CHCl$_3$, 125 MHz) δ:13.08, 28.58, 35.09, 35.54, 36.91, 39.84, 41.42, 42.10, 48.85, 111.83, 120.94, 123.67, 124.47, 124.52, 126.17, 126.62, 129.99, 130.04, 147.73. HRMS calculated for $C_{30}H_{27}NO_2$: 455.65, Observed: 456.65

3.6. References

1. Kwon, O.; Barlow, S.; Odom, S. A.; Beverina, L.; Thompson, N. J.; Zojer, E.; Brédas, J.-L.; Marder, S. A. Aromatic Amines: A Comparison of Electron-Donor Strengths. *J. Phys. Chem. A* **2005,** *109,* 9346-9352

2. Mann, C. K.; Barnes, K. K. *Electrochemical Reactions in Nonaqueous Systems*, Marcel Dekker Inc., New York, 1970, pp 260-269.

3. Shida, T. *Electronic Absorption Spectra of Radical* Ions, Elsevier Science Publishers B. V.: Amsterdam, 1988. pp 207-239.

4. Weiss, D. S.; Cowdery, J. R.; Young, R. H. in *Electron Transfer in Chemistry*, Balzani, V. (Ed.), Wiley-VCH, Verlag GmBH, 2001, Vol. 5, Part 2, pp 379-471.

5. Bender, T. P.; Graham, J. F.; Duff, J. M. Effect of Substitution on the Electrochemical and Xerographic Properties of Triarylamines: Correlation to the Hammet Parameter of the Substituent and Calculated HOMO Energy Level. *Chem. Mater.* **2001**, *13*, 4105-4111.

6. Swayamprabha, S. S.; Dubey, D. K.; Shahnawas; Yadav, R. A. K.; Nagar, M. R.; Sharma, A.; Tung, F.-C.; Jou, J.-H. Approaches for Long Lifetime Organic Light Emitting Diodes. *Adv. Sci.* **2021**, *8*, 2002254. DOI: 10.1002/advs.202002254.

7. Pak, S.; Kang, J.; Hwang, N.; Cho, S.; Lee, S. E.; Kim, Y. K.; Yoon, S. S. Fabrication of Blue Organic Light-Emitting Diodes Based on Indeno-Phenanthrene/Triphenylene Amine Derivatives. *J. Nanosci. Nanotech.* **2019**, *19*, 1597-1602.

8. Stolz, S.; Lemmer, U.; Hernandez-Sosa, G.; Mankel, E.; Correlation of Device Performance and Fermi-Level Shift in the Emitting Layer of Organic Light-Emitting Diodes with Amine-Based Electron Injection Layers. *ACS Appl. Mater. Interfaces* **2018**, *10*, 8877-8884.

9. Qin, Y.; Li, G.; Qi, T.; Huang, H. Aromatic Imide/Amide-Based Organic Small Molecules Emitters for Organic Light-Emitting Diodes. *Mater. Chem. Front.* **2020**, *4*, 1554-1568.

10. Wang, K.-L.; Jiang, J.-C.; Jhu, C.-H.; Wada, S.; Sassa, T.; Horie, M. High-Performance Organic Photorefractive Materials Containing 2-Ethylhexyl Plasticised Poly(triarylamine). *J. Mater. Chem. C* **2020**, *8*, 13357-13367.

11. Tsutsumi, N. Molecular Design of Photorefractive Polymers. *Polym. J.* **2016**, *48*, 571-588.

12. Masumura, K.; Nakanishi, I.; Thi Khuat, K. V.; Kinashi, K.; Sakai, W.; Tsutsumi, N. *Sci. Reports* **2019**, *9:739*. DOI: 10.1038/s41598-018-36980-2.

13. Patil, D. S.; Avhad, K. C.; Kadam, M. M.; Sekar, N. Synthesis of Red Emitting Triphenylamine Derived NLOphoric D–π–A Molecules: Photophysical and Viscosity Sensing Studies. *SN Applied Sciences* **2019**, *1:259*. DOI: 10.1007/s42452-019-0268-z.

14. Liu, F.; Yang, Y.; Cong, S.; Wang, H.; Zhang, M.; Bo, S.; Liu, J.; Zhen, Z.; Liu, X.; Qiu, L. Comparison of Second-Order Nonlinear Optical Chromophores with D-π-A, D-A-π-A and D-D-π-A Architectures: Diverse NLO Effects and Interesting Optical Behavior. *RSC Advance* **2014**, *4*, 52991-52999.

15. Tykwinski, R. R.; Gubler, U.; Martin, R. E.; Diederich, F.; Bosshard, C.; Günter, P. Structure-Property Relationships in Third-Order Nonlinear Optical Chromophores. *J. Phys. Chem. B* **1998**, *102*, 4451-4465.

16. Jadhav, M.; Vaghasiya, J. V.; Patil, D.; Soni, S. S.; Sekar, N. Effect of Donor Modification on the Photo-Physical and Photo-Voltaic Properties of *N*-alkyl/aryl Amine Based Chromophores. *New J. Chem.* **2019**, *43*, 8970-8981.

17. Estrella, L. L.; Balanay, M. P.; Kim, D. H. The Effect of Donor Group Rigidification on the Electronic and Optical Properties of Arylamine-Based Metal-Free Dyes for Dye Sensitized Solar Cells: A Computational Study. *J. Phys. Chem. A* **2016**, *120*, 5917-5922.

18. Ho, C.-L.; Wong, W.-Y. High Performance Arylamine-Based Metallated and Metal Free Organic Photosensitizers for Dye-Sensitized Solar Cells. *J. Photochem. Photobiol. C* **2016**, *28*, 138-158.

19. Liang, M.; Chen, J. Arylamine Organic Dyes for Dye-Sensitized Solar Cells. *Chem. Soc. Rev.* **2013**, *42*, 3453-3488.

20. Venkatesan, M.; Mandal, H.; Bheerappagari, R.; Bangal, P. R. Bimolecular Photoinduced Electron Transfer Between 7-Methylbenzo9[a]pyrene and Aromatic Amine Donors in Stationary and Static Regimes. *J. Photochem. Photobiol. A: Chem.* **2019**, *376*, 212-223.

21. Venkatesh, Y.; Munisamy, V.; Ramakrishna, B.; Kumar, P. H.; Mandal, H.; Bangal, P. R. Photoinduced Bimolecular Electron Transfer from Aromatic Amines to Pentafluorophenyl Porphyrin Combined with Ultrafast Charge Recombination Persistence with Marcus Inverted Region. *Phys. Chem. Chem. Phys.* **2017**, *19*, 5658-5673.

22. El-Nahass, M. N.; Fayed, T. A.; El-Morsi, M. A.; Photoinduced Intermolecular Electron Transfer from Donating Amines to Accepting Diarylethylenes in Different solvents. *J. Solution Chem.* **2015**, *44*, 1757-1776.

23. Samant, V.; Varne, M.; Palit, D. K. Dynamics of Intermolecular Electron Transfer from Amines to the Excited States of 9-Fluorenone. *J. Photochem. Photobiol. A: Chem.* **2013**, *264*, 1-11.

24. Dhenadhayalan, N.; Selvaraju, C. Role of Photoionization on the Dynamics and Mechanism of Photoinduced Electron Transfer Reaction of Coumarin 307 in Micelles. *J. Phys. Chem. B* **2012**, *116*, 4908-4920.

25. Kamino, B. A.; Morse, G. E.; Bender, T. P. Effect of Triarylamine Structure on the Photoinduced Electron Transfer to Boron Subphthalocyanine. *J. Phys. Chem. C* **2011**, *115*, 20716-20723.

26. Satpati, A. K.; Nath, S.; Kumbhakar, M.; Maity, D. K.; Semthilkumar, S.; Pal, H. Bimolecular Electron Transfer Reactions in Coumarin-Amine Systems: Donor-Acceptor Orientational Effect on Diffusion Controlled Reaction Rates. *J. Mol. Struct.* **2008**, *878*, 84-94.

27. Pan, Y.; Gao, Y.; Yan, L.; Pan, H.; Chen, J.; Yu, S. Reactivity of Aromatic Amines with Triplet 1,8-Dihydroxyanthraquinone: A Laser Flash Photolysis Study. *Spectrochim. Acta, A: Molecular and Biomolecular Spectroscopy* **2007**, *66A*, 63-67.

28. Pan, Y.; Fu, Y.; Liu, S.; Yu, H.; Gao, Y.; Guo, Q.; Yu, S. Studies on Photoinduced H-Atom and Electron Transfer Reactions of *o*-Naphthoquinones by Laser Flash Photolysis. *J. Phys. Chem. A* **2006**, *110*, 7316-7322.

29. Chakraborty, A.; Chakrabarty, D.; Seth, D.; Hazra, P.; Sarkar, N. Photoinduced Intermolecular Electron Transfer from Electron Donating Solvents to Coumarin Dyes in Bile Salt Aggregates: Role of Diffusion in Electron Transfer Reaction. *Spetochim. Acta, A: Molecular and Biomolecular Spectroscopy* **2006**, *63A*, 594-602.

30. Kumbhakar, M.; Nath, S.; Mukherjee, T.; Pal, H. Effect of Micellar Environment on Marcus Correlation Curve for Photoinduced Bimolecular Electron Transfer Reactions. *J. Chem. Phys.* **2005**, *123*, 034705. DOI:10.1063/1.1953579

31. Kumbhakar, M.; Nath, S.; Mukherjee, T.; Pal, H. Kinetics and Mechanism of Bimolecular Electron Transfer Reaction in Quinone-Amine Systems in Micellar Solution. *J. Chem. Phys.* **2005**, *122*, 084512. DOI: 10.1063/1.1856457.

32. Kumbhakar, M.; Nath, S.; Mukherjee, T.; Pal, H. Intermolecular Electron Transfer Between Coumarin Dyes and Aromatic Amines in Trixon-X-100 Micellar Solution: Evidence for Marcus Inverted Region. *J. Chem. Phys.* **2004**, *120*, 2824-2834.

33. Kumbhakar, M.; Nath, S.; Rath, M. C.; Mukherjee, T.; Pal, H. Electron Transfer Interaction of Dihydroxyquinones with Amine Quenchers: Dependence of the Quenching Kinetics on the Aliphatic and Aromatic Nature of the Amine Donors. *Photochem. Photobiol.* **2004**, *79*, 1-10.

34. Sasaki, Y.; Araki, Y.; Fujitsuka, M.; Ito, O.; Hirao, A.; Nishizawa, H. Photoinduced Electron Transfer and Electron-Mediating Systems from Aromatic Amines to Triplet States of C_{60} and C_{70} in the Presence of a Viologen Dication. *Photochem. Photobiol. Sci.* **2003**, *2*, 136-141.

35. Clark, C. D.; Hoffman, M. Z. Solvent Reorganization Energy in Excited-State Electron Transfer Reactions. Quenching and Geminate-Pair Back Electron Transfer. *J. Phys. Chem.* **1996**, *100*, 14688-14693.

36. Levin, P. P.; Costa, S. M. B.; Ferreira, L. F. V. Kinetics of Intersystem Electron Transfer within Triplet Radical Ion Pairs on Silica Studied by Diffuse Reflectance Laser Flash Photolysis. Bell-Shaped Energy Gap Dependence on the Surface. *J. Phys. Chem.* **1995**, *99*, 1267-1275.

37. Park, J.; Kim, D.; Suh, Y. D.; Kim, S. K. Comparative Study on Photoinduced Electron Transfer from *N,N*-Dimethylaniline (DMA) and 4,4'-Methylenebis(*N,N*-dimethylaniline) (BDMA) to C_{60} and C_{70} in Toluene. *J. Phys. Chem.* **1994**, *98*, 12715-12719.

38. Miyasaka, H.; Morita, K.; Kamada, K.; Nagata, T.; Kiri, M.; Mataga, N. Femtosecond-Picosecond Laser Photolysis Studies on Reduction Process of Excited Benzophenone with Tertiary Aromatic Amines in Acetonitrile Solution. *Bull. Chem. Soc. Jpn.* **1991**, *64*, 3229-3244.

39. Rajagopal, S.; Vijayalakshmi, N. Steric Effects in Photoinduced Electron Transfer Reactions of Ruthenium(II) Complexes with Aromatic Amines. *Ind. J. Chem. Section A.* **1991**, *30A*, 604-608.

40. Levin, P. P.; Pluzhnikov, P. F.; Kuzmin, V. A. Energy Gap Dependence for Intersystem Crossing within Charge Transfer Triplet Exciplexes. *Chem. Phys.* **1989**, *137*, 331-344.

41. Kitamura, N.; Kim, H. B.; Okano, S.; Tazuke, S. Photoinduced Electron Transfer Reactions of Ruthenium(II) Complexes. 1. Reductive Quenching of Excited Tris(2,2'-bipyridine)ruthenium^{2+} by Aromatic Amines. *J. Phys. Chem.* **1989**, *93*, 5750-5756.

42. Garrera, H. A.; Gsponer, H. E.; Garcia, N. A.; Cosa, J. J.; Prevatili, C. M. Solvent Effect and Activation Parameters for the Photoinduced Electron Transfer Between Ru(bpy)$_3$$^{2+}$ and Aromatic Amines. *J. Photochem.* **1986**, *33*, 257-260.

43. Mac, M.; Najbar, J.; Wirz, J. Fluorescence Quenching of Derivatives of Anthracene by Organic Electron Donors and Acceptors in Acetonitrile. Electron and Proton Transfer Mechanism. *Chem. Phys. Lett.* **1995**, *235*, 187-194.

44. Zhang, G.; Thomas, J. K.; Eremenko, A.; Kikteva, T.; Wilkinson, F. Photoinduced Charge-Transfer Reaction Between Pyrene and *N,N*-Dimethylaniline on Silica Gel Surfaces. *J. Phys. Chem. B* **1997**, *101*, 8569-8577.

45. Paul, A.; Samanta, A. Photoinduced Electron Transfer Reactions in Room Temperature Ionic Liquids: A combined Laser Flash Photolysis and Fluorescence Study. *J. Phys. Chem. B.* **2007**, *111*, 1957-1962.

46. Zhang, G.; Thomas, J. K. Effect of Charge Stabilization on Electron Transfer Reactions in Zeolites. *J. Phys. Chem. B* **2003**, *107*, 7254-7260.

47. Mataga, N.; Okada, T.; Kanda, Y.; Shioyama, H. Behavior of Radical Ion Pairs Produced by Photoinduced Electron Transfer in Polar Solutions. *Tetrahedron* **1986**, *42*, 6143-6148.

48. Chang, Y. J.; Chow, T. J. Triaryl Linked Donor Acceptor Dyads for High Performance Dye-Sensitized Solar Cells. *Tetrahedron* **2009**, *65*, 9626-9632.

49. Breimaier, S.; Winter, R. F. Electrochemical and spectroscopic Studies on Triarylamine-Polychlorotriphenylmethyl Dyads with Particularly Strong Triarylamine Donors. *Eur. J. Org. Chem.* **2021**, 4690-4700.

50. Shen, J.-J.; Zhong, Y.-W. Long-Range Ruthenium-Amine Electronic Communication Through the *para*-Oligophenylene Wire. *Sci. Reports* **2015**, *5*-13835. DOI: 10.1038/srep13835.

51. Wadas, T. J.; Chakraborty, S.; Lachicotte, R. J.; Wang, Q.-M.; Eisenberg, R. Facile Synthesis, Structure, and Luminescence Properties of Pt(diimine)bis(arylacetylide) Chromophore-Donor Dyads. *Inorg. Chem.* **2005**, *44*, 2628-2638.

52. Kirilov, P.; Matondo, H.; Vicendo, P.; Garrigues, J.-C.; Baboulène, M.; Nguyen, H.-P.; Rico-Lattes, I. Synthesis and Photophysical Properties of Novel Amphiphilic

Ruthenium(II) Complexes Containing 4,4'-Dialkylaminoethyl-2,2'-bipyridyl Ligands. *Appl. Organometal. Chem.* **2006**, *20*, 125-129.

53. Ajayakumar, G.; Gopidas, K. R. Long-Lived Photoinduced Charge Separation in New Ru(bipyridine)$_3^{2+}$ - Phenothiazine Dyads. *Photochem. Photobiol. Sci.* **2008**, *7*, 826-833.

54. Prasad, E.; Gopidas, K. R. Photoinduced Electron Transfer in Hydrogen Bonded Donor-Acceptor Systems. Study of the Dependence of Rate on Free Energy and Simultaneous Observation of Marcus and Rehm-Weller Behaviors. *J. Am. Chem. Soc.* **2000**, *122*, 3191-3196.

55. Smitha, M. A.; Prasad, E.; Gopidas, K. R. Photoinduced Electron Transfer in Donor-Acceptor Systems. Free Energy and Distance dependence Studies and an Analysis of the Role of Diffusion. *J. Am. Chem. Soc.* **2001**, *123*, 1159-1165.

56. Sessler, J. L.; Sathiosatham, M.; Brown, C. T.; Rhodes, T. A.; Wiederrecht, G. Hydrogen-Bond-Mediated Photoinduced Electron Transfer: Novel Dimethylaniline-Anthracene Ensembles Formed via Watson-Crick Base-Pairing. *J. Am. Chem. Soc.* **2001**, *123*, 3655-3660.

57. Lin, Z.; Lawrence, C. M.; Xiao, D.; Kireev, V. V.; Skourtis, S. S.; Sessler, J. L.; Beratran, D. N.; Rubtsov, I. V. Modulating Unimolecular Charge Transfer by Exciting Bridge Vibrations. *J. Am. Chem. Soc.* **2009**, *131*, 18060-18062.

58. Mataga, N. Migita, M.; Nishimura, T. Picosecond Chemistry of Some Exciplex Systems. *J. Mol. Structure*. **1978**, *47*, 199-219.

59. Yang, N. C.; Neoh, S. B.; Naito, T.; Ng, L.-K.; Chernoff, D. A.; McDonald, D. B. Chemistry of Exciplexes. Viscosity Effect on Intramolecular Exciplex Formation in Saturated Hydrocarbons. *J. Am. Chem. Soc.* **1980**, *102*, 2806-2810.

60. Okada, T.; Migita, M.; Mataga, N.; Sakata, Y.; Misumi, S. Picosecond Laser Spectroscopy of Intramolecular Heteroexcimer Systems. Time-Resolved Absorption Studies. *J. Am. Chem. Soc.* **1981**, *103*, 4715-4720.

61. Okada, T.; Karaki, I.; Matsuzawa, E.; Mataga, N.; Sakata, Y.; Misumi, S. Ultrafast Intersystem Crossing in Some Intramolecular Heteroexcimers. *J. Phys. Chem.* **1981**, *85*, 3957-3960.

62. Migita, M.; Okada, T.; Mataga, N.; Sakata, Y.; Misumi, S.; Nakashima, N.; Yoshihara, K. Picosecond Laser Spectroscopy of Intramolecular Heteroexcimer Systems. Time-Resolved Fluorescence Studies of p-(CH$_3$)$_2$NC$_6$H$_4$-(CH$_2$)$_n$-(9-Anthryl), p-(CH$_3$)$_2$NC$_6$H$_4$-(CH$_2$)$_n$-1-Pyrenyl) Systems and 9,9'-Bianthryl. *Bull. Chem. Soc. Jpn*. **1981**, *54*, 3304-3311.

63. Crawford, M. K.; Wang, Y.; Eisenthal, K. B. Effect of Conformation and Solvent Polarity on Intramolecular Charge Transfer: A Picosecond Laser Study. *Chem. Phys. Lett.* **1981**, *79*, 529-533.

64. Wang, Y.; Crawford, M. C.; Eisenthal, K. B. Picosecond Laser Studies of Intramolecular Excited-State Charge-Transfer Dynamics and Small Chain Relaxation. *J. Am. Chem. Soc*. **1982**, *104*, 5874-5878.

65. Heitele, H.; Michel-Beyerele, M. E. Electron Transfer through Aromatic Spacers in Bridged Electron-Donor-Acceptor Molecules. *J. Am. Chem. Soc.* **1985**, *107*, 8286-8288.

66. Okada, T.; Mataga, N.; Baumann, W.; Siemiarczuk, A. Picosecond Laser Spectroscopy of 4-(9-Anthryl)-N,N-dimethylaniline and Related Compounds. *J. Phys. Chem.* **1987**, *91*, 4490-4495.

67. Mataga, N.; Nishikawa, S.; Asahi, T.; Okada, T. Femtosecond-Picosecond Laser Photolysis Studies on the Photoinduced Charge Separation and Charge Recombination of a

Produced Ion Pair State of Some Typical Intramolecular Exciplex Compounds in Alkanenitrile Solvents. *J. Phys. Chem.* **1990**, *94*, 1443-1447.

68.   Tanaka, F.; Keawwangcha, S.; Rujkorakarn, R.; Mataga, N. Study of Photoinduced Electron Transfer in Pyrene-$(CH_2)_n$-*N,N*-dimethylaniline System by Molecular Dynamic Simulation. *Chem. Phys.* **2008**, *348*, 242-248.

69.   Rujkorakarn, R.; Tanaka, F. Three Representations of Photoinduced Electron Transfer Rates in Pyrene-$(CH_2)_n$-N,N-dimethylaniline Systems Obtained by Three Electron Transfer Theories. *J. Molecular Graphics and Modelling* **2009**, *27*, 571-577.

70.   Weller, A.; Staerk, H.; Treichel, R. Magnetic-field Effects on Geminate Radical-pair Recombination. *Faraday Discuss. Chem. Soc.* **1984**, *78*, 271-278.

71.   Staerk, H.; Busmann, H.-G.; Kühnle, W.; Weller, A. Solvent Effects on the Magnetic-Field-Dependent Reaction yields of Photogenerated Radical Ion Pairs. *Chem. Phys. Lett*. **1989**, *155*, 603-608.

72.   Busmann, H.-G.; Staerk, H.; Weller, A. Solvent Influence on the Magnetic Field Effect of Polymethylene-Linked Photogenerated Radical Ion Pairs. *J. Chem. Phys.* **1989**, *91*, 4098-4105.

73.   Werner, U.; Kühnle, W; Staerk, H. Magnetic Field Dependent Reaction Yields from Radical Ion Pairs Linked by a Partially Rigid Aliphatic Chain. *J. Phys. Chem.* **1993**, *97*, 9280-9287.

74.   Murov, S. L.; Carmichael, I.; Hug, G. L. *Handbook of Photochemistry*, Second Edition, Revised and Expanded. Marcel Dekker Inc. New York, 1993.

75.   Kavarnos, G. J. *Fundamentals of Photoinduced Electron Transfer*, VCH Publishers, Inc. New York, 1993.

76. Forster, M.; Hester, R. E. Photoionization of Dimethylaniline and of the Donor-Aromatic-Acceptor Molecules *p*-$(CH_3)_2NC_6H_4R$, R = CN, COOH, COOEt, CHO, NO_2, in Glasses of Ethanol and Etanediol/Water at 77-125 K. *J. Chem. Soc., Faraday Trans. 2* **1981**, *77*, 1521-1534.

77. Holcman, J.; Sehested, K. Dissociation of the OH Adduct of N,N-Dimethylaniline in Aqueous Solution. *J. Phys. Chem.* **1977**, *81*, 1963-1966.

78. Getoff, N.; Solar, S.; Richter, U.-B.; Haenel, M. W. Pulse Radiolysis of Pyrene in Aprotic Polar Organic Solvents; Simultaneous Formation of Pyrene Radical Cations and Radical Anions. *Radiat. Phys. Chem.* **2003**, *66*, 207-214.

79. Swinnen, A. M.; Van der Auweraer, M.; De Schryver, F. C.; Nakatani, K.; Okada, T.; Mataga, N. Photophysics of the Intramolecular Exciplex Formation in ω-(1-Pyrenyl)-α-N,N-dimethylaminoalkanes. *J. Am. Chem. Soc.* **1987**, *109*, 321-330.

80. Paddon-Row, M. N. Covalently Linked Systems Based on Organic Components. In *Electron Transfer Chemistry*; Balzani, V., Ed; Wiley-VCH: Weinheim, 2001; Vol. 3, pp 179-271.

81. Verhoeven, J. W. On the Role of Spin Correlation in the Formation, Decay, and Detection of Long-Lived Intramolecular Charge-Transfer States. *J. Photochem. Photobiol. C* **2006**, *7*, 40-60.

82. Hou, Y.; Zhang, X.; Chen, K.; Liu, D.; Wang, Z.; Liu, Q.; Zhao, J.; Barbon, A. Charge Separation, Charge Recombination, Long-Lived Charge Transfer State Formation and Intersystem Crossing in Organic Electron Donor/Acceptor Dyads. *J. Mater. Chem. C* **2019**, *7*, 12048-12074.

83.   Smit, K. J.; Warman, J. M. The Formation of Singlet and Triplet Charge Transfer States on Photo-Excitation of Carbazole-$(CH_2)_n$-Tetrachlorophthalimide Compounds Studied by Time-Resolved Microwave Conductivity. *J. Lumin*. **1988**, *42*, 149-154.

84.   Anglos, D.; Bindra, V.; Kuki, A. Photoinduced Electron Transfer and Long-Lived Charge Separation in Rigid Peptide Architectures. *J. Chem. Soc., Chem. Commun*. **1994**, 213-215.

85.   Klimkāns, A.; Larsson, S. Reorganization Energies in Benzene, Naphthalene and Anthracene. *Chem. Phys*. **1994**, *189*, 25-31.

86.   Zeng, Y.; Zimmt, M.B. Symmetry Effects in Photoinduced Electron Transfer Reactions. *J. Am. Chem. Soc*. **1991**, *113*, 5107-5109.

87.   Zeng, Y.; Zimmt, M.B. Symmetry Effects on Electron Transfer Reactions: Temperature Dependence as a Diagnostic Tool. *J. Phys. Chem*. **1992**, *96*, 8395-8403.

88.   Oliver, A. M.; Paddon-Row, M. N.; Kroon, J.; Verhoeven, J. W. Orbital Symmetry Effects on Intramolecular Charge Recombination. *Chem. Phys. Lett*. **1992**, *191*, 371-377.

89.   Wasielewski, M. R.; Niemczyk, M. P.; Johnson, D. G.; Svec, W. A.; Minsek, D. W. Ultrafast Photoinduced Electron Transfer in Donor-Spacer-Acceptor Molecules: Modification of Spacer Energetics as a Probe for Superexchange. *Tetrahedron* **1989**, *45*, 4785-4806.

Photoinduced Electron Transfer Studies of Adamantane-Bridged Dyads with Hydrocarbon Donors and Nitrobenzene Acceptor

4.1. Abstract

This chapter reports the synthesis, characterization and photophysical studies of four adamantane bridged compact dyads. The donors employed in the dyads are aromatic hydrocarbons anthracene, pyrene, diphenyl anthracene and perylene. Nitrobenzene, which is a well-known electron acceptor, was the acceptor component in all the dyads. Substitution of the adamantane-nitrobenzene groups did not alter the singlet excited state properties of the hydrocarbon donors. All the four dyads exhibited very low fluorescence due to PET from the singlet excited state of the hydrocarbons to the nitrobenzene. In laser flash photolysis studies, we observed transients assignable to long-lived radical ion products. In the case of AN-AD-NB and PY-AD-NB, prominent absorptions due to the local triplet states were also observed. In order to get some insight into the long-lived CS state formation we obtained the single crystal X-ray structures of two of the dyads. Based on the X-ray crystal structure we suggested that restricted rotation of the D and A chromophores in the dyads are responsible for the long lifetime of the charge separated state. The radical anion and radical cation moieties are held in spatially orthogonal orientations because of the adamantane structure, leading to a reduction in the coupling element for the recombination reaction.

4.2. Introduction

Nitroaromatics, due to the presence of electron withdrawing nitro groups, are considered as electron-poor molecules. Because of the electron deficient nature, nitroaromatics can easily undergo one-, two- or multi-electron reductions.[1] One-electron reduction of nitroaromatics leads to formation of their radical anions which are highly air sensitive as they can undergo very fast reaction with molecular oxygen to give superoxide ion. Two-electron reduction of nitroaromatics leads to formation of nitroso compounds and subsequently to hydroxyl amines. Multi-electron reduction of nitroaromatics give aryl amines as the final products. Most reducing agents are capable of reducing nitroaromatics. They can also be reduced electrochemically.

Because of the presence of the strong electron-withdrawing nitro group, nitrobenzene (NB) is expected to show intramolecular charge transfer (ICT) behavior. The photophysical properties of NB are therefore of great interest. The electronic spectra of NB, however, is very broad in all solvents and does not provide much information. The spectrum exhibited a strong band around 288 nm assigned to $\pi \rightarrow \pi^*$ transition and very weak, broad band in the 300-400 nm region.[2,3] Although the latter band is assigned to the $n \rightarrow \pi^*$ transition, this band is considered as a superposition of localized benzene- and nitromethane-type transitions with contribution from ICT excitation.[4] In addition, twisting of the nitro group upon excitation with possible formation of twisted intramolecular charge transfer (TICT) states is also proposed.[5] NB does not show fluorescence or phosphorescence and hence exact determination of the singlet and triplet energy levels is difficult.

Very little information is available about the excited state behavior of NB. Yip et al. have subjected few NB homologs to picosecond transient absorption spectroscopy and observed a transient absorbing in the 400-650 nm region.[6] This was attributed to the $n \rightarrow \pi^*$ triplet state,

116

which exhibited 800 ps lifetime. Based on triplet quenching studies, the energy of the $n \rightarrow \pi^*$ triplet is estimated as 58 kcal M^{-1}. The triplet-triplet absorption exhibited a 5 ps rise-time and hence the lifetime of the $n \rightarrow \pi^*$ singlet state was assumed to be less than 5 ps. Takezaki et al.[7,8] employed picosecond time-resolved transient grating method and obtained the singlet excited state lifetime as < 10 ps and triplet state lifetime of ~ 480 ps. The triplet state quantum yield was found to be 0.80.

Few reports are available where nitroaromatics were employed as acceptors in bimolecular PET reactions. Meyer and co-workers have studied the oxidative quenching of *tris*-bipyridylruthenium(II) dichloride ([Ru(bpy)$_3$]$^{2+}$, abbreviated as RuBP, in acetonitrile by thirteen nitroaromatics, including NB, *o*-, *m*- and *p*-dinitrobenzenes (DNB) and nitrobenzaldehydes.[9] The observed bimolecular quenching rate constants varied from 2.2×10^5 M^{-1} s^{-1} for NB to 8.6×10^9 M^{-1} s^{-1} for *p*-DNB. In transient absorption experiments, the authors could not observe absorptions assignable to radical ion products and this was attributed to very fast charge recombination reaction taking place in the solvent cage.

Previtali and co-workers have studied the bimolecular PET reactions between aromatic hydrocarbons naphthalene (NP), pyrene (PY) and dibenzanthracene by nitroaromatics such as *p*-DNB, *p*-nitrobenzaldehyde, *m*-nitrobenzaldehyde and *o*-nitroanisole.[10] They observed that the bimolecular quenching rate constants obtained using fluorescence lifetime measurements followed the Rehm-Weller type correlation with ΔG of the reaction (see Chapter 1, Figure 1.6). In laser flash photolysis experiments, radical cations of the aromatic hydrocarbons formed by electron transfer to the nitroaromatics were observed. Transient absorptions due to radical anions of the nitroaromatics were not observed and this was attributed to the low extinction coefficients

of the radical anion absorptions. They observed that charge recombination reactions in these systems lead to formation of the triplet states of the aromatic hydrocarbons.

Electron transfer quenching of the triplets of few aromatic hydrocarbons by nitroaromatics were also reported in the literature. For example, Previtali and co-workers have studied the quenching of the triplet excited states of anthracene (AN) and dibenz[a,h]anthracene by four nitroaromatics by laser flash photolysis.[11] Bimolecular quenching rate constants were determined and were found to follow the expected free energy relationship for outer sphere electron transfer. Transient absorption studies showed that electron transfer quenching of the triplet states lead to formation of radical ion products in methanol. Kuzmin et al. also have studied the quenching of triplet excited states of polycyclic aromatic hydrocarbons 1,2-benzpyrene and 1,2-benzanthracene by nitroaromatics.[12] The authors suggested that electron transfer from the triplet states is preceded by formation of an exciplex.

Although NB has been used as acceptor in few bimolecular PET reactions, we could find only one report where it is used in a covalently linked dyad, as the acceptor component.[13] The reduction potentials of 1,4-DNB (-0.69 V) and 1,3-DNB (-0.85 V) are very similar to the reduction potentials of 1,4-naphthaquinone (-0.63 V) and 9,10-anthraquinone (-0.86 V; all potentials are referenced to SCE), yet these nitro derivatives were never employed as acceptors in any covalently linked porphyrin or zinc porphyrin dyads. NB has not been widely used as acceptor in dyads most probably due to its low singlet energy, low singlet excited state lifetime, rapid intersystem crossing to the triplet state and very small triplet lifetime. Another important aspect is the photochemical reactivity of substituted nitroaromatics. Nitroaromatics are known to undergo photo reactions such as hydrogen abstraction and addition to double bonds.[14--17]

Lewis et al. studied the PET processes in the pyrenylurea-nitrobenzene π-stacked dyads **1-3** (Figure 4.1).[13] These molecules contain PY donor linked to NB acceptor through tertiary urea linkers. The tertiary urea linkers were selected for the study on the basis of earlier information that these linkers facilitate formation of strain-free folded conformations. The PET processes in these molecules were studied using femtosecond transient absorption technique in tetrahydrofuran and acetonitrile. Transient spectra obtained in the range 0 to 1900 ps is similar in both solvents, although the decay kinetics showed some differences.
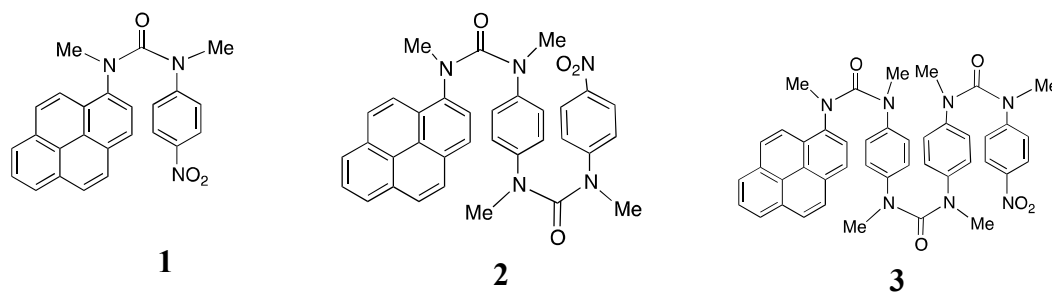

Figure 4.1. Structures of PY-NB dyads studied by Lewis et al.

Excitation of **1** using 355 nm light led to rapid formation of absorption at 600 nm which is attributed to the $S_2 \rightarrow S_n$ absorption of PY. This absorption decays within 100 fs to give a broad absorption at 495 nm and weak absorption at 420 nm. The 495 nm band decays with time constant of 33 ps leaving a spectrum with maxima at 410 and 520 nm, which did not decay during the 2 ns time window. The broad band at 495 nm was attributed to the $PY^{\bullet+}/NB^{\bullet-}$ charge transfer state and the long-lived absorptions at 410 and 520 nm are assigned to $^3PY^*$. Although both PY and NB absorbs the 355 nm laser light, based on the absorption spectra of PY and NB the authors suggested that two thirds of the incident light is absorbed by PY. The PY excited state initially formed transfers an electron to the NB acceptor to form the $PY^{\bullet+}/NB^{\bullet-}$ pair. Very

fast CR reaction takes place leading to formation of $^3PY^*$. Although one third of the light is absorbed by NB, the results suggested that the NB excited states did not lead to any observable photochemistry. Excited state processes taking place in **2** and **3** were very similar. Although the PY and NB moieties are separated by larger distances in **2** and **3**, the CR reactions occurred within 100 ps in these cases also. The CR reactions in both cases led to formation of $^3PY^*$, which was long lived under the experimental conditions.

Although nitroaromatics were rarely employed as acceptors in covalently linked dyads, they were used in several non-covalently linked dyads. In one of the early reports in this area, Nocera and co-workers studied the PET reaction in the non-covalently linked zinc porphyrin (ZnP)-DNB system **4** (Figure 4.2).[18]
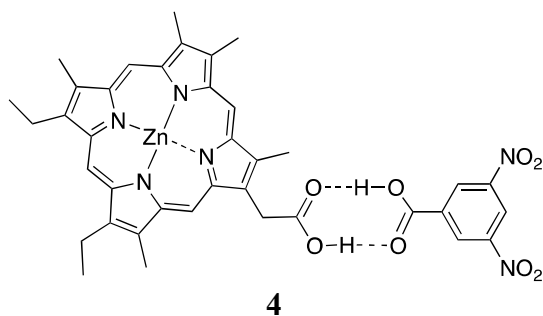

4

Figure 4.2. ZnP-DNB H-bonded D-A system designed by Nocera group

In **4** the ZnP donor and DNB acceptor are assembled through a carboxylic acid dimer-type hydrogen bonding interface. Excitation of ZnP leads to PET to the DNB acceptor. **4** provides the first direct experimental validation of PET taking place in synthetic, non-covalent systems. Comparison of **4** with Wasielewski's covalently linked ZnP-Q system, having comparable donor-acceptor separation and driving force, showed that PET rates are similar in these systems.[19] These results also confirmed previous theoretical predictions that hydrogen bond pathways for electron transfer can be competitive with covalent bond routes.[20-22]

Sessler and co-workers studied the PET process in the ZnP-DNB system **5**, where the ZnP is functionalized with guanine and the DNB is functionalized with cytosine.[23] The three-point hydrogen bonding interaction between guanosine and cytosine assembles the D-A dyad as shown in Figure 4.3. PET reaction in this system was studied in liquid crystals which reduced the PET rate by 2-3 orders of magnitude and made it possible to follow the reaction using time resolved electron paramagnetic resonance (TREPR). In **5**, PET occurs from the triplet state of ZnP to DNB and the CS state was detected in the TREPR study.
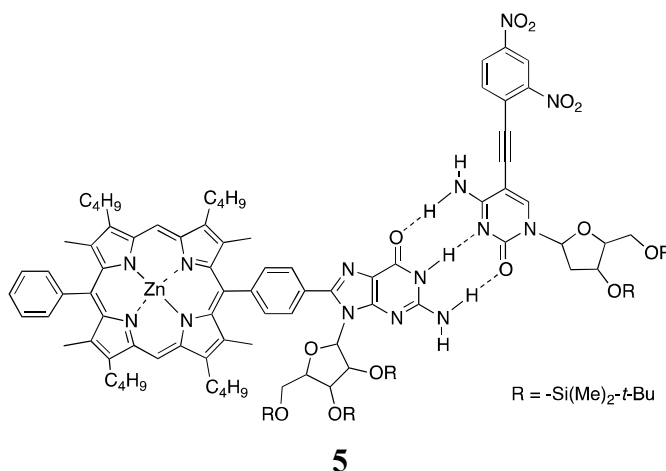

5

Figure 4.3. ZnP-DNB system assembled through guanine-cytosine base pairing

Nocera and co-workers have assembled RuBP donor - DNB acceptor systems through amidinium carboxylate salt bridges as shown in Figure 4.4.[24,25]
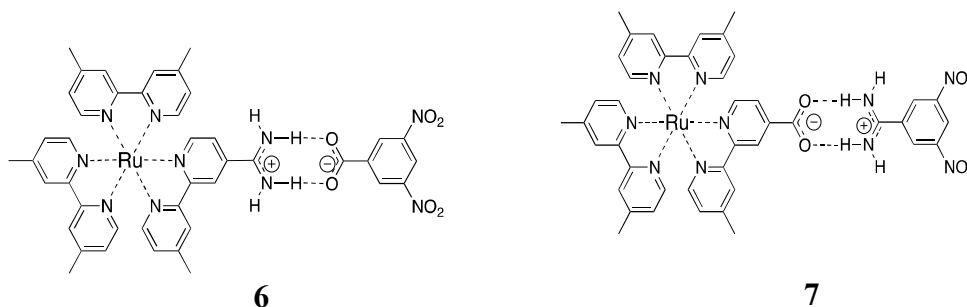

6   **7**

Figure 4.4. [Ru(bpy)$_3$]$^{2+}$-DNB pair assembled through amidinium-carboxylate bridge

In **6**, the amidinium part is on the RuBP moiety and carboxylate is on the DNB group. In **7** these groups are reversed. The salt bridge is polar and has a permanent dipole moment which is oriented towards the DNB group in **6** and towards the RuBP group in **7**. The presence of the negative charge on the DNB fragment reduces the electron transfer rate and hence k_{et} is ~ 100 times faster for **7**. Nocera and co-workers have used the amidinium-carboxylate salt bride to assemble a ZnP-DNB also (Figure 4.5).[26]
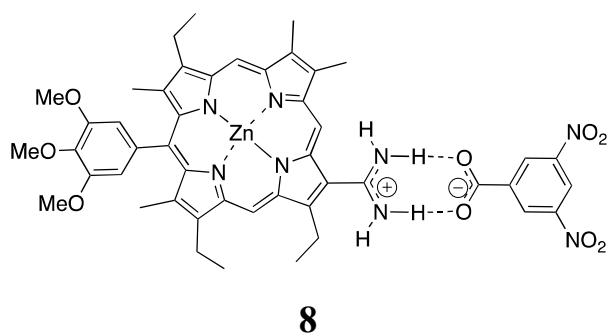

8

Figure 4.5. ZnP-DNB system assembled through amidinium-carboxylate bridge

Our research group has studied PET reactions in hydrogen-bonded pyrene – nitrobenzene and anthracene – nitrobenzene systems (Figure 4.6).[27,28] PET in these systems were studied using steady-state and time-resolved fluorescence experiments. We obtained k_{et} values in the range of $(6 – 9) \times 10^8$ s^{-1} for **9** and **10** (Figure 3.5).
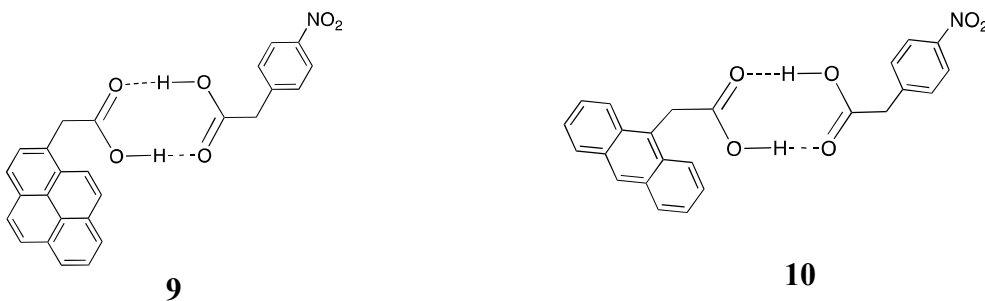

9

10

Figure 4.6. PY-NB and AN-NB hydrogen bonded D-A systems studied in our lab

Few β-cyclodextrin (β-CD) based non-covalent dyads also employed NB as acceptor. [29-30] In all the reports, the NB is attached to β-CD through the primary side as shown in Figure 4.7. The mono-6-*p*-nitrobenzoyl-β-cyclodextrin (NBCD) can encapsulate donor molecules within the β-CD cavity through the wider rim as shown in Figure 4.7. In one of the first reports, Wang et al. employed 2-dimethylaminonaphthalene (DNP) as the donor molecule.[29] Upon dissolving the donor DNP and acceptor NBCD in water, a fraction of DNP gets encapsulated inside the CD cavity to give the non-covalent dyad DNP@NBCD. Upon excitation of the DNP moiety, an electron is transferred from DNP to NB moiety of NBCD.
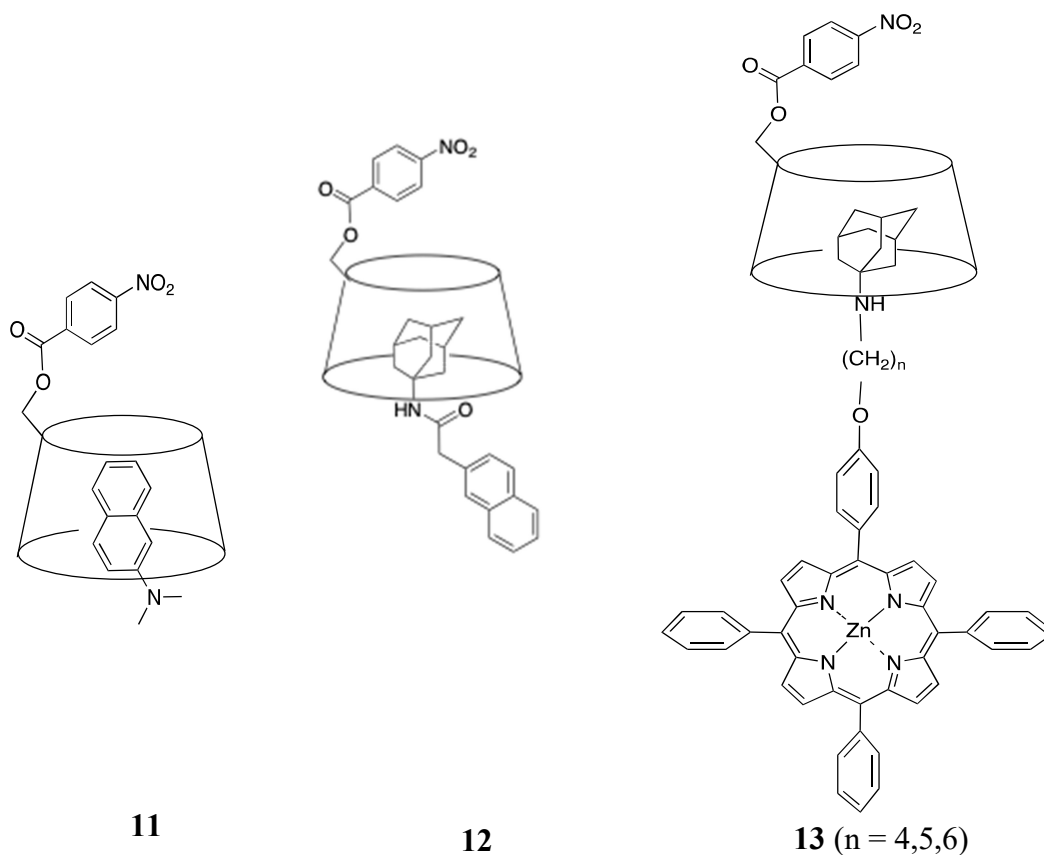

11　　　　**12**　　　　**13** (n = 4,5,6)

Figure 4.7. β-CD based non-covalent dyads with nitrobenzene acceptor

In aqueous solution adamantane (AD) derivatives show a very high propensity to get encapsulated in β-CD cavity. The association constant (K_a) for encapsulation of several AD derivatives in β-CD cavity is in the $10^4 - 10^5$ M^{-1} range.[32] Because of this, the donor group was linked to AD for **12** and **13**.[30,31] For dyad **13**, k_{et} values determined were in the range of $(8.7 - 13.7) \times 10^8$ s^{-1}.[31]

In almost all the non-covalently bound dyads, free moving donors and acceptors are also present in the solution and diffusion mediated PET pathways will also occur. The associated fraction of molecules is considered as an ensemble. The rate constant for PET in these cases are calculated using fluorescence lifetime experiments. The fluorescence decays will be bi-exponential due to the presence of associated ensemble and unassociated species. From the bi-exponential decays, k_{et} for electron transfer within the ensemble can be calculated. In most of these cases, the quantum yields and lifetimes of the charge separated (CS) state were not determined. In very few cases CS state lifetimes were determined using femtosecond flash photolysis and the values were found to lie in the picosecond time range.

In Chapter 3 of this thesis we have studied PET in two adamantane bridged systems, DMA-AD-AN and DMA-AD-PY. In these systems the aromatic hydrocarbons AN and PY acted as electron acceptors. In this chapter, PET reactions from the aromatic hydrocarbon donors, AN, PY, diphenyl anthracene (DPA) and perylene (PE) to NB acceptor linked through an AD spacer group, are studied. All the hydrocarbon molecules selected are good electron donors from their singlet excited states. The aim of the study is to see if the AD spacer helps in generating long-lived CS states in these D-AD-A systems also. We observed that the triplet states of the aromatic hydrocarbons are also formed in the flash photolysis of the AD bridged dyads (Chapter 3). We

suggested that a fraction of ^{1}CS state undergo ISC to the ^{3}CS state and the local triplets are formed from ^{3}CS. In linked D-A systems, ISC occurs in the CS state through the hyperfine interaction and this is possible only if the hyperfine interaction energy $\Delta E_{hfi} \geq 2J$, where $2J$ is the singlet-triplet spin exchange interaction energy (see Chapter 3). Since we are seeing slow formation of local triplets, we suggested that the AD spacer is capable of reducing the singlet-triplet coupling $2J$ such that $2J \approx \Delta E_{hfi}$ for the AD bridged systems. We have selected the DPA and PE systems because these molecules have inherently low triplet quantum yields. We were interested in knowing if the triplets of these molecules will be formed by ISC in the ^{1}CS state in these systems. Structures of molecules selected for the study and the abbreviations used are shown in Figure 4.8.

AN-AD-NB
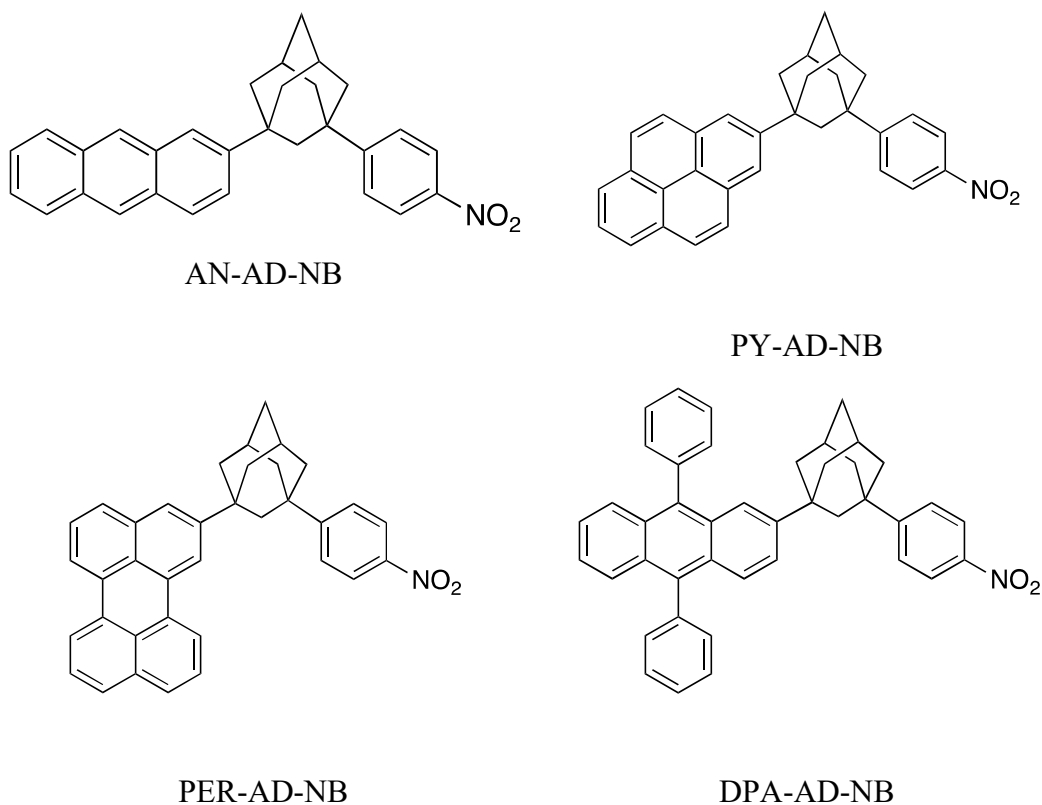
PY-AD-NB

PER-AD-NB

DPA-AD-NB

Figure 4.8. Structures of the dyads studied in this chapter.

In these dyads the aromatic hydrocarbons serve as donors and the NB moiety is the acceptor. The edge-to-edge distance between the donor and acceptor groups are four C-C single bonds (orthree sp^3 carbons), which is about 4.6 Å, as in the dyads reported in Chapter 3.

4.3. Results and Discussion

4.3.1. Synthesis and Characterization of dyads AN-AD-NB, PY-AD-NB, DPA-AD-NB and PER-AD-NB

Synthesis of AN-AD-NB and PY-AD-NB are reported in Chapter 3 of this thesis. These are compound **29** in Scheme 3.4 and compound **31** in Scheme 3.5, respectively. Procedures for the synthesis of these compounds and characterization data are presented in the experimental section of Chapter 3. Synthetic routes for DPA-AD-NB and PER-AD-NB are given in Scheme 4.1.
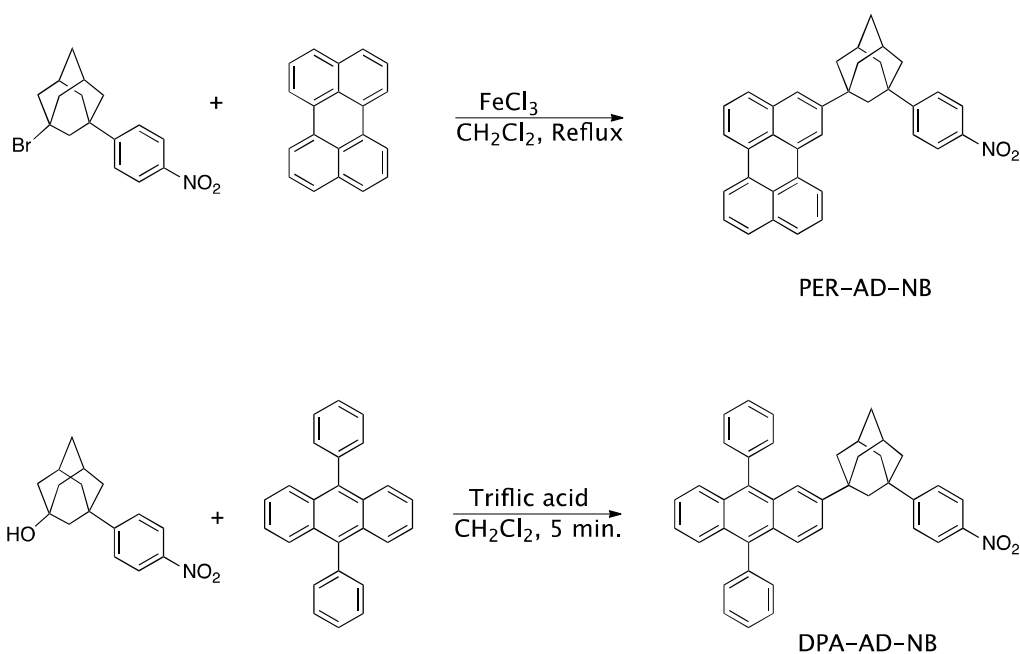
Scheme 4.1. Schemes for synthesis of PER-AD-NB and DPA-AD-NB

All the dyads are characterized by state-of-the-art spectroscopic techniques (see the experimental section).

126

4.3.2. Photophysical Studies of AN-AD-NB

Figure 4.9 shows the absorption spectra of AN, NB and AN-AD-NB (all in acetonitrile) overlaid in one plot. NB exhibit extremely weak absorptions above 300 nm. Above 350 nm, the absorption spectra of AN and AN-AD-NB are nearly identical except for increased absorption below 350 nm and the broadening of the absorption in the 390-400 nm region. The increase in absorbance below 350 nm is due to NB chromophore. This broadening in the 390-400 nm region may be due to charge transfer interaction as we have observed for the DMA systems reported in Chapter 3. The broadening, however, is much less for the AN-AD-NB system. The spectral comparison in Figure 4.9 shows that the singlet excited state of AN is not very much affected by substitution of the AD-NB moiety.

Figure 4.9 shows the absorption spectra of AN-AD-NB in few solvents. It can be seen from the figure that the spectrum is slightly red-shifted in less polar solvents such as chloroform and dichloromethane compared to that in the polar solvent acetonitrile. We have made similar observation in the case of the DMA based dyads reported in Chapter 3 also.
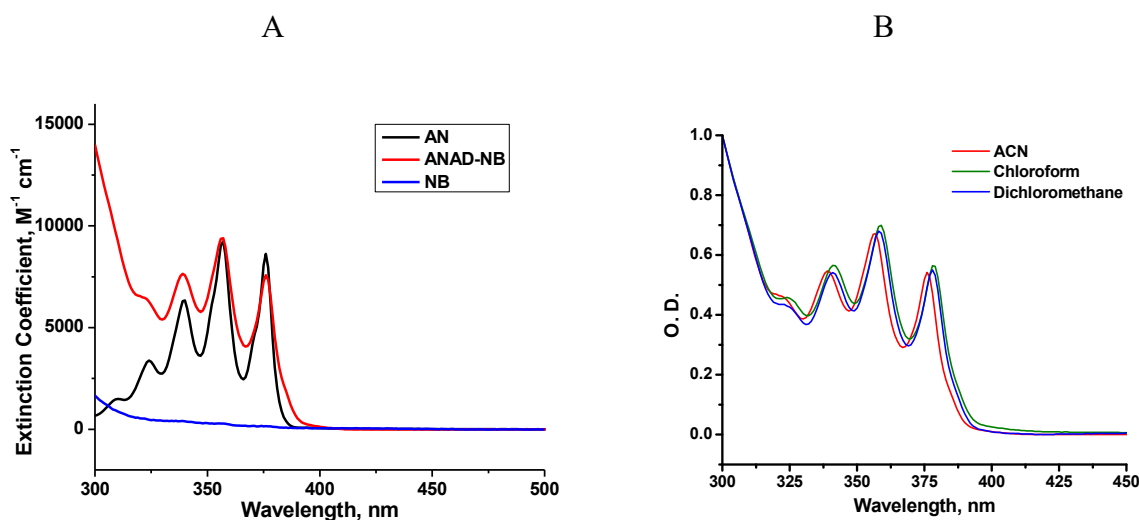
A   B

Figure 4.9. (A) Absorption spectra of NB (blue), AN (black) and AN-AD-NB (red) in acetonitrile and (B) absorption spectra of AN-AD-NB in few solvents compared.

Figure 4.10A shows a comparison of the emission spectra of optically matched solutions of AN and AN-AD-NB in acetonitrile under identical instrumental conditions. It can be seen that the emission of the AN moiety is quenched almost completely in the dyad as a result of PET from $^{1}AN^{*}$ to the acceptor NB. In Figure 4.10B, the emission spectrum of AN-AD-NB is multiplied by 100 and compared with that of AN. Figure 4.10B shows that the emission spectrum did not exhibit any additional feature when compared to that of AN.
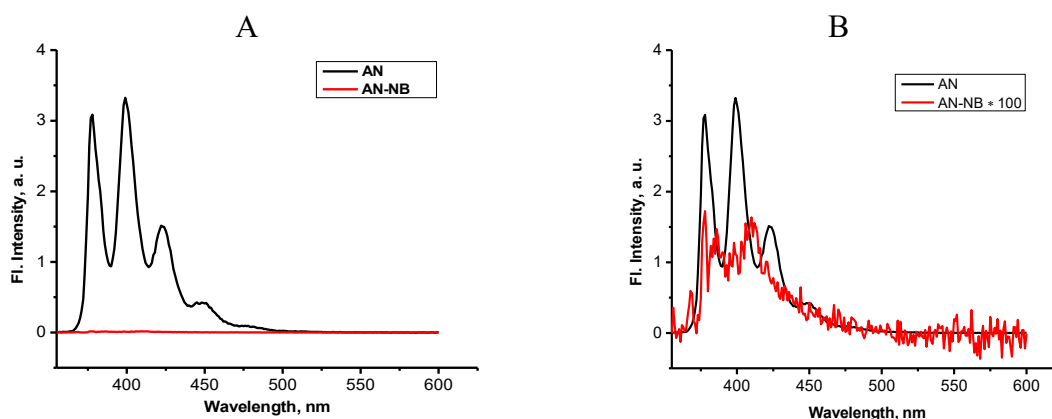

Figure 4.10. (A) Fluorescence spectra of optically matched solutions of AN and AN-AD-NB in acetonitrile under identical instrumental conditions. In (B), the emission spectra of AN-AD-NB is multiplied by 100. Excitation was at 360 nm and OD at the excitation wavelength was 0.05.

4.3.3. Photophysical Studies of PY-AD-NB

Figure 4.11A shows a comparison of the absorption spectra of PY, NB and PY-AD-NB in acetonitrile. In this case also, the increased absorption of PY-AD-NB at wavelengths below 350 nm can be attributed to the NB chromophore. Compared to PY, the absorption of PY-AD-NB is slightly broadened in the 345-375 nm region and this is may be due to charge transfer interactions. As in the case of the AN based dyad, the singlet excited states of PY are unaffected by the presence of the AD-NB group. Figure 4.11B shows a comparison of the absorption spectra of PY-AD-NB in three different solvents. It may be noted that the spectrum is slightly

blue shifted in the polar solvent acetonitrile. Similar observations were made earlier for the other systems also.
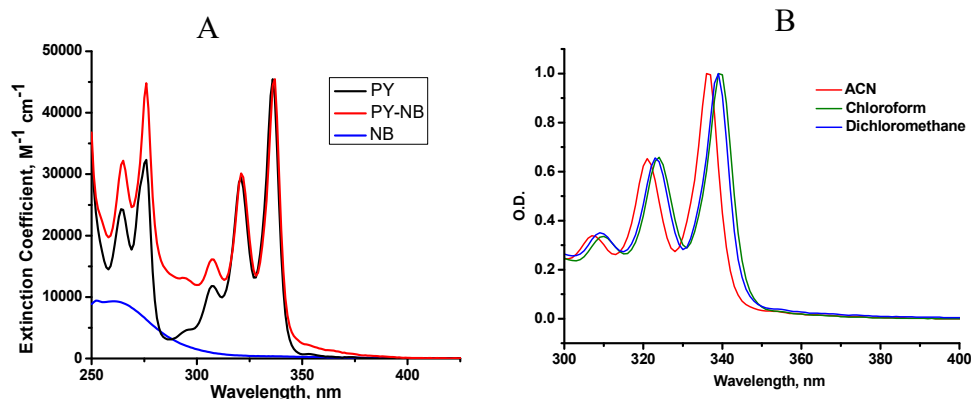

Figure 4.11. (A) Absorption spectra of NB (blue), PY (black) and PY-AD-NB (red) in acetonitrile and (B) absorption spectra of AN-AD-NB in few solvents compared

Figure 4.12 show a comparison of the emission spectra of optically matched solutions of PY and PY-AD-NB in acetonitrile under identical instrument conditions. It may be noted that the emission of PY is completely quenched because of PET to the acceptor NB. From the figure we estimate that the quenching is more than 90%.
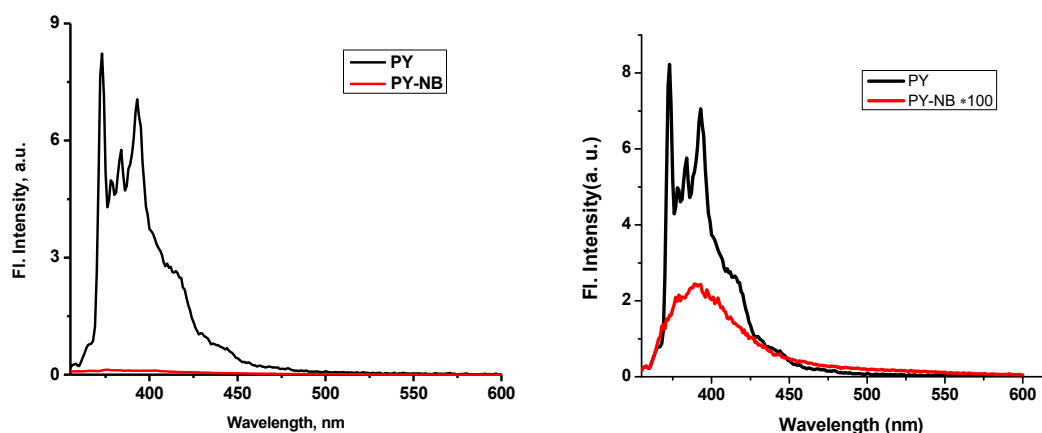

Figure 4.12. Fluorescence spectra of optically matched solutions of PY and PY-AD-NB in acetonitrile under identical instrumental conditions. Excitation was at 330 nm and OD at the excitation wavelength was < 0.05

4.3.4. Photophysical Studies of PER-AD-NB

Figure 4.13 compares the absorption spectrum of PER-AD-NB with that of PER. The increased absorption in the region below 350 nm is attributed to the NB moiety. The absorption onset was slightly shifted to the red for PER-AD-NB. It is to be noted that the broadening of the absorption on the long wavelength side is much less for PER-AD-NB. The maxima of all the three absorption bands of PER remain unaffected by substitution of the AD-NB moiety in this case.

Figure 4.13. Absorption spectra of PER (black) and PER-AD-NB (red) in acetonitrile. Concentrations were 5×10^{-6} M for both samples.

In Figure 4.14 we have compared the emission spectra of optically matched solutions of PER and PER-AD-NB under identical instrumental conditions. It can be seen that the emission intensity of the PER chromophore is highly quenched in the compact dyad due to PET process occurring from the singlet excited state of PER to ground state NB. It can also be noted that the emission profile of the dyad is the same as in the parent hydrocarbon and new emissions due to exciplex are not observed in the spectrum of PER-AD-NB.

Figure 4.14. Fluorescence spectra of optically matched solutions of PER (black) and PER-AD-NB (red) in acetonitrile under identical instrumental conditions.

4.3.5. Photophysical Studies of DPA-AD-NB

Figure 4.15 shows the absorption spectra of DPA and DPA-AD-NB dyad in acetonitrile. As in the earlier cases, the increased absorption at wavelengths below 350 nm can be attributed to the NB chromophore. In contrast to the cases of AN-AD-NB and PY-AD-NB, the broadening of absorption at the red end is much less for this dyad. The low wavelength absorptions in DPA remains unaffected in the dyad, suggesting that the singlet excited state of DPA is unaffected by substitution of AD-NB.
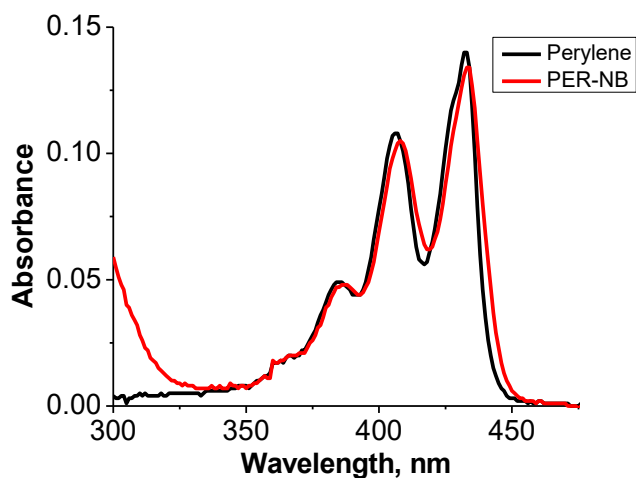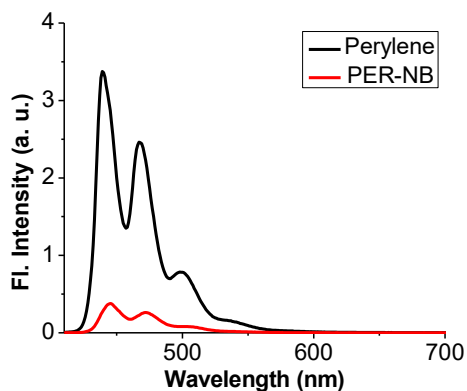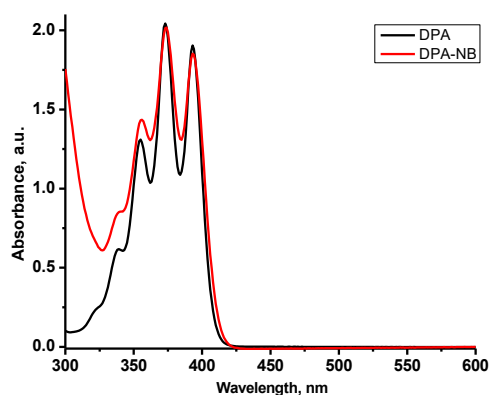

Figure 4.15. Absorption spectra of DPA (black) and DPA-AD-NB (red) in acetonitrile. Concentrations were 1×10^{-5} M for both samples.

Figure 4.16A compares the emission spectrum of DPA-AD-NB with that of DPA. It can be seen that the emission of the dyad is almost completely quenched by electron transfer to the NB acceptor. In Figure 4.16B, the emission spectrum of the dyad is multiplied by 100 and compared to that of DPA. It can be seen from Figure 4.16B that no new features are seen in the emission spectrum of DPA-AD-NB. The absorption and emission spectra in this case rule out the possibility of any charge transfer interaction in this case.
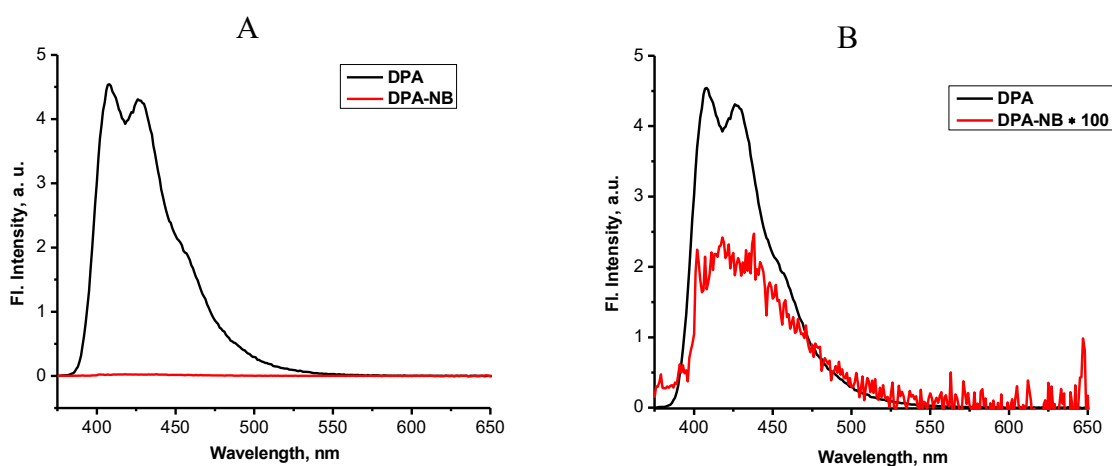
Figure 4.16. (A) Fluorescence spectra of optically matched solutions of DPA and DPA-AD-NB in acetonitrile under identical instrumental conditions. In (B), the emission spectra of DPA-AD-NB is multiplied by 100. Excitation was at 375 nm and OD at the excitation wavelength was 0.05

4.3.6. Electrochemical Aspects

Redox potentials and excitation energies of all the donors and acceptor studied in this chapter were reported in the literature[27,33-35,36-41] and we used these values to calculate ΔG_{PET} values for all the dyads. The reduction potential (E_{red}) of NB is – 1.17 V vs. SCE in acetonitrile.[27] In the dyad molecules studied in this chapter, the aromatic hydrocarbons are the excited state electron donor. Up on irradiation with 355 nm laser light, CS and CR reactions occur as shown in equations (4.1) to (4.3), where AR stands for the aromatic hydrocarbons, AN, PY, PER or DPA.

$$\text{AR-AD-NB} \xrightarrow{\text{h}\nu\ =\ 355\ \text{nm}} {}^{1}\text{AR*-AD-NB} \qquad (4.1)$$

$$^{1}\text{AR*-AD-NB} \xrightarrow{\text{ET}} {}^{\bullet+}\text{AR-AD-NB}^{\bullet-} \qquad (4.2)$$

$$^{\bullet+}\text{AR-AD-NB}^{\bullet-} \xrightarrow{\text{CR}} \text{AR-AD-NB} \qquad (4.3)$$
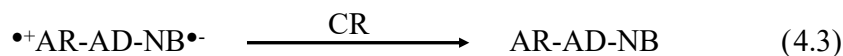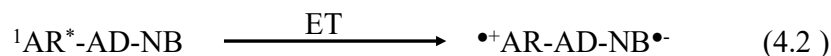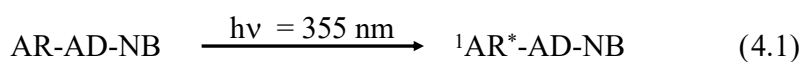
Relevant data for calculation of the ΔG_{PET} and ΔG_{CR} reactions are summarized in Table 4.1. The Weller equation (eq. 1.9) was used for the calculation of ΔG_{PET}. Values of ε_s = 37.5 for acetonitrile and d_{cc} = 12 Å (see Chapter 3) for center-to-center distance in the dyad, were used in the calculation. ΔG_{CR} values were calculated using equation 1.14 (see Chapter 1).

Table 4.1. Relevant data for AR-AD-NB dyads studied in this chapter

Dyad	$E_{0,0}$, eV	E_{ox}, V (vs SCE in)	Φ_F	τ_F, ns	ΔG_{PET}, eV	ΔG_{CR}, eV
AN-AD-NB	3.31	0.94	0.71	5.8	-1.24	-2.11
PY-AD-NB	3.33	1.08	0.72	100.0	-1.12	-2.25
DPA-AD-NB	3.15	1.22	0.90	8.2	-0.80	-2.39
PER-AD-NB	2.83	0.85	0.98	6.0	-0.81	-2.02

Since all the dyads have very low fluorescence quantum yields, single photon counting experiments could not be performed. Thus, it was not possible to obtain k_{CS} from the fluorescence lifetime of the dyads.

4.3.7. Flash Photolysis Experiments

4.3.7.1. Flash Photolysis of AN-AD-NB Dyad

Results obtained in the flash photolysis of AN-AD-NB dyad in acetonitrile using the 355 nm laser light are presented in Figure 4.17. Figure 4.17A shows the transient absorption spectra

obtained at 200, 300, 600 and 900 ns following the laser flash. The 355 nm laser excites the AN chromophore and the singlet excited state of AN formed then donates an electron to ground state NB. Electron transfer according to equation 4.2 leads to formation of $AN^{\bullet+}$ and $NB^{\bullet-}$. The $AN^{\bullet+}$ exhibit weak absorption at 430 nm and strong absorption at 720 nm.[42a] Thus, the relatively strong absorption at 720 nm can be assigned to $AN^{\bullet+}$. Decay profile of the 720 nm transient is given in Figure 4.17C. Fit of the data to a single exponential gave the lifetime of $AN^{\bullet+}$ as 1.4 µs, which gives $k_{CR} = 7.14 \times 10^5$ s^{-1}.
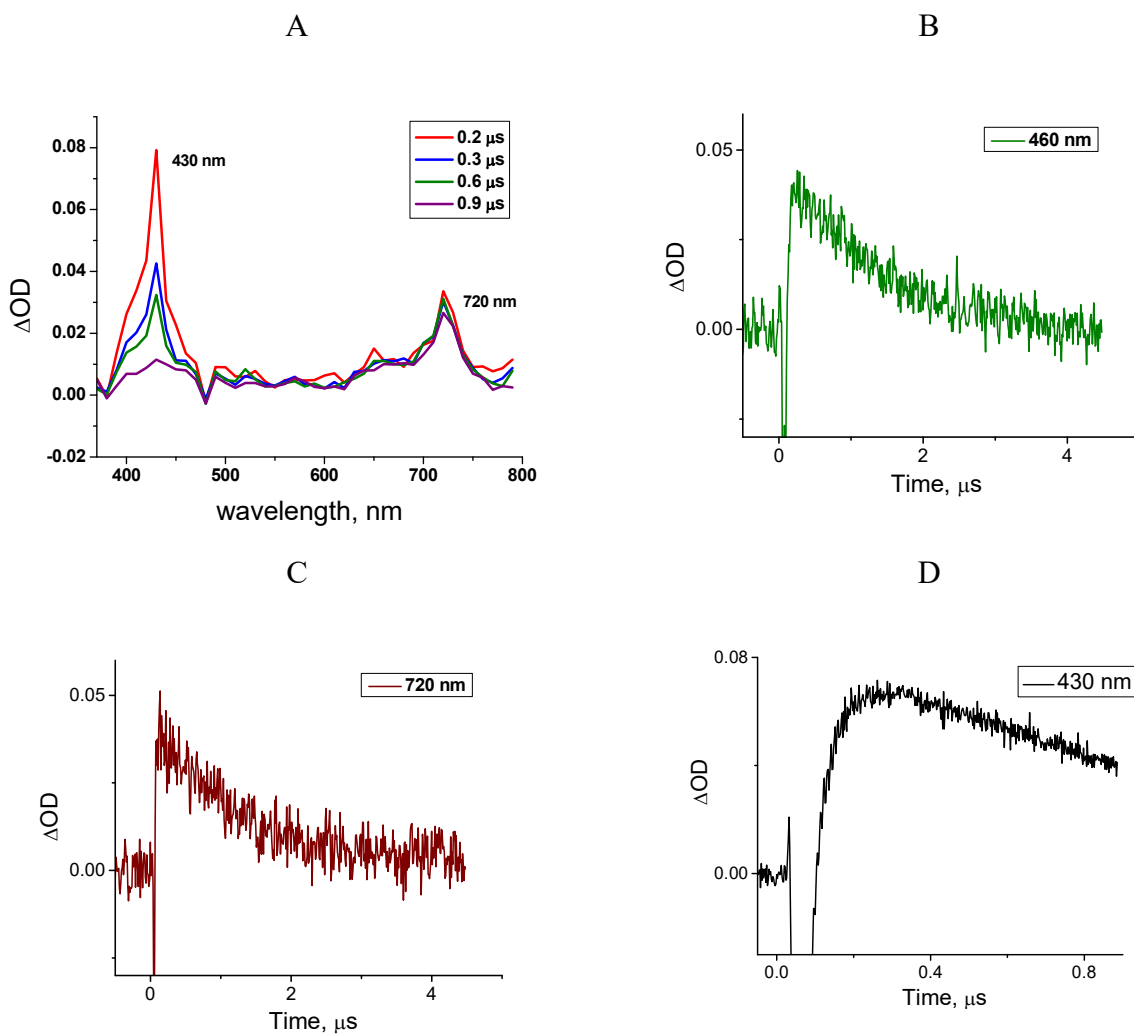

Figure 4.17. A: Transient absorption spectra at different times in the flash photolysis of AN-AD-NB. B-D are kinetic profiles under various conditions.

As mentioned in the introduction section of this chapter, spectrum of NB$^{\bullet-}$ was not reported in any flash photolysis experiments where NB served as acceptor. However, Shida obtained the absorption spectrum of NB$^{\bullet-}$ in pulse radiolysis and reported its absorption maximum as 465 nm.[42b] We can see that a weak, broad absorption is persisting in the transient spectrum even at 900 ns, which can be assigned to NB$^{\bullet-}$. Since there is considerable overlap of the ^{3}AN* and NB$^{\bullet-}$ absorptions in the 400-500 nm region, both these species are responsible for the transient absorption in this region. The strongest absorption in the transient spectra exhibited maximum at 430 nm, and we assign this to ^{3}AN*,[43a] formed from ^{3}CS state as in the case of AN-AD-DMA reported in Chapter 3. We saw a growth for the ^{3}AN* absorption in the flash photolysis of AN-AD-DMA studied in Chapter 3 of the thesis. In order to see if a growth component is present for the transient at 430 nm in the case of AN-AD-NB, the flash photolysis was performed at short timescales and the kinetic profile obtained is shown in Figure 4.17D. We can see a prominent growth component in the kinetic profile. This suggests that a fraction of the ^{1}CS state undergo intersystem crossing to ^{3}CS state, and the remaining fraction of ^{1}CS undergo CR reaction to the ground state. The ^{3}CS formed undergo very fast and quantitative CR to generate ^{3}AN*, which then decay to the ground state. Scheme 4.2 summarises the processes taking place when the AN chromophore of AN-AD-NB is excited.
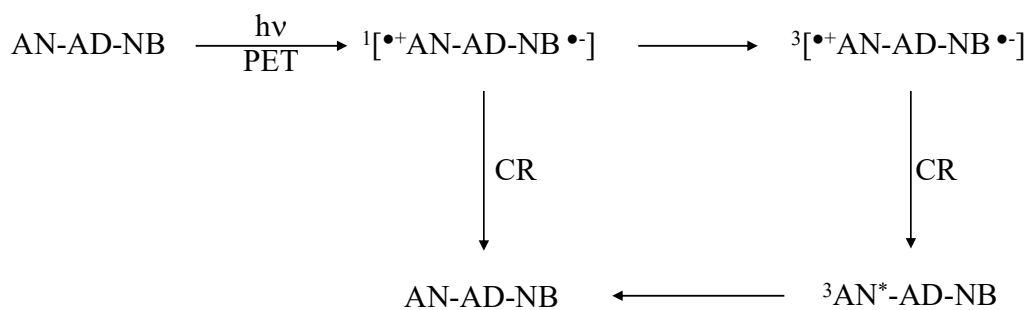
Scheme 4.2. CS and CR reactions possible in AN-AD-NB.

4.3.7.2. Flash Photolysis of PY-AD-NB Dyad

Dyad PY-AD-NB was subjected to flash photolysis using the 355 nm laser light from Nd-YAG laser and the results obtained are summarized in Figure 4.18. As in the case of AN-AD-NB, we expect formation of $^3PY^*$, $PY^{•+}$ and $NB^{•-}$ transients in the photolysis of PY-AD-NB. All these transients have closely spaced absorption maxima, which are: $^3PY^*$ - 415 nm,[43b] $PY^{•+}$ - 440 nm[42c] and $NB^{•-}$ - 460 nm.[42b] In Figure 4.18A, we have presented the transient absorption spectra obtained at 170 and 340 ns after the laser flash.
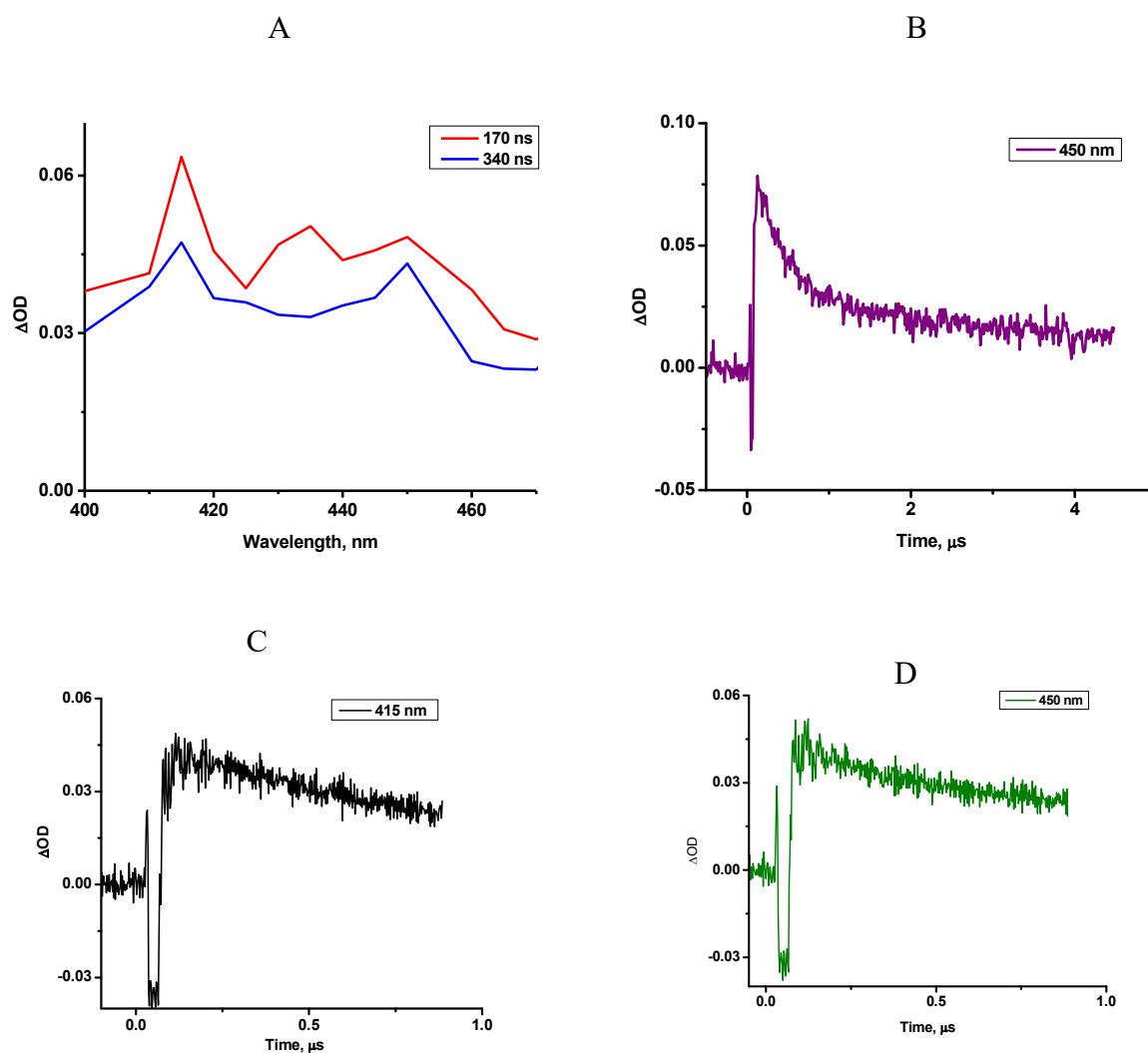

Figure 4.18. (A) Transient absorption spectra at 170 and 340 ns in the flash photolysis of PY-AD-NB. B-D are kinetic profiles at wavelengths indicated in the figures.

The transient is very broad suggesting that all the three expected transient absorptions are embedded within the broad spectra. Figure 4.18B shows decay of the transient at 450 nm and this can be attributed to $PY^{\bullet+}$ and $NB^{\bullet-}$. Since the radical anion and radical cation are expected to decay by CR to the ground state or undergo ISC to ^3CS, we expect the decay rates of these species to be the same. A fit of the decay profile with single exponential gave the lifetime as 1.6 μs ($k_{CR} = 7.15 \times 10^5$ s^{-1}). Thus, the PY-AD-NB system constitutes another example of long-lived charge separation brought by the AD bridge. Figure 4.18C shows the kinetic profile of the 415 nm transient. Growth of the triplet is evident in the figure. Figure 4.18D shows the decay profile of the 450 nm transient in short timescale. A growth section is not evident in this case. Figures 4.19A,B shows the behaviour of the transients towards oxygen. The 415 nm transient, assigned to $^3PY^*$ is quenched efficiently by oxygen whereas the transient absorption at 450 nm assigned to the radical ions is quenched only partially by oxygen. Based on the data presented in Figures 4.18 and 4.19, we conclude that the radical ions are formed immediately following excitation and the triplet is formed in a slow process. The mechanism outlined in Scheme 4.2 is applicable to PY-AD-NB dyad also.
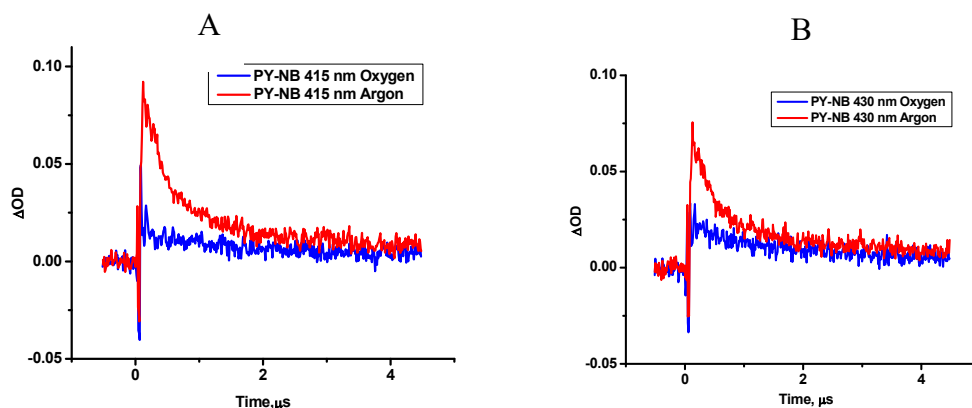
Figure 4.19. Decay profiles of 415 and 430 nm transients in the absence and presence (blue trace) of oxygen.

4.3.7.3. Flash Photolysis of PER-AD-NB Dyad
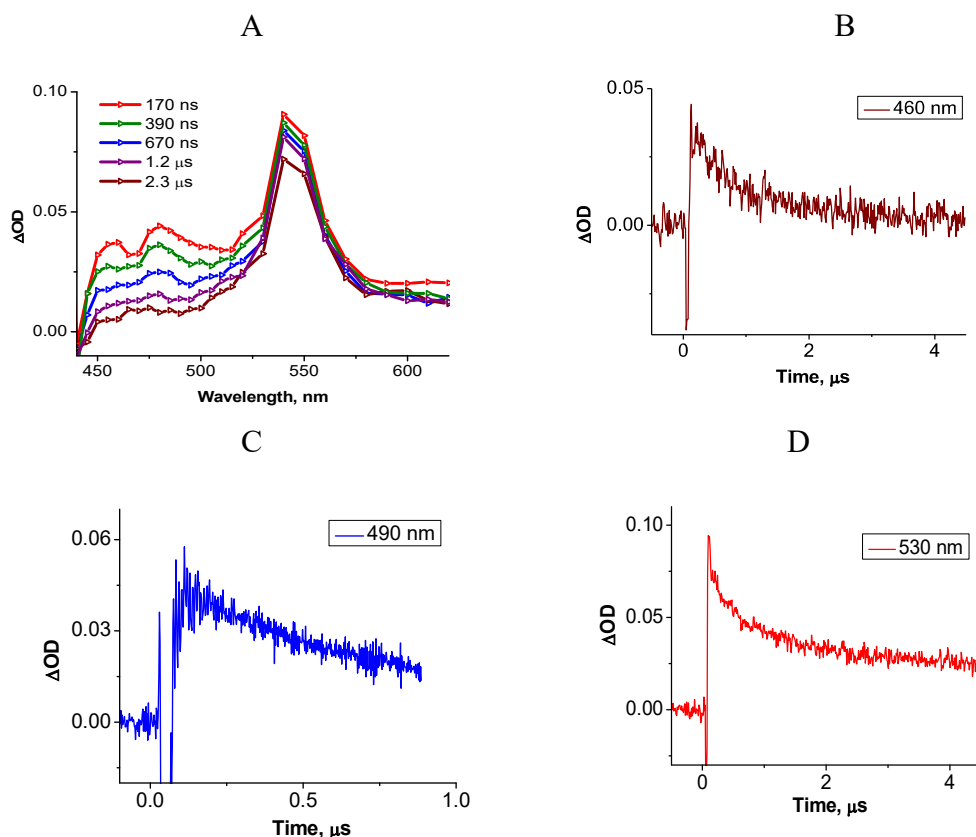
Figure 4.20. A: Transient absorption spectra obtained at different times in the flash photolysis of PER-AD-NB. B-D are kinetic profiles at the indicated wavelengths.

Figure 4.20 summarises the transient absorption data obtained for the PER-AD-NB dyad. Figure 4.20A shows the transient absorption spectra obtained at 170, 390, 670, 1200 and 2300 ns after the laser flash. The spectra exhibited three distinct absorptions, which are 460 nm, 490 nm and 540 nm. Based on literature the 460 nm peak is assigned to NB$^{\bullet-}$,[42b] the 490 nm assigned to ^{3}PER* absorption[43c] and the 540 nm transient assigned to PER$^{\bullet+}$.[44,45] Figure 4.20B shows the transient decay at 460 nm, assigned to the radical anion. This absorption may have some contribution from ^{3}PER* absorption. Since the radical anion and triplet absorptions overlap in the 450-500 nm region, the growth process associated with triplet formation (as in the case of AN-

AD-NB and PY-AD-NB systems), can be observed at short time delays at all wavelengths in this wavelength region. Kinetic profile obtained in the short time window at 490 nm is shown in Figure 4.20C. The transient absorption in the 520-570 nm region is assigned to PER$^{\bullet+}$ based on literature reports.[44,45] The decay profile at 530 nm is shown in Figure 4.20D. It may be noted that the transient is long-lived and a fit of the data gave lifetime of the CS state as 1.2 μs. Thus, the adamantane bridged PER-NB compact dyad is also capable of sustaining a long-lived photoinduced charge separation.

4.3.7.4. Flash Photolysis of DPA-AD-NB Dyad

In Figure 4.21, results of the flash photolysis of DPA-AD-NB in acetonitrile are presented. Figure 4.21A shows the transient absorption spectra taken at three different times following the laser flash. The spectra exhibited a broad peak in the 400-500 nm region and 3 peaks in the 500-750 nm region. DPA exhibit very poor ISC efficiency to its triplet state and in flash photolysis of DPA, absorptions due to the ^{3}DPA* has not been observed.[36,37] The triplet state of DPA, however, could be generated through sensitization experiments using anthracene[36] and benzophenone[37] as triplet energy donors. The T-T absorption spectrum of DPA is characterized by absorption maximum in the 440-455 nm region with a prominent shoulder at 425 nm.[36] As mentioned previously, the radical anion of NB exhibits weak absorption with maximum at 465 nm. Thus, the absorption band observed in the 400-500 nm region can be safely assigned to ^{3}DPA* and NB$^{\bullet-}$. The three peaks seen in the 550-750 nm region is assigned to DPA$^{\bullet+}$. Sioda obtained DPA$^{\bullet+}$ by electrochemical oxidation of DPA and recorded its absorption spectrum.[40] The spectrum was almost identical to the peak pattern seen in the 550-750 nm range in Figure

4.21A. Kochi and co-workers also reported an identical absorption spectrum for DPA$^{\bullet+}$.[41] Based on these reports, we assign the structured absorption in the 550-750 nm range in Figure 4.21A to DPA$^{\bullet+}$. Figure 4.21B shows the decay profile at 430 nm. A small growth pattern is seen in the initial part of the profile and this most probably is the growth of ^{3}DPA*. The kinetic profile obtained at 460 nm is shown in Figure 4.21C. The NB$^{\bullet-}$ and ^{3}DPA* contributes to this absorption. The decay profile of DPA$^{\bullet+}$ at 680 nm is shown in Figure 4.21D. The decay profile is very noisy due to the weak absorption and also low sensitivity of the photomultiplier in the long wavelength region.

A

B

C

D
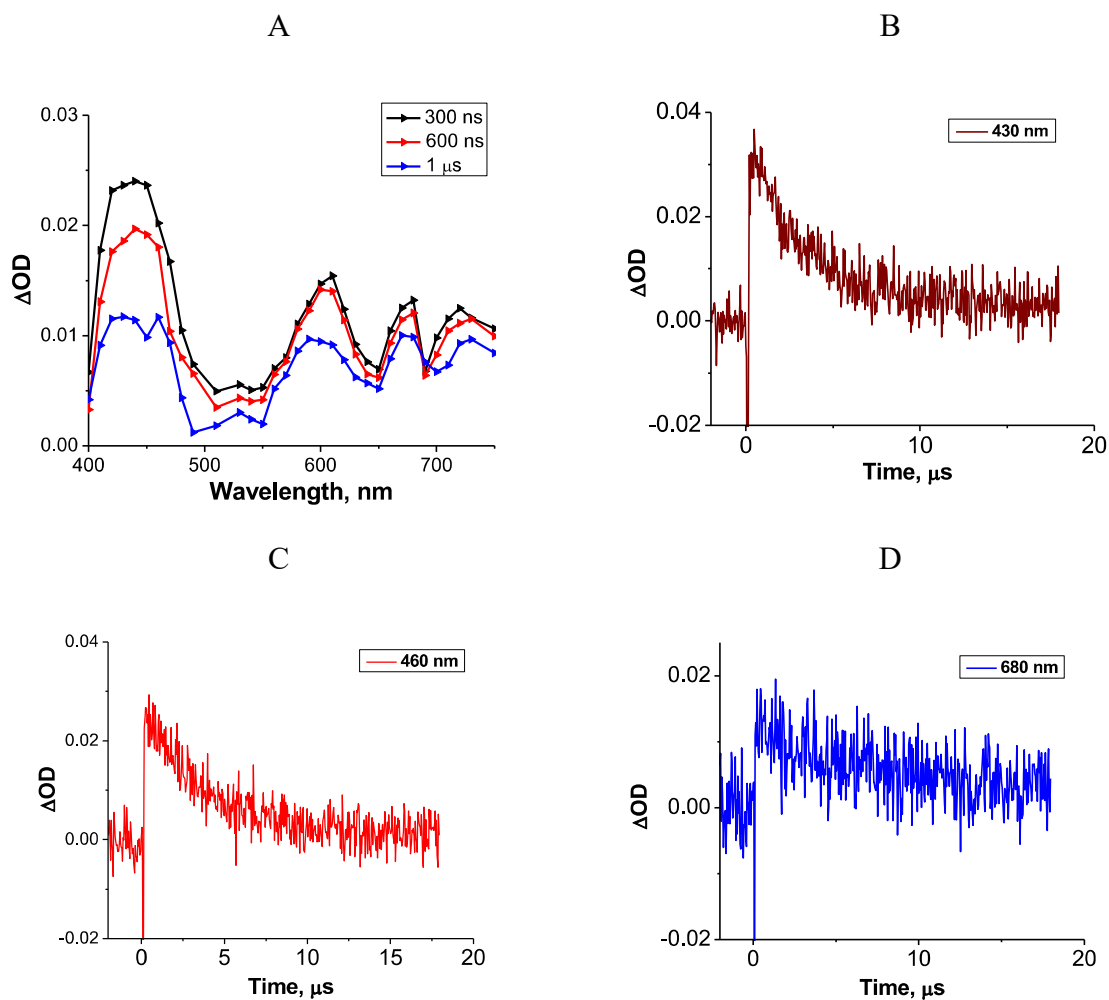
Figure 4.21. A: Transient absorption spectrum of DPA-AD-NB in acetonitrile at three different times. B-D are kinetic profiles at different wavelengths.

By fitting the data, we obtained the decay rate k_{CR} as 2.78×10^5 s^{-1}, which corresponds to CS state lifetime of 3.6 μs. Thus, the DPA-AD-NB constitutes another example of AD-bridged compact dyad that exhibit long CS state lifetime.

4.3.8. Long-Lived Charge Separation in Adamantane bridged dyads.

As mentioned in Chapters 1 and also 3, long-lived charge separation in compact dyads was possible only by the 'spin control' approach.[44-46] The CS state is long-lived in such systems because the CS state has triplet multiplicity and it is also the lowest energy excited state. All local triplets have energy higher than the ^{3}CS states in these cases and hence CR to local triplets will be energetically uphill. For the AD bridged dyads reported in Chapters 3 and 4, this is not the case. Figure 3.16 (Chapter 3) shows that the ^{1}CS state lies at 0.89 eV above the ^{3}AN* state and yet exhibits long lifetime. The CS state lifetimes of the AD bridged dyads reported in this chapter are also in the microsecond domain. The energy levels of the ^{1}CS (in red colour) and local triplet energy levels (blue colour) in these molecules are summarized in Figure 4.22.

Figure 4.22. Energy levels of ^{1}AR*, ^{1}CS and ^{3}AR* energy levels in the dyads

141

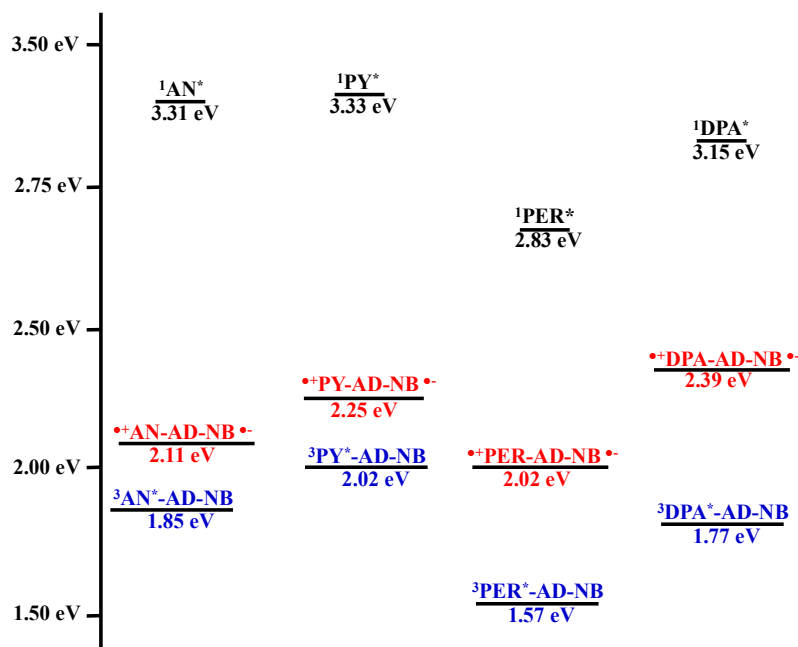An inspection of the figure confirms the following: (1) The ^{3}NB* lies at 2.52 eV, which is at a higher level with respect to all the ^{1}CS states. So, CR reaction from the ^{1}CS to ^{3}NB* will be energetically uphill for all the systems studied here. Thus, ^{3}NB* is not expected to be formed in any of these cases. (2) For all the dyads, the ^{1}CS state is higher in energy compared to the corresponding aromatic hydrocarbon triplets by more than 0.25 eV. In general, the energy difference between ^{1}CS and ^{3}CS, which is equal to 2J, is very small and amounts to only few cm$^-$^{1}. Hence, most probably, the ^{3}CS will also lie above the local hydrocarbon triplets in all these cases. Hence, the microsecond lifetime observed in all these cases cannot be attributed to 'spin control' effects.[44-46] We believe that the long-lived CS we are observing have singlet multiplicity. A fraction (20%) of ^{1}CS undergo ISC to ^{3}CS, which is extremely short lived as it undergoes ultrafast CR reaction to the local triplet. We reasoned that the structure of the dyad could be responsible for the long CS state lifetimes. In order to gain some insight into this aspect, we obtained the single crystal X-ray structures of two of the dyads studied in this chapter.

4.3.9. Single Crystal X-ray Structures of AN-AD-NB and PER-AD-NB
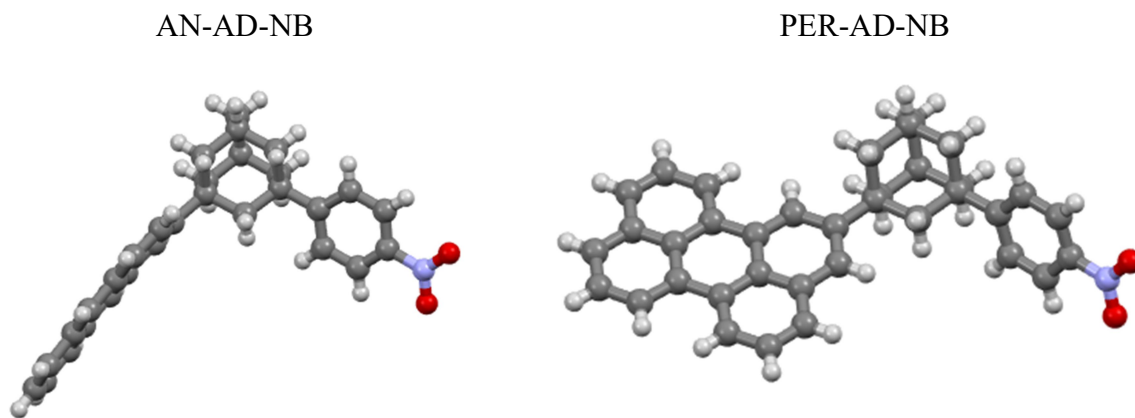
<div align="center">AN-AD-NB   PER-AD-NB</div>

Figure 4.23. Single crystal X-ray structures of AN-AD-NB and PER-AD-NB.

Single crystal X-ray structures of AN-AD-NB and PER-AD-NB are presented in Figure 4.23. We can see that for both the systems, the donor and acceptor chromophores are nearly orthogonal to each other and this may be an important reason for the long lifetime of the CS state. The X-ray structure is the structure of the molecules in the solid state. A careful analysis showed that in solution also, the donor and acceptor groups may remain orthogonal due to restricted rotation of the chromophores caused by the very close spatial disposition of the *ortho* hydrogens of the aromatic molecules with the hydrogen atoms on adjacent carbons of adamantane. In Figure 4.24, two conformations of AN-AD-NB are presented.

A

B
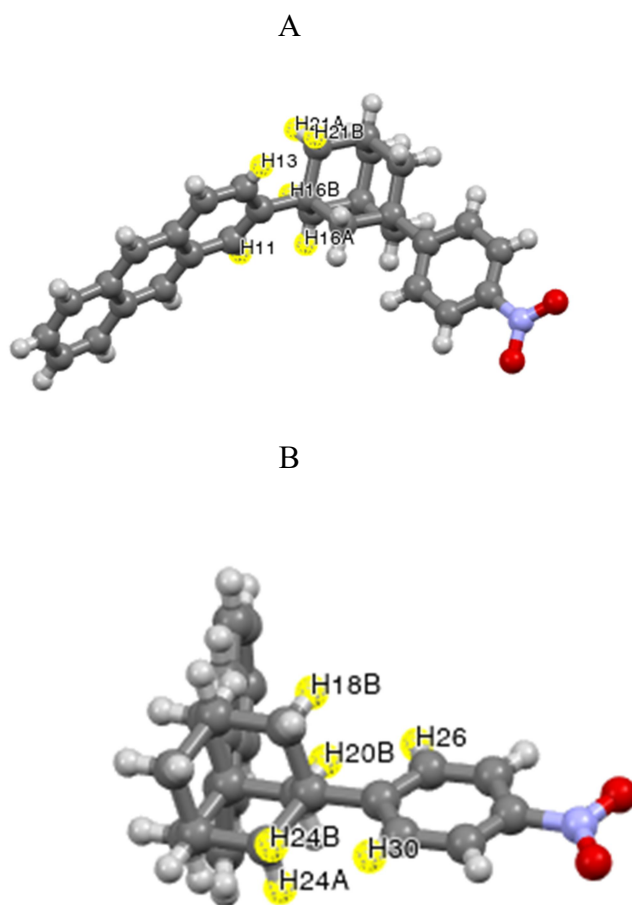
Figure 4.24. Conformations of AN-AD-NB showing spatial arrangement of *ortho* hydrogen atoms of the aromatics alongside adjacent hydrogen atoms of AD. (A) shows the interactions at the AN side and (B) shows interaction at the NB side.

In Figure 4.24A, we have marked *ortho* hydrogen atoms on the AN side. The H13 atom on the AN chromophore is placed in between the H21A and H21B of the adamantane ring. Again, the H11 of the AN ring is placed in between the H16A and H16B of the AD ring. Since both the *ortho* hydrogens of the AN chromophore are sterically strained, free rotation of the AN chromophore may be hindered. The steric strain on the NB side is shown in Figure 4.24B. The *ortho* hydrogen atom H30 is placed in between the H24A and H24B atoms of AD. Similarly, the *ortho* hydrogen atom H26 is placed in between the H18B and H20B of AD. Thus, free rotation of the NB moiety is also hindered due to steric congestion from spatially close hydrogen atoms on the AD group. Figure 4.25 shows the spatial proximity of *ortho* hydrogens on the PER and NB moieties to the nearby AD protons in PER-AD-NB. The hydrogen atoms are presented in yellow colour and the spatial interactions are marked by arrows. In this case also, we propose that the free rotation of the PER and NB moieties are hindered in solution state also.

Based on the discussion on the X-ray crystal structures of AN-AD-NB and PER-AD-NB, we propose the following to explain the long-lived CS states in the AD bridged dyads studied in Chapters 3 and 4 of this thesis. In the ground states of these molecules the donor and acceptor groups are orthogonal to each other. This conformation remains the same in the solution also. When the hydrocarbon chromophore is excited, the bond lengths for the excited chromophore may be different and this chromophore may undergo free rotation. Several conformations may be possible for the excited chromophore with respect to the ground state partner leading to facile PET. Once the CS state is generated, the molecules may return to its original conformation where the chromophores are orthogonal to each other. The radical cation present on the donor moiety will have very little interaction with the radical anion present on the acceptor because of the orthogonal conformations of the chromophores. As free rotation is hindered, only few

orientations will be possible and this will reduce the rates of CR reaction. In addition, the CR reaction in all the four dyads fall in the inverted region ($\Delta G_{CR} > 2.0$ eV) and this also contributes to the slow rate. CR reaction in the ^{3}CS to the local triplet is spin-allowed and very fast because the low energy gap (≤ 0.5 eV) between the two states. Thus, the long-lived charge separation in the AD bridged dyads can be attributed to the structure of AD bridge which nearly locks donor and acceptor chromophores in orthogonal orientations and the inverted region effects.
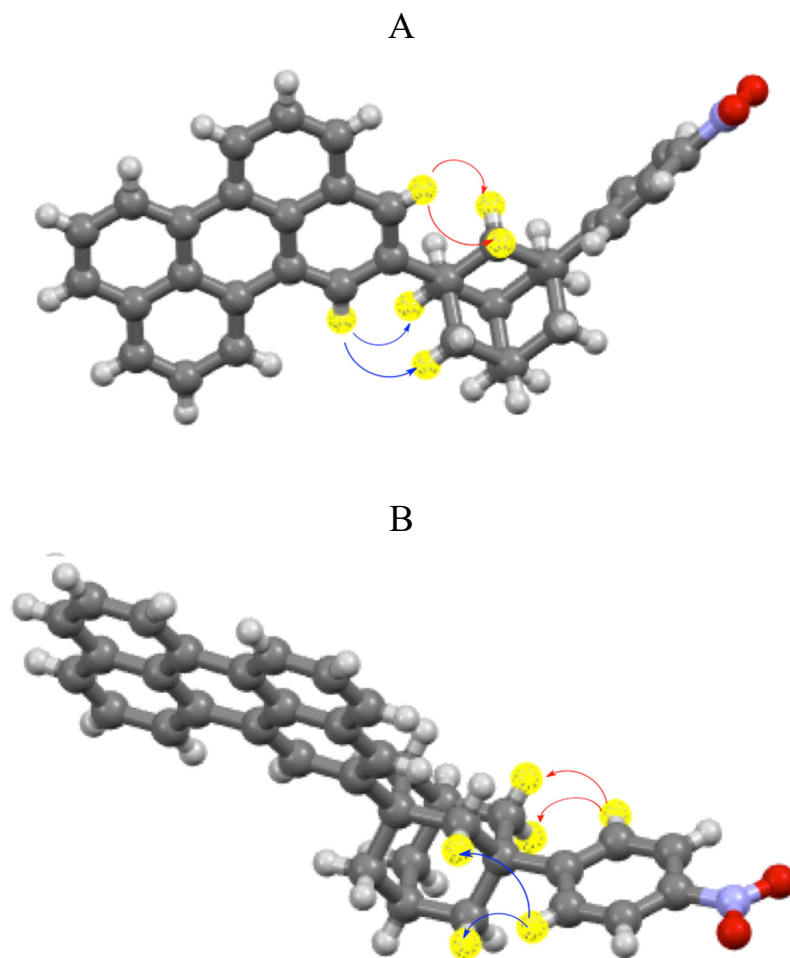
A

B

Figure 4.25. Conformations of PER-AD-NB showing spatial arrangement of *ortho* hydrogen atoms of the aromatics alongside adjacent hydrogen atoms of AD. (A) shows the perylene side interactions and (B) shows the nitrobenzene side interactions.

4.4. Conclusions

In this chapter we report the studies on four adamantane bridged donor-acceptor compact dyads. Aromatic hydrocarbons anthracene, pyrene, diphenyl anthracene and perylene served as donors and nitrobenzene served as acceptor. Facile electron transfer occurred in all dyads and the CS states were long lived in all cases. In the case of AN-AD-NB and PY-AD-NB, prominent absorptions due to the local triplet states were also observed. Triplet formation was less in the cases of DPA-AD-NB and PER-AD-NB. In order to get some insight into the long-lived CS state formation we obtained the single crystal X-ray structures of two of the dyads. The X-ray structures suggested that the free rotation of the D and A chromophores in these dyads are restricted, leading to reduced interaction in the ion-pair state, which is proposed as reason for the longevity of the CS state. Based on these studies we propose that use of adamantane as bridge can enhance the lifetimes of the CS states in compact dyads.

4.5. Experimental Section

4.5.1. Methods.

Experimental methods employed in this chapter are same as in Chapter 2 for all spectroscopic measurements. For the single crystal X-ray studies, the single crystals were mounted using oil (Infineum V8512) on a glass fibre. All measurements were made on a CCD area detector with graphite monochromated MoKα radiation. The data were collected using Bruker APEXII detector and processed using APEX2 from Bruker. All structures were solved by direct methods and expanded using Fourier techniques. The non-hydrogen atoms were refined anisotropically. Hydrogen atoms were included in idealized positions, but not refined.

4.5.2. **Synthesis of Compounds.**

4.5.2.1. **Synthesis of DPA-AD-NB:** To a mixture of diphenylanthracene (0.5 g, 2.47 mmol) and triflic acid (1.49 g, 9.9 mmol) in CH_2Cl_2 (30 mL), 1-hydroxy-3(4-nitrophenyl) adamantane (see Chapter 3, 0.68 g, 2.47 mmol) was added in one lot with vigorous stirring. After 5 minutes of stirring, the reaction was quenched by adding ice-water. CH_2Cl_2 (50 mL) was added and layers separated. The CH_2Cl_2 layer was washed free of acid, dried with anhydrous Na_2SO_4 and solvent removed to get a residue, which was chromatographed over silica gel. Elution with hexane gave unreacted diphenylanthracene. Further elution with hexane-chloroform (8:2) mixture gave the product DPA-AD-NB. Yield: 260 mg (45%), ^{1}H NMR (CDCl$_3$, 500 MHz) δ: 1.770 (s, 2H), 1.865-1.978 (m, 10H), 2.306 (s, 2H), 7.309-7.325 (t, 2H), 7.431-7.681 (m, 17H), 7.708 (d, 2H). ^{13}C NMR (CHCl$_3$, 125 MHz) δ:29.21, 35.59, 37.38, 37.95, 41.19, 42.12, 47.84, 121.40, 123.43, 123.47, 124.78, 124.94, 125.90, 126.94, 127.43, 128.40, 129.71, 129.86, 131.30, 131.37, 136.74, 137.04, 139.09, 139.18, 146.00, 158.08. HRMS calculated for $C_{42}H_{35}NO_2$: 585.75, Observed: 585.75.

4.5.2.2. Synthesis of PER-AD-NB: A solution of 1-bromo-3(4-nitrophenl)adamantane (Chapter 3**,** 670 mg , 2 mmol) in dry DCM (10 mL) was added drop-wise over a period of 15 min. to a well-stirred mixture of freshly sublimed FeCl$_3$ (326 mg, 2 mmol) and Perylene (500 mg, 2 mmol). After complete addition, the mixture was refluxed for 3 h and allowed to stand overnight and then poured into ice containing conc. HCl (5 mL). The DCM layer was separated, washed free of acid and dried over anhydrous CaCl$_2$. The solvent was removed and the residue obtained was crystallized from 20% Chloroform-Hexane mixture to give the product PER-AD-NB. Yield: 59 %. ^{1}H NMR (CDCl$_3$, 500 MHz) δ: 1.877 (m, 1H), 1.972-2.00 (m, 1H), 2.054-2.143 (m, 4H),2.412-2.485 (m, 8H) 7.469-7.546 (m, 4H), 7.592 (d, 2H), 7.608 (d, 2H), 8.166-8.207 (m,

4H), 8.207 (s, 1H), 8.469 (d, 2H). ^{13}C NMR (CHCl$_3$, 125 MHz) δ:37.13, 43.55, 43.80, 49.01, 26.83, 31.34, 36.45, 120.21, 121.3, 123.65, 124.01, 124.41, 125.33, 125.95, 126.22, 127.15, 128.19, 131.98, 133.78, 134.10, 135.88,145.15, 146.01, 145.45 . HRMS calculated for C$_{36}$H$_{29}$NO$_2$: 507.22, Observed: 507.23.

4.6. References

1. Mann, C. K.; Barnes, K. K. *Electrochemical Reactions in Nonaqueous Systems*, Marcel Dekker Inc., New York, 1970, pp 347 – 379.

2. Nagakura, S.; Kojima, M.; Maruyama, Y. Electronic Spectra and Electronic Structures of Nitrobenzene and Nitromesitylene. *J. Mol. Spectroscopy* **1964**, *13*, 174-192.

3. Vidal, B.; Murrel, J. N. The Effect of Solvent on the Position of the First Absorption Band of Nitrobenzene. *Chem. Phys. Lett.* **1975**, *31*, 46-47.

4. Kröhl, O.; Malsch, K.; Swiderek, P. The Electronic States of Nitrobenzene: Electron-Energy-Loss Spectroscopy and CASPT2 Calculations. *Phys. Chem. Chem. Phys.* **2000**, *2*, 947-953.

5. Sinha, H. K.; Yates, K. Ground and Excited-State Dipole Moments of Some Nitroaromatics. Evidence for Extensive Charge Transfer in Twisted Nitrobenzene Systems. *J. Chem. Phys.* **1990**, *93*, 7085-7093.

6. Yip, R. W.; Sharma, D. K.; Glasson, R.; Gravel, D. Picosecond Excited-State Absorption of Alkyl Nitrobenzene in Solution. *J. Phys. Chem.* **1984**, *88*, 5770-5772.

7. Takezaki, M.; Hirota, N.; Terazima, M. Nonradiative Relaxation Processes and Electronically Excited States of Nitrobenzene Studied by Picosecond Time-Resolved Transient Grating Method. *J. Phys. Chem. A* **1997**, *101*, 3443-3448.

8. Takezaki, M.; Hirota, N.; Terazima, M.; Sato, H.; Nakajima, T.; Kato, S. Geometries and Energies of Nitrobenzene Studied by CAS-SCF Calculations. *J. Phys. Chem. A* **1997**, *101*, 5190-5195.

9. Bock, C. R.; Connor, J. A.; Gutierrez, A. R.; Meyer, T. J.; Whitten, D. G.; Sullivan, B. P.; Nagle, J. K. Estimation of Excited-State Redox Potentials by Electron-Transfer Quenching. Application of Electron-Transfer Theory to Excited-State Redox Processes. *J. Am. Chem. Soc.* **1979**, *101*, 4815-4824.

10. Zanini, G. P.; Montejano, H. A.; Previtali, C. M. Photoinduced Electron-Transfer Quenching of Excited Singlet States of Polycyclic Aromatic Hydrocarbons by Organic Acceptors. *J. Chem. Soc. Faraday Trans.* **1995**, *91*, 1197-1202.

11. Montejano, H. A.; Avila, V.; Garrera, H. A.; Previtali, C. M. Solvent and Temperature Effects in the Electron Transfer Quenching of Triplet States of Aromatic Hydrocarbons by Nitrobenzenes. *J. Photochem. Photobiol. A Chem.* **1993**, *72*, 117-122.

12. Kuzmin, V. A.; Renge, I. V.; Borisevich, Y. E. Triplet Quenching of Polycyclic Hydrocarbons by Electron Acceptors. *Chem. Phys. Lett*. **1980**, *70,* 257-261.

13. Lewis, F. D.; Daublain, P.; Delos Santos, G. B.; Liu, W.; Asatryan, A. M.; Markarian, S. A.; Fiebig, T.; Raytchev, M.; Wang, Q. Dynamics and Mechanism of Bridge-Dependent Charge Separation in Pyrenylurea-Nitrobenzene π-Stacked Protophanes. *J. Am. Chem. Soc.* **2006**, *128*, 4792-4801.

14. Hurley, R.; Testa, A. C. Photochemical n → π* Excitation of Nitrobenzene. *J. Am. Chem. Soc.* **1966**, *88*, 4330-4332.

15. Hurley, R.; Testa, A. C. Nitrobenzene Photochemistry. II. Protonation in the Excited State. *J. Am. Chem. Soc.* **1967**, *89*, 6917-6919.

16. Charlton, J. L.; Liao, C. C.; de Mayo, P. Photochemical Synthesis. The Addition of Aromatic Nitro Compounds to Akenes. *J. Am. Chem. Soc.* **1971**, *93*, 2463-2471.

17. Maldotti, A.; Andreotti, L.; Molinari, A.; Tollari, S.; Penoni, A.; Cenini, S. Photochemical and Photocatalytic Reduction of Nitrobenzene in the Presence of Cyclohexene. *J. Photochem. Photobiol. A Chem.* **2000**, *133*, 129-133.

18. Turro, C.; Chang, C. K.; Leroi, G. E.; Cukier, R. I.; Nocera, D. G. Photoinduced Electron Transfer Mediated by a Hydrogen-Bonded Interface. *J. Am. Chem. Soc*. **1992**, *114*, 4013-4015.

19. Wasielewski, M. R.; Niemczyk, M. P.; Svec, W. A.; Pewitt, E. B. Dependence of Rate Constants for Photoinduced Charge Separation and Dark Charge Recombination on the Free Energy of Reaction in Restricted-Distance Porphyrin-Quinone Molecules. *J. Am. Chem. Soc*. **1985**, *107*, 1080-1082.

20. Beratan, D. N.; Onuchic, J. N.; Hopfield, J. J. Electron Tunneling Through Covalent and Noncovalent Pathways in Proteins. *J. Chem. Phys*. **1987**, *86*, 4488-4498.

21. Beratan, D. N.; Betts, J. N.; Onuchic, J. N. Protein Electron Transfer Rates Set by the Bridging Secondary and Tertiary Structure. *Science* **1991**, *252*, 1285-1288.

22. Onuchic, J. N.; Beratan, D. N. A Predictive Theoretical Model for Electron Tunneling Pathways in Proteins. *J. Chem. Phys*. **1990**, *92*, 722-733.

23. Berg, A.; Shuali, Z.; Asano-Someda, M.; Levanon, H.; Fuhs, M.; Möbius, K.; Wang, R.; Brown, C.; Sessler, J. L. A First High-Field EPR Study of Photoinduced Electron Transfer in a Base-Paired Porphyrin-Dinitrobenzene Supramolecular Complex. *J. Am. Chem. Soc*. **1999**, *121*, 7433-7434.

24. Robert, J. A.; Kirby, J. P.; Nocera, D. G. Photoinduced Electron Transfer within a Donor-Acceptor Pair Juxtaposed by a Salt Bridge. *J. Am. Chem. Soc.* **1995**, 117, 8051–8052.

25. Kirby, J. P.; Roberts, J. A.; Nocera, D. G. Significant Effect of Salt Bridges on Electron Transfer. *J. Am. Chem. Soc*. **1997**, *119*, 9230-9236.

26. Deng, Y.; Roberts, J. A.; Peng, S.-M., Chang, C. K.; Nocera, D. G. The Amidinium-Carboxylate Salt Bridge as a Proton-Coupled Interface to Electron Transfer Pathways. *Angew. Chem. Int. Ed*. **1997**, *36*, 2124-2127.

27. Prasad, E.; Gopidas, K. R. Photoinduced Electron Transfer in Hydrogen Bonded Donor-Acceptor Systems. Study of the Dependence of Rate on Free Energy and Simultaneous Observation of the Marcus and Rehm-Weller Behaviors. *J. Am. Chem. Soc.* **2000**, *122*, 3191-3196.

28. Smitha, M. A.; Prasad, E.; Gopidas, K. R. Photoinduced Electron Transfer in Hydrogen Bonded Donor-Acceptor Systems. Free Energy and Distance Dependence Studies and an Analysis of the Role of Diffusion. *J. Am. Chem. Soc.* **2001**, *123*, 1159-1165.

29. Wang. Y.-H.; Zhang, H.-M.; Liu, L.; Liang, Z.-X.; Guo, Q.-X.; Tung, C.-H.; Inoue, Y.; Liu, Y.-X. Photoinduced Electron Transfer in a Mono-6-*p*-nitrobenzoyl-β-cyclodextrin with Naphthalene Derivatives. *J. Org. Chem*. **2002**, *67*, 2529-2434.

30. Wang, Y.-H.; Fu, Y.; Zhu, M.-Z.; Huang, X.; Guo, Q.-X. Photoinduced Electron Transfer Reactions in a Host-Guest Assembly of Mono-6-*p*-nitrobenzoyl-β-cyclodextrin with N-(1-naphthylacetyl)-1-adamantamine. *Res. Chem. Intermed*. **2003**, *29*, 11-19.

31. Wang, Y.-H.; Zhu, M.-Z.; Ding, X.-Y.; Ye, J.-P.; Liu, L.; Guo, Q.-X. Photoinduced Electron Transfer Between Mono-6-*p*-nitrobenzoyl-β-cyclodextrin and Adamantanamine-C_n-porphyrins. *J. Phys. Chem*. *B* **2003**, *107*, 14087-14093.

32. Rekharsky, M. V.; Inoue, Y. Complexation Thermodynamics of Cyclodextrins. *Chem. Rev.* **1998**, *98*, 1875-1917.

33. Mataga, N.; Asahi, T.; Kanda, Y.; Okada, T. The Bell Shaped Energy Gap Dependence of the Charge Recombination Reaction of Geminate Radical Ion Pairs Produced by Fluorescence Quenching Reaction in Acetonitrile Solution. *J. Chem. Phys.* **1988**, *127*, 249-261.

34. Yamaji, M.; Maeda, H.; Nanai, Y.; Mizuno, K. Substitution Effects of C≡C Triple Bonds on the Fluorescent Properties of Perylene Studied by Emission and Transient Absorption Measurements. *Chem. Phys. Lett.* **2012**, *536*, 72-76.

35. Lewitzka, F.; Löhmannsröben, H.-G. The Deactivation of Singlet Excited Perylene by Aromatic Molecules in Solution. *Z. Phys. Chem. NF.* **1990**, *161*, 181-202.

36. Chattopadhyay, S. K.; Kumar, Ch. V.; Das, P. K. Triplet-Related Photophysics of 9,10-Diphenylanthracene. A Kinetic Study of Reversible Energy Transfer from Anthracene Triplet by Nanosecond Laser Flash Photolysis. *Chem. Phys. Lett.* **1983**, *98*, 250-254.

37. Susuki, T.; Nagano, M.; Watanabe, S.; Ichimura, T. Study of the Photophysics and Energy Transfer of 9,10-Diphenylanthracene in Solution. *J. Photochem. Photobiol. A: Chem.* **2000**, *136*, 7-13.

38. Gray, V.; Dzebo, D.; Lundin, A.; Alborzpour, J.; Abrahamsson, M.; Albinsson, B.; Moth-Poulsen, K. Photophysical Characterization of the 9,10-Disubstituted Anthracene Chromophore and its Applications in Triplet-Triplet Annihilation Photon Upconversion. *J. Mater. Chem. C* **2015**, *3*, 11111-11121.

39. Workentin, M. S.; Johnson, L. J. Wayner, D. D. M.; Parker, V. D. Reactivity of Aromatic Radical Cations. Rate Constants for Reactions of 9-Phenyl and 9,10-Diphenylanthracene Radical Cations with Acyclic Amines. *J. Am. Chem. Soc.* **1994**, *116*, 8279-8287.

40. Sioda, R. E. Electrolytic Oxidation of 9,10-Diphenylanthracene and Properties of Its Radical Cation and Anion. *J. Phys. Chem.* **1968**, *72*, 2322-2300.

41. Masnovi, J. M.; Seddon, E. A.; Kochi, J. K. Electron Transfer from Anthracenes. Comparison of Photoionization, Charge-Transfer Excitation and Electrochemical Oxidation. *Can. J. Chem.* **1984**, *62*, 2552-2559.

42. Shida, T. *Electronic Absorption Spectra of Radical Ions*, Elsevier Science Publishers B. V., Amsterdam, 1988. (a) p. 69; (b) p. 329; (c) p. 86; (d) p. 87.

43. Murov, S. L.; Carmichael, I.; Hug, G. *Handbook of Photochemistry*, Second Edition, Revised and Expanded, Marcel Dekker, New York, 1993. (a) p. 103; (b) p. 122; (c) p. 118; (d) p. 104.

44. Grellmann, K. H.; Watkins, A. R. The Photoionization of Perylene in Acetonitrile Solutions. *Chem. Phys, Lett.* **1971**, *9*, 439-443.

45. Konuk, R.; Cornelisse, J.; McGlynn, S. P. Photoionization of Perylene in Polar Solvents. *J. Chem. Phys.* **1985**, *82*, 3929- 3933.

46. Smit, K. J.; Warman, J. M. The Formation of Singlet and Triplet Charge Transfer States on Photo-Excitation of Carbazole-$(CH_2)n$-Tetrachlorophthalimide Compounds Studied by Time-Resolved Microwave Conductivity. *J. Lumin.* **1988**, *42*, 149-154.

47. Anglos, D.; Bindra, V.; Kuki, A. Photoinduced Electron Transfer and Long-Lived Charge Separation in Rigid Peptide Architectures. *J. Chem. Soc., Chem. Commun.* **1994**, 213-215.

48. van Dijk, S. I.; Groen, C. P.; Hartl, F.; Brouwer, A. M.; Verhoeven, J. W. Long-Lived Triplet State Charge Separation in Novel Piperidine-Bridged Donor-Acceptor Systems. *J. Am. Chem. Soc.* **1996**, *118*, 8425-8432.

ABSTRACT

Name of the Student: Daisymol K. B.   **Registration No. : 10CC15J39005**

Faculty of Study: Chemical Science   **Year of Submission: 2023**

AcSIR academic centre/CSIR Lab: CSIR-NIIST, Thiruvananthapuram

Name of the Supervisor(s): Dr. K.R. Gopidas

Title of the thesis: Design, Synthesis and Photo-physical Studies of Donor-Acceptor Systems for Achieving Long-Lived Charge-Separated State

---

We synthesized a few novel Donor-Acceptor dyads for achieving long lived Charge Separated (CS) states adopting several strategies. Photoinduced electron transfer in two donor-acceptor dyads with bis(phenylethynyl)anthracene as light absorber and acceptor and phenothiazine as donor were investigated in Chapter 2. Electron transfer in these systems is analyzed in the light of Marcus theory and the slow back electron transfer was attributed to inverted region effects. The fact that both dyads reported in Chapter 2 did not generate the local triplet suggest that spin-orbit coupling or hyperfine-induced intersystem crossing pathways are not operating in these molecules and hence, the long-lived CS state in these molecules can be attributed to the inverted region effect, which is made possible by lack of intersystem crossing in the parent hydrocarbon. The dyads in chapter 3 and 4 which employ adamantane moiety as bridge and the CS state lifetimes obtained exhibited more than thousand-fold larger when compared to the same dyad systems bridged through C3-alkyl chains. In addition to the long-lived CS state decays, slow formation of acceptor triplets was also observed in nanosecond flash photolysis and both these features are first-time observations for compact dyads. Thus, our studies in the thesis confirm that the adamantane bridge can be used to enhance charge separated states in compact dyads.

Details of the publications emanating from the thesis work

1. Daisymol, K. B.; Gopidas, K. R. Thousand-Fold Enhancement of Charge Separated State Lifetimes Caused by an Adamantane Bridge in Dimethylaniline-Anthracene and Dimethylaniline-Pyrene Dyads. *J. Phys. Chem. Lett.* **2023**, 14, 4, 977–982.

2. Daisymol, K. B.; Gopidas, K. R. Long-Lived Photoinduced Charge Separation in Adamantane-Bridged Donor-Acceptor Systems: A Case of Adamantane Bridge Conferring Orthogonal Donor-Acceptor Orientation and Restricted Rotation. (Manuscript Communicated- J. Am. Chem. Soc).

List of posters presented in conferences

1. "Synthesis of Nanographite Materials from Diazonium Salts, and its Functionalization, Characterization and Energy Applications", Kurisingal B. Daisymol; Sadasivan P. Prakash; Karical R. Gopidas, ; East Asian Symposium (EAS8-2017). CSIR-National Institute for Interdisciplinary Science and Technology, Thiruvananthapuram 695 019, Kerala, India, September, 20-22, **2017**.

Letter

Thousand-Fold Enhancement of Charge-Separated State Lifetimes Caused by an Adamantane Bridge in Dimethylaniline−Anthracene and Dimethylaniline−Pyrene Dyads

Kurisingal B. Daisymol and Karical R. Gopidas*

Read Online

ACCESS | Metrics & More | Article Recommendations | SI Supporting Information

ABSTRACT: A long-standing challenge in photoinduced electron transfer research is the design of compact donor−acceptor dyads that can generate long-lived charge-separated (CS) states for use as sensitizers in solar energy harvesting. Reports of dyads exhibiting CS state lifetimes in the microsecond time domain are very rare. Herein, we report two compact donor−bridge−acceptor dyads exhibiting lifetimes in the microsecond domain. We employed an adamantane moiety as a bridge, and the lifetimes obtained are nearly 1000-fold larger when compared to those of the same donor−acceptor dyads bridged through C_3-alkyl chains. In addition to long-lived CS state decays, slow formation of acceptor triplets was also observed via nanosecond flash photolysis. The long lifetime of the CS state is attributed to the extremely small value of the electronic coupling matrix element for the charge recombination compared to charge separation.
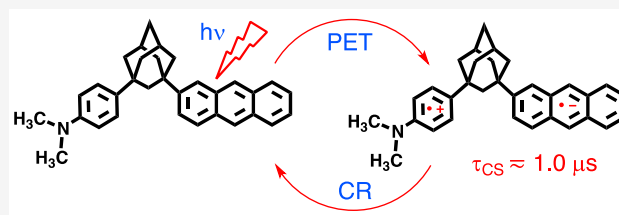
Photogenerated radical-ion pairs (RP) in linked donor−acceptor (D−A) dyads are extremely short-lived because of the very fast charge recombination (CR) reaction either to the D−A ground state or to a low-lying local triplet (^{3}D* or ^{3}A*).[1,2] Applications of photoinduced electron transfer (PET) in practically relevant areas such as artificial photosynthesis, solar water splitting, and photocatalytic reactions require CS states with near-microsecond lifetimes; hence, enhancing CS state lifetimes is a major goal in photochemistry. Most of the studies in this area envisaged the natural photosynthetic reaction center as a model and designed covalently linked triads, tetrads, and higher-order systems.[3−6] However, covalent synthesis of large molecular arrays is highly inefficient and expensive, and hence, the assembly of such arrays through noncovalent interactions was also attempted.[7,8] The covalent and noncovalent approaches have very little success in extending the CS state lifetimes beyond the nanosecond domain. The amount of energy that can be stored in the CS state is also very important. In large molecular arrays, a long-lived CS state is possible because of sequential electron transfer steps that increase the distance between the charge centers. Energy is lost in each of these steps, and as a result, the CS state will store only ∼50% of the excitation energy in a typical tetrad. In this context, the design of compact dyads that can exhibit long CS state lifetimes and also store energy in excess of 2.0 eV looks extremely attractive and important.[9] In this work, we employed adamantane (AD) as the bridge between D and A moieties and obtained enhanced CS state lifetimes from picoseconds to a few hundred nanoseconds when compared to those of the same D−A systems bridged through alkyl chains.

The spin control approach, in which the CS state is generated with triplet spin multiplicity, can lead to CS states with microsecond lifetimes.[10−12] In these molecules, a local triplet state lies below the CS state in nonpolar solvents. When excited, the CS state generated in the singlet state (^{1}CS) undergoes intersystem crossing (ISC) to give ^{3}CS. Ultrafast CR reaction in the ^{3}CS leads to the formation of local triplets. When the spin control strategy works, energy level reversal occurs in polar solvents such that the energy of the ^{3}CS state becomes lower than that of the local triplet. Excitation in polar solvents leads to formation of the ^{3}CS state, which will be long-lived because CR to the local triplet is endergonic and CR to the ground state is spin forbidden. A notable example is an *N*-alkylnaphthalimide acceptor linked to a 4-methoxyaniline donor through a piperidine bridge, reported by Verhoeven and co-workers.[12] Excitation of the acceptor leads to a short-lived ^{1}CS state in nonpolar solvents, whereas in polar solvents, a long-lived ^{3}CS state is observed. The spin control strategy can work only if the ^{3}CS is the lowest triplet in the dyad, and only a few examples are known.[10−12] The amount of energy that can be stored in the ^{3}CS state is also small.

In this study, we used dimethylaniline (DMA) as the donor and anthracene (AN) and pyrene (PY) as excited state

electron acceptors. Bimolecular PET reactions in DMA−AN and DMA−PY systems have been studied under various conditions.[13−16] PET leads to formation of a short-lived DMA radical cation (DMA$^{\bullet+}$) and an AN or PY radical anion (AN$^{\bullet-}$ or PY$^{\bullet-}$, respectively). Very fast CR occurs to the ground state and also to triplet state of AN or PY. Thus, the long-lived transients in the bimolecular PET reactions are ^{3}AN* or ^{3}PY*. PET in methylene chain-linked systems such as DMA−(CH$_2$)$_n$−AN and DMA−(CH$_2$)$_n$−PY, where n varied from 1 to 16, were also investigated in great detail using steady state and time-resolved fluorescence as well as nanosecond and picosecond transient absorption spectroscopies.[17−27] PET reactions in these systems lead to a short-lived CS state, $^{\bullet+}$DMA−(CH$_2$)$_n$−AN$^{\bullet-}$ [or $^{\bullet+}$DMA−(CH$_2$)$_n$−PY$^{\bullet-}$] initially, the fate of which actually depends on n. For short chain systems ($n < 6$), the CS state is very short-lived and decays to the ground state. For systems for which $n > 6$, the CS decays to the ground state and also to the acceptor triplets. In this study, we used AD-bridged systems that separate the D and A moieties by three carbon atoms (or four C−C bonds), and we expect a photochemistry similar to that of the DMA−(CH$_2$)$_3$− AN or DMA−(CH$_2$)$_3$−PY system. For these systems, solvent-dependent photochemistry was reported.[18−20] In nonpolar solvents, ultrafast formation of an exciplex was observed. In the polar solvent acetonitrile, conformation-dependent photo-chemistry was observed. Molecules that exist in the folded conformation undergo ultrafast (<2 ps) exciplex formation, and molecules in the extended conformation gave the CS states [$^{\bullet+}$DMA−(CH$_2$)$_3$−AN$^{\bullet-}$ or $^{\bullet+}$DMA−(CH$_2$)$_3$−PY$^{\bullet-}$].[18−20] For the DMA−(CH$_2$)$_3$−AN system, the CS state is formed within 2.7 ps and undergoes charge recombination to the ground state in 0.7 ns. For the DMA−(CH$_2$)$_3$−PY system, the RP state is formed within 11 ps and undergoes charge recombination in 1.1 ns.[25] In both cases, acceptor triplet excited states (^{3}AN* and ^{3}PY*) were not formed. In this work, we replaced the -(CH$_2$)$_3$- chain with a 1,3-AD bridge and designed the DMA−AD−AN and DMA−AD−PY dyads. Photoexcitation of these dyads led to formation of the RP states with lifetimes close to 1 μs. The energy stored in the $^{\bullet+}$DMA−(CH$_2$)$_3$−AN$^{\bullet-}$ radical pair is ∼2.7 eV. In addition to the CS state, formation of acceptor triplets was also observed. Thus, replacement of the methylene chain with the rigid adamantane moiety led to the drastic alteration of the photochemical processes in the D−A system.

To the best of our knowledge, AD has never been employed as a bridging moiety in any D−bridge−A dyad designed for PET. However, the AD-bridged trichromophoric system phenanthrene−AD−biphenyl−AD−naphthalene was studied by Tan et al., who reported singlet−singlet and triplet−triplet energy transfers.[28] Because AD is a very rigid, saturated molecule with no absorption above 250 nm, it is not expected to perturb the electronic states of D or A.

Structures of the DMA−AD−AN and DMA−AD−PY AD-bridged systems along with the previously studied methylene-bridged systems[18−25] are shown in Figure 1. Synthesis and characterization of the dyads are given in Section 2 of the Supporting Information. The 1,3-AD bridge keeps the D and A moieties at a fixed edge-to-edge distance (R_e) of ∼4.6 Å, as in the case of rigid norbornylogous-bridged systems studied in detail by Paddon-Row et al. (Section 3 of the Supporting Information).[4] DMA−AD−PY tends to aggregate in an acetonitrile solution even at low concentrations, and dichloro-
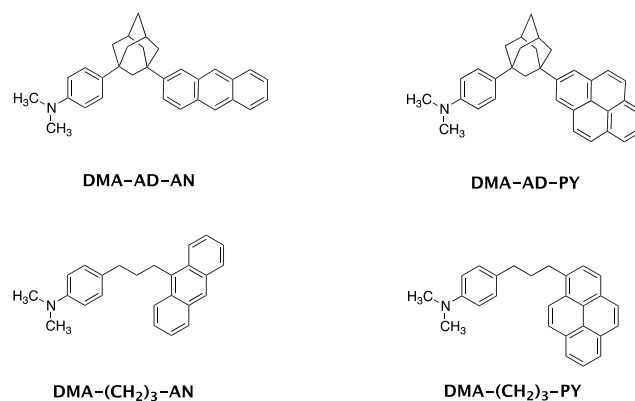

Figure 1. Structures of the DMA−AD−AN and DMA−AD−PY dyads along with previously studied DMA−(CH$_3$)$_3$−AN and DMA−(CH$_3$)$_3$−PY systems.

methane solutions are used for this study. For DMA−AD−AN, studies are performed in acetonitrile.

In Figure 2A−E, we present the photophysical data for the dyads. The absorption spectrum of DMA−AD−AN in acetonitrile is shown in Figure 2A along with spectra of the components DMA and AD. Absorption spectra of DMA−AD−PY and the components in dichloromethane are shown in Figure 2B. Compared to the parent hydrocarbons, the dyads exhibited increased absorption in the region below 320 nm, which can be attributed to DMA, and a small shoulder in the higher-wavelength region. The vibronic band maxima of AN and PY absorptions remain unaffected in the dyads. Figure 2C compares the fluorescence spectra of optically matched solutions of AN and DMA−AD−AN obtained under identical instrument conditions. Similarly, Figure 2D compares the emissions of PY and DMA−AD−PY under identical conditions. Panels C and D of Figure 2 show that the fluorescence of the dyads is strongly quenched when compared to that of the parent hydrocarbon, AN (or PY). Normalized fluorescence spectra of the parent hydrocarbons and dyads are shown in Section 4 of the Supporting Information. Normal-ization shows that the spectra are broadened in the long-wavelength region, but emissions attributable to the excimer or exciplex are absent in the emission spectra of DMA−AD−AN and DMA−AD−PY. From the fluorescence intensities, we estimated the percentage quenching as 95% for DMA−AD−AN and 80% for DMA−AD−PY.

Fluorescence decay profiles of the dyads are shown in panels E and F of Figure 2. The decays were biexponential with a fast component that contributed to >90% of the decay and a slow component (5−7%). We assign the fast component of the decay to PET taking place in the dyads (Section 5 of the Supporting Information).

Fluorescence quenching observed for the dyads is attributed to electron transfer taking place from the donor DMA to the singlet excited state of the acceptor hydrocarbon, leading to formation of the CS state.

$$\text{DMA−AD−AN} \xrightarrow{h\nu} \text{DMA−AD −}^1\text{AN*} \xrightarrow{\text{ET}} {}^{\bullet+}\text{DMA−AD−AN}^{\bullet-}$$
(1)
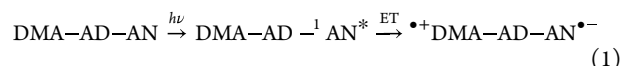
The rate constant for this process, k_{CS}, was obtained in the usual way from the fluorescence decay data (Section 5 of the Supporting Information). We obtained k_{CS} values of 4.06×10^9 and 4.60×10^8 s^{-1} for DMA−AD−AN and DMA−AD−PY, respectively. These rates were 1−2 orders of magnitude smaller
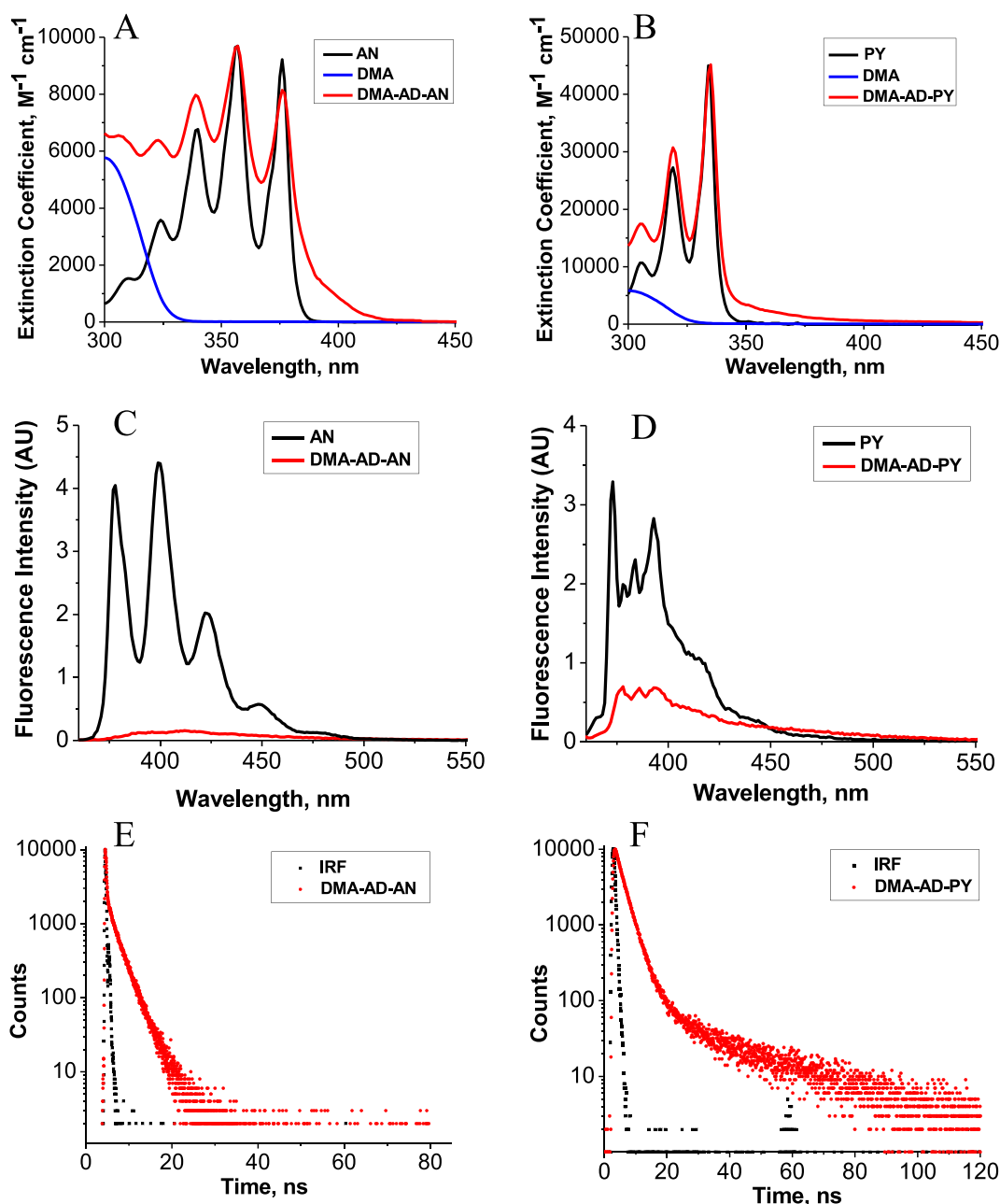
Figure 2. Photophysical data for DMA−AD−AN and DMA−AD−PY. (A) Absorption spectra of DMA, AN, and DMA−AD−AN. (B) Absorption spectra of DMA, PY, and DMA−AD−PY. (C) Fluorescence spectra of optically matched solutions of AN and DMA−AD−AN (λ_{exc} = 350 nm; OD_{350} = 0.05). (D) Fluorescence spectra of optically matched solutions of PY and DMA−AD−PY (λ_{exc} = 330 nm; OD_{330} = 0.05). (E) Fluorescence decay profile of DMA−AD−AN with a lamp profile (λ_{exc} = 331 nm; λ_{em} = 395 nm). (F) Emission decay profile of DMA−AD−PY with a lamp profile (λ_{exc} = 331 nm; λ_{em} = 375 nm).

than those of the corresponding -(CH$_2$)$_3$- bridged systems.[18−20,25]

Transient absorption spectra obtained at different times for DMA−AD−AN are shown in Figure 3. The spectra showed peaks at 430, 470, and 720 nm and are nearly identical to the transient absorption spectrum obtained at early times in the intermolecular PET between AN and DMA.[13] On the basis of this and other literature reports, the 430 nm peak is assigned to ^{3}AN*,[29] the 470 nm peak is assigned to DMA$^{\bullet+}$,[30−32] and the absorption features around 700 nm are assigned to AN$^{\bullet-}$.[33] DMA$^{\bullet+}$ and AN$^{\bullet-}$ are formed by the electron transfer reaction

in eq 1. The insets in Figure 3 show decay profiles of the transients at 430 and 470 nm. The decay rates of DMA$^{\bullet+}$ at 470 nm and AN$^{\bullet-}$ at 720 nm were the same and were attributed to CR reaction to the ground state. Fitting the decay at 470 nm to a single exponential gave a CR rate k_{CR} of 1.15 × 10^6 s^{-1}, which gave $\tau_{CS} = 1/k_{CR}$ = 872 ns. Fits of the data with residuals are shown in Section 6 of the Supporting Information. The τ_{CS} value of 872 ns obtained for DMA−AD−AN in the polar solvent acetonitrile is among the highest ever reported for a compact dyad. A fit of the 430 nm decay
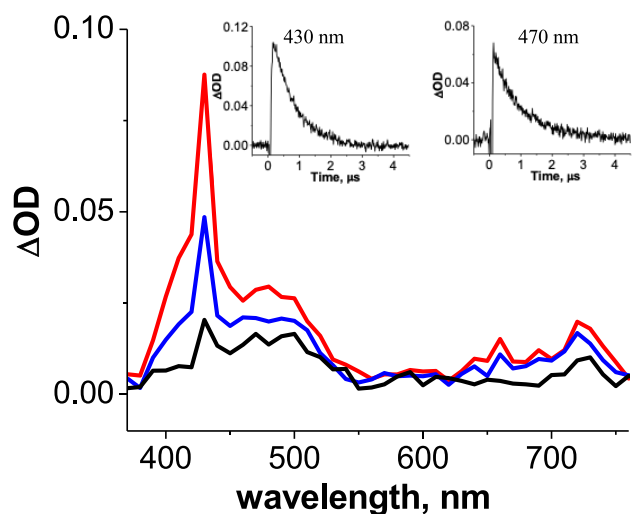
Figure 3. Transient absorption spectra obtained at 390 ns (red), 780 ns (blue), and 1.24 μs (black) in the flash photolysis of DMA−AD− AN in acetonitrile (OD$_{355}$ = 0.5 for the solution). The insets show the decay profiles at 430 and 470 nm. See Section 6 of the Supporting Information for the decay profile and the fit of the decay data.

gave a triplet lifetime τ_T of 740 ns. A fit of the data with residuals is given in Section 6 of the Supporting Information.

The transient absorption spectra obtained in the flash photolysis of DMA−AD−PY at different times are shown in Figure 4. The spectra are broad because of overlapping
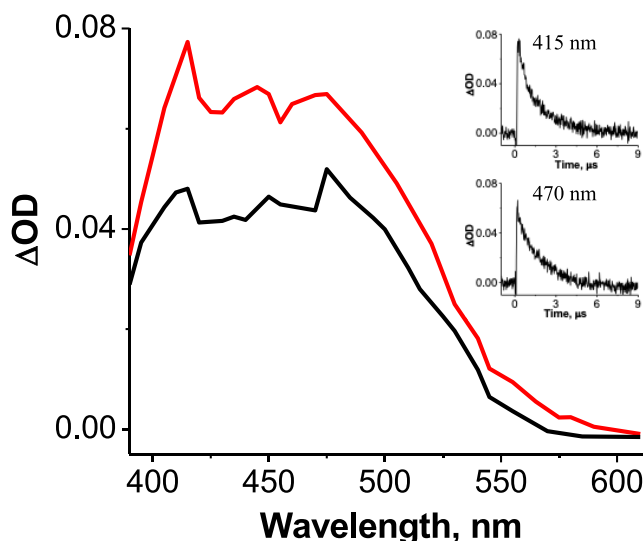

Figure 4. Transient absorption spectra obtained at 250 ns (red) and 750 ns (black) in the flash photolysis of DMA−AD−PY in dichloromethane (OD$_{355}$ = 0.5 for the solution). The insets show the decay profiles at 415 and 470 nm.

absorptions of ^{3}PY* (415 and 470 nm),[34] PY$^{•-}$ (495 nm),[35,36] and DMA$^{•+}$ (470 nm).[30−32] The overlapping nature of the transients makes it difficult to determine exact lifetimes, but it may be noted from the insets that lifetimes of all of the transients are slightly greater than 1.0 μs.

The formation of the acceptor triplets in the flash photolysis of the dyads is very intriguing. Using an optically matched solution of AN in acetonitrile, we calculated the quantum yield (Φ_T) of ^{3}AN* in the case of DMA−AD−AN (Section 7 of the

Supporting Information). We obtained a Φ_T of 0.21. In short time windows, the formation of the triplet can be observed as shown in Figure 5. A similar growth pattern is absent for the
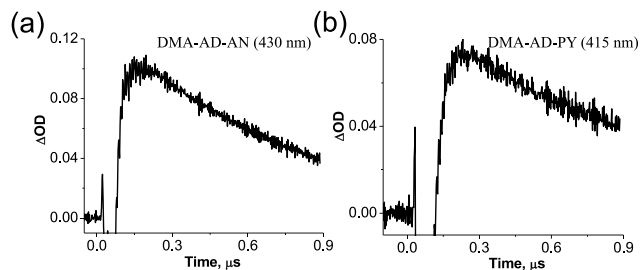

Figure 5. Slow growth of triplet absorptions in the flash photolysis of (A) DMA−AD−AN and (B) DMA−AD−PY. A fit of the growth at 430 nm in the case of DMA−AD−AN is given in Section 6 of the Supporting Information.

DMA$^{•+}$ (470 nm) and AN$^{•-}$ (720 nm) absorptions. Kinetic profiles of the 470 and 720 nm transients taken in the short time window did not show the growth pattern (see Section 8 of the Supporting Information), suggesting that DMA$^{•+}$ and AN$^{•-}$ are formed within the laser pulse through PET reaction (eq 1) and the ^{3}AN* is formed in a slow reaction.

Because the triplets exhibited slow growth, it can be safely assumed that this species is formed through CR reaction in the radical pair state. On the basis of this argument, the photo processes taking place in DMA−AD−AN are summarized in Figure 6. Excitation with 355 nm light leads to the formation of
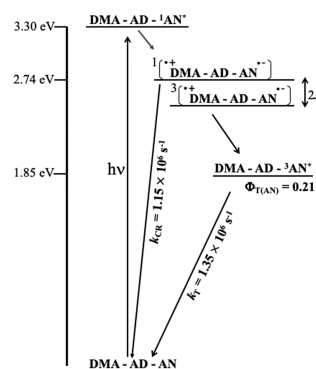

Figure 6. Photo processes taking place in DMA−AD−AN. The energy levels of the various transients and rate constants are also shown.

DMA−AD−^{1}AN*, which undergoes ultrafast electron transfer to generate the ^{1}CS state, $^{•+}$DMA−AD−AN$^{•-}$. A major fraction of ^{1}CS undergoes CR to the ground state. A small fraction of the ^{1}CS state undergoes ISC to form the ^{3}CS state, which requires spin realignment in the radical pair. The ^{3}CS formed undergoes ultrafast and quantitative spin-allowed CR to the local triplet. In linked dyads, the spin multiplicity change is caused by the hyperfine interaction between the unpaired electrons and the nuclear spins. However, a spin multiplicity change can occur only if the hyperfine interaction energy ΔE_{hfi} > 2J, where 2J is the spin exchange interaction energy. Previous studies have shown that ^{3}AN* is not formed when DMA− (CH$_2$)$_3$−AN is flash photolyzed, as ΔE_{hfi} < 2J. However, 2J values decrease exponentially with distance and ^{3}AN* formation could be observed for DMA−(CH$_2$)$_n$−AN when n

≥ 6, where R_e > 8.8 Å. Similar results are also observed in rigid DMN[n]DCV dyads.[4] In these cases, triplet formation was observed only for systems for which $n \geq 6$ ($R_e \geq 6.8$ Å). For the $n = 6$ system, Φ_T was 0.03, which increased to 0.4 for the $n = 10$ system ($R_e \sim 11.5$ Å). For DMA−AD−AN, $R_e \sim 4.6$ Å, and hence, formation of ^{3}AN* with a Φ_T of ~0.2 is unusual. Most probably the AD spacer is also capable of reducing $2J$ values, and the slow formation of ^{3}AN* suggests that $2J \approx \Delta E_{hfi}$ for DMA−AD−AN.

Figure 6 shows that the energy of the local triplet state DMA−AD−^{3}AN* lies 0.89 eV lower than the ^{1}CS state. The energy difference between the ^{1}CS and ^{3}CS states ($2J$) is normally only a few inverse centimeters. In compact dyads, $2J$ can be larger, but in any case, it cannot be larger than 0.89 eV. Hence, we believe that the ^{3}CS state is also far above the local triplet level in DMA−AD−AN. Thus, the ^{3}CS is not the lowest triplet in the molecule and the CS state is long-lived not because of the spin control effect discussed above. Figure 6 suggests that the long-lived CS state we observe in the case of the DMA−AD−AN compact dyad has singlet multiplicity.

CS state lifetimes exceeding 1.0 ns have not been reported for compact dyads where the the energy of the CS state is higher than those of local triplets.[1,2] τ_{CS} values of >1.0 ns have been reported only in cases in which the ^{3}CS is the lowest triplet in the dyad, which is not true in the DMA−AD−AN dyad we report here. For the alkyl chain-bridged systems shown in Figure 1, $\tau_{CS} \leq 1.0$ ns.[25] In the case of rigid dyad DMN[4]DMV, where R_e = 4.6 Å, $\tau_{CS} \ll 1.0$ ns.[4] For DMN[6]DMV where R_e = 6.8 Å, τ_{CS} was 0.5 ns.[4] τ_{CS} values observed for AD-bridged systems studied here are nearly 1000 times larger. Even for most of the triad molecules also, reported τ_{CS} values are < 1.0 μs.[2−6] In this context, observation of τ_{CS} values of >800 ns for DMA−AD−AN and DMA−AD−PY is extremely important and constitutes a significant advance in the study of PET reactions.

Rate constants k_{et} (k_{CS} or k_{CR}) for CS and CR reactions depend on the electronic matrix element that couples the reactant and product states (V), Gibbs free energy change (ΔG), and reorganization energy (λ), according to the Marcus equation for nonadiabatic electron transfer.

$$k_{et} = (2\pi/\hbar)V^2(4\pi\lambda k_B T)^{-1/2} \exp[-(\Delta G + \lambda)^2/4\lambda k_B T] \tag{2}$$

where $\hbar$ is Planck's constant divided by 2π, k_B is the Boltzmann constant, and T is the temperature.[37] An inspection of the data shows that k_{CS} and k_{CR} values for the AD-bridged systems are 1−3 orders of magnitude lower than those of the -(CH$_2$)$_3$- bridged systems, which have identical ΔG and λ values. Hence, the observed differences in k_{CS} and k_{CR} for the two systems must be due to differences in V values, which can be attributed to the AD bridge. For DMA−AD−AN, we have calculated electronic coupling for the CS (V_{CS}) and CR (V_{CR}) reactions using experimentally obtained k_{et} and calculated ΔG and λ values (Section 6 of the Supporting Information). The calculations gave a V_{CS} of 322 cm^{-1} and a V_{CR} of 0.532 cm^{-1}. The V_{CR} obtained is 3 orders of magnitude smaller than V_{CS}. Thus, the long τ_{CS} obtained in this study is attributed to the AD bridge, which exhibits extremely small electronic coupling for the CR reaction. The V_{CS} value reported here is comparable to the V_{CS} of 392 cm^{-1} for DMN[4]DMV.[1] V_{CR} was not calculated for this system because τ_{CR} was too short.

It has long been recognized that long CS state lifetimes can be achieved in principle, if V_{CS} is much larger than V_{CR}. Early studies by Zeng and Zimmt,[38,39] Oliver et al.,[40] and Wasielewski et al.[41] employed tools such as molecular symmetry, molecular shape, and geometrical isomerism to increase CS state lifetimes, but the enhancements attained were small. If we can establish that the AD bridge can enhance CS state lifetimes in dyads, it would be an important development in the study of PET reactions. Studies in this direction are in progress in our laboratory.

■ ASSOCIATED CONTENT

ⓈI Supporting Information

The Supporting Information is available free of charge at https://pubs.acs.org/doi/10.1021/acs.jpclett.2c03453.

> Materials and methods, synthesis and characterization of dyads, normalized fluorescence spectra, calculation of electron transfer rates, decay profiles of transient absorptions with fits and residuals, calculations of triplet quantum yields, kinetic profiles in short time windows, and calculations of ΔG, λ, V_{CS}, and V_{CR} (PDF)

■ AUTHOR INFORMATION

Corresponding Author

Karical R. Gopidas − *Photosciences and Photonics, Chemical Sciences and Technology Division, CSIR-National Institute for Interdisciplinary Science and Technology, Trivandrum 695019, India; Academy of Scientific and Innovative Research (AcSIR), Ghaziabad 201002, India;* ● orcid.org/0000-0003-2897-7633; Email: gopidaskr@gmail.com

Author

Kurisingal B. Daisymol − *Photosciences and Photonics, Chemical Sciences and Technology Division, CSIR-National Institute for Interdisciplinary Science and Technology, Trivandrum 695019, India; Academy of Scientific and Innovative Research (AcSIR), Ghaziabad 201002, India*

Complete contact information is available at:
https://pubs.acs.org/10.1021/acs.jpclett.2c03453

Notes

The authors declare no competing financial interest.

■ REFERENCES

(1) Verhoeven, J. W. On the Role of Spin Correlation in the Formation, Decay, and Detection of Long-Lived Intramolecular Charge-Transfer States. *J. Photochem. Photobiol. C* **2006**, *7*, 40−60.

(2) Hou, Y.; Zhang, X.; Chen, K.; Liu, D.; Wang, Z.; Liu, Q.; Zhao, J.; Barbon, A. Charge Separation, Charge Recombination, Long-Lived Charge Transfer State Formation and Intersystem Crossing in Organic Electron Donor/Acceptor Dyads. *J. Mater. Chem. C* **2019**, *7*, 12048−12074.

(3) Fukuzumi, S.; Lee, Y.; Nam, W. Mimicry and Functions of Photosynthetic Reaction Centers. *Biochem. Soc. Trans.* **2018**, *46*, 1279−1288.

(4) Paddon-Row, M. N. Covalently Linked Systems Based on Organic Components. In *Electron Transfer Chemistry*; Balzani, V., Ed.; Wiley-VCH: Weinheim, Germany, 2001; Vol. 3, pp 179−271.

(5) Gust, D.; Moore, T. A.; Moore, A. L. Covalently Linked Systems Containing Porphyrin Units. In *Electron Transfer Chemistry*; Balzani, V., Ed.; Wiley-VCH: Weinheim, Germany, 2001; Vol. 3, pp 272–336.

(6) Guldi, D. M. Fullerene-Porphyrin Architectures; Photosynthetic Antenna and Reaction Center Models. *Chem. Soc. Rev.* 2002, 31, 22–36.

(7) Wasielewski, M. R. Self-Assembly Strategies for Integrating Light Harvesting and Charge Separation in Artificial Photosynthetic Systems. *Acc. Chem. Res.* 2009, 42, 1910–1921.

(8) KC, C. B.; D'Souza, C. B. Design and Photochemical Study of Supramolecular Donor-Acceptor Systems Assembled via Metal-Ligand Axial Coordination. *Coord. Chem. Rev.* 2016, 322, 104–141.

(9) Verhoeven, J. W.; van Ramesdonk, H. J.; Groeneveld, M. M.; Benniston, A. C.; Harriman, A. Long-Lived Charge-Transfer States in Compact Donor-Acceptor Dyads. *ChemPhysChem.* 2005, 6, 2251–2260.

(10) Smit, K. J.; Warman, J. M. The Formation of Singlet and Triplet Charge Transfer States on Photo-Excitation of Carbazole-$(CH_2)n$-Tetrachlorophthalimide Compounds Studied by Time-Resolved Microwave Conductivity. *J. Lumin.* 1988, 42, 149–154.

(11) Anglos, D.; Bindra, V.; Kuki, A. Photoinduced Electron Transfer and Long-Lived Charge Separation in Rigid Peptide Architectures. *J. Chem. Soc., Chem. Commun.* 1994, 213–215.

(12) van Dijk, S. I.; Groen, C. P.; Hartl, F.; Brouwer, A. M.; Verhoeven, J. W. Long-Lived Triplet State Charge Separation in Novel Piperidine-Bridged Donor-Acceptor Systems. *J. Am. Chem. Soc.* 1996, 118, 8425–8432.

(13) Mac, M.; Najbar, J.; Wirz, J. Fluorescence Quenching of Derivatives of Anthracene by Organic Electron Donors and Acceptors in Acetonitrile. Electron and Proton Transfer Mechanism. *Chem. Phys. Lett.* 1995, 235, 187–194.

(14) Zhang, G.; Thomas, J. K.; Eremenko, A.; Kikteva, T.; Wilkinson, F. Photoinduced Charge-Transfer Reaction Between Pyrene and *N,N*-Dimethylaniline on Silica Gel Surfaces. *J. Phys. Chem. B* 1997, 101, 8569–8577.

(15) Paul, A.; Samanta, A. Photoinduced Electron Transfer Reactions in Room Temperature Ionic Liquids: A combined Laser Flash Photolysis and Fluorescence Study. *J. Phys. Chem. B* 2007, 111, 1957–1962.

(16) Zhang, G.; Thomas, J. K. Effect of Charge Stabilization on Electron Transfer Reactions in Zeolites. *J. Phys. Chem. B* 2003, 107, 7254–7260.

(17) Okada, T.; Fujita, T.; Kubota, M.; Masaki, S.; Mataga, N.; Ide, R.; Sakata, Y.; Misumi, S. Intramolecular Electron Donor-Acceptor Interactions in the Excited State of (Anthracene)-$(CH_2)_n$-(N,N-Dimethylaniline) Systems. *Chem. Phys. Lett.* 1972, 14, 563–568.

(18) Chuang, T. J.; Cox, R. J.; Eisenthal, K. B. Picosecond Studies of the Excited Charge-Transfer Interactions in Anthracene-$(CH_2)_3$-*N*, *N*-Dimethylaniline Systems. *J. Am. Chem. Soc.* 1974, 96, 6828–6831.

(19) Crawford, M. K.; Wang, Y.; Eisenthal, K. B. Effects of Conformation and Solvent Polarity on Intramolecular Charge Transfer: A Picosecond Laser Study. *Chem. Phys. Lett.* 1981, 79, 529–533.

(20) Crawford, M. K.; Wang, Y.; Eisenthal, K. B. Picosecond Laser Studies of Intramolecular Excited-State Charge-Transfer Dynamics and Small Chain Relaxation. *J. Am. Chem. Soc.* 1982, 104, 5874–5878.

(21) Okada, T.; Migita, M.; Mataga, N.; Sakata, Y.; Misumi, S. Picosecond Laser Spectroscopy of Intramolecular Heteroexcimer Systems. Time-Resolved Absorption Studies of *p*-$(CH_3)_2NC_6H_4(CH_2)_n$(1-pyrenyl) and -(9anthryl) systems. *J. Am. Chem. Soc.* 1981, 103, 4715–4720.

(22) Okada, T.; Karaki, I.; Matsuzawa, N.; Mataga, N.; Sakata, Y.; Misumi, S. Ultrafast Intersystem Crossing in Some Intramolecular Heteroexcimers. *J. Phys. Chem.* 1981, 85, 3957–3960.

(23) Migita, M.; Okada, T.; Mataga, N.; Sakata, Y.; Misumi, S.; Nakashima, N.; Yoshihara, K. Picosecond Laser Spectroscopy of Intramolecular Heteroexcimer Systems. Time-Resolved Fluorescence Studies of *p*-$(CH_3)_2NC_6H_4$-$(CH_2)_n$-(9-Anthryl), *p*-

(CH_3)_2NC_6H_4(CH_2)_n-(1-Pyrenyl) Systems and 9,9'-Bianthryl. *Bull. Chem. Soc. Jpn.* 1981, 54, 3304–3311.

(24) Okada, T.; Mataga, N.; Baumann, W.; Siemiarczuk, A. Picosecond Laser Spectroscopy of 4-(9-Anthryl)-N,N-dimethylaniline and Related Compounds. *J. Phys. Chem.* 1987, 91, 4490–4495.

(25) Mataga, N.; Nishikawa, S.; Asahi, T.; Okada, T. Femtosecond-Picosecond Laser Photolysis Studies on the Photoinduced Charge Separation and Charge Recombination of a Produced Ion Pair State of Some Typical Intramolecular Exciplex Compounds in Alkanenitrile Solvents. *J. Phys. Chem.* 1990, 94, 1443–1447.

(26) Wasielewski, M. R.; Minsek, D. W.; Niemczyk, M. P.; Svec, W. A.; Yang, N. C. Intramolecular Light-Induced Electron Transfer in a Rigid, Fixed-Distance Anthracene-N, N-Dimethylaniline System. Exciplex-like Behavior. *J. Am. Chem. Soc.* 1990, 112, 2823–2824.

(27) Tanaka, F.; Keawwangchai, S.; Rujkorakarn, R.; Mataga, N. Study of Photoinduced Electron Transfer in Pyrene-$(CH_2)_n$-N, N-dimethylaniline system by Molecular Dynamic Simulation. *Chem. Phys.* 2008, 348, 242–248.

(28) Tan, Z.; Kote, R.; Samaniego, W. N.; Weininger, S. J.; McGimpsey, W. G. Intramolecular Singlet-Singlet and Triplet-Triplet Energy Transfer in Adamantyl-Linked Trichromophores. *J. Phys. Chem. A* 1999, 103, 7612–7620.

(29) Murov, S. L.; Carmichael, I.; Hug, G. L. *Handbook of Photochemistry*, 2nd ed.; Marcell Dekker, Inc.: New York, 1993; p 103.

(30) Shida, T. *Electronic Absorption Spectra of Radical Ions*; Elsevier Science Publishers B.V.: Amsterdam, 1988; p 208.

(31) Forster, M.; Hester, R. E. Photoionization of Dimethylaniline and of the Donor-Aromatic-Acceptor Molecules *p*-$(CH_3)_2NC_6H_4R$, R = CN, COOH, COOEt, CHO, NO_2, in Glasses of Ethanol and Etanediol/Water at 77–125 K. *J. Chem. Soc., Faraday Trans. 2* 1981, 77, 1521–1534.

(32) Holcman, J.; Sehested, K. Dissociation of the OH Adduct of N,N-Dimethylaniline in Aqueous Solution. *J. Phys. Chem.* 1977, 81, 1963–1966.

(33) Shida, T. *Electronic Absorption Spectra of Radical Ions*; Elsevier Science Publishers B.V.: Amsterdam, 1988; p 69.

(34) Murov, S. L.; Carmichael, I.; Hug, G. L. *Handbook of Photochemistry*, 2nd ed.; Marcell Dekker, Inc.: New York, 1993; p 123.

(35) Shida, T. *Electronic Absorption Spectra of Radical Ions*; Elsevier Science Publishers B.V.: Amsterdam, 1988; p 85.

(36) Getoff, N.; Solar, S.; Richter, U.-B.; Haenel, M. W. Pulse Radiolysis of Pyrene in Aprotic Polar Organic Solvents; Simultaneous Formation of Pyrene Radical Cations and Radical Anions. *Radiat. Phys. Chem.* 2003, 66, 207–214.

(37) Marcus, R. A.; Sutin, N. Electron Transfer in Chemistry and Biology. *Biochim. Biophys. Acta* 1985, 811, 265–322.

(38) Zeng, Y.; Zimmt, M. B. Symmetry Effects in Photoinduced Electron Transfer Reactions. *J. Am. Chem. Soc.* 1991, 113, 5107–5109.

(39) Zeng, Y.; Zimmt, M. B. Symmetry Effects on Electron Transfer Reactions: Temperature Dependence as a Diagnostic Tool. *J. Phys. Chem.* 1992, 96, 8395–8403.

(40) Oliver, A. M.; Paddon-Row, M. N.; Kroon, J.; Verhoeven, J. W. Orbital Symmetry Effects on Intramolecular Charge Recombination. *Chem. Phys. Lett.* 1992, 191, 371–377.

(41) Wasielewski, M. R.; Niemczyk, M. P.; Johnson, D. G.; Svec, W. A.; Minsek, D. W. Ultrafast Photoinduced Electron Transfer in Donor-Spacer-Acceptor Molecules: Modification of Spacer Energetics as a Probe for Superexchange. *Tetrahedron* 1989, 45, 4785–4806.